ALGORITHM DEVELOPMENT FOR USING OPTIMAL CONTROL IN STRUCTURAL OPTIMIZATION SUBJECTED TO SEISMIC AND WIND FORCES

by Franklin Y. Cheng
Curators' Professor

Chris Pantelides
Graduate Assistant

Department of Civil Engineering
University of Missouri-Rolla
Rolla, MO 65401-0249
1988

CIVIL ENGINEERING STUDY
STRUCTURAL SERIES 88-1-15

ALGORITHM DEVELOPMENT FOR
USING OPTIMAL CONTROL IN STRUCTURAL OPTIMIZATION
SUBJECTED TO SEISMIC AND WIND FORCES

by
Franklin Y. Cheng
Curators' Professor

Chris Pantelides
Graduate Assistant

Department of Civil Engineering
University of Missouri-Rolla
Rolla, MO 65401
1988

50272-101

REPORT DOCUMENTATION PAGE	1. REPORT NO. Structural Series 88-1-15	2.	3. Recipient's Accession No. PB90 133471/AS

4. Title and Subtitle
Algorithm Development for Using Optimum Control in Structural Optimization Subjected to Seismic and Wind Forces

5. Report Date
January, 1988

6.

7. Author(s)
Franklin Y. Cheng and Chris P. Pantelides

8. Performing Organization Rept. No.
Structural Series

9. Performing Organization Name and Address

Civil Engineering Department
University of Missouri-Rolla
Rolla, MO 65401

10. Project/Task/Work Unit No.

11. Contract(C) or Grant(G) No.

(C)

(G) NSF CEE 8403875

12. Sponsoring Organization Name and Address

National Science Foundation
Washington, D.C.

13. Type of Report & Period Covered
Final

14.

15. Supplementary Notes

16. Abstract (Limit: 200 words)
        The present study deals with the optimal design of building structures equipped with active control systems. The control systems considered are the active mass damper, the active tendon system, and a combination of the two systems. Optimal control algorithms have been extensively studied for possible adoption in the structural optimization. The studies included the Ricatti closed-loop algorithm based on classical control theory, non-optimal closed-loop control in the frequency-domain, and instantaneous open-loop, closed-loop, and open-closed-loop algorithms in the time-domain. Although all the above mentioned algorithms were investigated for their effectiveness in structural control, the time-domain algorithms have been extensively studied for the combined effect of structural optimization with optimal control. Also included in this study are a critical-mode control algorithm and the resulting spillover effect on the uncontrolled modes, the optimal location of controllers in conjunction with the critical-mode control algorithm, and the time-delay in the application of the control forces. The structural optimization is formulated as a constrained minimization problem for which the design variables are the floor stiffnesses of the building and certain control parameters. The objective function is the structural weight of the building. The constraints include floor drifts, floor displacements, control forces, and natural frequencies.

17. Document Analysis   a. Descriptors

Analysis	Frameworks	Tendon
Control	Mass Damper	Wind
Design	Optimization	
Earthquake	Structures	

b. Identifiers/Open-Ended Terms

c. COSATI Field/Group

18. Availability Statement

19. Security Class (This Report) UNCLASSIFIED	21. No. of Pages 285
20. Security Class (This Page) UNCLASSIFIED	22. Price

(See ANSI-Z39.18)   See Instructions on Reverse   OPTIONAL FORM 272 (4-77)
(Formerly NTIS-35)

ABSTRACT

The present study deals with the optimal design of building structures equipped with active control systems. The control systems considered are the active mass damper, the active tendon system, and a combination of the two systems.

Optimal control algorithms have been extensively studied for possible adoption in the structural optimization. The studies included the Ricatti closed-loop algorithm based on classical control theory, non-optimal closed-loop control in the frequency-domain, and instantaneous open-loop, closed-loop, and open-closed-loop algorithms in the time-domain. Although all the above mentioned algorithms were investigated for their effectiveness in structural control, the time-domain algorithms have been extensively studied for the combined effect of structural optimization with optimal control. Also included in this study are a critical-mode control algorithm and the resulting spillover effect on the uncontrolled modes, the optimal location of controllers in conjunction with the critical-mode control algorithm, and the time-delay in the application of the control forces.

The structural optimization is formulated as a constrained minimization problem for which the design variables are the floor stiffnesses of the building and certain control parameters. The objective function is the structural weight of the building. The constraints include floor drifts, floor displacements, control forces, and natural frequencies.

Structural optimization can yield a safer and more economical structure based on rational stiffness redistribution while satisfying a set of constraints. This study shows that active control systems are effective in reducing the effects of an earthquake on the safety and serviceability of structures. The combination of structural optimization and active control can further reduce the control forces and consequently reduce the total structural cost. This is achieved by minimizing the required control energy, to determine the optimal weighting matrices, while the structural response is still bound by the constraints imposed for structural optimization.

The critical-mode control algorithm is developed in order to reduce the amount of computation time which is important in the structural optimization scheme. The spillover effect on the uncontrolled modes is shown to be considerable. For seismic structures the prospect of applying critical-mode control is promising since the response is governed by the few lowest modes.

The critical-mode control algorithm is also used to determine the optimal location of a limited number of controllers. Two methods are investigated; the first is based on the modal shapes and the second upon the minimization of the control energy and response performance indices.

The issue of time-delay is investigated in order to be utilized in the optimal control algorithms used in the structural optimization process. It is recognized that as control system technology advances the effect of time-delay may become negligible.

ACKNOWLEDGMENTS

TABLE OF CONTENTS

LIST OF ILLUSTRATIONS

List of Illustrations (continued)

List of Illustrations (continued)

List of Illustrations (continued)

List of Illustrations (continued)

List of Illustrations (continued)

LIST OF TABLES

NOMENCLATURE

AMD   active mass damper

ARE   algebraic Ricatti equation

AT   active tendon

$[A_d]$ plant matrix for structure with AMD

$[A]_j$ transfer matrix of jth story equipped with AT

$[A_m]$ transfer matrix of mth story equipped with AMD

$[A(N)]$ transfer matrix product for AT

$[A_m(N)]$ transfer matrix product for AMD

$[A_t]$ plant matrix for structure equipped with AT

a constant for structural weight function

$\{B_d\}$ location vector for structure with AMD

$[B_t]$ location matrix for structure with AT

$[\tilde{B}]$ cross-correlation matrix

b_j jth floor constant for structural weight function

$\bar{C}$ constant, function of tendon stiffness

C_h, C_χ decay coefficient

C_p, C_w pressure coefficient

$\bar{C}_d$ DFF gain

$\bar{C}_v$ VFF gain

$\{C_d\}$ excitation influence vector for structure with AMD

$\{C_t\}$ excitation influence vector for structure with AT

$[C]$ damping matrix

$[C_D]$ damping matrix for structure equipped with AMD

c damping coefficient

c_d	damping coefficient of AMD
c_g	ground damping
c_j	damping coefficient for jth floor
DFF	displacement feedback force
$[D]$	lower triangular correlation matrix
E	wind spectrum coefficient
$\bar{F}(h)$	mean wind velocity
$\{F(h,t)\}$	wind velocity vector
$\{\bar{F}(h)\}$	mean wind velocity vector
$\tilde{f}$	shear velocity constant
$f_j(t)$	jth dynamic component of wind velocity
$G1, G2$	ideal gains
$G(i,j)$	element of ideal gain matrix
$[G_t]$	coefficient matrix for AT open-loop control force
$g_j(\{k\})$	jth general constraint
$g_m(\omega)$	gain of AMD controller
$g_t(\omega)$	gain of AT controller
g_1, g_2	real gains
$H_g(i\omega)$	frequency response function
$H_g(s)$	transfer function
h_j	height at jth floor
h_0	roughness length
$\mathcal{H}$	Hamiltonian
$[I], [I]_c$	identity matrix
$[IK]$	ideal gain matrix
i	imaginary unit number
J	quadratic performance index for AT

J_D	quadratic performance index for AMD
$J_{Dp}(t)$	instantaneous time-dependent performance index for AMD
JE	control energy performance index
J_E	control energy performance index
J_R	response performance index
$J_p(t)$	instantaneous time-dependent performance index for AT
K_A, K_U	gain for closed-loop control
K_P, K_O	gain for closed-loop control
Kc_j	active tendon stiffness
Kc_N	active mass damper stiffness
$\{k\}$	design variables vector
$[K]$	stiffness matrix
$[K]_c$	gain matrix for critical-mode control
$[K_D]$	stiffness matrix for structure with AMD
$[\overline{K}]$	time-invariant gain matrix
$[K(t)]$	time-varying gain matrix
k	stiffness
k_d	stiffness of AMD system
k_g	ground stiffness
k_j	stiffness of jth floor
k_{md}	proportionality constant for AMD
k min	minimum allowable stiffness
k_t	tendon stiffness
L	number of frequency intervals
LF	Lagrangian function
l	counter
M	number of tendon controllers

MRE	matrix Ricatti equation
$[M]$	mass matrix
$[M_D]$	mass matrix for structure with AMD
m	mass
m_d	mass of AMD
m_g	ground mass
m_j	mass of jth floor
$\overline{m}$	number of critical modes
N	number of floors of the structure
n	frequency
PMD	passive mass damper
$P_r(h_j, t)$	dynamic wind pressure at jth floor
$\overline{P}_r(h_j)$	mean wind pressure at jth floor
$\{\hat{P}2(t)\}$	response vector for critical-mode algorithm
$[P]$	solution of ARE for a structure with AT
$[P_D]$	solution of ARE for a structure with AMD
$[\hat{P}1(t)]$	response matrix for critical-mode algorithm
$[P(t)]$	time-varying solution of MRE
prm, prt	proportionality constant
$[Q]$	response weighting matrix for structure with AT
$[Q]_c, [Q]_r$	composite weighting matrix for critical-mode control
$[Q]_{cr}, [Q]_{rc}$	composite weighting matrix for critical-mode control
$[Q_D]$	response weighting matrix for structure with AMD
R_D	control weighting constant for structure with AMD
$R0$	feedback gain
$R1$	loop gain
$[R]$	control weighting matrix for structure with AT

$[RK]$	real gain matrix
$[RKR]$	real gain submatrix
r	dimensionless quantity
$S(h,n)$	wind design spectrum
$S_j(n)$	wind spectrum at jth floor
$S^C(r,n)$	wind co-spectrum
S^2	power spectrum of white noise
$S_m(\omega)$	power spectral density of state at mth floor
$\{S2_d(t)\}$	coefficient for AMD control force
$\{S1_d\}^T$	coefficient matrix for AMD control force
$\{S2(t)\}$	coefficient matrix for AT control force
$[S1]$	coefficient matrix for AT control force
$\{TC\}$	composite vector
$\{TC\}_c, \{TC\}_r$	composite vector for critical-mode control
$[T]$	transfer matrix of AMD
$[TB]$	composite matrix
$[TB]_c, [TB]_r$	composite matrix for critical-mode control
$[T_d]$	modal transformation matrix for system with AMD
$[TR]_i$	gain transformation matrix
$[T_t]$	modal transformation matrix for system with AT
t	time
t_f	final time-instant
t_0	initial time-instant
t_x	time-delay in application of DFF
$t_{\dot{x}}$	time-delay in application of VFF
$U(t)$	actuator displacement
$u, u(t)$	horizontal component of AT control force

u_d max	allowable AMD control force
$u_d(t)$	AMD control force
u_i max	allowable control force for ith AT
$u_i(t)$	AT control force
$u^*d(t)$	optimal AMD control force
$\bar{u}$	Fourier transform of AT control force
$\bar{u}_d$	Fourier transform of AMD control force
$\{u(t)\}$	control force vector for AT
$\{u^*(t)\}$	optimal control force vector for AT
VFF	velocity feedback force
$V(t)$	feedback voltage
W	structural weight of building
$\{W(t)\}$	wind forces vector
$X_d(t)$	absolute displacement of AMD
$X_g(t)$	ground displacement
X_j, $X_j(t)$	jth floor absolute displacement
X_{N+1}	displacement of AMD
$\ddot{X}_g(t)$	ground acceleration
$\bar{X}_j$	Fourier transform of jth floor displacement
$x(t)$	relative displacement
$x_d(t)$	relative displacement of AMD
x_j max	jth floor allowable relative displacement
$x_j(t)$	jth floor relative displacement
$\bar{x}_g$	Laplace transform of input ground displacement
$\{x(t)\}$	vector of relative displacements for structure with AT
Y_j	shear force in columns of jth floor
$\bar{Y}_j$	Fourier transform of shear force in columns of jth floor

$\{y(t)\}$	vector of relative displacements for structure with AMD
$\{Z\}_j$	Fourier transform of state at jth floor
$\{Z\}_0$	Fourier transform of state at basement floor
$\{z(t)\}$	state-vector for structure with AT system
$\{z_D(t)\}$	state-vector for structure with AMD system
z_g	ground displacement
$\bar{z}_g$	Laplace transform of ground displacement
α	scalar
$\{\beta(t)\}$	uncorrelated wind velocity vector
$\beta_j(t)$	jth uncorrelated wind velocity
$\{\Gamma(t)\}$	forcing term
$\{\gamma_D\}$	location vector for structure with AMD
$[\gamma]$	location matrix for structure with AT
Δn_i	frequency interval
Δt	time-increment
$\delta(t)$	Dirac delta function
$\{\delta\}$	excitation influence coefficient for structure with AT
$\{\delta_D\}$	excitation influence coefficient for structure with AMD
ε_d	normalized loop gain for AMD
ε max	allowable normalized loop gain for AMD or AT
ε_t, ε_{ti}	normalized loop gain for ith AT
ζ_g	ground damping
$[\tilde{H}]$	cross-correlation matrix
$\{\eta(t)\}$	random process vector
$\Theta_m(t)$	coefficient for AMD control force
$\Theta_t(t)$	coefficient for AT control force
θ	angle between tendon and horizontal

κ	Von Karman's constant
$\{\Lambda_d(t - \Delta t)\}$	numerical integration vector for structure with AMD
$\{\Lambda_t(t - \Delta t)\}$	numerical integration vector for structure with AT
$\{\Lambda_t(t - \Delta t)\}_c$	integration vector for critical-mode control
$\{\lambda(t)\}$	vector of Lagrange multipliers
$\{M_j\}$	real part of jth eigenvector
μ_j	real part of jth eigenvalue
ν	coherence coefficient
$\{\xi(t)\}$	uncorrelated wind velocity vector
$\{\hat{\xi}(t)\}$	response vector for instantaneous algorithms
$[\hat{\Xi}(t)]$	response vector for instantaneous closed-loop
ρ	air density
σ_d	standard deviation of AMD control force
σ_d max	standard deviation of allowable AMD control force
σ_{ti}	standard deviation of ith AT control force
σ_{ti} max	standard deviation of allowable AT control force
σ_{xj}	standard deviation of jth floor relative displacement
σ_{xj} max	standard deviation of allowable displacement
σ_d^2	mean square response of AMD control force
σ_m^2	mean square response of state at mth floor
σ_{ti}^2	mean square response of ith AT control force
τ	dummy variable of integration
τ_d	normalized feedback gain for AMD
τ max	allowable normalized feedback gain for AMD or AT
τ_t, τ_{ti}	normalized feedback gain for ith AT
$\{Y_j\}$	imaginary part of jth eigenvector
υ_j	imaginary part of jth eigenvalue

$\Phi\ddot{X}_g(\omega)$ power spectral density of earthquake

$[\varphi_t]$ modal plant matrix

$[\varphi_t]_c$ critical modal plant matrix

$[\varphi_t]_j$ modal plant submatrix

$[\varphi_t]_r$ residual modal plant matrix

ϕ_{ji} phase angle

χ horizontal dimension

$\{\psi_d(t)\}$ modal response vector for structure with AMD

$\{\psi_t(t)\}$ modal response vector for structure with AT

$\{\psi_t(t)\}_c$ critical-modes modal response vector

$\{\psi_t(t)\}_r$ residual-modes modal response vector

$[\hat{\Psi}(t)]$ response matrix for instantaneous open-closed-loop

ω forcing frequency

ω_d natural frequency of PMD

ω_g ground frequency

ω_1 fundamental frequency of structure without control

Special Symbols

$\{0\}$ null vector

$\{\ \}^{T}$ transpose of a vector

$\{\dot{x}(t)\}$ first time-derivative of $x(t)$

$\{\ddot{x}(t)\}$ second time-derivative of $x(t)$

$[0]$ null matrix

$[\ ]^{-1}$ inverse of a matrix

$[\ ]^{T}$ transpose of a matrix

$[\dot{P}(t)]$ time-derivative of $[P(t)]$

$\exp[A]$ exponential matrix of $[A]$

$\|z\|^{2}$ magnitude of vector z

$\dfrac{\partial \mathscr{H}}{\partial x}$ partial derivative of $\mathscr{H}$ with respect to x

δJ variation of J

∞ infinity

I. INTRODUCTION

A. LITERATURE REVIEW

Structural control implies that performance and serviceability of a structure are controlled so that they remain within prescribed limits during the application of environmental loads. Structural control is achieved by using passive or active control devices. The passive devices utilize the fact that energy dissipating mechanisms can be activated by the motion of the structure itself. Base-isolation of the superstructure from the foundation using steel-reinforced rubber bearings is an example of passive control for earthquake resistant structures. Dynamic absorbers used in the vibration control of machinery are mass-spring systems appended to the structure. They have been applied to tall buildings in the form of passive tuned mass dampers, such as the John Hancock building in Boston (60), and the Citicorp Center in New York (46). Passive devices although effective in reducing the response, are limited to just one mode of vibration as pointed out by Chang and Soong (6).

Active control devices require external energy for their operation. The devices under consideration can be classified into four categories: 1) active mass damper, 2) active tendons, 3) appendages, and 4) pulse control.

Dynamic absorbers or mass dampers can be coupled with an external power supply and an electrohydraulic actuator to form active mass dampers. The actuator is operated by an active control algorithm which can be non-optimal, sub-optimal or optimal, where the optimality refers to the minimization of a cost functional. The cost functional to be minimized is the total energy of the system, including the work done by the control forces. The active control algorithm is implemented on a digital or analog computer. Such active devices produce a larger reduction in response than passive devices. Active mass dampers, or active tuned mass dampers as they are sometimes called, can be used for wind or earthquake excited structures.

Active tendons, or cables, are a second category of active control systems for civil engineering structures. The tendons can be tensioned using hydraulic rams. Internal forces are generated that are used to adjust the deformations of the structure. Displacement and velocity sensors are used to monitor the response due to external excitations. If the response exceeds certain limits the controller determines the required adjustments with the aid of the control algorithm, and activates the hydraulic actuators which tension the tendons. The feasibility of using active tendons to control seismic structures was tested experimentally by Soong, Reinhorn and Yang (15,53).

A third category of active control systems for tall buildings is that of appendages. Appendages are attachments to the top of the building that resemble aircraft wings with variable geometry. The appendages are movable and their position is computed based on current

2

deformation measurements. Simulation studies by Soong and Skinner for structures equipped with appendages have shown substantial reductions in the displacements of tall buildings under wind gusts (54).

Pulse control is a fourth class of active structural control. Pulses are thrusts applied over a short period of time in the form of either air and gas jets or tendon prestressing. These thrusts are applied using pulse generators located at various positions in the structure. The pulses are applied to the structure at discrete time-intervals and their intensity is computed by a control algorithm based on response measurements. Pulse control experiments have been carried out by Masri, Bekey and Caughey using jets (35).

The application of control theory to aircraft and satellite systems has been extensive. The problems that are identified and solved range from stochastic control of aircraft in turbulence (22), to spacecraft attitude control (31). Several studies and experiments of active control have been carried out in the aerospace field. The experiments were performed to actively damp vibrational motion of flexible structures. Schaechter has performed an experiment employing a pinned-free flexible beam (49). The experiment demonstrated active dynamic control, adaptive control, and associated hardware requirements and mechanization difficulties. Hallauer, Skidmore, and Gehling, studied the modal-space active damping of a plane grid, theoretically and experimentally (21). Meirovitch et al., studied the nonlinear control of an experimental beam (39). The above studies are examples of laboratory implementations to either validate theoretical

control concepts, or determine the reason for difficulties and ineffectiveness in control strategies.

In the field of active control as applied to civil engineering structures, the effort has been concentrated in the development of optimal control algorithms. Recently some experimental work has also been done. Abdel-Rohman, Quintana and Leipholz have examined the active control of flexible structures in terms of closed-loop control, and a combination of closed-loop and open-loop control (2). The classical Ricatti approach was used. The weighting matrices were found by trial and error, and the equations of motion were approximated by a limited number of modes. Abdel-Rohman and Leipholz presented a general approach that solves the optimal control problem (1). In their approach a quadratic performance index is minimized and constraints are imposed on the structure's deflections, accelerations, and on the magnitude of the control forces. A deterministic excitation was used for simulation studies.

Basharkah and Yao attempted to find an optimum gain matrix in the application of active control to civil engineering structures (4). The technique was based upon a stochastic approach and modal analysis in order to reduce the displacement response of building structures to earthquakes. The topic of optimum gain matrices was studied by Cheng and Pantelides in the context of optimum weighting matrices. The concept of reducing the control force levels by finding the optimum weighting matrices was formulated as an optimization problem to minimize control energy (13).

4

Yang has studied the application of the active mass damper or active tendon systems to tall buildings subject to earthquake excitations (61). The random vibration analysis was formulated in terms of the transfer matrix approach, thus obtaining the frequency response of the structure directly. Parametric studies of the efficiency of the non-optimal control law were carried out in terms of the control parameters of normalized feedback and loop gains. Yang and Samali applied the transfer matrix approach to tall buildings in along-wind motion (65). The active tendon or active mass damper systems were investigated. The random wind flow was assumed stationary in time and non-homogenous in space. The standard deviations of the response and of the control forces were computed for a range of the control parameters of normalized feedback and loop gains.

Cheng and Pantelides presented an algorithm for optimal design of structural systems equipped with active tendon and/or active mass damper systems (9,10) which is given in Chapter IV. The structure was subjected to a stochastic earthquake excitation and a non-optimal control law was used. The analysis was performed in the frequency-domain using the transfer matrix method. The structural optimization was carried out using structural weight as the objective function, and the standard deviations of the displacement response and of the control forces as constraints. It was observed that the optimum structure with the active control system can effectively reduce the response.

5

Meirovitch and Silverberg studied the control of structures subject to seismic excitation, using the independent modal-space control method (IMSC) (42). In this method the structure is controlled by controlling individual modes independently of one another (37,41,44). In the IMSC one first designs modal controls so as to control the lower modes. These modal controls do not represent actual controls because they are derived in the modal domain, so an expression is formulated to relate the modal controls to the actual controls. An optimal IMSC closed-loop control scheme was applied to a three-story structure subjected to a real accelerogram. The results were satisfactory.

The topic of controlling only a few modes of vibration of a flexible dynamic system has received considerable attention. Martin and Soong have showed that modal control theory can be applied fruitfully to affect direct control of specific structural modes (34). Balas has presented the feedback control of N modes of a flexible system and has treated the problem of control spillover into the uncontrolled modes (3). Meirovitch and Öz have presented an independent modal-space control scheme for the control of positional, attitude, and elastic motions for a discretized model of a distributed-parameter flexible spacecraft (40). The control scheme was demonstrated for non-optimal and optimal proportional control laws as well as for on-off control. Recently, a stochastic independent modal-space estimation and control method was presented by Öz and Meirovitch (45). The method is capable of estimating and controlling

all the modes of a distributed-parameter system in a noisy environment.

Yang and Lin have studied an optimal open-loop critical-mode control algorithm for tall buildings under stationary earthquake excitations (63). The control systems considered were the active tendon or the active mass damper systems. The critical-mode control was found to be superior to the global control, insofar as the amount of on-line computations was concerned. The spillover effect, resulting from the excitation of the uncontrolled modes by the control forces, was found to be negligible under certain conditions. It was also observed that the optimal critical-mode control is likely to be as effective as the optimal global control, since the response of tall buildings under earthquake excitations is usually dominated by a few lowest modes. Yang and Lin have also applied the optimal open-loop critical-mode algorithm to buildings excited by an earthquake modelled as a non-stationary random process (64). It was shown that the building response and the required active control forces computed based on the stationary earhquake model are conservative.

In this study Chapter IX presents the derivation of a critical-mode optimal control algorithm based on the instantaneous closed-loop control. The algorithm is used to evaluate the spillover effect on the residual modes, and to study the problem of optimal location of a limited number of controllers.

The concept of the instantaneous optimal control was introduced by Saridis and Lobbia in their search for simplified optimal stochastic control algorithms (48). Instead of minimizing an integral performance index it was proposed to minimize a sequence of single-stage processes. Thus the optimality of the control is achieved at each instant of time. The benefit of instantaneous optimal control algorithms was the simplicity of the derived control law as compared to the traditional control law based on the integral performance index.

The concept of instantaneous optimal control algorithms was recently adopted by Yang, Akbarpour and Gaemmaghami for analysis of seismic structures (62). In their approach instead of an integral performance index, a time-varying performance index is minimized. The optimal open-loop, closed-loop, and open-closed-loop algorithms were developed. The instantaneous nature of these algorithms allowed the consideration of the on-line measurement of the earthquake excitation for the open-loop and open-closed-loop algorithms. The resulting optimal control laws are simpler than the classical Ricatti approach.

The instantaneous optimal open-loop algorithm was used by Cheng and Pantelides for the structural optimization of seismic structures equipped with an active mass damper or active tendon system (11), which is given in Chapter VI. The objective function to be minimized was structural weight and constraints were imposed on the maximum floor displacements and maximum control forces. It was found that structural optimization combined with active control produces an

8

efficient and economical design, while keeping the control forces within a practical range.

Recently Kobori, Kanayama and Kamagata, presented an approach on "dynamic intelligent" building systems to control earthquake motions (27). A combination of open-loop and closed-loop control was proposed. It was suggested that open-loop control will remove the natural period of the structure from the seismic spectral peak period, and closed-loop control will reduce the inertia force created by the seismic excitation. The algorithm was applied to an experimental three degree-of-freedom model.

Recently, Lin, Chung, Soong and Reinhorn have made an experimental study of a standardized model under base excitation supplied by the earthquake simulator at SUNY/Buffalo (32). The Ricatti closed-loop and the instantaneous control algorithms were tested, and comparisons were made between analytical and experimental results.

Time-delay in the application of active control is an important problem in the implementation of structural control. The problem was considered in an experimental study of the active tendon system carried out by Chung, Reinhorn, and Soong (15). The time-delay for the single degree-of-freedom experimental model was incorporated in the elements of the gain matrix of the optimal control algorithm. Another interesting problem in the implementation of active control is the determination of optimal controller locations when, due to practical and economic considerations only a limited number of them are available. Soong and Chang have developed a minimum control energy

criterion within the framework of modal control to address the problem (52). Simulations for a three-story structure showed that the arrangement that satisfied the minimum control energy criterion also produced the minimum response.

The use of structural optimization techniques as an ordered approach to design decisions has been extensively developed in the past two decades. Structural optimization with the aid of the electronic computer, can relieve the designer from repetitive calculations and reanalysis. Many types of optimization problems can be identified. An efficient structural optimization program ODRESB-3D, was developed by Truman and Cheng, based on optimality criteria (14,55,56). The procedure can be used for design and sensitivity analysis of three-dimensional reinforced concrete and steel buildings, subject to multi-component earthquake excitations. Multiple constraints are included in the optimization such as displacement, stress, frequency and drift constraints. The algorithm includes several analysis capabilities including static, modal analysis and the ATC-03 analysis procedures. The modal analysis was used to study multi-component excitations, and the ATC-03 provisions were used to study the effects of the ATC-03 parameters such as soil profile, geographic location, plan and vertical irregularities, and ATC-03 stability function.

Geometric non-linearities such as the P-Δ effect can also be taken into account in the optimization of tall buildings as demonstrated by Cheng and Botkin (7). Recently Cheng and Juang have developed an optimization algorithm designated as ODSEWS-2D-II, for

structural design of two-dimensional structures with various building codes including UBC, Chinese-TJ-11-78, ATC-3-06 Tentative Provisions and others. The objective is to obtain the minimum weight or minimum cost of a structural system subject to static, earthquake and wind forces (8,23). Included are studies on the assessment of ATC-3-06 parameters, the effect of soil-structure interaction of the ATC-3-06 provisions, the effectiveness of various bracing systems in designing aseismic structures, the effect of the P-Δ forces and the vertical ground excitations on the optimum design, the comparison of various seismic code provisions, the comparison of minimum weight and minimum cost design, and the influence of story drift constraint and displacement constraint on optimum design.

A method for vibration control of large space structures by integrating the structural and control design has been presented by Khot, Eastep and Venkayya (25). The objective was to reduce the structural response under an initial disturbance. The cost function was the weight of the structure, with a constraint on the damping parameter of the closed-loop system.

Recently, Cheng and Pantelides presented an algorithm for combining structural optimization and active control of structural systems (12,13). The algorithm is based on optimal instantaneous algorithms for structures subject to seismic and wind excitations. The optimal weighting matrices in the performance index were found by minimizing the control energy of the control system. The critical-mode control algorithm for the instantaneous optimal closed-loop scheme was derived, and the spillover effect was demonstrated for earthquake

11

excited structures. For wind excited structures, the reduction of floor displacements and enhancement of human comfort was shown. The objective of structural optimization is to yield a safer and more economical structure based on a rational stiffness redistribution while satisfying a set of constraints. Active control is effective in reducing the earthquake effects on the safety and serviceability of the structure. The combination of structural optimization and active control can further reduce the control forces, and a more economical structure-control system can be produced.

B. UNDERLINE OBJECTIVE

The safety and serviceability of seismic structures can be improved by using active control devices. At the design stage the building can be designed with the presence of the control system in mind. However in order to achieve economy of both structural material and control energy, the combined structure-control system should be optimized.

The main objective of this study is to integrate the design of a structural system with the active control system in an optimal manner. Earthquake excitation is considered in the form of ground acceleration or power spectral density of ground acceleration. Wind forces are generated using wind design spectra. Two active control systems are considered, the active mass damper and active tendon systems. Both frequency-domain and time-domain control algorithms are considered. From previous studies by Cheng and Juang (8), and Cheng and Truman (14), it is known that structural weight is a reliable objective

function for member resizing and is used in this study. The design variables are the structural stiffness and control parameters. The constraints include displacements, natural frequencies, drifts, and control forces. The optimization algorithm uses an interior penalty function strategy and Powell's search algorithm (47).

Other objectives in this study are: 1) to study the fundamental concepts of the Ricatti optimal closed-loop algorithm for the passive mass damper, active mass damper, and active tendon systems, 2) to discuss the assumptions inherent in the Ricatti optimal closed-loop algorithm and compare the simulations with experimental results, 3) to derive the non-optimal closed-loop control in the frequency-domain based on the transfer matrix concept for the combined active mass damper and active tendon systems, 4) to derive the instantaneous optimal control algorithms in the time-domain for open-loop, closed-loop and open-closed-loop strategies, 5) to investigate the importance of the weighting matrices in the performance index and to derive optimal weighting matrices by the minimization of control energy, 6) to study the influence of time-delay and methods of compensating for it, 7) to derive the critical-mode optimal control algorithm and study the spillover effect on the uncontrolled modes, 8) to utilize the critical-mode optimal control algorithm with the modal and performance index methods in order to determine optimal locations of controllers, 9) to compare the various optimal control algorithms, 10) to study the effect of wind-induced excitations on the controlled structure, and 11) to illustrate by numerical examples the design

13

procedures of the numerical optimization technique, and the benefits of using a combined optimum structure-control design.

A brief discussion of the contents of each Chapter in this dissertation is given below.

In Chapter II the structural control systems are categorized into three classifications. First, according to whether they are passive or active. Secondly, the active control systems are categorized in terms of implementation strategy into open-loop, closed-loop, and open-closed-loop control. Finally the active control systems are classified according to the optimality of the control scheme as optimal, sub-optimal, and non-optimal control algorithms.

Chapter III gives a brief discussion of the assumptions inherent in the Ricatti optimal closed-loop algorithm. The fundamental concepts for the active tendon, active mass damper, and passive mass damper are discussed. The Ricatti optimal closed-loop algorithm is derived using both the active tendon and active mass damper systems. Comparisons with experimental results are made and numerical simulations are presented.

In Chapter IV the non-optimal closed-loop control based on the transfer matrix concept is described. The statistics of the response for both the active tendon, active mass damper and a combination of the two systems are derived. The active tendon and active mass damper control forces are described in terms of the feedback and loop gains. Numerical examples demonstrate power spectral density comparisons of

the response for the active tendon, active mass damper and combination of the two systems.

The instantaneous optimal control algorithms for open-loop, closed-loop, and open-closed-loop strategies are derived in Chapter V. The algorithm for a combined active tendon and active mass damper system is proposed. The solution of the motion equations in state-space using modal decomposition is described in detail. The importance of the weighting matrices in the performance index is emphasized, and numerical examples illustrate the resulting variations of the control forces and the response. Simulation of the response under earthquake and wind excitations is demonstrated with the aid of numerical examples, and a comparison is made with the Ricatti closed-loop algorithm.

The structural optimization formulation for both optimal and non-optimal control algorithms is described in detail in Chapter VI. The design variables, objective function, and constraints pertaining to the control algorithms derived in Chapters III, IV, and V are outlined. The numerical optimization algorithm is described, and numerical applications of the structural optimization with the active control systems are demonstrated.

In Chapter VII the topic of minimization of control energy is discussed in the context of optimal weighting matrices used in the performance index. Numerical examples illustrate the concept as applied to an instantaneous closed-loop algorithm.

15

Chapter VIII deals with the topic of time-delay. The general considerations for the time-delay problem are outlined. Compensation methods for a single-degree of freedom and a multiple-degree of freedom systems are suggested.

In Chapter IX the critical-mode optimal control algorithm is derived for the instantaneous optimal closed-loop control. The control spillover effect is demonstrated both theoretically and numerically. The critical-mode algorithm is then used to study the problem of optimal location of a limited number of controllers for an earthquake excited structure.

In Chapter X the work is reviewed, and the conclusions based on the results are outlined.

Appendix A contains the derivation of the power spectral density of filtered white noise for earthquake excitations. This is used in Chapter IV in conjunction with the non-optimal closed-loop control algorithm.

Appendix B contains the derivation of artificial wind loads based on wind design spectra used with the optimal control algorithms of Chapters III, and V.

Appendix C contains the development of the various expressions for the performance indices used in the optimal control algorithms of Chapters III, V and IX.

Appendix D describes the optimality conditions and optimal control solutions for the optimal control algorithms of Chapters III, V and IX.

Appendix E contains the derivations for the motion equations and transfer matrix relations for the non-optimal closed-loop control presented in Chapter IV.

Appendix F contains the computer programs for the optimization algorithm of Chapter VI, and the control algorithms described in Chapters III, IV, and V.

II. PROTECTIVE SYSTEMS FOR EARTHQUAKE HAZARD MITIGATION

A. PASSIVE AND ACTIVE CONTROL SYSTEMS

The dynamic response of structures to earthquake and wind excitations can exceed tolerable limits for human comfort, structural stability and structural integrity. Passive and active control systems have been developed in order to reduce the effect of wind excitations and earthquake ground motion on the structure. Passive control system applications exist in many parts of the world (46,60). Active control systems have been tested in the laboratory and the results are very promising (15,35,53,54).

Passive control systems are mechanical devices that do not require external energy for their operation. They redirect the energy transmitted by the ground motion to structural elements which can dissipate it in such a way that the rest of the structure responds with minimum deformations. The same concept is applied for wind forces. Examples of passive control systems are rubber and lead-core base isolators, limited-slip bolted joints and passive tuned mass dampers.

Active control systems require an outside energy source. Control forces are applied in order to minimize the effect of the seismic excitation or to correct the position of the structure. Active control systems include active tendons, active mass dampers, appendages, and pulse control by means of jets.

Passive control systems have their shortcomings. Base isolators are not suitable for high-rise buildings because large overturning moments can cause uplift of the foundation pads. Another shortcoming is that large sidesway at the foundation level may render the structure unstable. Tuned mass dampers are efficient in tall buildings; their operation, however, is limited to one mode of vibration only. Extensive studies have been performed on experimental applications of active control systems including active tendons, appendages, and pulse control.

B. ACTIVE CONTROL IMPLEMENTATION SCHEMES

There are three active control schemes or strategies by which the active control law can be implemented to a structure :

1. Open-loop disturbance-compensated control

2. Closed-loop control

3. Open-closed-loop disturbance-compensated control

In the open-loop disturbance-compensated scheme shown in Figure 1, the control law requires information about the earthquake excitation. The diagram for implementation of this scheme using an active tendon is shown in Figure 2. An accelerometer placed at the basement of the building measures the earthquake ground acceleration. This information is used to calculate the required control force based on the active control algorithm for open-loop control, which is then applied to the structure.
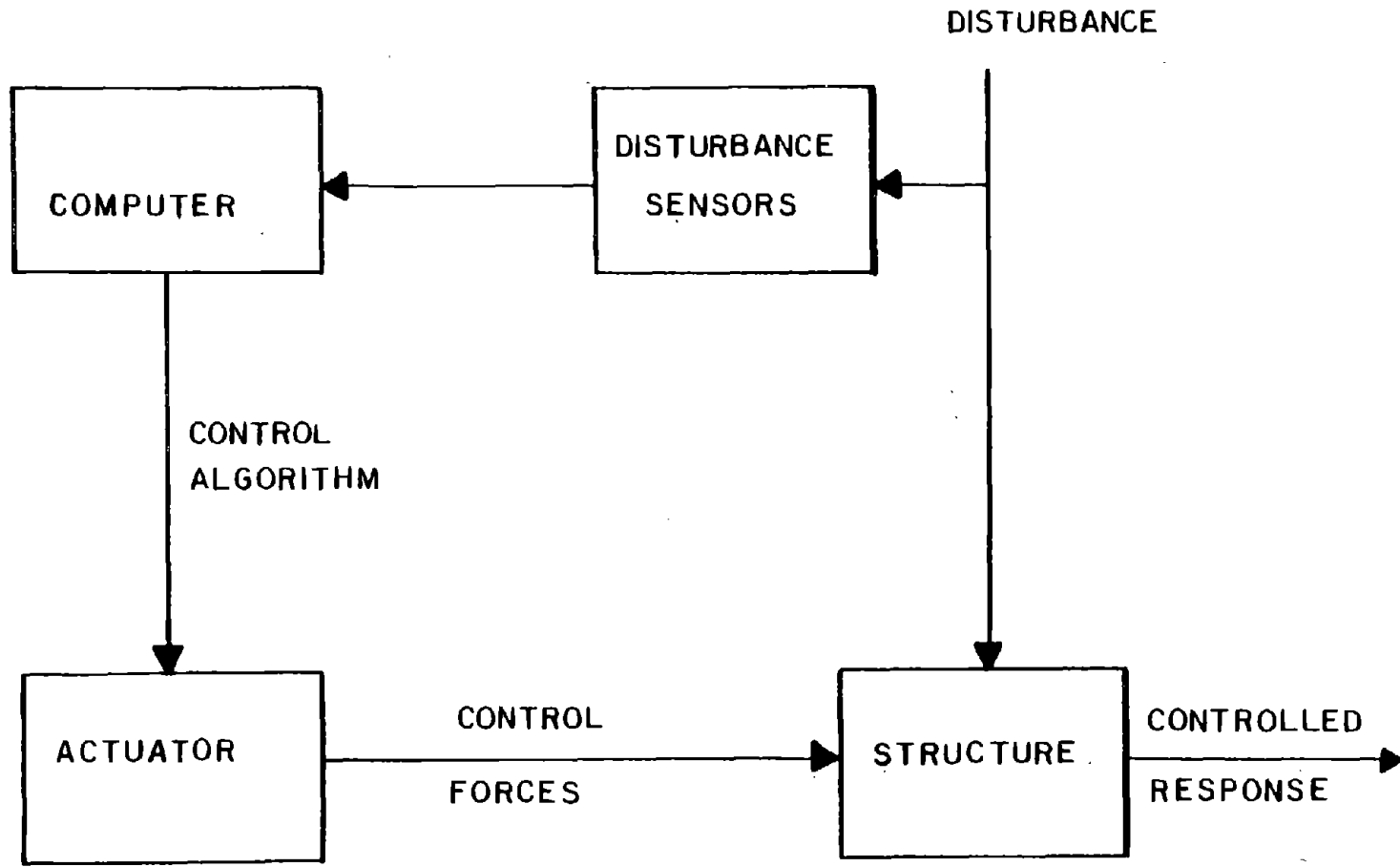
DISTURBANCE

Figure 1. Open-loop Disturbance-compensated Control
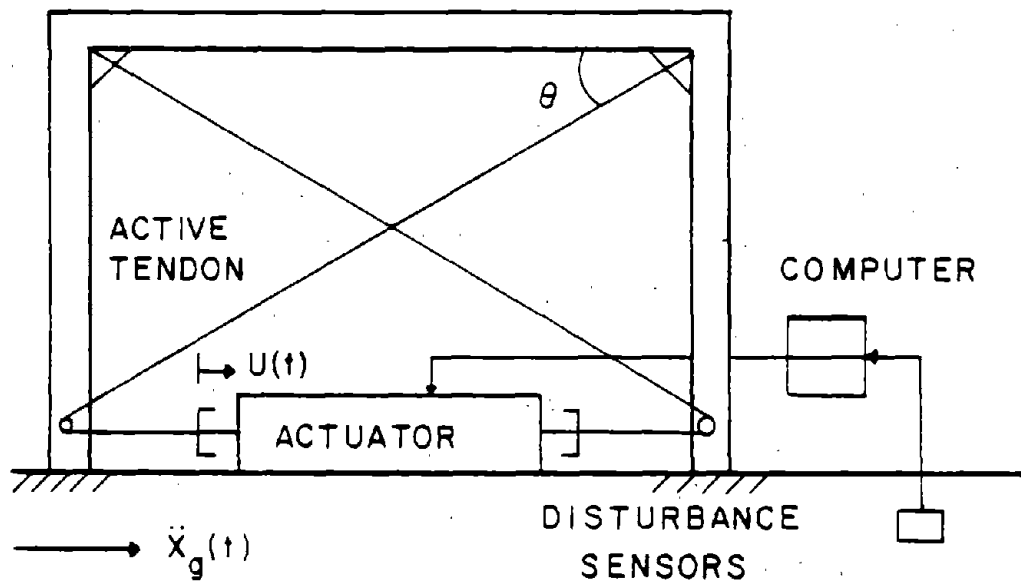
Figure 2. Open-loop Control Implementation

In the closed-loop scheme shown in Figure 3, the control law requires measurement of the relative displacements and velocities of the structure. The diagram for this scheme is shown in Figure 4 for the active tendon system. The sensed information is used to calculate the required control force based on the closed-loop active control algorithm, which is then applied to the structure.

The open-closed-loop disturbance-compensated scheme is a combination of the open-loop compensated and closed-loop control schemes as shown in Figure 5. The diagram for implementation of this scheme with an active tendon is shown in Figure 6. Both the earthquake ground acceleration and sensed relative displacements and velocities are used to calculate the required control forces based on the active control algorithm, which are then applied to the structure.

For wind excitations it may be difficult to measure the wind pressures on the structure and hence the closed-loop control scheme may be the best scheme to be used. The absolute displacements and velocities are measured and the control forces are calculated based on the active control algorithm for wind excitations. In this study all three active control schemes are used for earthquake and wind excitations.

DISTURBANCE

CONTROLLED
RESPONSE

ACTUATOR

CONTROL
FORCES

STRUCTURE

COMPUTER

RESPONSE
SENSORS
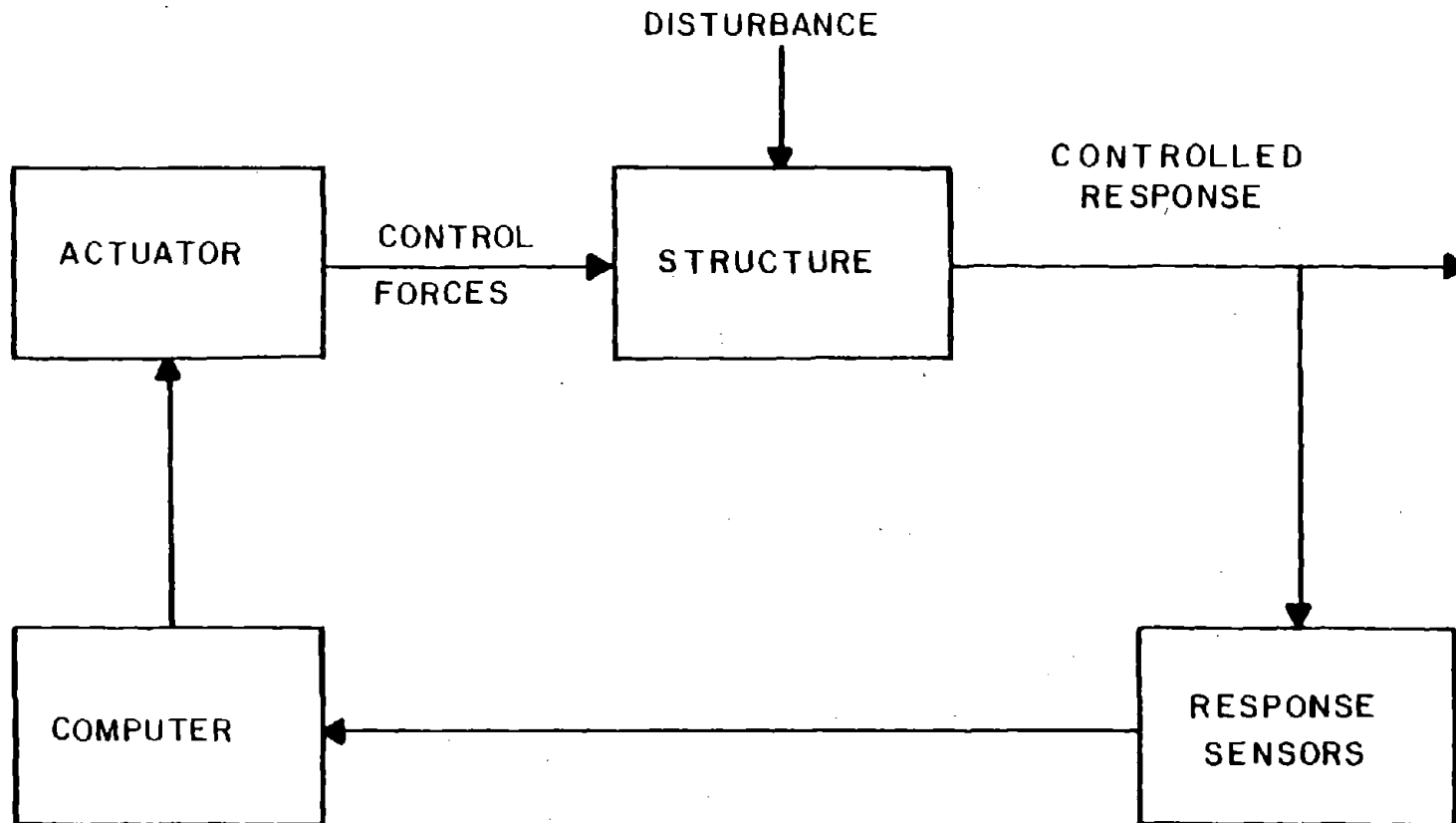
Figure 3. Closed-loop Control
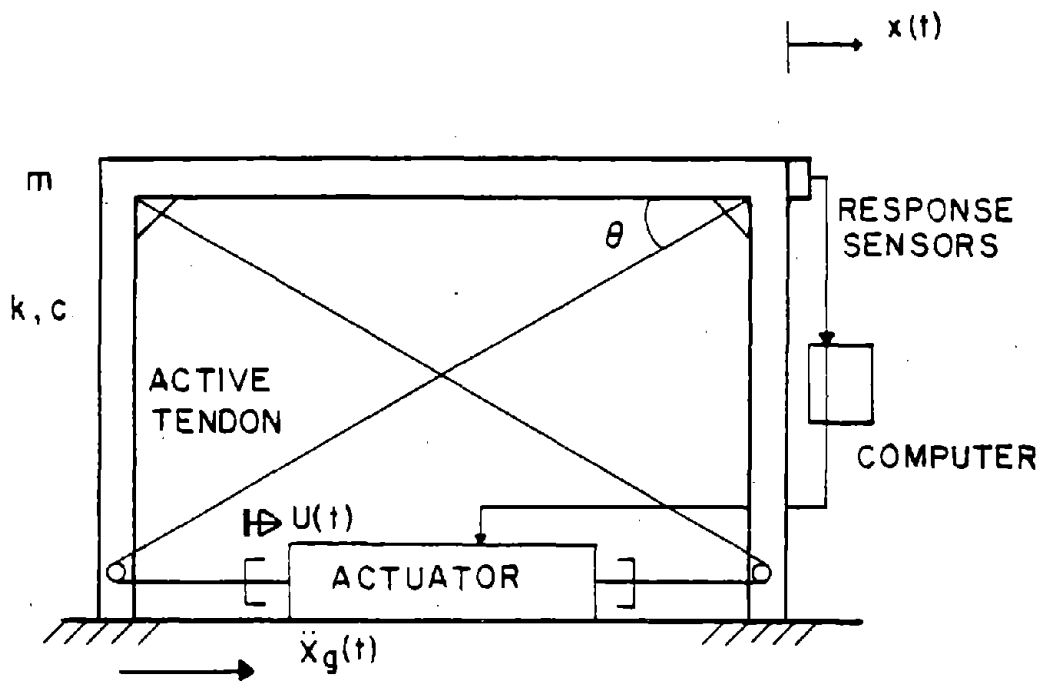
Figure 4. Closed-loop Control Implementation
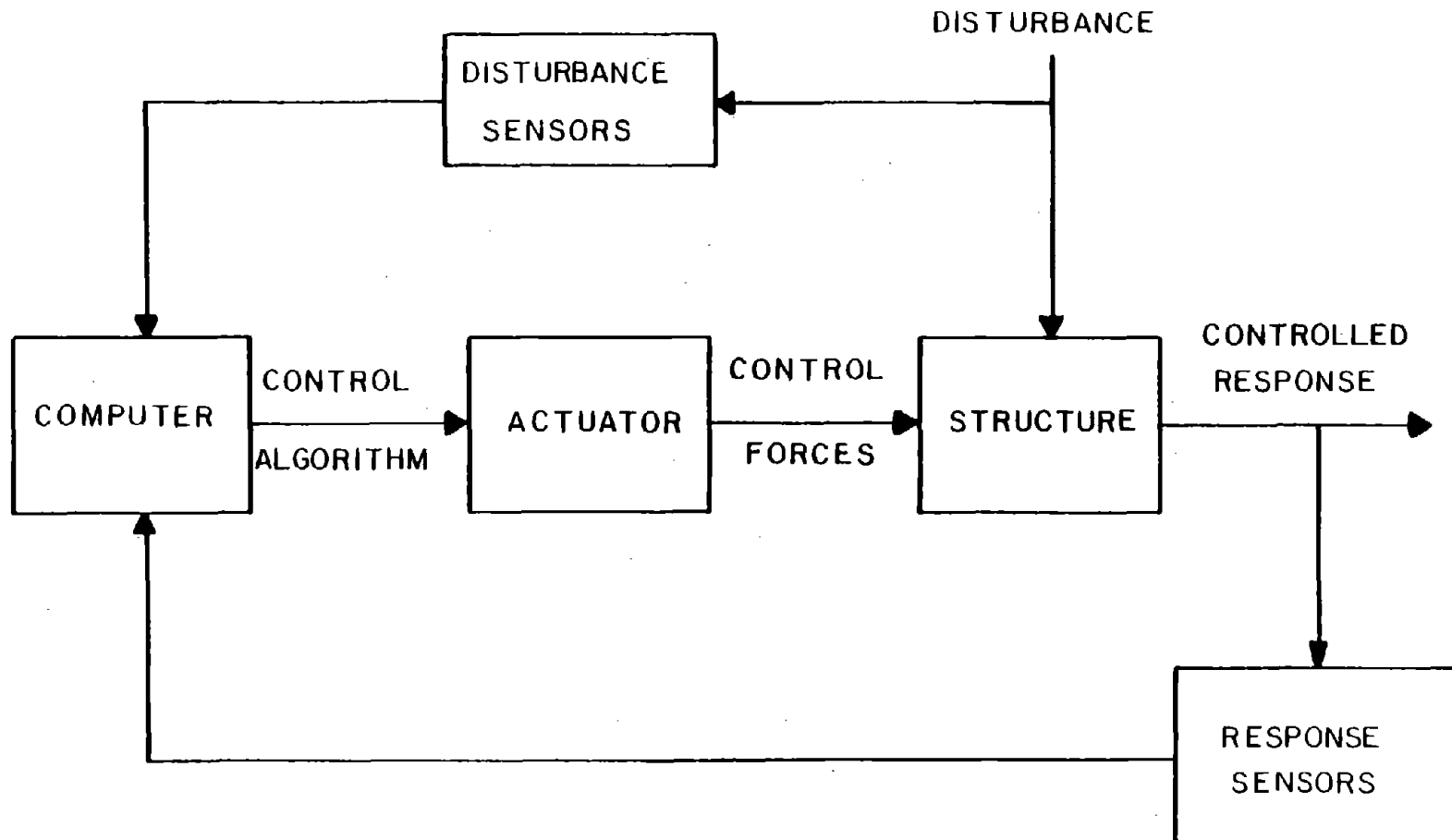
Figure 5. Open-closed-loop Disturbance-compensated Control
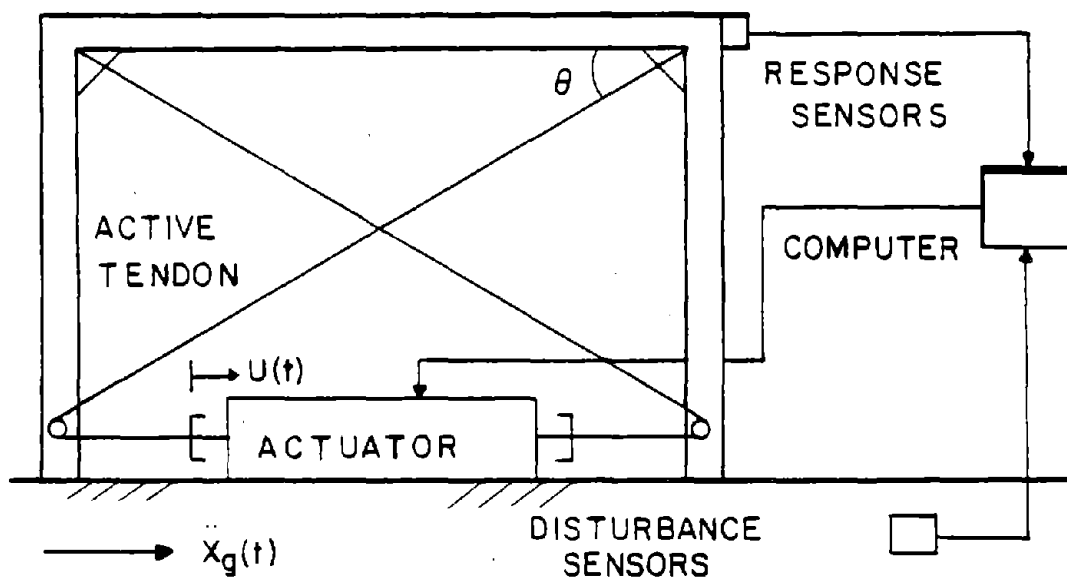
Figure 6. Open-closed-loop Control Implementation

C. ACTIVE CONTROL ALGORITHMS

An efficient and capable control algorithm is essential to the application of an active control system. The control algorithm is to be used in order to calculate the magnitude of the control forces. These control forces are to be calculated in real-time according to the active control law and control scheme employed in the control algorithm. There are three types of control algorithms:

1. Optimal control algorithms

2. Sub-optimal control algorithms

3. Non-optimal control algorithms

The difference between optimal and non-optimal control algorithms lies in the manner in which the control law is derived. Optimal control algorithms employ a control law based on the minimization of a performance index. The performance index, or cost functional, to be minimized represents the total energy of the system including the work done by the control forces. It is a compromise between the reduction of the structure's response and the control energy required to achieve this reduction. The optimal control law is, therefore, the result of a constrained optimization problem which can be stated as follows: Find the optimal control forces that minimize the performance index and satisfy the equation of motion for the actively controlled structure. Depending on the particular performance index that is chosen, one can have many categories of optimal control algorithms. In this study, the following two categories are examined :

a. Ricatti optimal control algorithm

b. Instantaneous optimal control algorithms

In the Ricatti optimal control algorithm, an integral performance index is minimized, following traditional concepts of optimal control theory. However, the optimal forces are derived by ignoring the external disturbance or by assuming that it is a white noise process. In the instantaneous optimal control algorithms, an instantaneous time-dependent performance index is minimized. The advantage of the instantaneous optimal control algorithms is that they include the external disturbance in the derivation of the control forces. In addition they result in simpler expressions for the optimal control forces. In this study both the Ricatti optimal control algorithm and the instantaneous optimal control algorithms are used and compared.

Sub-optimal control implies that the performance index does not include all the characteristics of the system. For example the structure's response could be minimized without consideration for minimizing the control forces. Thus a simplified control model results at the expense of global optimality.

Non-optimal control algorithms are based on the particular control scheme that is employed. The control forces are calculated based on conditions other than the minimization of a performance index. The result is that the magnitude of the control forces is no longer the minimum required. In this study only a closed-loop scheme will be considered, using the transfer matrix approach.

III. RICATTI OPTIMAL CLOSED-LOOP CONTROL

The classical optimal control approach is developed in this Chapter for seismic structures equipped with active control systems. Both the active tendon (AT) and active mass damper (AMD) systems are studied. The earthquake excitation is applied as a ground acceleration in time function. The Chapter includes a brief description of the earthquake excitations used. A discussion of the fundamentals of control systems including the AT, AMD, and passive mass damper systems is presented. The development begins with a closed-loop algorithm applied to an initial-conditions problem. This algorithm is extended to include external disturbances. Finally a comparison with experimental results obtained by Chung, Reinhorn, and Soong (15) shows good agreement between experimental and simulation results.

A. EARTHQUAKE EXCITATION

A real ground earthquake accelerogram record and several artificial acceleration records are used in this study. The first accelerogram is a real record of the north-south component of the El-Centro earthquake, of May 1940. An artificial accelerogram known as the EE1 record is also used for simulations. Finally an impulsive triangular acceleration was used to test the Ricatti optimal closed-loop algorithm.

29

B. CONCEPTS FOR RESPONSE REDUCTION USING PASSIVE CONTROL

The passive mass damper (PMD) system does not require external power; it dissipates the input energy passively, by transferring the energy from the structure to the mass damper, the spring and the damping devices. The configuration is shown in Figure 7 where it is to be noted that the electrohydraulic actuator is not present. This system is widely used in vibration isolation of centrifugal machines or other equipment where the excitation is of known constant frequency. For earthquake or wind excitations, however, many frequency components of the forcing function exist. For the PMD to be most effective in limiting the response over a wide range of excitation frequencies, it is necessary to select the parameters of the mass, spring, and damping of the passive system in an optimal manner.

The basic principle for the application of the PMD is that of the vibration absorber early suggested by Ormonroyd and Den Hartog (43). In the case of the vibration absorber, the frequency of the mass damper ω_d is tuned to that of the exciting frequency ω, in order to eliminate the vibrations. The primary structure is modelled as a mass m resonating on a spring k. The absorber is tuned to resonate such that the motion of its mass m_d becomes relatively large, and the motion of the mass of the primary system m is minimized. For a fixed mass ratio (m_d/m) and a fixed spring constant k_d, the frequency response of m is independent of the absorber's damping constant c_d at two distinct frequencies. The response passes through two invariant points P1 and P2 regardless of the value of the damping constant c_d. Den Hartog optimized absorber performance by first choosing k_d so that P1 and P2

30
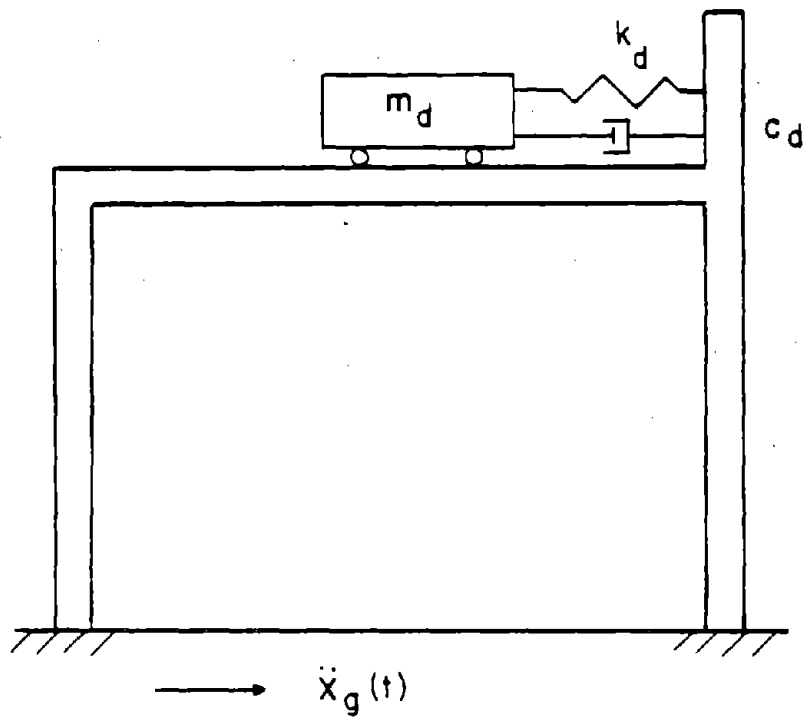
Figure 7. Passive Mass Damper

are adjusted to equal height, and then by finding c_d to make the curve pass through one of the invariant points with a horizontal tangent. A detailed discussion of optimal tuning and damping parameters was given by Den Hartog (19). This optimization procedure was extended to multiple-degree of freedom discrete undamped systems by Lewis (30).

C. CONCEPTS FOR RESPONSE REDUCTION USING ACTIVE CONTROL

A brief discussion of the underlying concepts for the use of active control is given in this Section. The description is qualitative and brings out the basic features of the active tendon and active mass damper and the manner in which these systems reduce the response.

1. Active Tendon (AT). The purpose of a control system is the reduction of the structure's response under seismic or wind loads. In order to illustrate the manner in which this is achieved, let us consider a single degree of freedom structure equipped with an active tendon, subjected to a ground acceleration. As shown in Figure 4, $x(t)$ is the relative displacement of the structure with respect to the ground, and m, k, c are the mass, stiffness and damping of the structure. The ground acceleration is denoted by $\ddot{X}_g(t)$, $U(t)$ is the actuator displacement, and θ the angle between the tendon and the horizontal. The movement of the actuator is regulated by the optimal closed-loop algorithm. For closed-loop control, the measurement of the displacement and velocity response is required and is obtained from the sensors.

The motion equation for the system of Figure 4 is

$$m\,\ddot{x}(t) + c\,\dot{x}(t) + k\,x(t) \;=\; -m\,\ddot{X}_g(t) - u(t) \tag{3.1}$$

where $u(t)$ is the horizontal component of the control force produced by the actuator displacement, through tensioning of the tendons. Using the Ricatti closed-loop algorithm, the feedback control force $u(t)$ is shown in Section D of this Chapter to be composed of two parts: 1) the displacement feedback control force, and 2) the velocity feedback control force. It is also a function of θ, the tendon stiffness, and the actuator movement. Thus the feedback control force can be written

$$u(t) \;=\; \overline{C}(\overline{C}_d\,x(t) + \overline{C}_v\,\dot{x}(t)) \tag{3.2}$$

where $\overline{C}$ is a function of the tendon stiffness and angle θ, and $\overline{C}_d$ and $\overline{C}_v$ are the feedback control force gains and are positive quantities. Equation 3.2 states that the feedback control force is a closed-loop active control force proportional to the relative displacement and velocity of the structure. Substituting Equation 3.2 in Equation 3.1

$$m\,\ddot{x}(t) + c\,\dot{x}(t) + k\,x(t) \;=\; -m\,\ddot{X}_g(t) - \overline{C}\,(\overline{C}_d\,x(t) + \overline{C}_v\,\dot{x}(t)) \tag{3.3}$$

Transferring the last term of Equation 3.3 to the left side

$$m\,\ddot{x}(t) + (c + \overline{C}\,\overline{C}_v)\,\dot{x}(t) + (k + \overline{C}\,\overline{C}_d)\,x(t) \;=\; -m\,\ddot{X}_g(t) \tag{3.4}$$

The equation of motion if no control were present is

$$m\,\ddot{x}(t) + c\,\dot{x}(t) + k\,x(t) \;=\; -m\,\ddot{X}_g(t) \tag{3.5}$$

33

Comparing Equations 3.4 and 3.5 for the controlled and no control case, one can make the following observations: 1) The stiffness of the structure has been increased from k to $(k + \overline{C}\,\overline{C}_d)$, 2) the damping of the structure has been increased from c to $(c + \overline{C}\,\overline{C}_v)$, 3) the controlled frequency has been increased since the stiffness has increased and the mass has not changed. It is evident that the consequences of using active control are beneficial in reducing the dynamic response of the structure.

2. <u>Active Mass Damper (AMD)</u>. The same single-story structure considered for the active tendon system is used here, equipped with an active mass damper of mass m_d, which is placed on the top floor as shown in Figure 8. The AMD is connected to the structure through a spring of stiffness k_d and a hydraulic damper c_d. The electrohydraulic actuator is also connected to the mass m_d which produces the active control force.

The equation of motion for the system and the Ricatti closed-loop optimal control result in similar expressions as those derived for the active tendon system. These results are described in detail for the general case of an N-story structure in Section E of this Chapter. The main conclusions, however, are the same ones reached for the active tendon case. The active control force improves the stiffness and damping characteristics of the structure and effectively reduces the response due to earthquake or wind excitations.

34
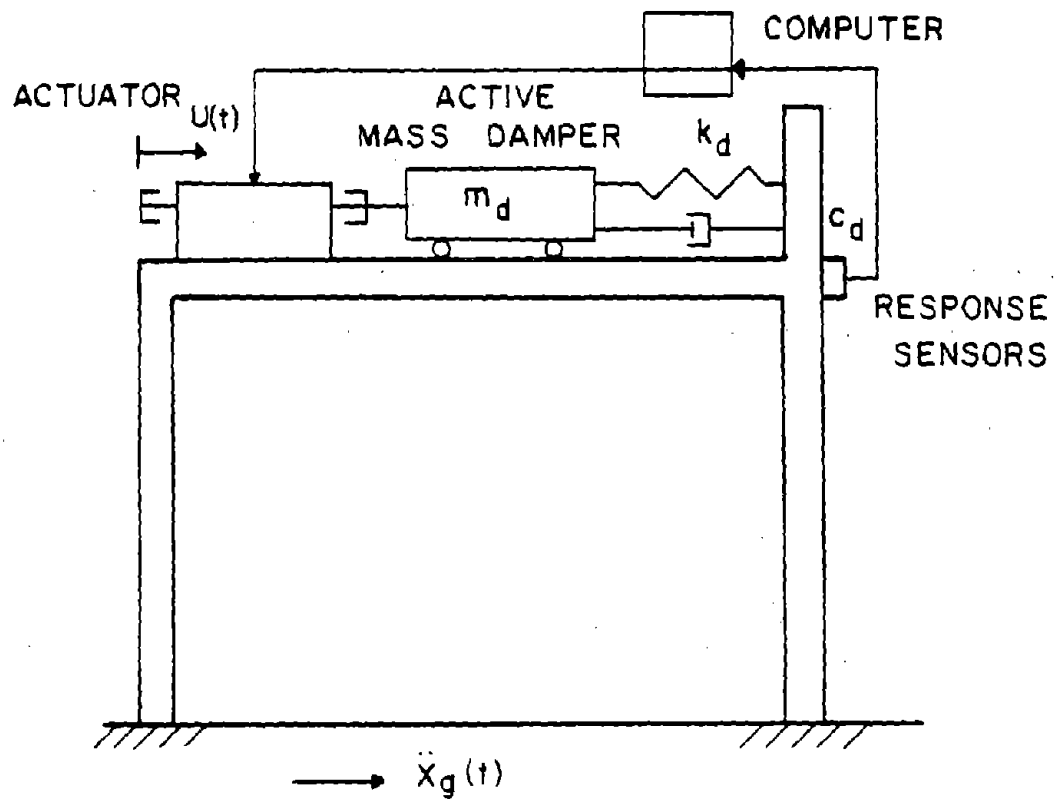
Figure 8. Active Mass Damper

The active mass damper control reduces the response more effectively than the passive mass damper, at the expense of external power. The parameters of mass, damping and spring constants are selected in an optimal manner as described for the PMD.

D. ALGORITHM FOR INITIAL CONDITIONS

The subject of this Section is to study the response when the external disturbance is set equal to zero and the motion is produced by the initial values of displacement or velocity.

1. Formulation Using Classical Approach. In order to apply the results of classical optimal control theory, the equation of motion, Equation 3.1, is cast into its state-form by using the state-vector, defined as

$$\{z(t)\} = \left\{ \frac{\{x(t)\}}{\{\dot{x}(t)\}} \right\} \tag{3.6}$$

The equation of motion for an N-story shear building equipped with active tendons at some floors as shown in Figure 9a is

$$[M]\{\ddot{x}(t)\} + [C]\{\dot{x}(t)\} + [K]\{x(t)\} = [\gamma]\{u(t)\} + \{\delta\}\ddot{X}_g(t) \tag{3.7}$$

In Equation 3.7, $x_j(t)$ is the floor relative displacement defined as

$$x_j(t) = X_j(t) - X_g(t) \qquad j = 1, \ldots, N \tag{3.8}$$

where $X_j(t)$ is the floor absolute displacement and $X_g(t)$ the ground displacement. Vector $\{u(t)\}$ is the control force vector of dimension $[N \times r]$, where $r =$ number of controllers. In Equation 3.7, $[M]$, $[C]$ and $[K]$
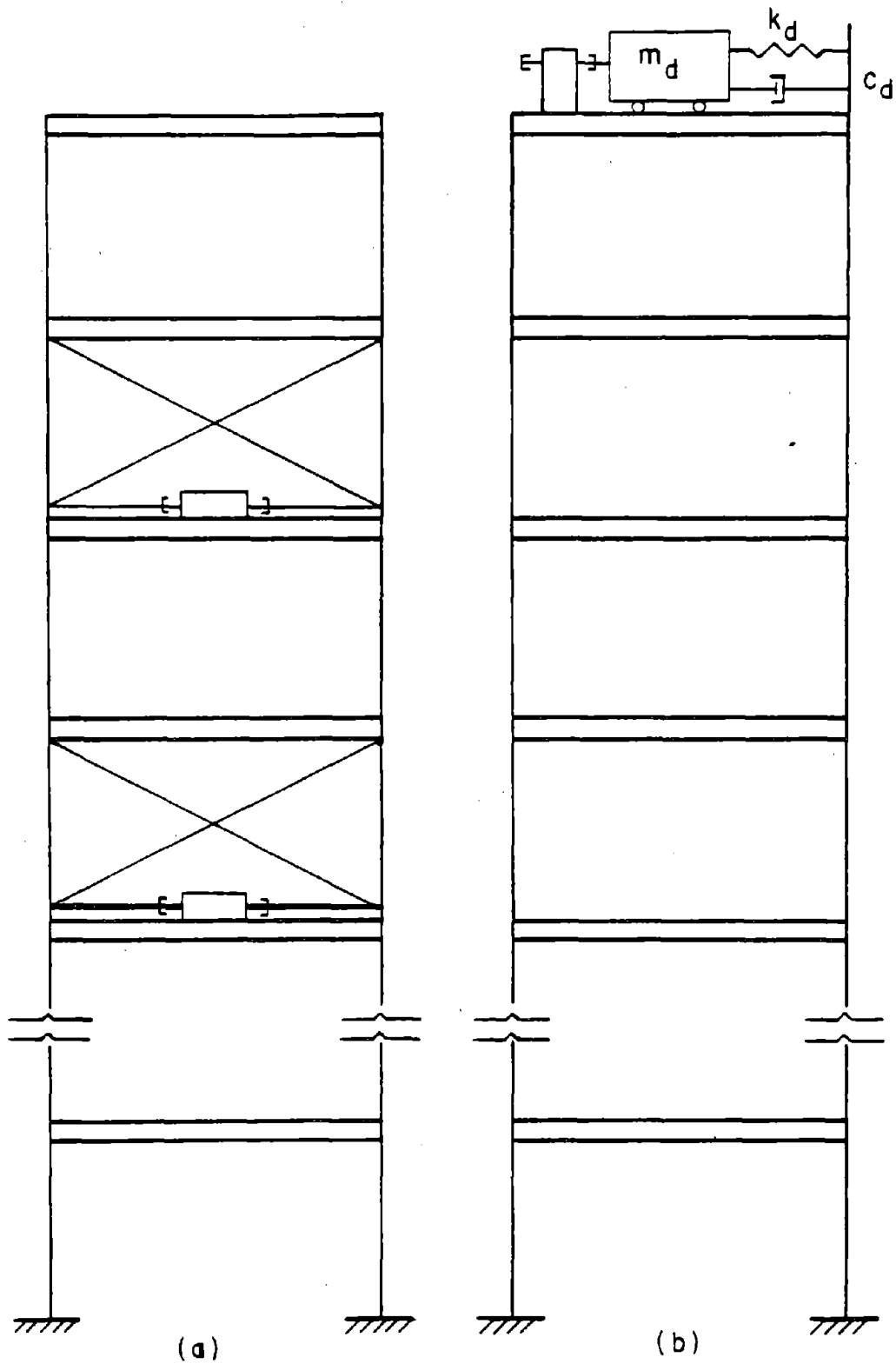
Figure 9. Tall Building Equipped with Active Control System:
(a) Active Tendon; (b) Active Mass Damper

are the mass, damping and stiffness matrices of the structure, respectively, of dimension $[N \times N]$, $[\gamma]$ is an $[N \times r]$ matrix relating the location of the controllers to the structure, and $\{\delta\}$ is a vector of coefficients for the earthquake excitation $\ddot{X}_g(t)$. For an active tendon system matrix $[\gamma]$ has the form

$$
[\gamma] \;=\; \begin{bmatrix}
-1 & 1 & & & & & \\
& -1 & 1 & & & & \\
& & -1 & 1 & & & \\
& & & \cdot & \cdot & & \\
& & & & \cdot & \cdot & \\
& & & & & \cdot & \cdot \\
& & & & & -1 & 1 \\
& & & & & & -1
\end{bmatrix}
\tag{3.9}
$$

and vector $\{\delta\}$ has the form

$$
\{\delta\}^T \;=\; \{\, -m_1,\ -m_2,\ -m_3,\ \dots\ ,-m_N \,\}
\tag{3.10}
$$

where m_j is the mass of the jth floor. Rewriting Equation 3.7

$$
\begin{aligned}
\{\ddot{x}(t)\} \;=\; & -\;[M]^{-1}[C]\{\dot{x}(t)\} - [M]^{-1}[K]\{x(t)\} + [M]^{-1}[\gamma]\{u(t)\} \\
& + [M]^{-1}\{\delta\}\,\ddot{X}_g(t)
\end{aligned}
\tag{3.11}
$$

Using the definition of the state-vector, Equation 3.11 can be written as

$$
\begin{aligned}
\left\{ \begin{array}{c} \{\dot{x}(t)\} \\ \{\ddot{x}(t)\} \end{array} \right\}
\;=\;
& \left[\begin{array}{c|c} 0 & [I] \\ \hline -[M]^{-1}[K] & -[M]^{-1}[C] \end{array} \right]
\left\{ \begin{array}{c} \{x(t)\} \\ \{\dot{x}(t)\} \end{array} \right\} \\
& + \left[\begin{array}{c} 0 \\ \hline [M]^{-1}[\gamma] \end{array} \right] \{u(t)\}
+ \left\{ \begin{array}{c} 0 \\ \hline [M]^{-1}\{\delta\} \end{array} \right\} \ddot{X}_g(t)
\end{aligned}
\tag{3.12}
$$

38

Rewritting Equation 3.12 in compact form

$$\{\dot{z}(t)\} = [A_t]\{z(t)\} + [B_t]\{u(t)\} + \{C_t\}\ddot{X}_g(t) \tag{3.13}$$

where

$$[A_t] = \left[\begin{array}{c|c} 0 & [I] \\ \hline -[M]^{-1}[K] & -[M]^{-1}[C] \end{array}\right] , \quad [B_t] = \left[\begin{array}{c} 0 \\ \hline [M]^{-1}[\gamma] \end{array}\right]$$

$$\{C_t\} = \left\{\begin{array}{c} 0 \\ \hline [M]^{-1}\{\delta\} \end{array}\right\} \tag{3.14}$$

For free vibrations one can set the excitation equal to zero and the state-equation becomes

$$\{\dot{z}(t)\} = [A_t]\{z(t)\} + [B_t]\{u(t)\} \tag{3.15}$$

This case can be physically materialized when initial conditions are imposed on $\{z(t)\}$ with no external excitation. The classical control theory has been developed based exactly on such a model.

The optimal control force vector $\{u^*(t)\}$, is to be derived by minimizing a standard quadratic performance index J given by

$$J = \frac{1}{2}\int_{t_0}^{t_f} \left(\{z(t)\}^T [Q]\{z(t)\} + \{u(t)\}^T [R]\{u(t)\}\right) dt \tag{3.16}$$

and satisfying the state-equation, Equation 3.15. In Equation 3.16 t_0 is the initial and t_f the final time-instant under consideration. Matrix $[Q]$ is a $[2N \times 2N]$ positive semi-definite matrix, and $[R]$ is an $[r \times r]$ positive definite matrix. The performance index, J, represents a balance between structural response and control energy. When the elements of $[Q]$ are large, the response is reduced at the expense of

large control forces. When the elements of $[R]$ are large, the control forces are small but the response is not reduced appreciably. Detailed discussion of Equation 3.16 is given in Appendix C. Assume that the system is controllable, i.e., the available control force is sufficient to bring the system from any initial state to any desired final state. Assume also that the system is observable, i.e., the system response output yields sufficient information to determine the state-vector at any time t. Variational calculus yields the solution to the optimization problem. Define the Hamiltonian $\mathcal{H}$ as

$$\mathcal{H} = \frac{1}{2}\{z(t)\}^T [Q]\{z(t)\} + \frac{1}{2}\{u(t)\}^T [R]\{u(t)\} \\ + \{\lambda(t)\}^T ([A_t]\{z(t)\} + [B_t]\{u(t)\})$$

(3.17)

where $\{\lambda(t)\}$ is the vector of Lagrange multipliers of dimension $[2N \times 1]$. The necessary conditions for optimality are given in standard textbooks on control theory, such as Elbert (20)

$$\frac{\partial \mathcal{H}}{\partial \{z(t)\}} = -\{\dot{\lambda}(t)\} \quad \rightarrow \quad -\{\dot{\lambda}(t)\} = [Q]\{z(t)\} + [A_t]^T\{\lambda(t)\}$$

(3.18)

$$\frac{\partial \mathcal{H}}{\partial \{u(t)\}} = \{0\} \quad \rightarrow \quad [R]\{u(t)\} + [B_t]^T\{\lambda(t)\} = \{0\}$$

(3.19)

$$\frac{\partial \mathcal{H}}{\partial \{\lambda(t)\}} = \{0\} \quad \rightarrow \quad [A_t]\{z(t)\} + [B_t]\{u(t)\} - \{\dot{z}(t)\} = \{0\}$$

(3.20)

with the transversality condition

$$\{\lambda(t_f)\} = \{0\}$$

(3.21)

From Equation 3.20 note that this condition is the state-equation. From Equation 3.19 the optimal control is derived as

$$\{u^*(t)\} = -[R]^{-1} [B_i]^T \{\lambda(t)\} \tag{3.22}$$

Complete derivation of Equation 3.22 is given in Appendix D. Note that the requirement for $[R]$ to be positive definite arises from Equation 3.22. The Lagrange multipliers $\{\lambda(t)\}$ are still not known but can be solved for, by using the first necessary condition of Equation 3.18.

Assume a solution of the form

$$\{\lambda(t)\} = [P(t)]\{z(t)\} \tag{3.23}$$

which when substituted in Equation 3.22 implies a closed-loop control, since

$$\begin{aligned} \{u^*(t)\} &= -[R]^{-1} [B_i]^T [P(t)] \{z(t)\} \\ &= -[K(t)]\{z(t)\} \end{aligned} \tag{3.24}$$

Substituting Equations 3.23 and 3.24 in Equation 3.18 gives

$$\left([\dot{P}(t)] + [P(t)][A_i] + [A_i]^T [P(t)] - [P(t)][B_i][R]^{-1} [B_i]^T [P(t)] + [Q] \right) \{z(t)\} = \{0\} \tag{3.25}$$

and from Equation 3.21 we get

$$[P(t_f)]\{z(t_f)\} = \{0\} \tag{3.26}$$

For a non-zero state $\{z(t)\}$, the non-trivial solution is

$$-[\dot{P}(t)] = [P(t)][A_i] + [A_i]^T [P(t)] - [P(t)][B_i][R]^{-1} [B_i]^T [P(t)] + [Q] \tag{3.27}$$

$$[P(t_f)] = [0] \tag{3.28}$$

Equation 3.27 is the matrix Ricatti equation (MRE). There are many efficient algorithms available for the solution of the MRE. Vaughan

41

presented a solution in terms of negative exponentials (57). Davison and Maki developed a method based on an iterative exponential solution (18). Both methods are more efficient than a standard Runge-Kutta approach which requires a small integration step to ensure stability, and thus large computational times. After the solution of the MRE is found it is substituted in Equation 3.24 to obtain the optimal control. From Equation 3.24 note that this is a proportional type of control, i.e. the control force vector is proportional to the response. In practice this type of control can be achieved using a gain amplifier.

For simulation results once the optimal control is calculated, the state-vector at time t can be found by substituting $\{u(t)\}$ in Equation 3.15 and solving for $\{z(t)\}$. The solution of Equation 3.15, a vector linear differential equation is available in standard textbooks on control theory (20). A method for the solution of this type of problem is presented in Chapter V.

2. <u>Asymptotic Behavior of Matrix Ricatti Equation</u>. The Ricatti equation solution for $[P(t)]$ may reach steady state conditions for time t far away from t_f. This relationship between t and t_f is a basic characteristic of the classical optimal control problem of subsection 1 of this Section, also known as the regulator problem. It permits the use of steady state values in determining the control force vector. From the results given in Equations 3.27 and 3.28 note that the MRE requires a time-dependent solution. Moreover from Equation 3.24 it is obvious that the gain matrix $[K(t)]$ is also time-dependent. For an infinite final time t_f, i.e. $t_f = \infty$, it can be shown (20) that the

42

time-dependent MRE becomes time-invariant. Setting in Equation 3.27, $[\dot{P}(t)] \equiv [0]$ produces the so-called algebraic Ricatti equation (ARE), given by

$$[P][A_t] + [A_t]^T[P] - [P][B_t][R]^{-1}[B_t]^T[P] + [Q] = [0] \qquad (3.29)$$

Hence the gain matrix $[\bar{K}]$ becomes time-invariant and the optimal control is given as

$$\begin{aligned}\{u^*(t)\} &= -[R]^{-1}[B_t]^T[P]\{z(t)\} \\ &= -[\bar{K}]\{z(t)\}\end{aligned} \qquad (3.30)$$

The solution of the ARE is simpler than that of the MRE and there are many good algorithms available. An algorithm which is based on an iterative technique was presented by Kleinman (26). Another algorithm developed by Laub uses an eigenvector approach based on Schur vectors (29). However the validity of the bound $t_f \rightarrow \infty$ has to be examined for the particular case of earthquake excitation. It is shown in the next Section that the assumption is valid if t_f is taken to be longer than the earthquake duration.

The advantage of the ARE over the MRE is that the gain matrix in Equation 3.30 is constant and thus the optimal control forces can be obtained proportional to the response $\{z(t)\}$. It should be emphasized that in a real system the closed-loop control requires the measurement of the full state-vector, i.e., $2N$ sensors are required to measure the response. When analog differentiators are used to determine the velocities $\{\dot{x}(t)\}$, then the number of sensors is reduced to N. Such a scheme was used by Chung, Reinhorn, and Soong in experiments carried out on a reduced model at SUNY/Buffalo (15).

E. ALGORITHM FOR EXTERNAL DISTURBANCES

In this Section the more general problem that includes the external disturbance is studied. The state-equation to be used in this Section is given by Equation 3.13. In the first subsection the optimal control algorithm for the case of active tendon controllers is developed, and in the second subsection the algorithm for the active mass damper is developed. Both control systems are shown in Figure 9.

1. Formulation for Active Tendon System. The optimal control vector $\{u^*(t)\}$ is to be found by minimizing the performance index of Equation 3.16 and satisfying the state-equation given by Equation 3.13. The Hamiltonian in this case is given by

$$
\begin{aligned}
\mathscr{H} \;=\; & \frac{1}{2}\{z(t)\}^T \, [Q]\,\{z(t)\} + \frac{1}{2}\{u(t)\}^T \, [R]\,\{u(t)\} \\
& + \{\lambda(t)\}^T \Big([A_t]\,\{z(t)\} + [B_t]\,\{u(t)\} + \{C_t\}\,\ddot{X}_g(t) \Big)
\end{aligned}
\tag{3.31}
$$

The necessary conditions for optimality are the same as those given in Equations 3.18 − 3.21, except Equation 3.20 now includes the earthquake excitation term

$$
[A_t]\,\{z(t)\} + [B_t]\,\{u(t)\} + \{C_t\}\,\ddot{X}_g(t) - \{\dot{z}(t)\} \;=\; \{0\}
\tag{3.32}
$$

Proceeding in a similar fashion as was done for the initial conditions case, assume the relation

$$
\{\lambda(t)\} \;=\; [P(t)]\,\{z(t)\}
\tag{3.33}
$$

and substitute Equation 3.33 into Equations 3.18, 3.19 and 3.32 to obtain

$$\left([\dot{P}(t)] + [P(t)][A_t] + [A_t]^T[P(t)] - [P(t)][B_t][R]^{-1}[B_t]^T[P(t)] + [Q]\right)\{z(t)\}$$
$$+ [P(t)]\{C_t\}\ddot{X}_g(t) = \{0\} \tag{3.34}$$

Note that Equation 3.26 still holds. The earthquake excitation is unknown before the earthquake occurs, therefore, backward solution of Equation 3.34 subject to the final condition of Equation 3.28 is not feasible. If we set the earthquake excitation $\ddot{X}_g(t)$ equal to zero, then Equation 3.34 reduces to Equation 3.25. Therefore strictly speaking the Ricatti matrix obtained from the solution of the reduced equation, Equation 3.25, does not correspond to the optimal closed-loop control for the earthquake excited structure. The Ricatti closed-loop control is truly optimal only if the earthquake excitation is either zero or a white noise process. In that respect it can be considered as a sub-optimal control. However the solution based on Equation 3.25 was found to be effective in both numerical simulations and experimental results and is used in this study. When compared with other optimal control algorithms the Ricatti closed-loop control is as effective. The external excitation is present in the algorithm since from Equation 3.30 the optimal control is a function of the forced response.

The asymptotic behavior of the MRE given in Equations 3.27 and 3.28 was tested for a single-story structure equipped with an active tendon and subject to different excitations. It was found that typically the elements of $[P(t)]$ remain constant over the entire duration of the earthquake excitation t_f, and drop rapidly to zero near t_f. This asymptotic behavior is shown in Figure 10. Hence $[P(t)]$ establishes a
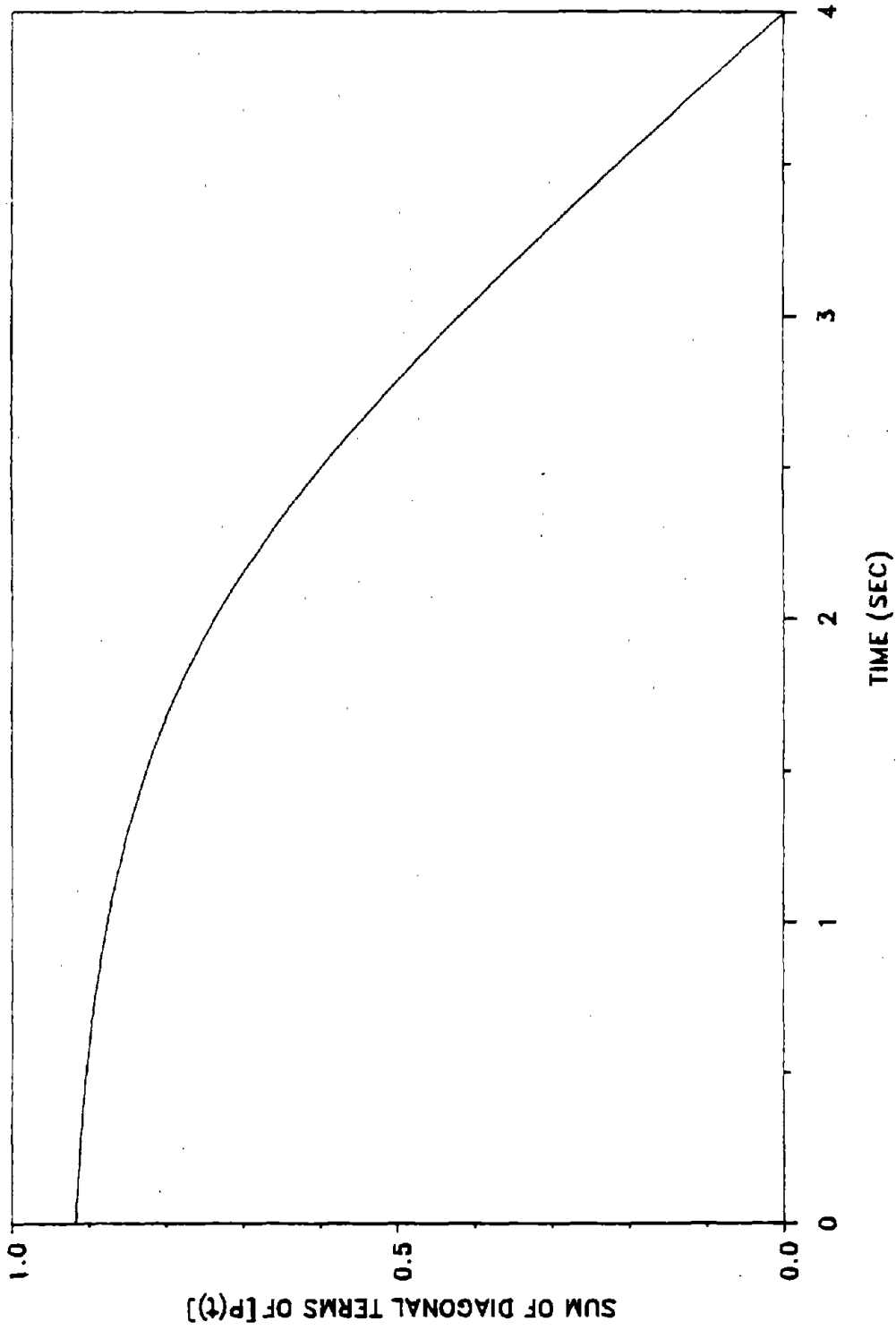
Figure   10.   Asymptotic Behavior of Matrix Ricatti Equation

46

steady-state in a short time starting from t_f backwards. As a result, the MRE can be approximated by the ARE and $[P(t)]$ replaced by $[P]$ which is time-invariant. This is true as long as t_f is longer than the earthquake duration. For the simulations in this study, Equation 3.29 is used to solve for the Ricatti matrix and Equation 3.30 to solve for the optimal control. The response is found using Equation 3.13.

It is to be noted that $[P]$ is a symmetric matrix of order $[2N \times 2N]$ and hence a system of only $[N \times (N+1)/2]$ non-linear equations has to be solved. The case when a certain floor is not equipped with an active tendon is taken care of by deleting the corresponding column in the $[\gamma]$ matrix.

2.   <u>Formulation for Active Mass Damper</u>.   The structural system with the AMD is shown in Figure 9b.   The state-vector is modified in this case to include the relative displacement of the AMD with respect to the top floor displacement $x_d(t)$

$$x_j(t) = X_j(t) - X_g(t) \qquad\qquad j = 1, ... , N \qquad\qquad (3.35)$$

$$x_d(t) = X_d(t) - X_N(t) \qquad\qquad\qquad (3.36)$$

Define the state-vector as

$$\{z_D(t)\} = \left\{ \frac{\{y(t)\}}{\{\dot{y}(t)\}} \right\} \qquad\qquad (3.37)$$

where $\{z_D(t)\}$ is of dimension $[(2N+2) \times 1]$, $N =$ number of floors, and $\{y(t)\}$ is given by

$$\{y(t)\}^T = \{x_1(t), x_2(t), ... , x_N(t), x_d(t)\} \qquad\qquad (3.38)$$

47

The equation of motion is given by

$$[M_D]\{\ddot{y}(t)\} + [C_D]\{\dot{y}(t)\} + [K_D]\{y(t)\} = \{\gamma_D\} u_d(t) + \{\delta_D\} \ddot{X}_g(t) \qquad (3.39)$$

where $[M_D]$, $[C_D]$ and $[K_D]$ are the mass, damping and stiffness matrices, respectively, of the combined structure and mass-damper system of dimension $[(N+1) \times (N+1)]$ given as

$$[M_D] = \begin{bmatrix} m_1 & & & & & \\ & m_2 & & & & \\ & & \ddots & & & \\ & & & & m_n & \\ & & & & m_d & m_d \end{bmatrix} \qquad (3.40)$$

$$[C_D] = \begin{bmatrix} (c_1 + c_2) & -c_2 & & & & & \\ -c_2 & (c_2 + c_3) & -c_3 & & & & \\ & & \ddots & & & & \\ & & & -c_{n-1} & (c_{n-1} + c_n) & -c_n & \\ & & & & -c_n & c_n & -c_d \\ & & & & & & c_d \end{bmatrix} \qquad (3.41)$$

48

$$
[K_D] \; = \; \begin{bmatrix} (k_1 + k_2) & -k_2 & & & & & \\ -k_2 & (k_2 + k_3) & -k_3 & & & & \\ & & & \ddots & & & \\ & & & & & & \\ & & -k_{n-1} & (k_{n-1} + k_n) & -k_n & \\ & & & -k_n & k_n & -k_d \\ & & & & & k_d \end{bmatrix} \qquad (3.42)
$$

where k_d, m_d and c_d are the stiffness, mass and damping of the mass damper, respectively. The scalar $u_d(t)$ is the control force due to the active mass damper and $\{\gamma_D\}$ and $\{\delta_D\}$ are $[(N+1) \times 1]$ vectors given by

$$
\{\gamma_D\}^T \; = \; \{0, 0, 0, \dots, -1, 1\} \qquad (3.43)
$$

$$
\{\delta_D\}^T \; = \; \{-m_1, -m_2, -m_3, \dots, -m_N, -m_d\} \qquad (3.44)
$$

The state-form of Equation 3.39 is

$$
\{\dot{z}_D(t)\} \; = \; [A_d]\{z_D(t)\} + \{B_d\}\, u_d(t) + \{C_d\}\, \ddot{X}_g(t) \qquad (3.45)
$$

where

$$
[A_d] \; = \; \left[\begin{array}{c|c} 0 & [I] \\ \hline -[M_D]^{-1}[K_D] & -[M_D]^{-1}[C_D] \end{array} \right] \;,\quad \{B_d\} = \left[\begin{array}{c} 0 \\ \hline [M_D]^{-1}\{\gamma_D\} \end{array} \right]
$$
$$
\{C_d\} \; = \; \left\{ \begin{array}{c} 0 \\ \hline [M_D]^{-1}\{\delta_D\} \end{array} \right\} \qquad (3.46)
$$

The optimal control force $u_d(t)$ is to be found by minimizing the performance index J_D, given by

$$J_D = \frac{1}{2} \int_{t_0}^{t_f} \left(\{z_D(t)\}^T [Q_D] \{z_D(t)\} + R_D u_d^2(t) \right) dt \tag{3.47}$$

and satisfying the state-equation, Equation 3.45 where $[Q_D]$ is a $[(2N+2) \times (2N+2)]$ positive semidefinite weighting matrix, and R_D is a positive scalar. Following the same procedure as for the AT case the optimal control is found to be

$$u_d^{\bullet}(t) = -R_D^{-1} \{B_d\}^T [P_D] \{z_D(t)\} \tag{3.48}$$

where $[P_D]$ is the solution to the following ARE

$$[P_D][A_d] + [A_d]^T [P_D] - [P_D]\{B_d\} R_D^{-1} \{B_d\}^T [P_D] + [Q_D] = [0] \tag{3.49}$$

Once the optimal control has been determined from Equation 3.48, the response is obtained for simulation purposes by solving Equation 3.45.

F. SINGLE DEGREE-OF-FREEDOM SUBJECT TO INITIAL CONDITIONS

In order to illustrate the Ricatti optimal closed-loop control, an example with initial conditions only is presented. The structure is similar to the one shown in Figure 4, with the following structural properties: Structural stiffness $k = 100$ *kips/in* (17513 *kN/m*), mass $m = 4$ *kip* $-$ *sec²/in* (700 *Mg*), and three percent of critical damping, or equivalently, $c = 1.2$ *kip* $-$ *sec /in* (210 *Mg/* sec). The weighting matrix $[Q]$, is a $[2 \times 2]$ diagonal matrix whose diagonal elements are set equal, i.e., $Q(1,1) = Q(2,2)$. The weighting matrix for the control forces is just a scalar, R. The structure is subjected to an initial displacement of 0.2 *in* (5.08 *mm*). Two cases for control are considered.

50

In Case 1, the elements of matrix $[Q]$ are set to the value $Q(1,1) = Q(2,2) = 1.0$ and $R = 0.01$. In Case 2, matrix $[Q]$ is the same, but $R = 0.001$. The response was calculated for these two cases, and compared to the case when no control was applied. From Figure 11, it is obvious that the displacement response has been reduced effectively. It is interesting to note that in Case 2, the structure comes to rest faster than Case 1. The same observations are made for the velocity response as shown in Figure 12. However, as can be seen from Figure 13, Case 2 requires a larger control force than Case 1. Thus, depending on the weighting matrices that are used, one can achieve different reduction levels in response with the associated control force.

G. COMPARISONS WITH EXPERIMENTAL RESULTS

In order to verify the analytical results obtained in the last Section, they were compared to experimental results obtained at the National Center for Earthquake Engineering Research at the University of New York at Buffalo (15). The experimental setup was a single-story structure as shown in Figure 4 with structural and control properties as given in Table I.   This is a 1 : 4 scaled model of a prototype structure. The elements of the weighting matrices $[Q]$ and R are chosen as

$$[Q] = \begin{bmatrix} k & 0 \\ \hline 0 & 0 \end{bmatrix}, \qquad R = k_t \tag{3.50}$$

where k is the structure stiffness, k_t is the tendon stiffness and their values are given in Table I.

51
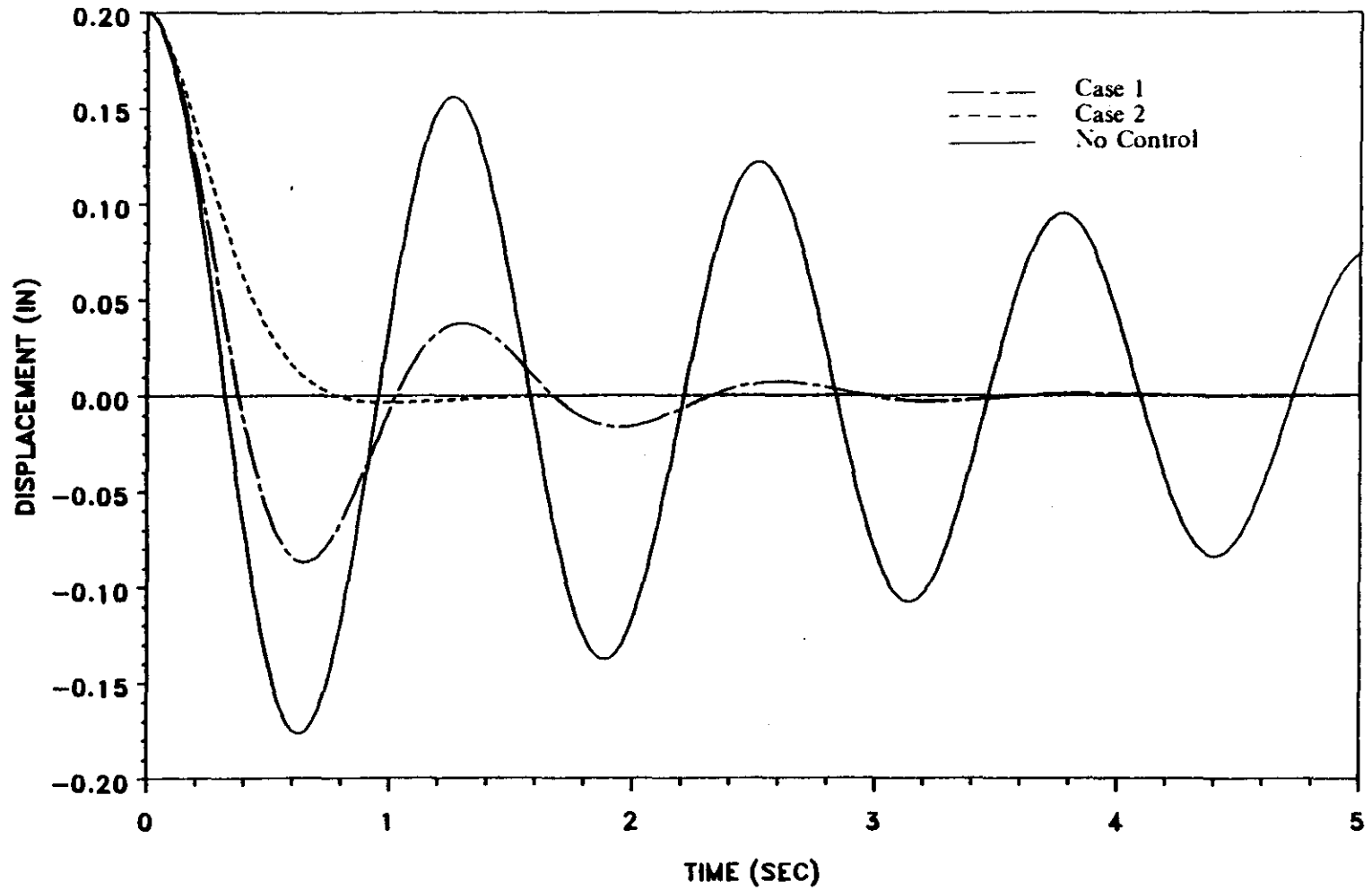
Figure   11.   Displacement Response of SDOF System
          (1 in = 25.4 mm)

52
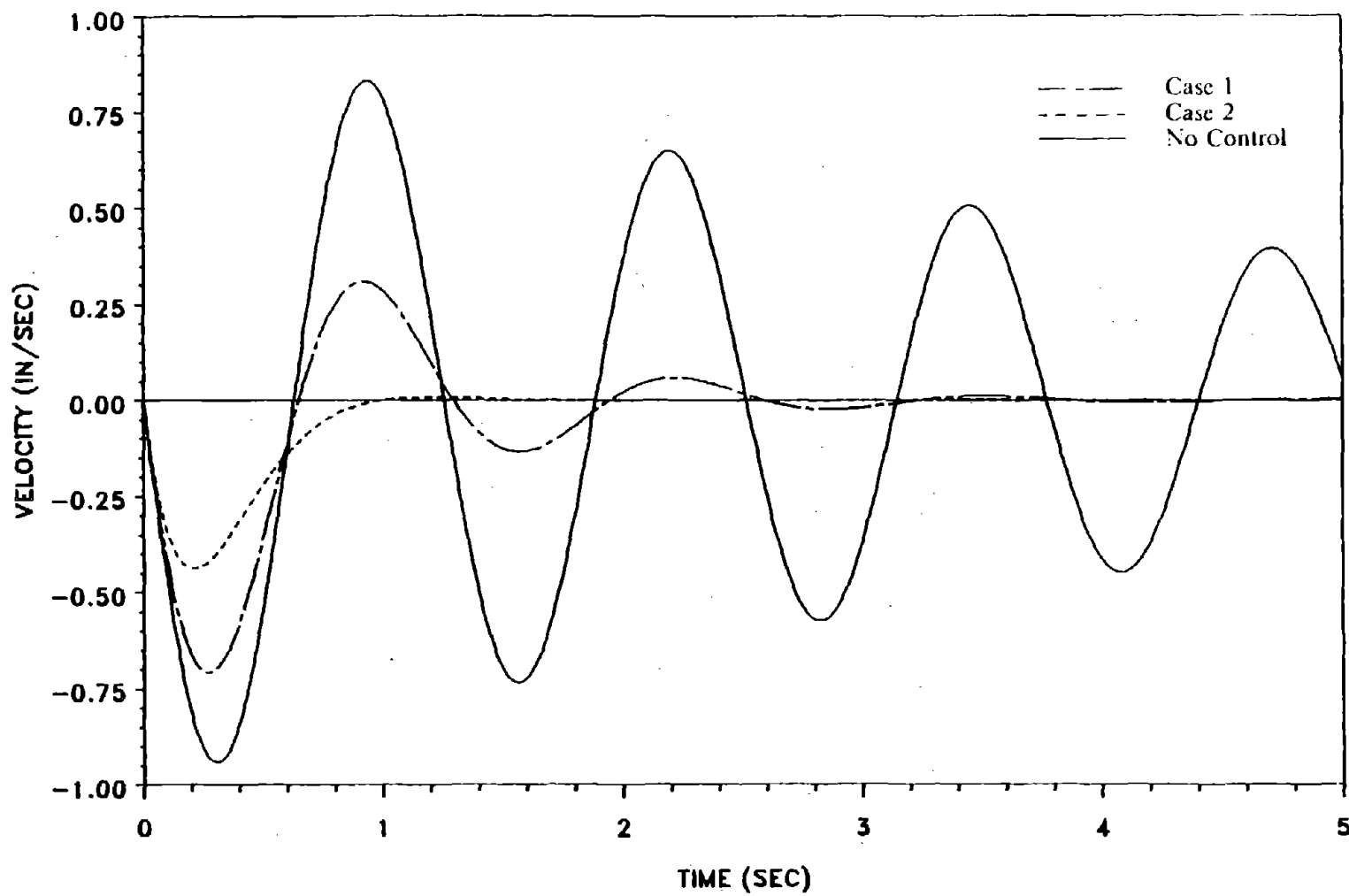
Figure 12. Velocity Response of SDOF System
(1 in/sec = 25.4 mm/sec)
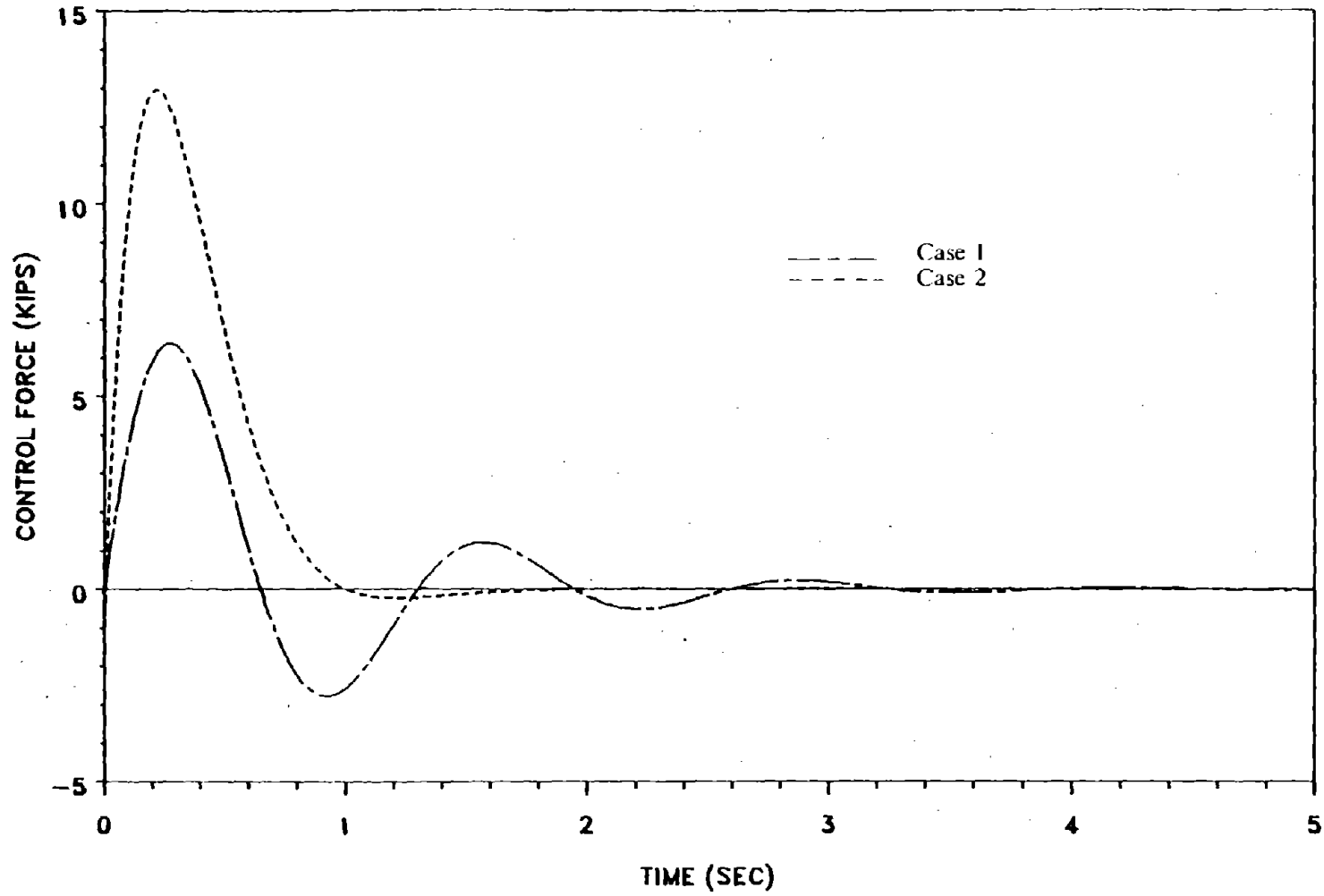
Figure   13.   Control Forces for SDOF System
(1 kip = 4.45 kN)

TABLE I. EXPERIMENTAL DATA
(1 lb-sec^2 /in = 175 Kg)
(1 lb/in = 175 N/m)

Parameter	Quantity
mass	16.69 lb-sec^2/in
structure stiffness	7934 lb/in
tendon stiffness	2124 lb/in
tendon angle	36 degrees
natural frequency	3.47 Hz
damping factor	1.24 %
geometry scaling factor	1 : 4

Figures 14 and 15 show good agreement between analytical and experimental results obtained under the same conditions. The differences are due to inaccuracies in the mathematical model, system and measurement noise, and interactions between the control system and the structure.
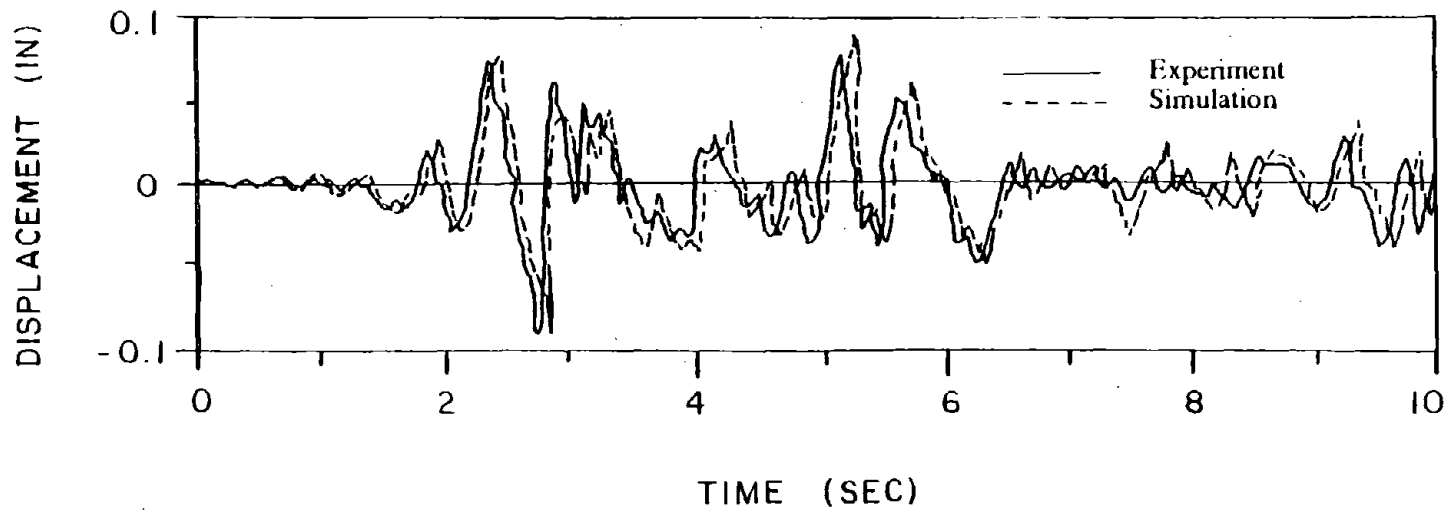
Figure 14. Comparison of Displacement Response with Experiment
(1 in = 25.4 mm)
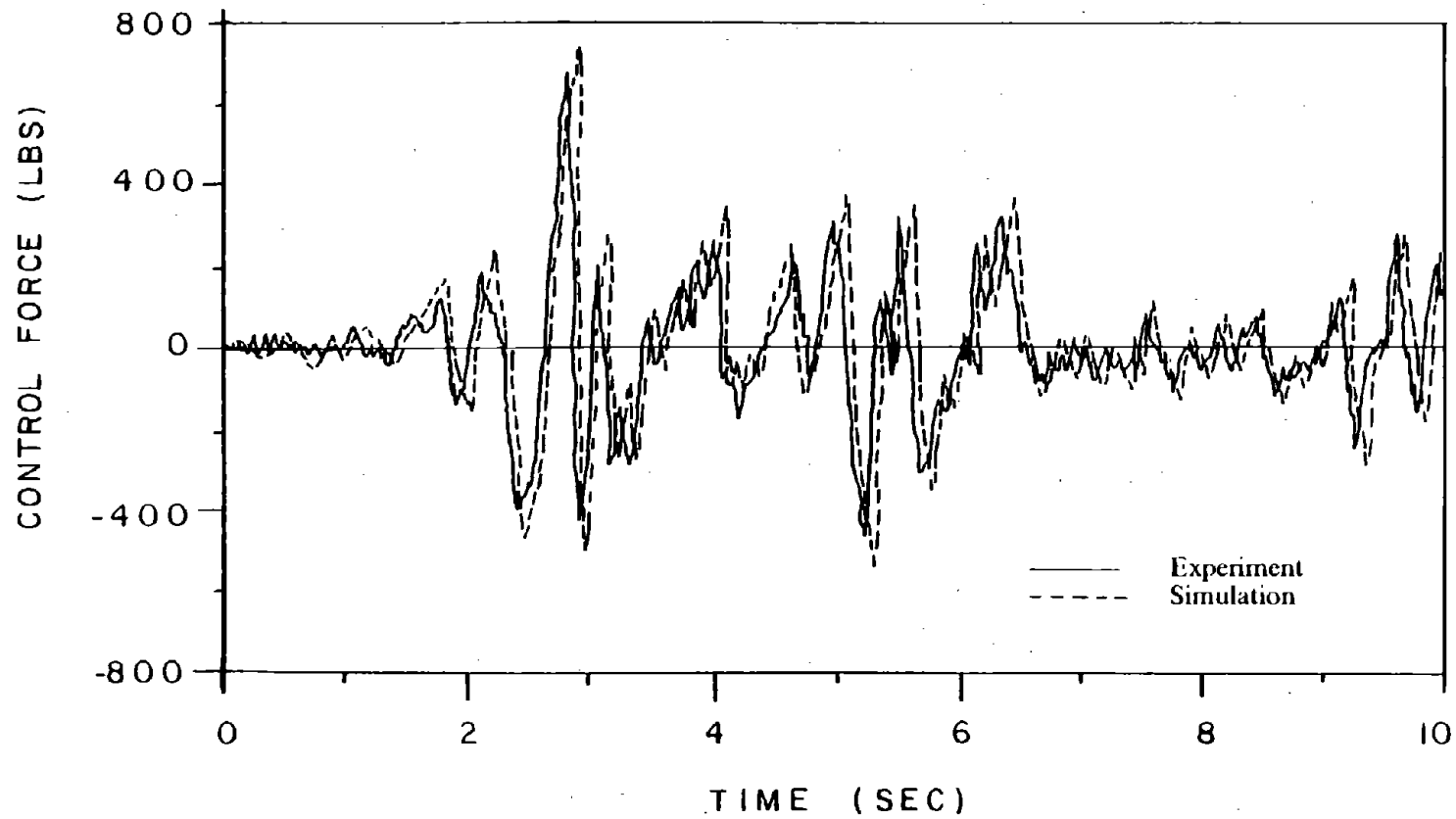
Figure 15. Comparison of Control Force with Experiment
(1 lb = 4.45 N)

IV. NON-OPTIMAL CLOSED-LOOP CONTROL

In this Chapter a closed-loop control scheme using the transfer matrix approach of dynamic analysis is developed. Three active control systems are investigated in this study: 1) an active tendon system installed between adjacent floors as shown in Figure 9a, 2) an active mass damper installed at the top floor of the building as shown in Figure 9b, and 3) a combination of the active tendon and active mass damper systems as shown in Figure 16. The effectiveness of these two control systems in reducing the structural response under earthquake excitations is examined.

The procedure for analysis follows the transfer matrix approach in the frequency-domain instead of the classical modal approach. The transfer matrix approach determines the structural response directly without having to calculate the natural frequencies and modes. This results in considerable simplification of the calculations.

The present closed-loop active control algorithm is not optimal. The control forces are not determined according to the minimization of a performance index but according to a simple closed-loop control law. This implies that the magnitude of the control forces is not the minimum possible. However, the control forces do not require on-line computations for their regulation.

The transfer matrix approach for controlled response has been used by Yang for earthquake excitations (61), and Yang and Samali for wind excitations (65). Two important features are different in the derivations presented herein. First, each floor of the structure does

59
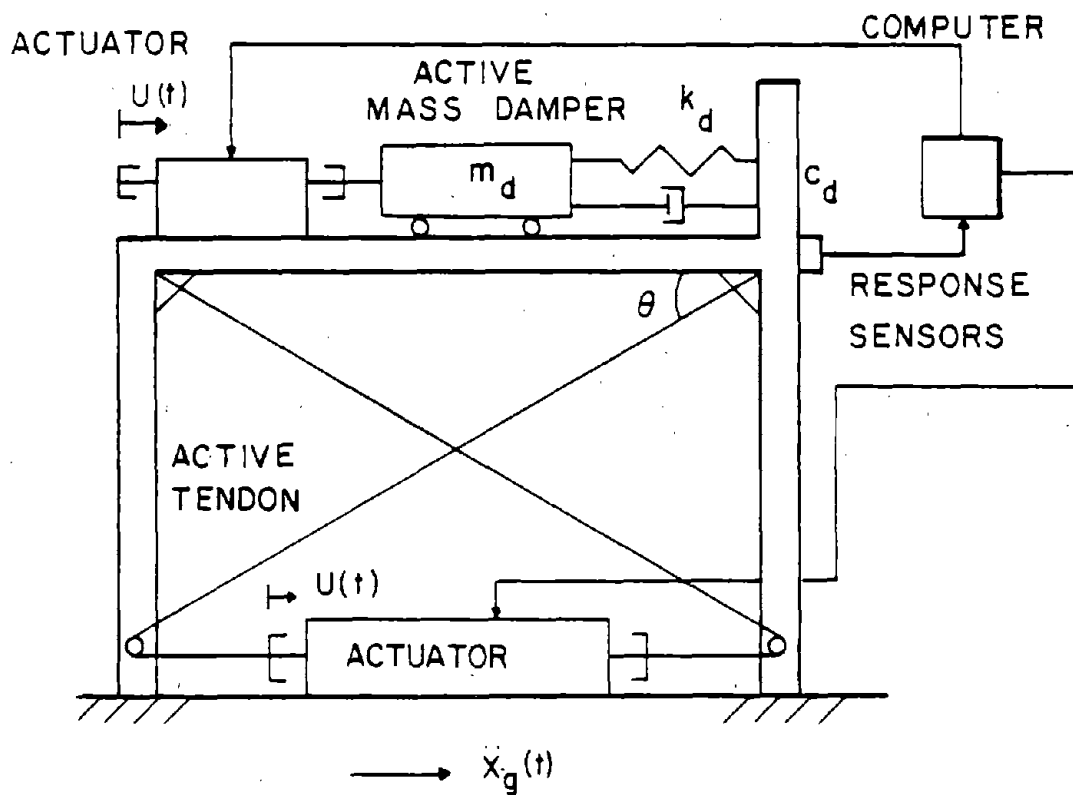
Figure 16. Combined Active Mass Damper and Tendon System

not have to be identical to the others. This is required for the optimization algorithm to be implemented. Secondly, this derivation includes a combined active tendon-mass damper system, as shown in Figure 16. This combined system resulted in improved performance of the control system.

A. EARTHQUAKE EXCITATION

The earthquake ground acceleration is modelled as a stochastic process and a random vibration analysis is carried out to determine the stochastic response of buildings equipped with active control systems. It is assumed that the strong shaking portion of typical earthquake accelerograms is stationary, i.e. the statistics are time-invariant. The corresponding structural response is also stationary. The earthquake ground acceleration, $\ddot{X}_g(t)$, has been modelled as a stationary random process with zero mean and a power spectral density $\Phi\ddot{X}_g(\omega)$. The power spectral density function used herein is a filtered white noise, known as the Kanai-Tajimi function (24). It is derived based on a model of the ground as a linear filter. The complete derivation is given in Appendix A. The power spectral density of filtered white noise obtained from Appendix A is given as

$$\Phi\ddot{X}_g(\omega) = \frac{\left[1 + 4\zeta_g^2 \frac{\omega^2}{\omega_g^2}\right] S^2}{\left(1 - \frac{\omega^2}{\omega_g^2}\right)^2 + 4\zeta_g^2 \frac{\omega^2}{\omega_g^2}} \qquad (4.1)$$

In Equation 4.1 ζ_g = ground damping, ω_g = ground frequency, ω = forcing frequency, and S^2 = power spectrum of white noise. With proper selection of the ground properties, ζ_g and ω_g, Equation 4.1 can be used to represent earthquake excitations with different power spectral density shapes. For example using $S^2 = 1.0 \ m^2/\sec^3/rad$, $\omega_g = 18.85 \ rad/\sec$, and two values for the ground damping $\zeta_g = 0.15$, or $\zeta_g = 0.65$, two different curves can be obtained as shown in Figure 17. When $\zeta_g = 0.15$ (Curve A in Figure 17), a narrow-band excitation is obtained which can influence the response within only a narrow range of frequencies. When $\zeta_g = 0.65$ (Curve B in Figure 17), a wide-band excitation is obtained. It is to be noted that at the frequency $\omega = \omega_g$ resonance occurs. As ω_g tends to infinity, i.e. the ground assumes infinite stiffness, $\Phi \ddot{X}_g(\omega) = S^2$, the input is not a filtered white noise anymore, i.e., it remains a white noise process.

B. COMBINED ACTIVE MASS DAMPER AND TENDONS

The structural model chosen for the present study is an N-story shear building equipped with a number of active tendons and an active mass damper, as shown in Figures 16 and 18. The following assumptions are made to simplify the analysis: 1) the mass of each floor is concentrated at the floor level, 2) linear elasticity is provided by massless columns between neighboring floors, 3) the structural response is described by the displacement and shear force in each story, 4) active tendon controllers are installed between two neighboring floors either above or below the jth floor, 5) an AT controller is regulated by two sensors placed on the floors above and

62
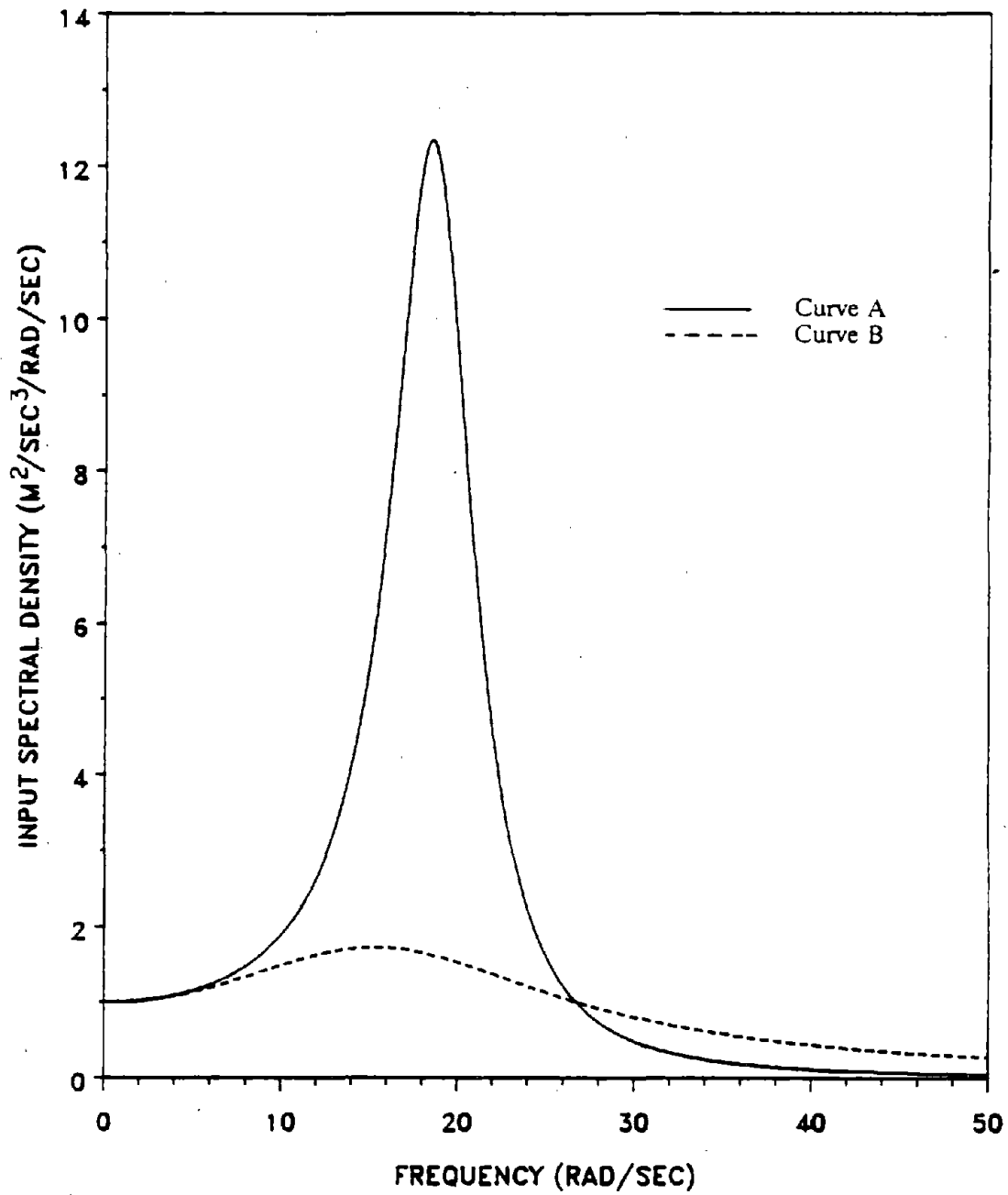
Figure 17. Input Power Spectral Density

63
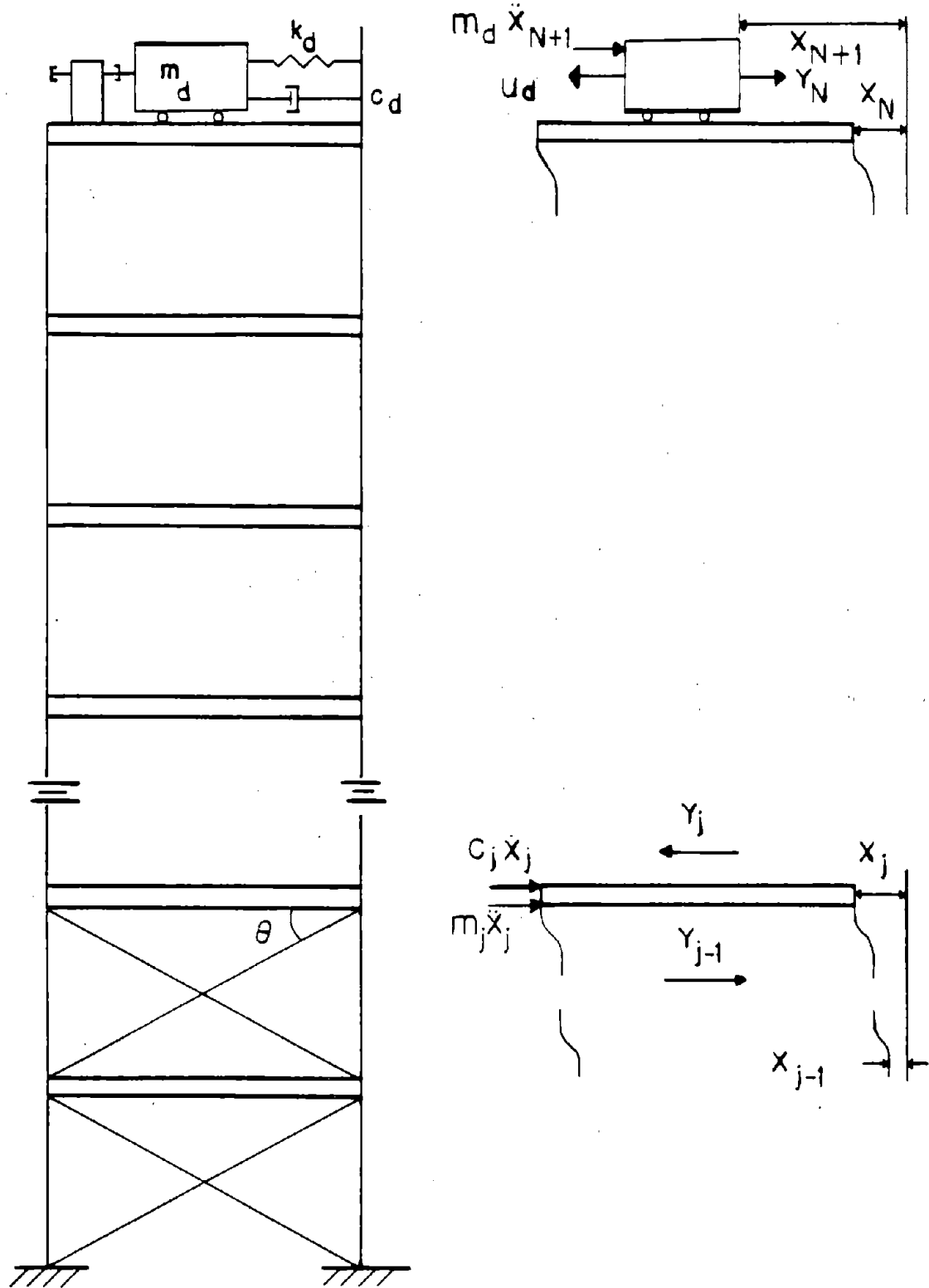
Figure 18. Structural Model and Active Control Systems

below it, 6) an active mass damper is placed on the top floor, and 7) an acceleration sensor is placed at the top floor to regulate the AMD controller.

Let X_j and Y_{j-1} be the displacement of the jth floor, and the resultant shear force in the columns of the jth floor, respectively, as shown in Figure 18. Also let X_{N+1} be the displacement of the AMD, and Y_N be the force exerted on the mass of the damper m_d from the elastic spring k_d and dashpot c_d. The equations of motion of a typical floor can be written

$$Y_j = Y_{j-1} + m_j \ddot{X}_j + c_j \dot{X}_j, \qquad 1 \leq j \leq (N-1) \tag{4.2}$$

$$Y_{j-1} = k_j (X_j - X_{j-1}) + u_j, \qquad 1 \leq j \leq (N-1) \tag{4.3}$$

where N = number of floors, u_j is the active control force in the horizontal direction from the jth tendon and m_j, c_j, and k_j are the mass, damping coefficient and elastic stiffness of the jth floor, respectively. The equations of motion for the Nth floor and AMD are

$$Y_N = k_d (X_{N+1} - X_N) + c_d (\dot{X}_{N+1} - \dot{X}_N) \tag{4.4}$$

$$u_d = m_d \ddot{X}_{N+1} + Y_N \tag{4.5}$$

$$Y_N = Y_{N-1} + m_N \ddot{X}_N + c_N \dot{X}_N + u_d \tag{4.6}$$

$$Y_{N-1} = k_N (X_N - X_{N-1}) + u_N \tag{4.7}$$

Note that u_d is the AMD control force and that the quantities Y_j, X_j, X_N, X_{N+1}, u_d, and u_j are all functions of time. Assuming zero initial

conditions and taking the Fourier transforms of Equations 4.2 and 4.3 yields

$$\{Z\}_L = [A(L)] \{Z\}_0, \qquad 1 \leq L \leq (N-1) \tag{4.8}$$

Taking the Fourier transforms of Equations 4.4 and 4.7 yields

$$\{Z\}_N = [A]_N \{Z\}_{N-1} + \left\{ \frac{0}{g_m(\omega)\overline{X}_N} \right\} \tag{4.9}$$

$$\{Z\}_{N+1} = [T] \{Z\}_N - \left\{ \frac{0}{g_m(\omega)\overline{X}_N} \right\} \tag{4.10}$$

in which an overbar denotes the Fourier transform of a quantity. In Equations 4.8 through 4.10 the symbol $\{Z\}_j$ is the state-vector defined in terms of the diplacement and shear force Fourier transforms as

$$\{Z\}_j = \left\{ \frac{\overline{X}_j}{\overline{Y}_j} \right\} \tag{4.11}$$

Detailed derivations of the above equations are given in Appendix E. The notation $[A(L)]$ is a matrix product defined as

$$[A(L)] = [A]_L \cdots [A]_2 [A]_1 \tag{4.12}$$

where $[A]_j$ is the transfer matrix of the $j th$ floor given by

$$\{Z\}_j = [A]_j \{Z\}_{j-1} \tag{4.13}$$

$$[A]_j = \begin{bmatrix} 1 & \dfrac{1}{Kc_j} \\ (-\omega^2 m_j + i\omega c_j) & 1 + \dfrac{(-\omega^2 m_j + i\omega c_j)}{Kc_j} \end{bmatrix} \tag{4.14}$$

where

$$i = \sqrt{-1} \tag{4.15}$$

$$Kc_j = k_j + g_t(\omega) \tag{4.16}$$

In Equation 4.16, $g_t(\omega)$ is the gain of the AT controller and is described in Section C of this Chapter. If a certain floor does not have a tendon controller, $g_t(\omega) = 0$. In Equations 4.9 and 4.10, $g_m(\omega)$ is the gain of the AMD controller and is described in Section D of this Chapter. The notation $\{Z\}_{N+1}$ is defined as the boundary condition

$$\{Z\}_{N+1} = \left\{ \frac{\overline{X}_{N+1}}{0} \right\} \tag{4.17}$$

and matrix $[T]$ is the transfer matrix of the AMD, given by

$$[T] = \begin{bmatrix} 1 & \dfrac{1}{k_d + i\omega\, c_d} \\ -m_d\omega^2 & 1 - \dfrac{m_d\omega^2}{k_d + i\omega\, c_d} \end{bmatrix} \tag{4.18}$$

The earthquake ground acceleration of Appendix A, given by Equation 4.1 is used as the earthquake input. The structural response and active control statistics will be stationary random processes with zero mean. The power spectral density of the response state-vector at the mth floor is given by

$$S_m(\omega) = \| \{Z\}_m \|^2\ \omega^{-4}\ \Phi\ddot{X}_g(\omega) \tag{4.19}$$

where $\Phi\ddot{X}_g(\omega)$ is given in Equation 4.1 and $\| \{Z\}_m \|^2$ is the magnitude of the state-vector $\{Z\}_m$, detailed derivation of which is given in Appendix E. When the relative displacement of the mth floor to the ground is

required, $\overline{X}_m$ in Equation 4.19 should be replaced by $(\overline{X}_m - 1)$. The mean square response vector at the *mth* floor level, σ_m^2, is given by

$$\sigma_m^2 = \int_{-\infty}^{\infty} \|Z_m\|^2 \; \omega^{-4} \; \Phi \ddot{X}_g(\omega) \; d\omega \tag{4.20}$$

The mean square value of the control force from the *ith* AT controller, σ_{ti}^2, is given by

$$\sigma_{ti}^2 = \int_{-\infty}^{\infty} \|\bar{u}\|^2 \; \omega^{-4} \; \Phi \ddot{X}_g(\omega) \; d\omega \tag{4.21}$$

where $\bar{u}$ is given in Section C of this Chapter. The mean square value of the AMD control force, σ_d^2, is given by

$$\sigma_d^2 = \int_{-\infty}^{\infty} \|\bar{u}_d\|^2 \; \omega^{-4} \; \Phi \ddot{X}_g(\omega) \; d\omega \tag{4.22}$$

where $\bar{u}_d$ is given in Section D of this Chapter.

C. ACTIVE TENDON SYSTEM

In the special case when no AMD is present, the solution is simplified considerably and the response is given by

$$\{Z\}_N = [A(N)] \; \{Z\}_0 \tag{4.23}$$

Applying the boundary conditons

$$\{Z\}_N = \left\{ \begin{array}{c} \overline{X}_N \\ 0 \end{array} \right\}, \qquad\qquad \{Z\}_0 = \left\{ \begin{array}{c} 1 \\ \overline{Y}_0 \end{array} \right\} \tag{4.24}$$

to Equation 4.23 gives

$$\left\{ \frac{\overline{X}_N}{0} \right\} = \left[\begin{array}{c|c} A11(N) & A12(N) \\ \hline A21(N) & A22(N) \end{array} \right] \left\{ \frac{1}{\overline{Y}_0} \right\} \tag{4.25}$$

The unknown quantities can be found as

$$\overline{Y}_0 = -\frac{A21(N)}{A22(N)} \tag{4.26}$$

$$\overline{X}_N = A11(N) + A12(N)\,\overline{Y}_0 \tag{4.27}$$

Consequently the state-vector and AT control force can be easily obtained. The statistics of the response are still given by Equations 4.20 and 4.21.

The active tendon control force is due to: 1) the elongation of the tendon $\left[(X_j - X_{j-1})\cos\theta \right]$ resulting from the motion of the building, and 2) the movement of the hydraulic ram $U(t)$. Let k_t denote the tendon stiffness. The active tendon control force u in the horizontal direction is given by

$$u = k_t \left[(X_j - X_{j-1})\cos\theta + U \right] \cos\theta \tag{4.28}$$

where u, X_j, X_{j-1} and U are functions of time. The controller considered is an electrohydraulic servomechanism similar to that described in reference (61). For the jth tendon controller, the building motions are sensed by velocity sensors placed on the floor above and below it, i.e., the jth and $(j-1)th$ floors

$$\dot{X}_j = \frac{dX_j}{dt}, \qquad\qquad \dot{X}_{j-1} = \frac{dX_{j-1}}{dt} \tag{4.29}$$

69

The sensed motions are transmitted to the controller in the form of an electric voltage $V(t)$, which is proportional to the sensed motions

$$V(t) = prt\,(\dot{X}_j - \dot{X}_{j-1})$$ (4.30)

where prt is a proportionality constant. The displacement of the hydraulic rams $U(t)$ is regulated by the feedback voltage $V(t)$, through the relation

$$\dot{U}(t) + R1\,U(t) = R1\left(\frac{V(t)}{R0}\right)$$ (4.31)

in which $R1$ is the loop gain and $R0$ is the feedback gain of the controller. The electrohydraulic mechanism is shown in detail in Figure 19. The definitions of the loop and feedback gain in terms of the gains K_A, K_U, K_P, and K_O, are

$$R1 = K_A\,K_U\,K_P\,K_O$$ (4.32)

$$R0 = K_O$$ (4.33)

A possible arrangement for providing the feedback control force is shown schematically in Figure 20. Taking the Fourier transform of Equations 4.28, 4.30 and 4.31

$$\bar{u} = k_t\,\cos\theta\left[\cos\theta + \frac{\tau_t\,\varepsilon_t\,(\frac{i\omega}{\omega_1})}{\varepsilon_t + (\frac{i\omega}{\omega_1})}\right](\bar{X}_j - \bar{X}_{j-1})$$ (4.34)

in which $\omega_1 =$ fundamental frequency of the structure without control, ε_t is the normalized loop gain, and τ_t is the normalized feedback gain for the active tendon system,

70
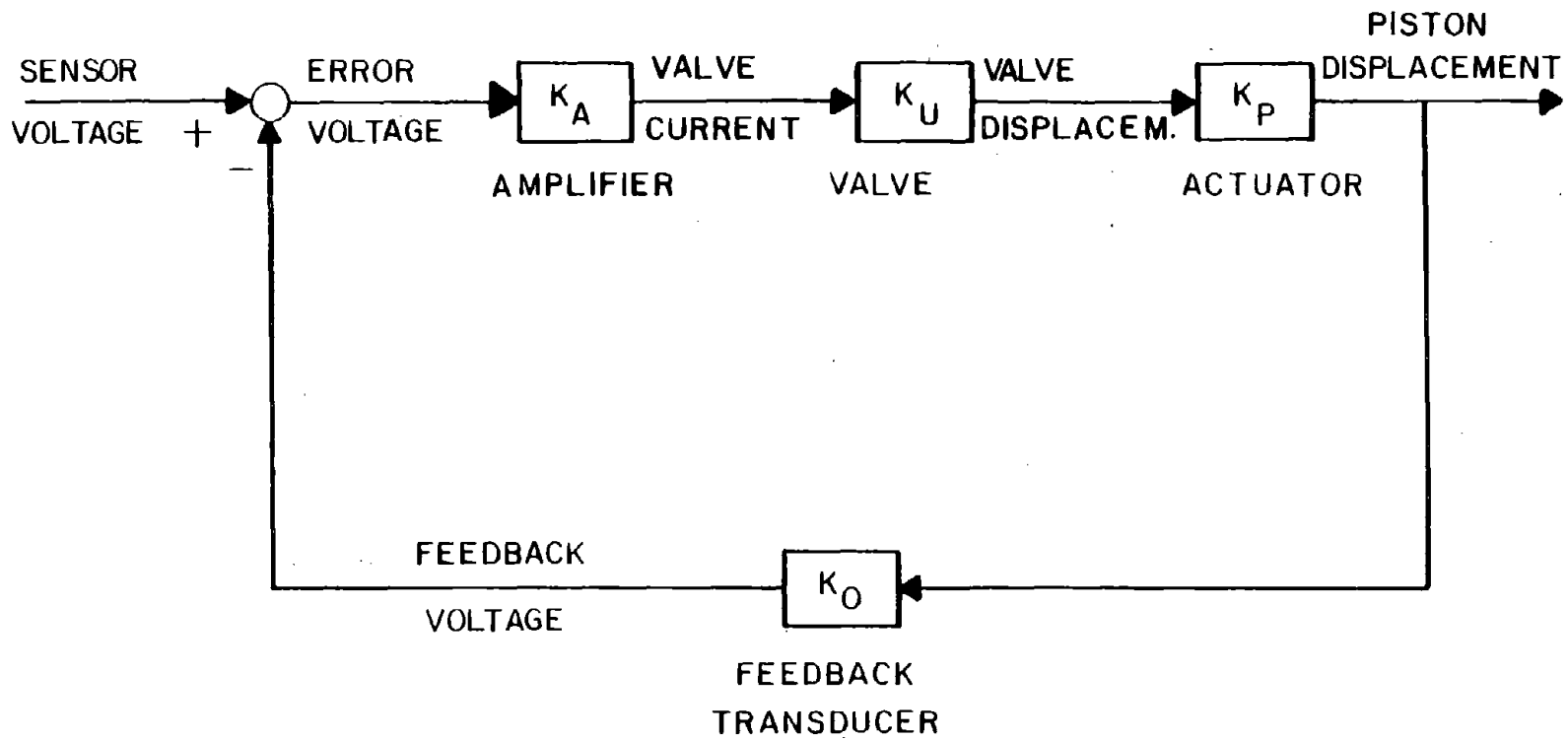
Figure 19. Electrohydraulic Servomechanism

71
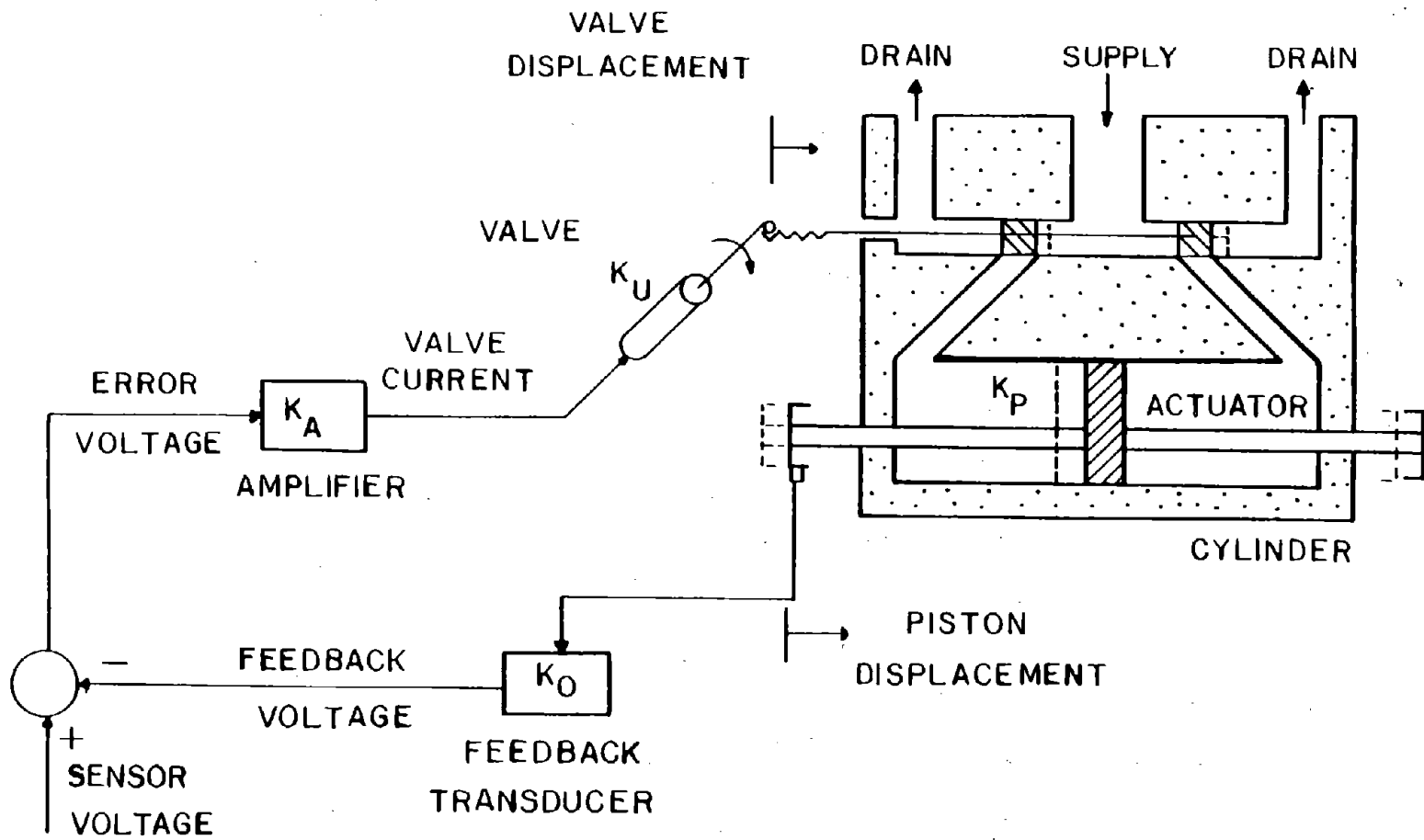
Figure 20. Schematic for Electrohydraulic Actuator

$$\varepsilon_t = \frac{R1}{\omega_1}, \qquad\qquad \tau_t = prt\frac{\omega_1}{R0} \qquad\qquad (4.35)$$

The expression $g_t(\omega)$ can now be established from Equation 4.34 as

$$\bar{u} = g_t(\omega)(\overline{X}_j - \overline{X}_{j-1}) \qquad\qquad (4.36)$$

$$g_t(\omega) = k_t \cos\theta \left[\cos\theta + \frac{\tau_t\,\varepsilon_t\,(\frac{i\omega}{\omega_1})}{\varepsilon_t + (\frac{i\omega}{\omega_1})} \right] \qquad\qquad (4.37)$$

It is important to note that $\bar{u}$ is a function of the forcing frequency ω.

D. ACTIVE MASS DAMPER SYSTEM

In the case where only an AMD is used, the transfer matrix relations of Equations 4.8 through 4.10 can be used again with one difference. In matrix $[A]_j$ of Equation 4.14 the quantity $g_t(\omega)$ in the term Kc_j is set equal to zero. Consequently the state-vector and AMD control force can be obtained using the same general expressions. The statistics of the response are still given by Equations 4.20 and 4.22.

The active mass damper control force is regulated by an acceleration sensor on the top floor. The voltage that is proportional to this sensed acceleration is

$$V(t) = prm\,\ddot{X}_N \qquad\qquad (4.38)$$

where *prm* is a proportionality constant. The displacement of the hydraulic rams is still given by Equation 4.31. Let the Fourier transform of the AMD control force be given by

$$\bar{u}_d \ = \ g_m(\omega)\, \overline{X}_N \tag{4.39}$$

Taking the Fourier transform of Equations 4.31 and 4.38 combined with Equation 4.39 yields the result

$$\bar{u}_d \ = \ k_{md} \left[\frac{\tau_d\, \varepsilon_d\, (\frac{i\omega}{\omega_1})^2}{\varepsilon_d + (\frac{i\omega}{\omega_1})} \right] \overline{X}_N \tag{4.40}$$

Hence

$$g_m(\omega) \ = \ k_{md} \left[\frac{\tau_d\, \varepsilon_d\, (\frac{i\omega}{\omega_1})^2}{\varepsilon_d + (\frac{i\omega}{\omega_1})} \right] \tag{4.41}$$

where k_{md} is a proportionality constant, τ_d is the normalized feedback gain, and ε_d the normalized loop gain for the mass damper, respectively,

$$\varepsilon_d \ = \ \frac{R1}{\omega_1}, \qquad\qquad \tau_d \ = \ prm\, \frac{\omega_1^2}{R0} \tag{4.42}$$

E. COMPARISON OF RESPONSE FOR THREE CONTROL SYSTEMS

The three active control system models described in this Chapter, i.e., the active tendon, active mass damper, and combined active mass damper and tendons are examined in this example. The structural model is an eight-story shear building, with the following properties: $m_j = 314\,Mg$, $k_j = 3 \times 10^5\,kN/m$, $c_j = 90\,Mg/\sec$, $j = 1, ..., 8$. The earthquake excitation used is that of Equation 4.1, of the Kanai-Tajimi spectral density function, with the following parameters : $\omega_g = 18.85\,rad/\sec$, $\zeta_g = 0.65$, and $S^2 = 4.65 \times 10^{-4}\,m^2/\sec^3 / rad$. The control parameters are: $k_t = 15 \times 10^3\,kN/m$, $\theta = 25\ degrees$, $m_d = 27\,Mg$, $k_d = 957.2\,kN/m$, $c_d = 23\,Mg/\sec$, and $k_{md} = 15 \times 10^3\,kN/m$. In addition, the normalized gains are fixed at the following values: $\tau_t = \varepsilon_t = 8$, $\tau_d = 4$, and $\varepsilon_d = 0.4$. The structure is first subjected to the earthquake excitation without any active control system (Case 1); in Case 2, the structure is equipped with eight active tendons, one on each floor; in Case 3 the structure is equipped with an active mass damper on the top floor, and in Case 4 the structure is equipped with an active mass damper and two active tendons at the bottom two floors. The power spectral densities of the response for the four cases were calculated. In Figure 21, the spectral density of the eighth floor relative displacement is shown. The advantage of the combined system in Case 4 over that of the AMD alone of Case 3 is that the response of the higher modes is reduced in addition to the first mode. From Figure 22, it can be seen that all systems reduce the base shear force. Note that the vertical axis for both of these figures is based on the logarithmic scale of base 10.
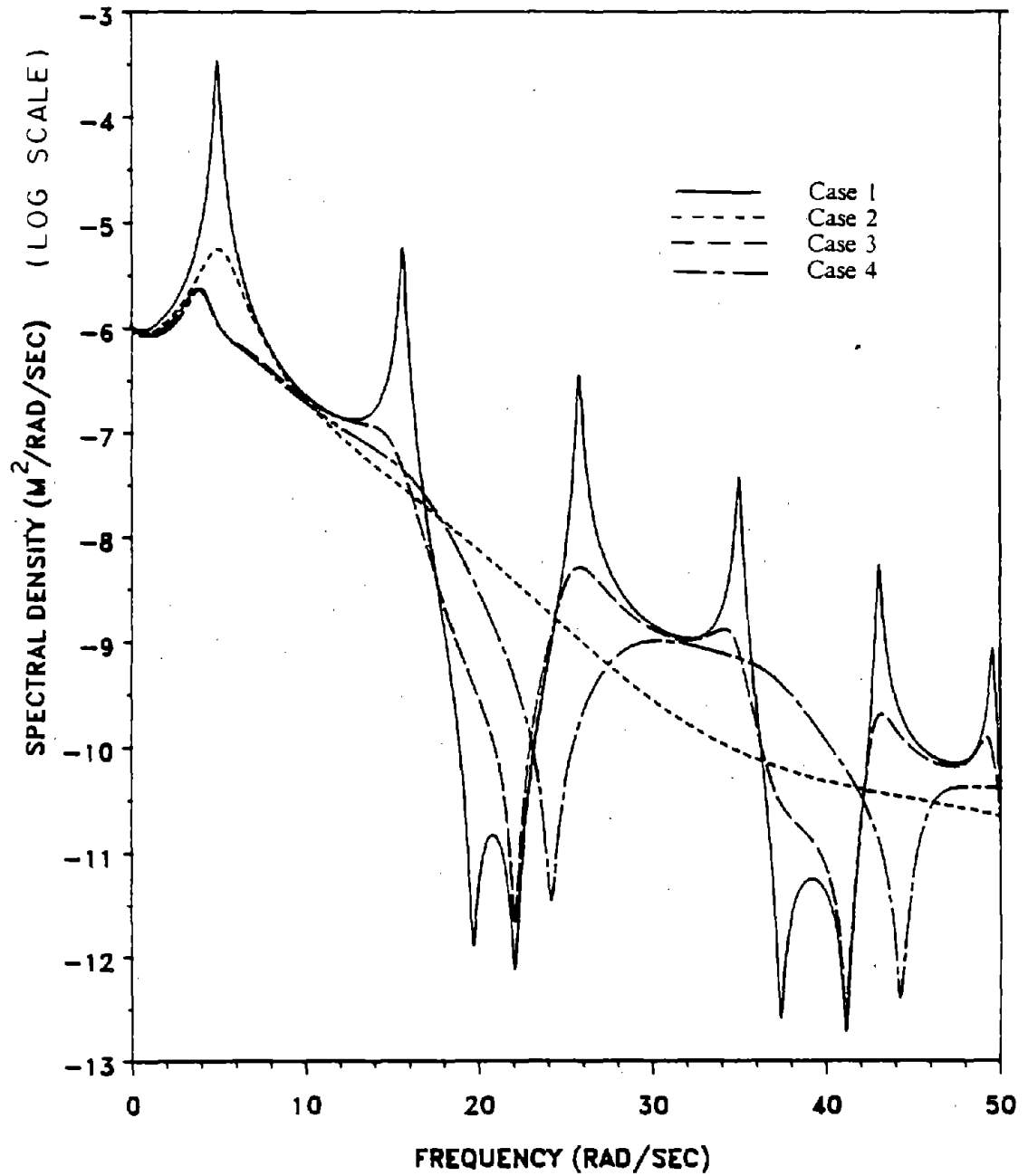
Figure 21.   Spectral Density of Top Floor Relative Displacement

76
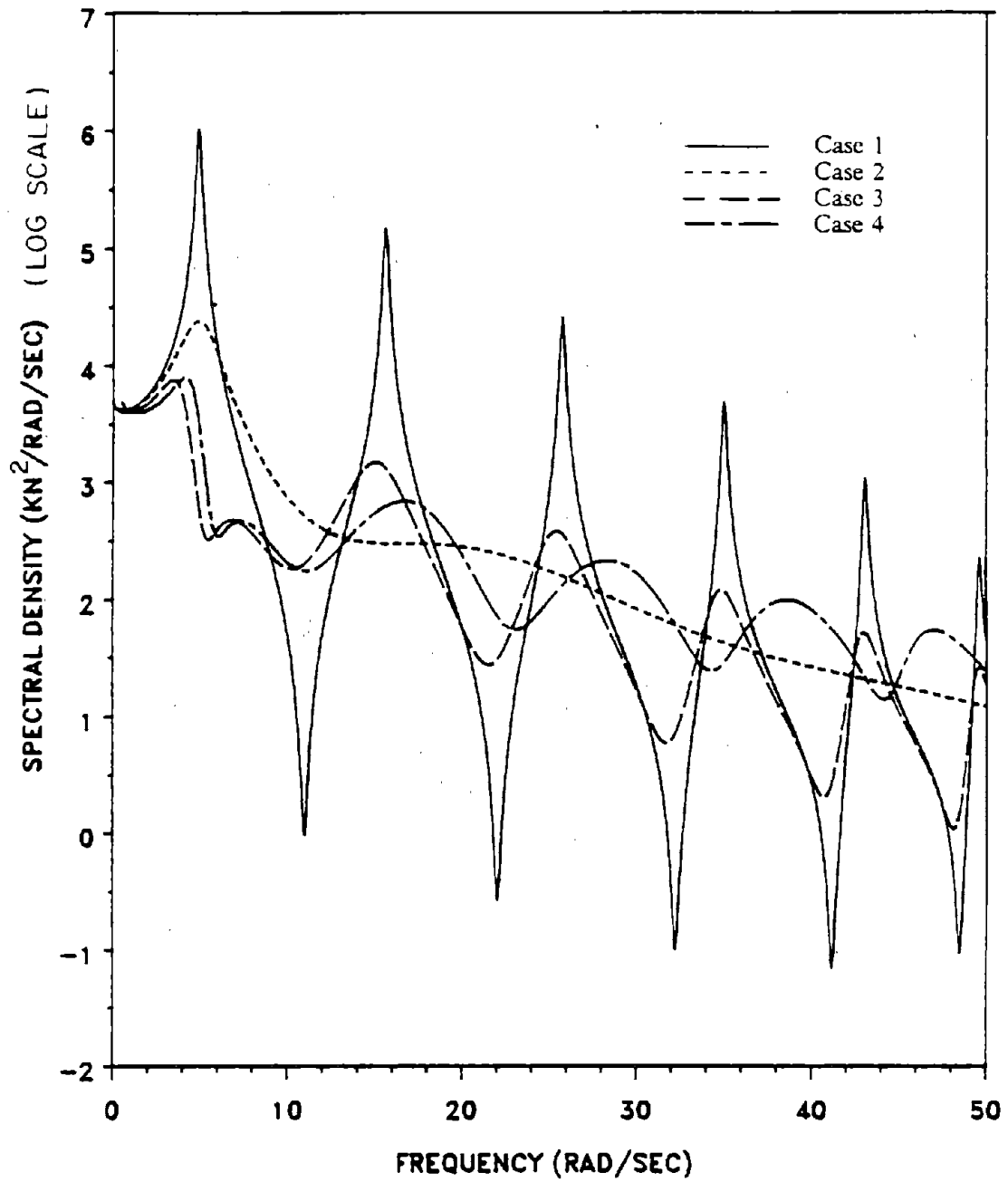
Figure 22. Spectral Density of Base Shear Force

V. INSTANTANEOUS OPTIMAL CONTROL ALGORITHMS

The difficulty of not knowing the earthquake ground motion
apriori has made it necessary to consider the assumption of a white
noise excitation in the derivation of the Ricatti closed-loop control
in Chapter III. The instantaneous optimal control algorithms resolve
this issue with the added advantage that the optimal control
expressions are simpler than those of the Ricatti closed-loop control.

This simplification was introduced in the study of discrete-time
systems by Saridis and Lobbia (48), in which they developed stochastic
algorithms. The main idea is that instead of minimizing the integral
performance index used for the Ricatti algorithm, minimization of a
sequence of single-stage processes was proposed. The term
"per-interval" optimal controller was used, meaning that optimality
was achieved at each instant of time. This idea was adopted for the
case of control of earthquake-excited structures by Yang, Akbarpour
and Gaemmaghami (62). Cheng and Pantelides extended the same concept
to the optimum design of seismic structures equippped with active mass
damper or active tendons (11,12,13). Cheng and Pantelides have also
adopted the instantaneous algorithms for optimal control of
wind-excited structures (12).

In this Chapter, the instantaneous optimal control algorithms are
developed for all three control schemes, i.e., open-loop, closed-loop,
and open-closed-loop. In Chapter VI these algorithms are used in the
structural optimization of seismic structures. Their simplicity in

establishing the control gain matrix is of paramount importance in their application to the optimization algorithm.

A. EARTHQUAKE EXCITATION

The earthquake acceleration records described in Section A, of Chapter III are also used herein. Their use allows comparisons to be made between the Ricatti closed-loop and instantaneous optimal control algorithms.

B. WIND EXCITATION

Artificial wind velocities are generated for simulation. The wind flow is assumed stationary in time and non-homogenous in space. It is known that the wind velocity has two components, steady and turbulent flow. The logarithmic law is used to obtain the steady flow component at different floor heights, which is then adjusted for different averaging times and terrain conditions.

The fluctuating component is obtained from design spectra for wind which vary with height above the ground. These design spectra establish the autospectrum for the structure based on which the fluctuating components of the wind velocities are created. These components are then correlated spatially using a transformation matrix which is based on an experimental coherence function. From the mean and fluctuating velocities, the mean and fluctuating windward and leeward pressures are obtained for each floor. These pressures multiplied by the tributary area of each floor constitute the

spatially discretized time-histories of the artificial wind forces. The complete derivation of the wind forces is given in Appendix B.

C. INSTANTANEOUS OPEN-LOOP DISTURBANCE-COMPENSATED ALGORITHM

In addition to the simplicity of the instantaneous optimal control algorithms, their instantaneous nature is advantageous because of their ease of implementation in real-time. In the present algorithm the earthquake excitation is assumed to be measured by accelerometers installed at the basement of the building. The structural and control system for this type of control are shown in Figure 2. The accelerometer is used to measure the earthquake ground acceleration in real-time. Thus at any instant of time t, the ground excitation record, $\ddot{X}_g(t)$, at the basement of the building is available up to that time instant. Thus the only measurement required for instantaneous open-loop control is that of the excitation as pointed out by Yang et al. (62). Experimental evaluation of the instantaneous algorithms was carried out by Lin, Soong and Reinhorn (33). In this Section the optimal control is derived, based on the measurement of the excitation for both the active mass damper and active tendon systems.

1. _Active Tendon System (AT)_. The optimal control $\{u^*(t)\}$ is to be derived by minimizing instead of the integral performance index J of Equation 3.16, an instantaneous time-dependent performance index $J_p(t)$ defined as

$$J_p(t) = \{z(t)\}^T [Q] \{z(t)\} + \{u(t)\}^T [R] \{u(t)\} \tag{5.1}$$

and satisfying the state-equation of Equation 3.13. The performance index $J_p(t)$ is minimized at every time instant t, for all t in the interval $0 \leq t \leq t_f$, where t_f is the earthquake duration. Detailed discussion of Equation 5.1 is given in Appendix C.

First consider the solution of Equation 3.13, assuming the optimal control $\{u^*(t)\}$ has been derived, and the earthquake excitation $\ddot{X}_g(t)$ has been measured upto and including time t. The response $\{z(t)\}$ can be found analytically as follows. Let the state vector be expressed in terms of the modal transformation matrix $[T_t]$ of the plant matrix $[A_t]$

$$\{z(t)\} = [T_t]\{\psi_t(t)\} \tag{5.2}$$

where $[T_t]$ is a $[2N \times 2N]$ matrix constructed from the eigenvectors of matrix $[A_t]$ as

$$[T_t] = \left[\{M_1\}, \{Y_1\}, \dots, \{M_j\}, \{Y_j\}, \dots, \{M_N\}, \{Y_N\} \right] \tag{5.3}$$

in which $\{M_j\}$ and $\{Y_j\}$ are the real and imaginary parts of the jth eigenvector of matrix $[A_t]$. Substituting Equation 5.2 in the state-equation, Equation 3.13, yields

$$[T_t]\{\dot{\psi}_t(t)\} = [A_t][T_t]\{\psi_t(t)\} + [B_t]\{u(t)\} + \{C_t\}\ddot{X}_g(t) \tag{5.4}$$

Premultiplying Equation 5.4 by $[T_t]^{-1}$ yields the modal state-equation as

$$\{\dot{\psi}_t(t)\} = [\varphi_t]\{\psi_t(t)\} + \{\Gamma(t)\} \tag{5.5}$$

where $[\varphi_t]$ is the modal plant matrix defined as

$$[\varphi_t] = [T_t]^{-1}[A_t][T_t] \tag{5.6}$$

81

and the vector $\{\Gamma(t)\}$ is made up of the control force and excitation terms

$$\{\Gamma(t)\} = [T_r]^{-1} [B_r] \{u(t)\} + [T_r]^{-1} \{C_r\} \ddot{X}_g(t) \tag{5.7}$$

The advantage of Equation 5.5 over the original state-equation, Equation 3.13, is that now the modal plant matrix is decoupled

$$[\varphi_r] = \begin{bmatrix} [\varphi_r]_1 & & & & \\ & [\varphi_r]_2 & & & \\ & & \ddots & & \\ & & & [\varphi_r]_j & \\ & & & & \ddots \\ & & & & & [\varphi_r]_N \end{bmatrix} \tag{5.8}$$

where each sub-matrix $[\varphi_r]_j$ is a $[2 \times 2]$ matrix given by

$$[\varphi_r]_j = \begin{bmatrix} \mu_j & \upsilon_j \\ -\upsilon_j & \mu_j \end{bmatrix}, \qquad j = 1, \dots, N \tag{5.9}$$

in which μ_j and υ_j are the real and imaginary parts, respectively, of the jth eigenvalue of matrix $[A_r]$. The initial conditions at time $t = 0$ are

$$\{\psi_r(t)\} = \{0\}, \qquad \{\overset{\bullet}{u}(0)\} = \{0\}, \qquad \ddot{X}_g(0) = 0 \tag{5.10}$$

The solution of Equation 5.5 is given by the integral

$$\{\psi_t(t)\} = \int_0^t \exp[[\varphi_t](t-\tau)] \ \{\Gamma(\tau)\} \, d\tau \tag{5.11}$$

where τ is a dummy variable of integration, and $\exp[[\varphi_t](t-\tau)]$ is a $[2N \times 2N]$ exponential matrix. Making use of the initial conditions, one can perform the integration of Equation 5.11 numerically by the trapezoidal rule. Let $t = n\Delta t$, then

$$\{\psi_t(t)\} = \sum_{l=1}^{n-1} \exp[[\varphi_t](n-l)\Delta t] \{\Gamma(l\Delta t)\} \Delta t \ + \ \{\Gamma(t)\}\left(\frac{\Delta t}{2}\right) \tag{5.12}$$

where Δt, is the time-increment. In order to simplify Equation 5.12 define the summation term as

$$\{\Lambda_t(t-\Delta t)\} = \sum_{l=1}^{n-1} \exp[[\varphi_t](n-l)\Delta t] \{\Gamma(l\Delta t)\} \Delta t \tag{5.13}$$

so that Equation 5.12 can be written in the form

$$\{\psi_t(t)\} = \{\Lambda_t(t-\Delta t)\} + \{\Gamma(t)\}\left(\frac{\Delta t}{2}\right) \tag{5.14}$$

It can be shown that the term $\{\Lambda(t)\}$ can be expressed in recurrent form using previous information as

$$\{\Lambda_t(t-\Delta t)\} = \exp[[\varphi_t]\Delta t] \ \{\{\Lambda_t(t-2\Delta t)\} + \{\Gamma(t-\Delta t)\}(\Delta t)\} \tag{5.15}$$

Substituting Equation 5.14 into Equation 5.2 we can recover the state-vector in physical coordinates as

$$\{z(t)\} = [T_t]\left\{ \{\Lambda_t(t-\Delta t)\} + \{\Gamma(t)\}\left(\frac{\Delta t}{2}\right) \right\} \tag{5.16}$$

In Equation 5.16, $\{\Lambda_t(t-\Delta t)\}$ is known from previous measurements up to $(t-\Delta t)$, and in order to evaluate $\{z(t)\}$ at time t, only one measurement of $\ddot{X}_g(t)$ is needed. The optimal control force $\{u^*(t)\}$ is obtained from the optimal control law.

This optimal control law is derived as follows. Substitute Equation 5.16 in the performance index of Equation 5.1, and in order to obtain the extremum, set the variation of $J_p(t)$ equal to zero

$$\delta J_p(t) \equiv 0 \tag{5.17}$$

The optimal control is obtained as

$$\{u^*(t)\} = [G_t]\{\Theta_t(t)\} \tag{5.18}$$

where

$$[G_t] = \left[[B_t]^T [Q][B_t] \left(\frac{\Delta t}{2}\right)^2 + [R] \right]^{-1} \tag{5.19}$$

$$\{\Theta_t(t)\} = -[B_t]^T [Q][T_t]\{\Lambda_t(t-\Delta t)\}\left(\frac{\Delta t}{2}\right) - [B_t]^T [Q]\{C_t\}\ddot{X}_g(t)\left(\frac{\Delta t}{2}\right)^2 \tag{5.20}$$

Thus the optimal control forces are computed from the measured base acceleration $\ddot{X}_g(t)$ and previous information at $(t-\Delta t)$, keeping the real-time on-line computational effort minimal. The response state-vector is obtained from Equation 5.16 after the optimal value of the control forces is obtained from Equation 5.18. The derivative of $\{z(t)\}$ is then obtained from Equation 3.13.

2. <u>Active Mass Damper System (AMD)</u>. The development for the active mass damper follows parallel lines to that for the active tendon. The state-equation, Equation 3.45, can be decoupled by using the modal transformation

$$\{z_D(t)\} = [T_d]\{\psi_d(t)\} \tag{5.21}$$

where $[T_d]$ is constructed from the eigenvectors of matrix $[A_d]$

$$[T_d] = \left[\{M_1\}, \{Y_1\}, \dots, , \{M_j\}, \{Y_j\}, \dots, \{\tilde{M}_N\}, \{Y_N\}, \{M_{N+1}\}, \{Y_{N+1}\} \right] \tag{5.22}$$

Note that now $[T_d]$ is a $[(2N+2) \times (2N+2)]$ matrix. Minimization of the instantaneous performance index

$$J_{Dp}(t) = \{z_D(t)\}^T [Q_D]\{z_D(t)\} + R_D u_d^2(t) \tag{5.23}$$

leads to the optimal control for the active mass damper

$$\dot{u_d}(t) = \frac{\Theta_m(t)}{\{B_d\}^T [Q_D]\{B_d\}\left(\frac{\Delta t}{2}\right)^2 + R_D} \tag{5.25}$$

$$\Theta_m(t) = -\{B_d\}^T [Q_D][T_d]\{\Lambda_d(t - \Delta t)\}\left(\frac{\Delta t}{2}\right) - \{B_d\}^T [Q_D]\{C_d\}\ddot{X}_g(t)\left(\frac{\Delta t}{2}\right)^2 \tag{5.26}$$

Note that $\{\Lambda_d(t - \Delta t)\}$ is similar to the expression for $\{\Lambda_t(t - \Delta t)\}$ but is of dimension $[(2N+2) \times 1]$.

D. INSTANTANEOUS CLOSED-LOOP ALGORITHM

The control forces are regulated by the feedback response state-vector $\{z(t)\}$ alone, i.e., the only measurements required are those of the response at time t. This can be done by placing displacement and velocity sensors at the floor levels. The structure and control system for this type of control are shown in Figure 4. There is a definite advantage of this algorithm for the case of wind excitations which are difficult to measure for application with the open-loop algorithm.

From the open-loop case we know that the state-equation, Equation 3.13, can be solved using the trapezoidal rule given by Equation 5.16. The optimal tendon control force vector $\{u^*(t)\}$ is to be derived that minimizes the instantaneous performance index of Equation 5.1 and satisfies the state-equation, Equation 5.16. The Lagrangian function is given by

$$LF = \{z(t)\}^T [Q] \{z(t)\} + \{u(t)\}^T [R] \{u(t)\} + \{\lambda(t)\}^T \left\{ \{z(t)\} - [T_r] \{\Lambda_r (t - \Delta t)\} - [T_r] \{\Gamma(t)\} \left(\frac{\Delta t}{2}\right) \right\} \tag{5.27}$$

Substituting $\{\Gamma(t)\}$ from Equation 5.7

$$LF = \{z(t)\}^T [Q] \{z(t)\} + \{u(t)\}^T [R] \{u(t)\} + \{\lambda(t)\}^T \left\{ \{z(t)\} - [T_r] \{\Lambda_r (t - \Delta t)\} - \left\{ [B_r] \{u(t)\} + \{C_r\} \ddot{X}_g(t) \right\} \left(\frac{\Delta t}{2}\right) \right\} \tag{5.28}$$

The necessary conditions for optimality are

$$\frac{\partial LF}{\partial \{z(t)\}} = \{0\} \quad \rightarrow \quad 2[Q]\{z(t)\} + \{\lambda(t)\} = \{0\} \tag{5.29}$$

$$\frac{\partial LF}{\partial \{u(t)\}} = \{0\} \quad \rightarrow \quad 2[R]\{u(t)\} - [B_r]^T \{\lambda(t)\} \left(\frac{\Delta t}{2}\right) = \{0\} \tag{5.30}$$

86

$$\{z(t)\} - [T_i]\{\Lambda_t(t - \Delta t)\} - \left\{[B_t]\{u(t)\} + \{C_t\}\ddot{X}_g(t)\right\}\left(\frac{\Delta t}{2}\right) = \{0\} \tag{5.31}$$

Solving for $\{u^{\bullet}(t)\}$ from Equations 5.29 through 5.31 one obtains the optimal control

$$\{u^{\bullet}(t)\} = -\left(\frac{\Delta t}{2}\right)[R]^{-1}[B_t]^T[Q]\{z(t)\} \tag{5.32}$$

Thus the optimal control forces are computed from the measured response. The response state-vector can be derived from Equation 5.16 as

$$\{z(t)\} = [\hat{\Xi}(t)]\{\hat{\xi}(t)\} \tag{5.33a}$$

$$[\hat{\Xi}(t)] = \left[[I] + \frac{(\Delta t)^2}{4}[B_t][R]^{-1}[B_t]^T[Q]\right]^{-1} \tag{5.33b}$$

$$\{\hat{\xi}(t)\} = \left\{[T_i]\{\Lambda_t(t - \Delta t)\} + \{C_t\}\ddot{X}_g(t)\left(\frac{\Delta t}{2}\right)\right\} \tag{5.33c}$$

and the derivative of $\{z(t)\}$ can be obtained from Equation 3.13.

The derivation for the active mass damper system follows parallel reasoning with the result

$$\dot{u}_d(t) = -\left(\frac{\Delta t}{2}\right)\left(\frac{1}{R_D}\right)\{B_d\}^T[Q_D]\{z_D(t)\} \tag{5.34}$$

The result for the response state-vector is similar to that of Equation 5.33.

E. INSTANTANEOUS OPEN-CLOSED-LOOP DISTURBANCE-COMPENSATED ALGORITHM

This algorithm requires the measurement of the ground excitation and the response. The structure and control system for this type of control are shown in Figure 6. The optimal control $\{u^*(t)\}$ is to be of the form

$$\{u(t)\} = [S1]\{z(t)\} + \{S2(t)\} \tag{5.35}$$

where $[S1]$ is a constant gain matrix, and $\{S2(t)\}$ a vector containing the measured excitation upto and including time t. The necessary conditions for optimality are the same as for the closed-loop case. Combining Equations 5.29 through 5.31 and Equation 5.35, it can be shown that the optimal control vector is of the form of Equation 5.35 with

$$[S1] = -\left(\frac{\Delta t}{4}\right)[R]^{-1}[B_t]^T\left[\ [I] + [Q][B_t][R]^{-1}[B_t]^T\frac{(\Delta t)^2}{8}\ \right]^{-1}[Q] \tag{5.36}$$

$$\{S2(t)\} = [S1]\left\{ [T_t]\{\Lambda_t(t-\Delta t)\} + \{C_t\}\ddot{X}_g(t)\left(\frac{\Delta t}{2}\right) \right\} \tag{5.37}$$

The response state-vector can be derived from Equation 5.16 as

$$\{z(t)\} = [\hat{\Psi}(t)]\{\hat{\xi}(t)\} \tag{5.38a}$$

$$[\hat{\Psi}(t)] = \left[\ [I] - [B_t][S1]\left(\frac{\Delta t}{2}\right)\ \right]^{-1}\left[\ [I] + [B_t][S1]\left(\frac{\Delta t}{2}\right)\ \right] \tag{5.38b}$$

$$\{\hat{\xi}(t)\} = \left\{ [T_t]\{\Lambda_t(t-\Delta t)\} + \{C_t\}\ddot{X}_g(t)\left(\frac{\Delta t}{2}\right) \right\} \tag{5.38c}$$

and the derivative of $\{z(t)\}$ can be obtained from Equation 3.13. The derivation for the AMD yields

$$u_d^{\bullet}(t) \;=\; \{S1_d\}^T \{z_D(t)\} + S2_d(t) \tag{5.39}$$

where

$$\{S1_d\}^T \;=\; -\left(\frac{\Delta t}{4R_D}\right) \{B_d\}^T \left[\; [\,I\,] + \frac{[Q_D]\,\{B_d\}\,\{B_d\}^T (\Delta t)^2}{8R_D} \right]^{-1} [Q_D] \tag{5.40}$$

$$S2_d(t) \;=\; \{S1_d\}^T \left\{ [T_d]\,\{\Lambda_d(t-\Delta t)\} + \{C_d\}\,\ddot{X}_g(t)\left(\frac{\Delta t}{2}\right) \right\} \tag{5.41}$$

The response state-vector can be derived similar to Equation 5.38.

F.   COMPARISON OF INSTANTANEOUS OPTIMAL CONTROL ALGORITHMS

The instantaneous algorithms are compared in this example. All three algorithms, i.e., the open-loop, closed-loop and open-closed-loop algorithms were derived based on different assumptions concerning the nature of the signal which creates the control forces. In the open-loop case the control forces depend on the measured excitation, in the closed-loop case on the measured response, and in the open-closed-loop case on both the measured response and excitation. For simulation results one has to input the excitation in order to get the response. Similarly the measured response is assumed to be known in order to calculate the control forces. Therefore all three control schemes should yield the same answer. This fact was confirmed by extensive results carried out on an eight-story shear building, equipped with eight active tendons, for both wind and earthquake excitations. The instantaneous open-loop and closed-loop algorithms were compared, and the results were identical.

G. COMPARISON OF RICATTI AND INSTANTANEOUS OPTIMAL ALGORITHMS

The Ricatti closed-loop and instantaneous algorithms are compared in this example. Theoretically both algorithms should yield the same results, as was mentioned in Section F of this Chapter. However, the Ricatti closed-loop algorithm was derived based on an integral rather than an instantaneous performance index. Consequently the gain matrix, which depends on the solution of the ARE, is of different form than that of the instantaneous algorithms. As a consequence, different control forces and different responses are obtained. However, by modifying the weighting matrices, approximately equal control forces and response can be obtained for the two schemes. Hence the two schemes of Ricatti and instantaneous algorithms can be compared. An eight-story shear building with eight active tendons is the model for this example. The structural properties are: $m_j = 105\,Mg$, $k_j = 1 \times 10^5\,kN/m$, $j = 1,\dots,8$, and three percent critical damping. The earthquake excitation used is the N-S component of the El-Centro earthquake ground acceleration of May 18, 1940, shown in Figure 23. The weighting matrices, $[Q]$ and $[R]$, are considered to be diagonal in this example. For the Ricatti closed-loop algorithm, the following were chosen: $Q(l,l) = 1000$, $l = 1,\dots,16$, and $R(i,i) = 0.13 \times 10^{-3}$, $i = 1,\dots,8$. For the instantaneous algorithm the elements of $[Q]$ and $[R]$ were found by trial and error as: $Q(l,l) = 1 \times 10^5$, $l = 1,\dots,16$, and $R(1,1) = 0.50 \times 10^{-3}$, $R(2,2) = 0.44 \times 10^{-3}$, $R(3,3) = 0.41 \times 10^{-3}$, $R(4,4) = 0.31 \times 10^{-3}$, $R(5,5) = 0.24 \times 10^{-3}$,

90
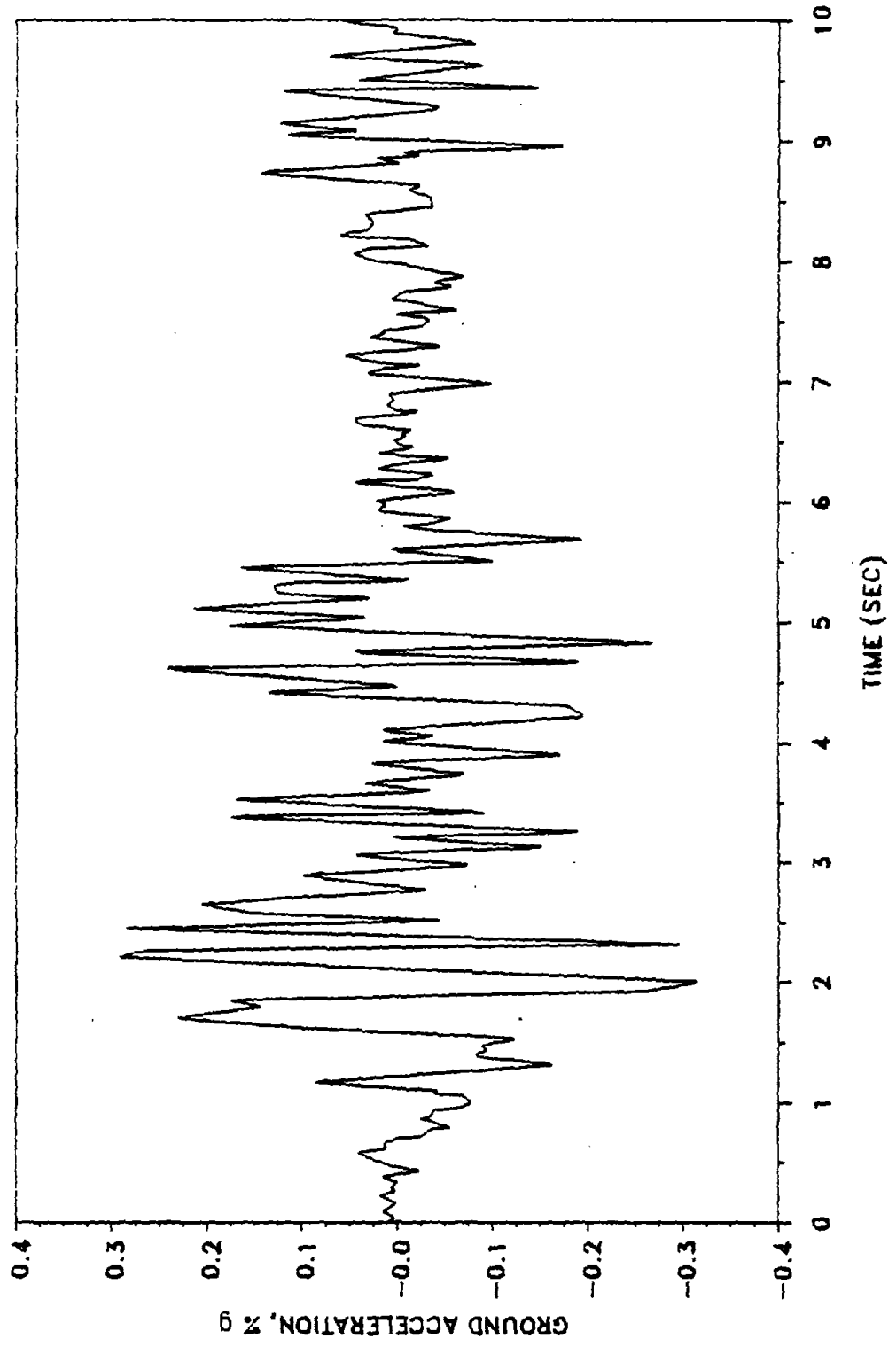
Figure 23. N-S Component of El-Centro Earthquake of May 18, 1940

$R(6,6) = 0.15 \times 10^{-3}$, $R(7,7) = 0.80 \times 10^{-4}$, $R(8,8) = 0.20 \times 10^{-4}$. The maxima of the control forces using the above chosen weighting matrices are approximately equal. A comparison of the eighth floor relative displacement, using the two schemes, is shown in Figure 24. Figure 25 shows a comparison of the eighth floor control force. It can be observed that almost identical results are obtained.

H.   HUMAN COMFORT ENHANCEMENT IN WIND-EXCITED STRUCTURES

The equations of motion and optimal control expressions for wind forces for a structure equipped with the AT or AMD systems are the same as for earthquake forces except that two changes have to be made. First the relative displacements, velocities and accelerations have to be replaced by their absolute counterparts. Secondly, the forcing function instead of the earthquake acceleration, $\{C_i\}\ddot{X}_g(t)$, has to be replaced by the discretized wind forces vector $\{W(t)\}$ which was derived in Appendix B. The optimal control laws for both the AT and AMD systems have the same form as for the earthquake excitation.

An eight-story shear building is considered for analysis under the artificial wind loads. The structural properties of the building are: $m_j = 105\,Mg$, $k_j = 1 \times 10^5\,kN/m$, $j = 1,...,8$, and three percent critical damping. The tributary area for each floor is $100\,m^2$, and the interstory height $h_j = 4\,m$. The instantaneous algorithms were applied for two cases. In the first case, eight tendons were assumed to be acting, one on each floor.   The weighting matrices were assumed diagonal with the values: $Q(l,l) = 1.0 \times 10^5$, $l = 1,...,16$, and $R(i,i) = 0.9 \times 10^{-3}$, $i = 1,...,8$. A sample of the artificial wind load which was created based on the
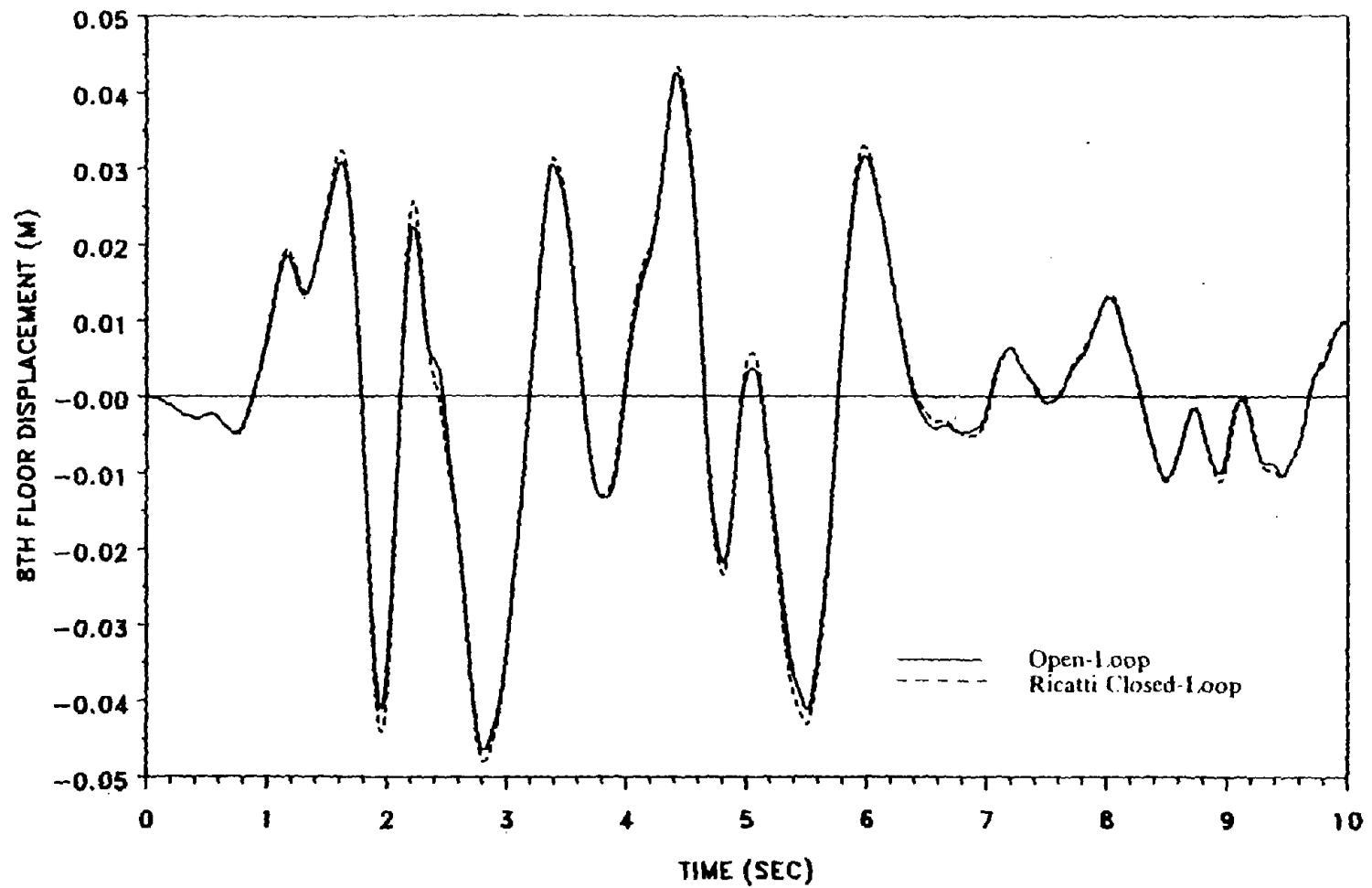
Figure 24. Comparison of Eighth Floor Relative Displacement for

94
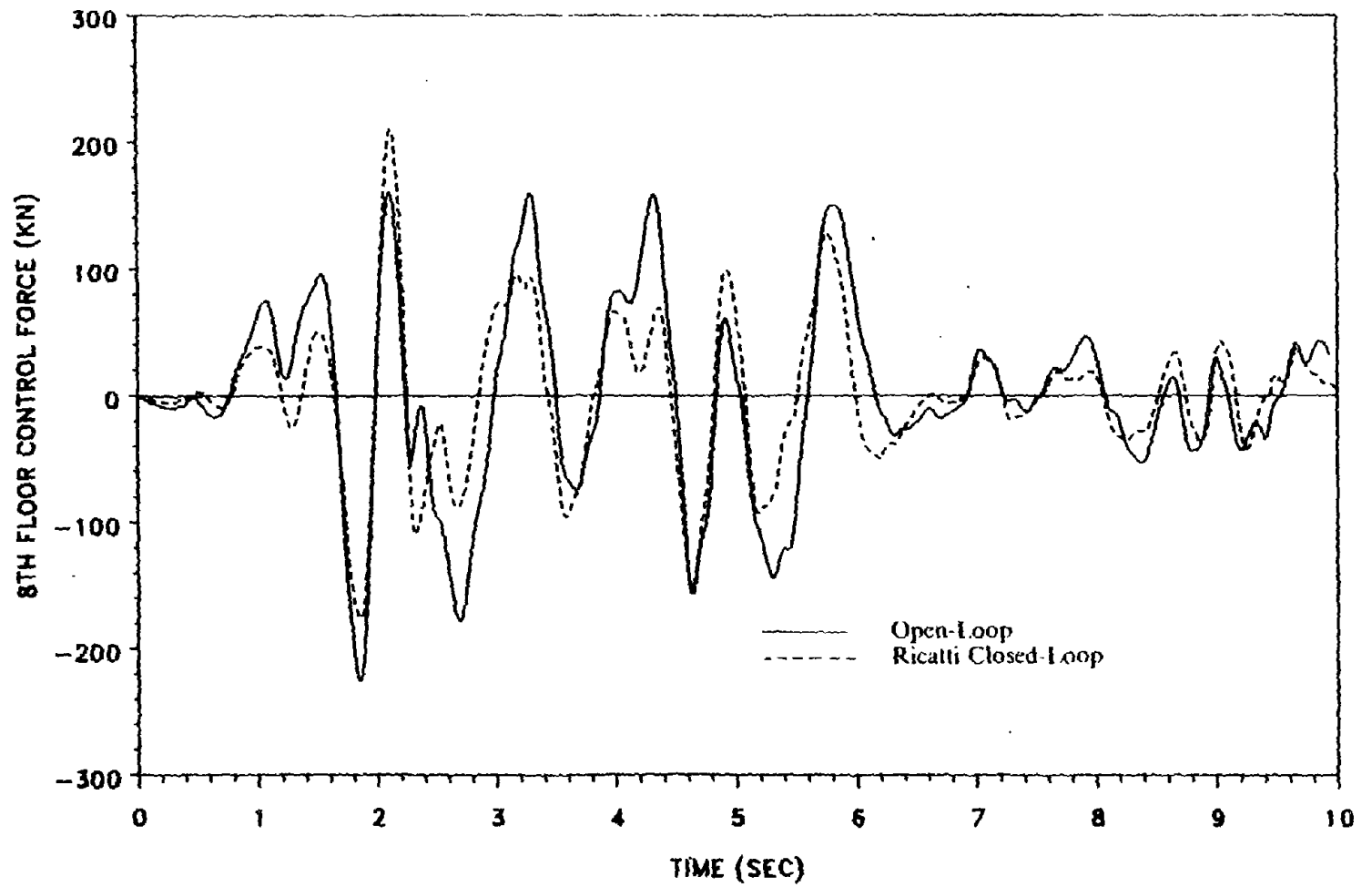
Figure 25. Comparison of Eighth Floor Control Force for

derivation of Appendix B is given in Figure 26. Figure 27 shows the wind pressure transducer proposed by Mayne (36) to measure wind pressures on buildings. The device was used by Lam and Lam (28) in full-scale tests to assess the wind loads on the claddings of high-rise buildings. The eighth floor displacement with and without the tendons is compared in Figure 28. Figure 29 shows the acceleration response for the controlled and uncontrolled cases. It may be observed that the response is significantly reduced in magnitude. According to criteria for human comfort from studies by Chang (5), and Warwaruk (59), the comfort limits are defined in Table II. From Figure 29 one can observe that the eighth floor acceleration is reduced from the "annoying" to the "perceptible" range. The second case is the same building equipped with only an active mass damper, having the following properties: $m_d = 5\,Mg$, $k_d = 10\,kN/m$, and $c_d = 0.7\,Mg/\sec$. The acceleration response of the eighth floor to the wind excitation is compared to the uncontrolled case in Figure 30. Again it is observed that the acceleration is reduced from the "annoying" to the "perceptible" range.

I. WEIGHTING MATRICES

From the Ricatti closed-loop and instantaneous algorithms it is obvious that the control forces vector is a function of the weighting matrices $[Q]$ and $[R]$. These matrices are assumed constant. Thus the level of the control forces depends on these matrices. As can be seen from Equations 3.30, 5.19, 5.32, and 5.40 for a fixed matrix $[Q]$, if $[R]$ is reduced, then the control force increases. This behavior is
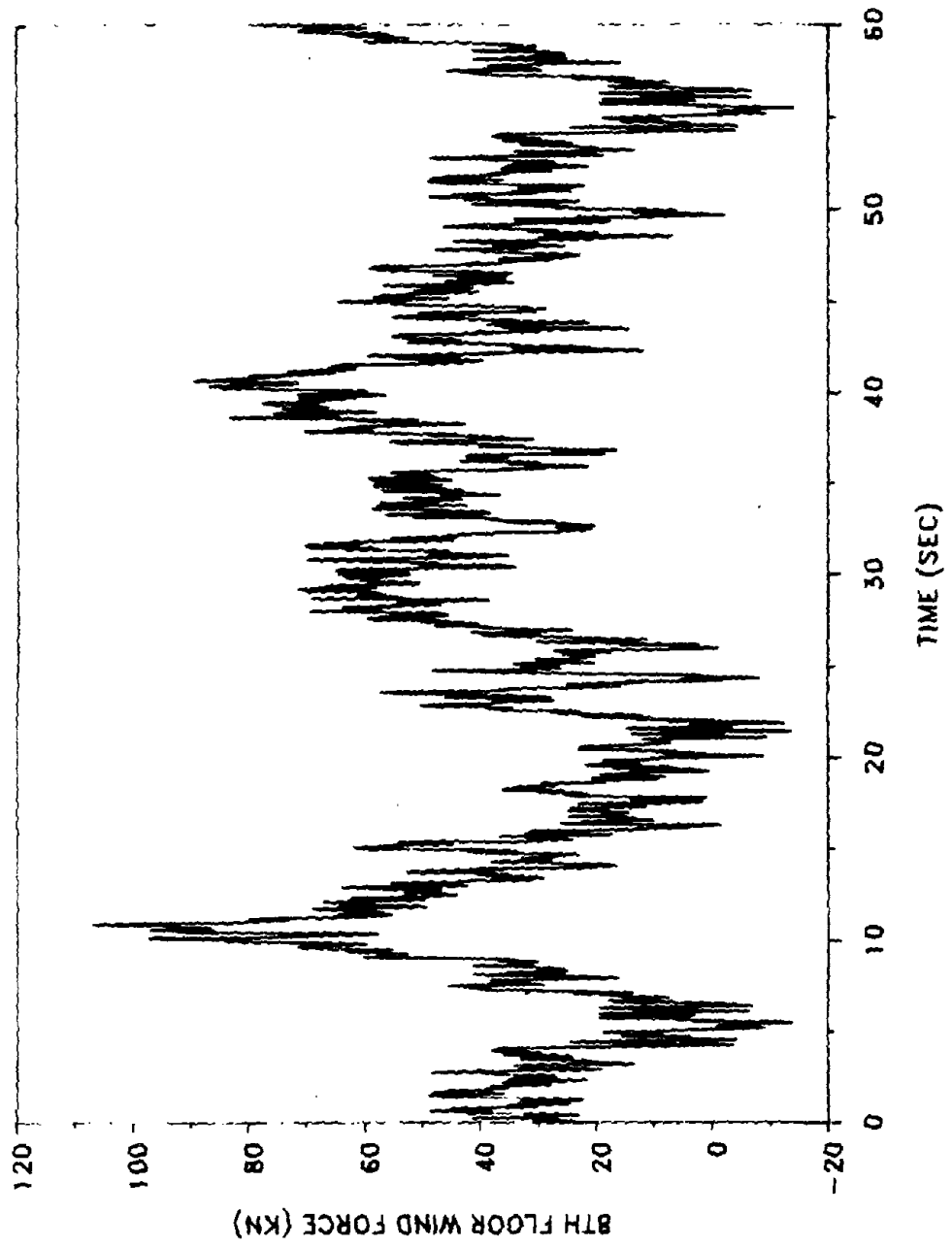
Figure 26. Eighth Floor Wind Force
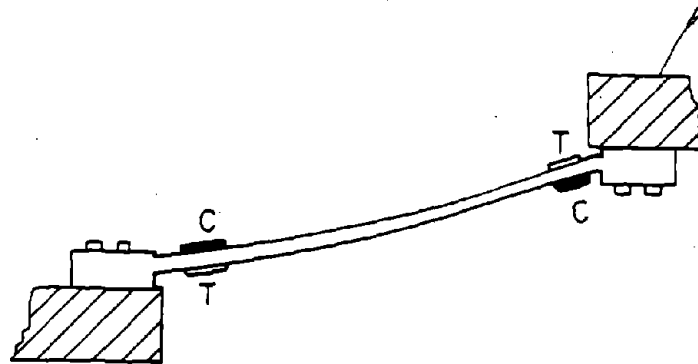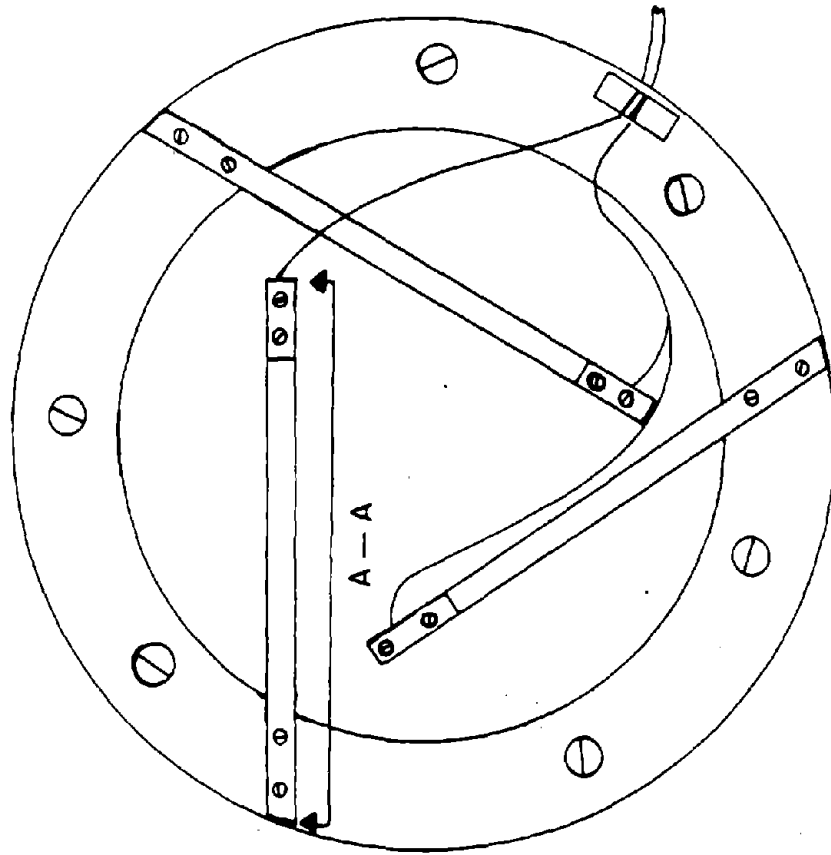
SECTION   A — A

Figure 27.   Wind Pressure Transducer

0.06

0.04

0.02

8TH FLOOR DISPLACEMENT (M)

-0.00

-0.02

No Control
Eight AT

-0.04

0   10   20   30   40   50   60

TIME (SEC)
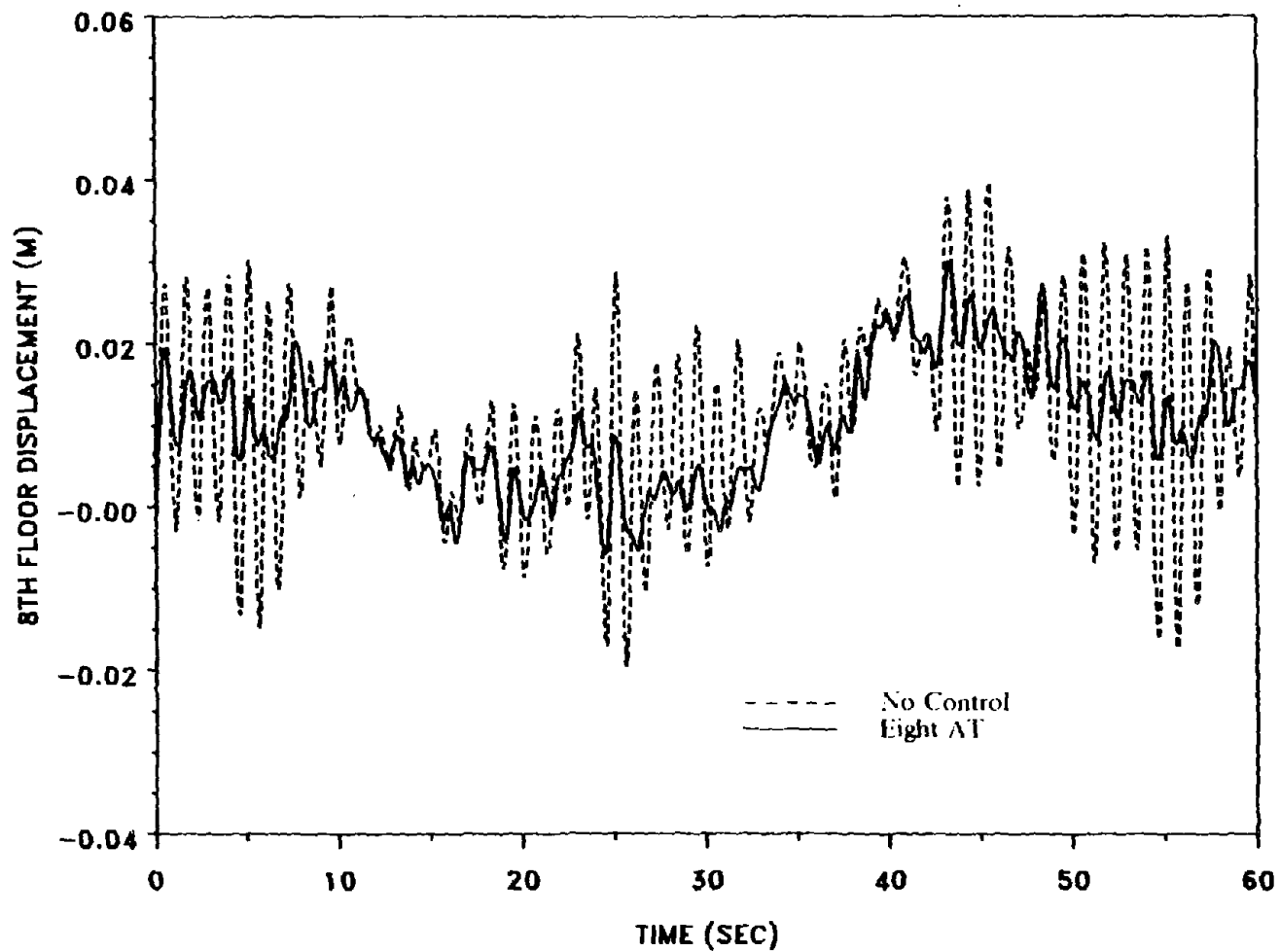
Figure   28.   Comparison of Eighth Floor Displacement for Active
Tendons System under Wind Forces
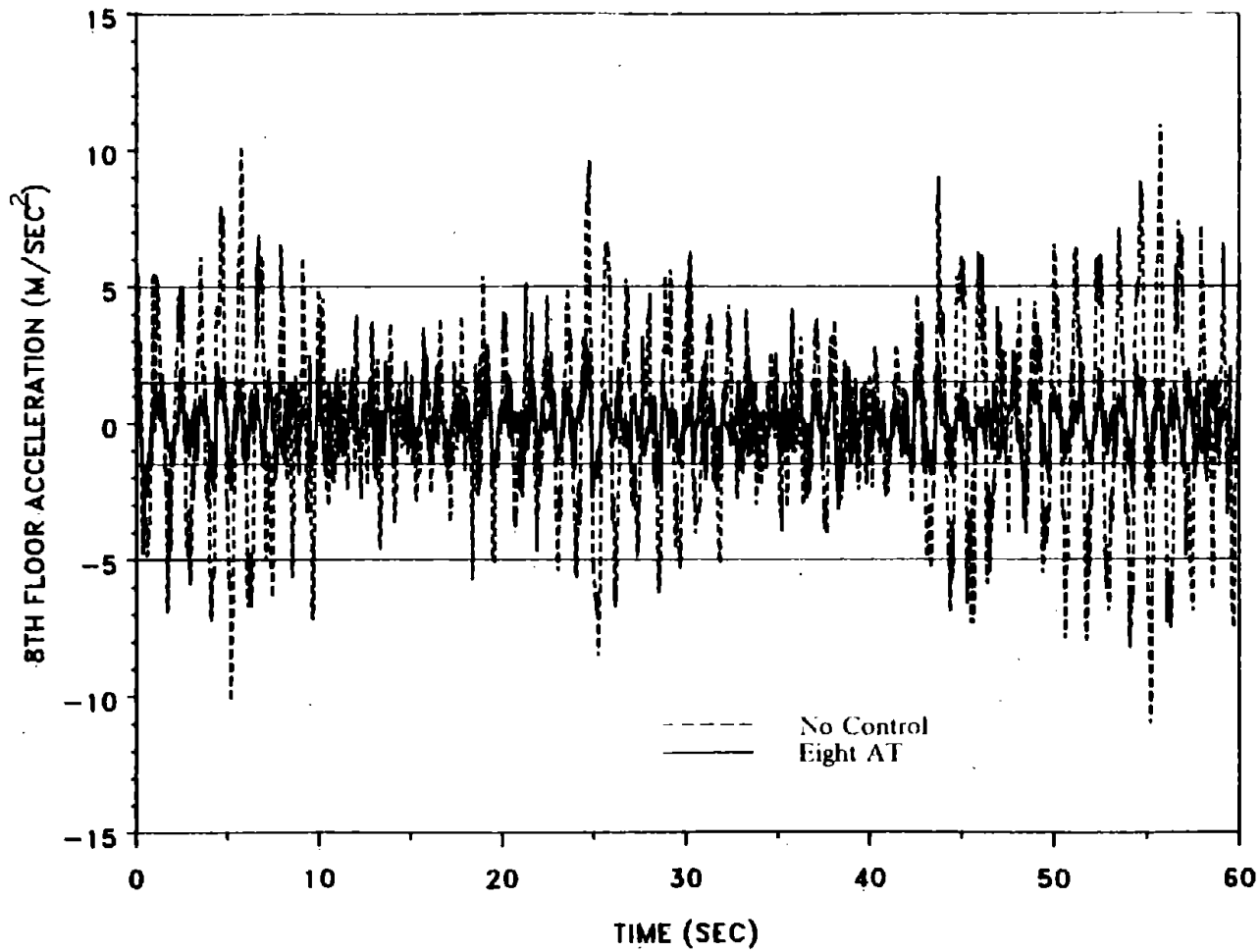
Figure 29. Comparison of Eighth Floor Acceleration for Active
Tendons System under Wind Forces

TABLE II. HUMAN COMFORT CRITERIA

Range	Comfort Limit	Acceleration, %g
A.	Not Percreptible	< 0.5
B.	Perceptible	0.5 - 1.5
C.	Annoying	1.5 - 5.0
D.	Very Annoying	5.0 - 15.0
E.	Intolerable	> 15.0
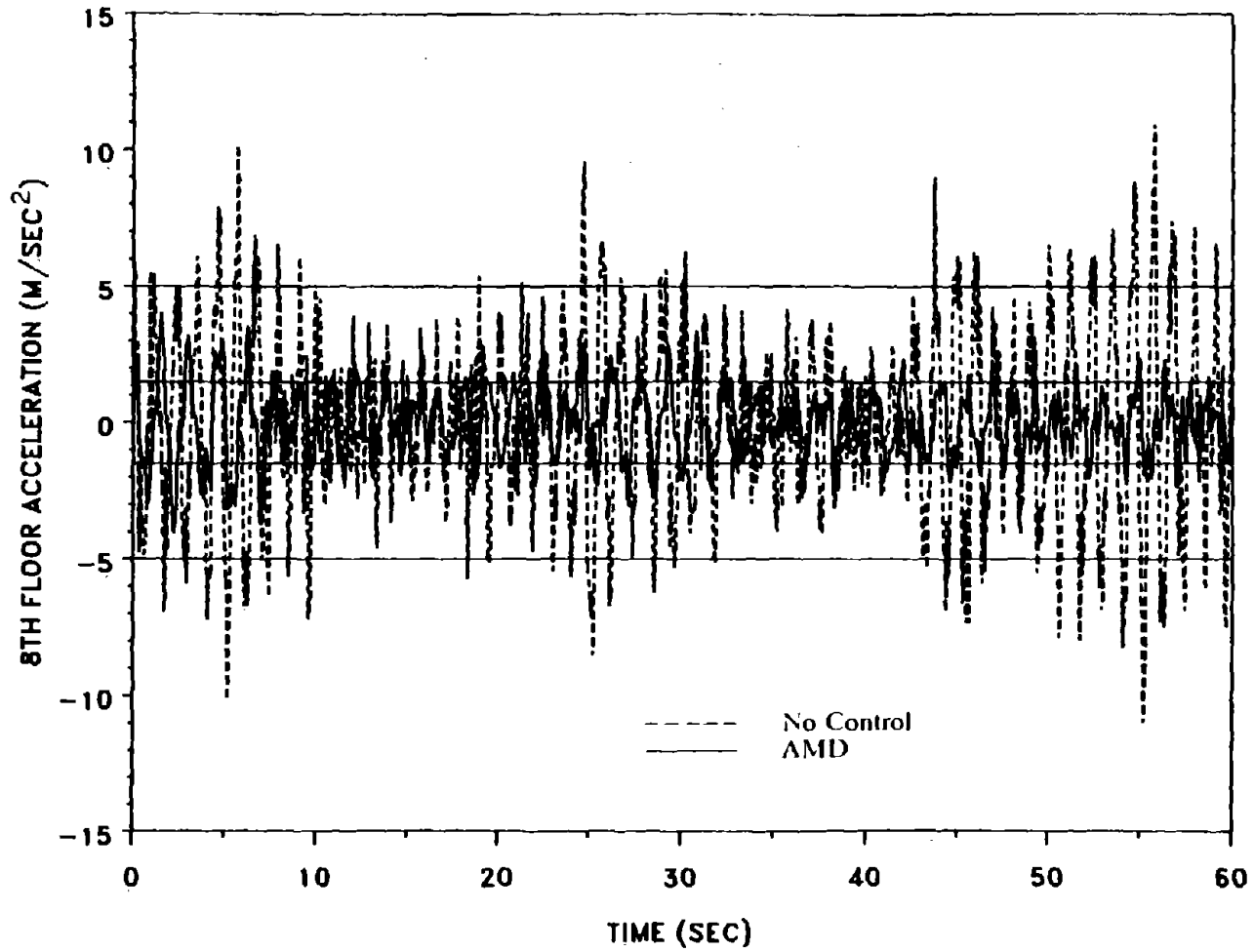
Figure 30. Comparison of Eighth Floor Acceleration for Active
Mass Damper under Wind Forces

demonstrated by the following example. The eight-story structure of the previous Section, with the same structural properties, is equipped with eight tendons. Both weighting matrices $[Q]$ and $[R]$ are assumed diagonal. The diagonal elements of matrix $[Q]$ are all set equal to the value $Q(l,l) = 1. \times 10^5$, $l = 1, ..., 16$, and the diagonal elements of the $[R]$ matrix are all set equal and allowed to vary as shown in Figure 31. In Figure 31 the maxima of the first, fourth, and eighth floor control forces and floor displacements are shown. It is observed that with decreasing values of $R(i,i)$, the displacements decrease but the control forces increase. Hence different levels of control can be achieved by varying the elements of the weighting matrices. In physical terms this implies that the amplifier gains of the control devices must be established according to these weighting matrices. The subject of searching for the optimal weighting matrices that will produce the minimum control forces is treated in Chapter VII.
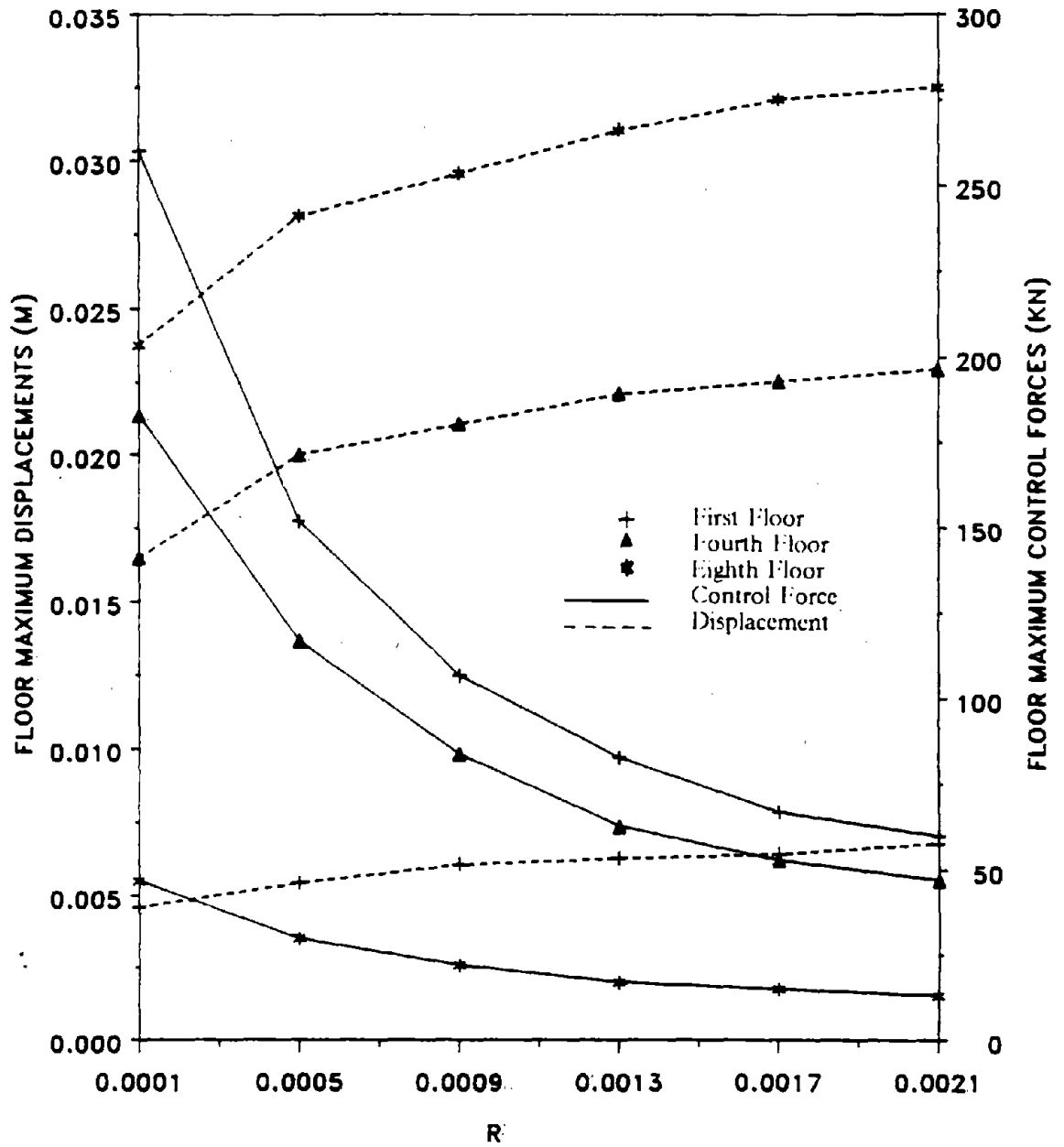
Figure 31. Variation of Control Forces and Floor Displacements with Weighting Matrices

103

VI. STRUCTURAL OPTIMIZATION USING ACTIVE CONTROL

The structural optimization procedure is described for both the non-optimal closed-loop and optimal control algorithms. The objective function is structural weight and is the same for both optimal and non-optimal control algorithms. The design variables for the non-optimal control include the structure's floor stiffnesses and the normalized loop and feedback gains of the control system. The constraints are expressed in terms of the standard deviations of floor relative displacements and control forces. The design variables for the optimal control algorithms are the structure's floor stiffnesses. The constraints are expressed in terms of the maximum floor relative displacements and maximum control forces.

A. OBJECTIVE FUNCTION

The objective function for both optimal and non-optimal control algorithms is approximated by a linear structural weight function given by

$$W = a + \sum_{j=1}^{N} b_j k_j \tag{6.1}$$

where W is the structural weight of the building and k_j the floor stiffnesses, assumed to be in the elastic range. The constants a, and b_j are chosen to approximate the actual relationship between the structural weight and structural stiffness based on structural member properties.

B. FORMULATION OF OPTIMIZATION PROBLEM

The formulation of the optimization problem is different for the optimal and non-optimal algorithms. The design variables for the non-optimal algorithm include the control parameters of normalized loop and feedback gains in addition to the floor stiffnesses.

1. Non-optimal Closed-loop Control. The structural optimization problem for the non-optimal closed-loop algorithm is formulated as follows: Find k_j, τ_{ti}, ε_{ti}, τ_d, ε_d that will minimize the structural weight W of Equation 6.1, subject to the following constraints

$$\sigma_{xj} \leq \sigma_{xj} \, \text{max} \qquad j = 1, \dots, N \qquad\qquad (6.2)$$

$$\sigma_{ti} \leq \sigma_{ti} \, \text{max} \qquad i = 1, \dots, M \qquad\qquad (6.3)$$

$$\sigma_d \leq \sigma_d \, \text{max} \qquad\qquad\qquad\qquad (6.4)$$

$$k_j \geq k \, \text{min} \qquad j = 1, \dots, N \qquad\qquad (6.5)$$

$$\tau_{ti} \leq \tau \, \text{max} \qquad i = 1, \dots, M \qquad\qquad (6.6)$$

$$\varepsilon_{ti} \leq \varepsilon \, \text{max} \qquad i = 1, \dots, M \qquad\qquad (6.7)$$

$$\tau_d \leq \tau \, \text{max} \qquad\qquad\qquad\qquad (6.8)$$

$$\varepsilon_d \leq \varepsilon \, \text{max} \qquad\qquad\qquad\qquad (6.9)$$

where σ_{xj} and σ_{xj} max are the standard deviations of the relative displacement of the jth floor and the allowable displacement, respectively. The quantity σ_{xj} can be obtained from the response statistics of Equation 4.20. The quantities σ_{ti}, and σ_{ti} max are,

105

respectively, the standard deviations of the ith tendon active control force given by Equation 4.21 and the allowable. Similarly σ_d and σ_d max are, respectively, the standard deviations of the active mass damper control force given in Equation 4.22 and the allowable. Side constraints are imposed on the floor elastic stiffnesses k min, and the normalized feedback and loop gains of the active tendon and active mass damper systems. The number of floors is N and the number of tendon controllers is M. The implementation of standard deviation expressed in the constraints is in the sense that for a given maximum displacement and a probability of not exceeding that value, the standard deviation of the displacement can be obtained. A Gaussian probability distribution is assumed.

2. <u>Optimal Control Algorithms</u>. The structural optimization problem for the optimal control algorithms is formulated as follows: Find k_j, that will minimize the structural weight of Equation 6.1, subject to the following constraints

$$x_j(t) \leq x_j \text{ max} \qquad j = 1, \dots, N \qquad (6.10)$$

$$u_i(t) \leq u_i \text{ max} \qquad i = 1, \dots, M \qquad (6.11)$$

$$u_d(t) \leq u_d \text{ max} \qquad (6.12)$$

$$k_j \geq k \text{ min} \qquad j = 1, \dots, N \qquad (6.13)$$

where $x_j(t)$, and x_j max are the relative displacement of the jth floor and the maximum allowable, respectively. The ith active tendon control force and the maximum allowable are denoted by $u_i(t)$ and u_i max, repectively.

106

The active mass damper control force and the maximum allowable are denoted by $u_d(t)$ and u_d max, repectively.

C. OPTIMUM STRUCTURE USING NON-OPTIMAL CLOSED-LOOP CONTROL

1. Example 1: Two-story Building. The optimization procedure is applied to a two-story building shown in Figure 32 for earthquake excitation. The objective is to find the minimum structural weight that satisfies the imposed constraints. The design variables are the floor stiffnesses, and the normalized loop and feedback gains. Three case studies are made. In Case A, the structure is equipped with two active tendons whose stiffness k_t is allowed to vary according to the variation of the jth floor stiffness, k_j, in the optimization procedure as $k_t = 0.05 k_j$. In Case B, the stiffness of the tendons is fixed at $k_t = 40 \, kips/in \ (7000 \, kN/m)$. In Case C, an active mass damper is included in addition to the two tendons. The earthquake excitation used is that of Equation 4.1, of the Kanai-Tajimi spectral density function, with the following parameters: $\omega_g = 18.85 \, rad/sec$, $\zeta_g = 0.65$, and $S^2 = 4.65 \times 10^{-4} \, m^2/sec^3/rad$. The structural properties for all three Cases are: $m_1 = m_2 = 2 \, kip - sec^2/in \ (350 \, Mg)$, $c_1 = c_2 = 1.6 \, kip - sec/in \ (280 \, Mg/sec)$, $\theta = 25 \, degrees$. The active mass damper parameters for Case C are: $m_d = 0.04 \, kip - sec^2/in \ (7 \, Mg)$, $k_d = 6.11 \, kip/in \ (1070 \, kN/m)$, $c_d = 0.10 \, kip - sec/in \ (17.5 \, Mg/sec)$, and $k_{md} = 25 \, kip/in \ (4378 \, kN/m)$. The constraints for all three cases are: σ_{x1} max $= 0.035 \, in \ (0.89 \, mm)$, σ_{x2} max $= 0.070 \, in \ (1.78 \, mm)$, σ_{t1} max $= \sigma_{t2}$ max $= 10 \, kips \ (44.48 \, kN)$, τ max $= \varepsilon$ max $= 10$. Additional constraints are imposed for Case C as $\tau_d \leq 6$, and $\varepsilon_d \leq 6$.
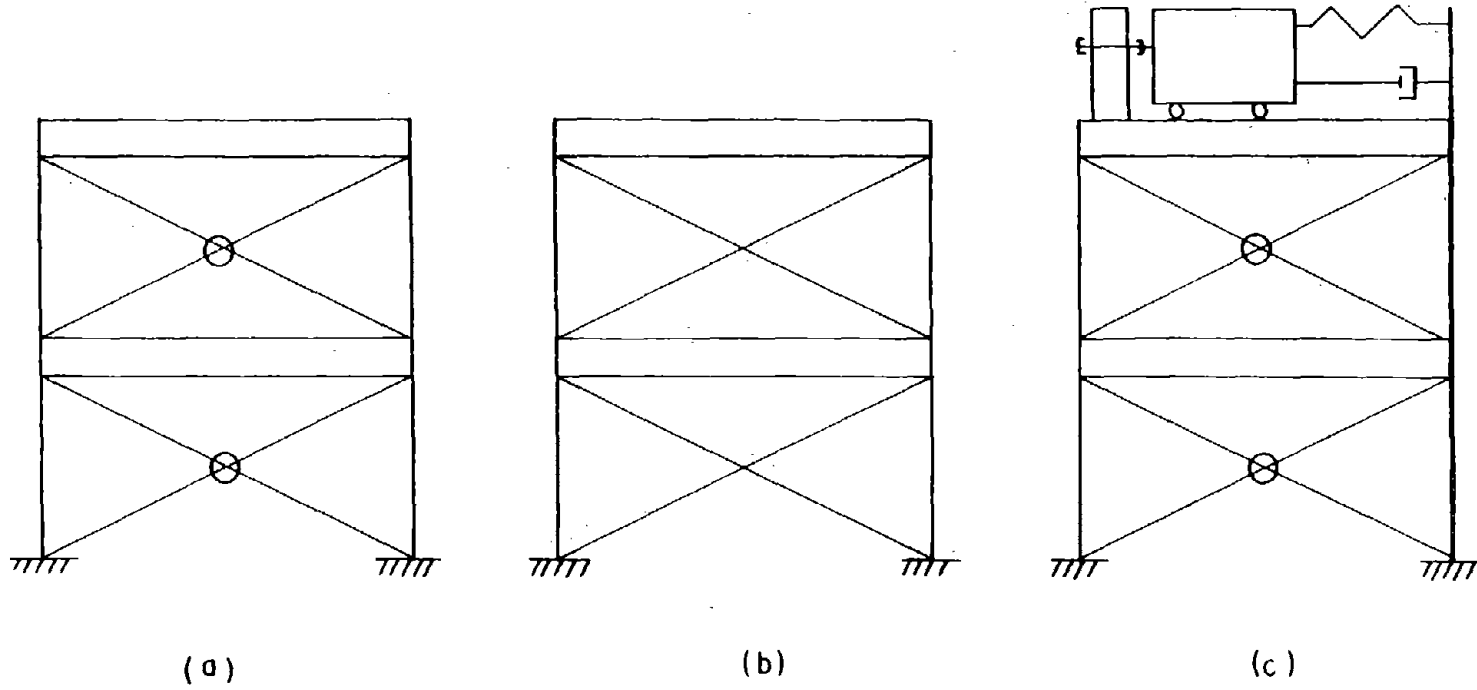
Figure 32. Two-story Shear Building:
(a) Case A, (b) Case B, (c) Case C

From Figures 33 and 34, one can observe that Case C gives the least structural weight. From Figure 35, it is evident that the active tendon control forces of Case B require a larger τ_l. The ε_l values, however, reach upper bound for all three cases as shown in Figure 36. The same active tendon control force standard deviations are obtained at the optimum for all three cases. In Case C, τ_d reaches an upper bound, whereas ε_d goes to a small value, as shown in Figure 37. In all three cases, the displacement constraint of the second floor and the control force constraints are active. The difference between Case A and Case B is very small, in terms of the structural weight. It appears that the combined active tendon and active mass damper system is advantageous over the other two cases.

2. **Example 2: Eight-story Building.** The three active control system models described in Chapter IV, i.e. the active tendon, active mass damper, and combined active mass damper and tendons are compared in this example. The eight-story structure is first optimized, subjected to the earthquake excitation without any active control system (Case 1); in Case 2 the structure is equipped with eight active tendons; in Case 3 the structure is equipped with an active mass damper on the top floor, and in Case 4 the structure is equipped with an active mass damper and two active tendons at the two bottom floors. All four cases are shown in Figure 38. The design variables are floor stiffnesses, and normalized loop and feedback gains. The structural properties are: $m_j = 314\,Mg$, $k_j = 3 \times 10^5\,kN/m$, $c_j = 90\,Mg/\sec$, $j = 1,...,8$. The earthquake excitation is that of the Kanai-Tajimi function, given
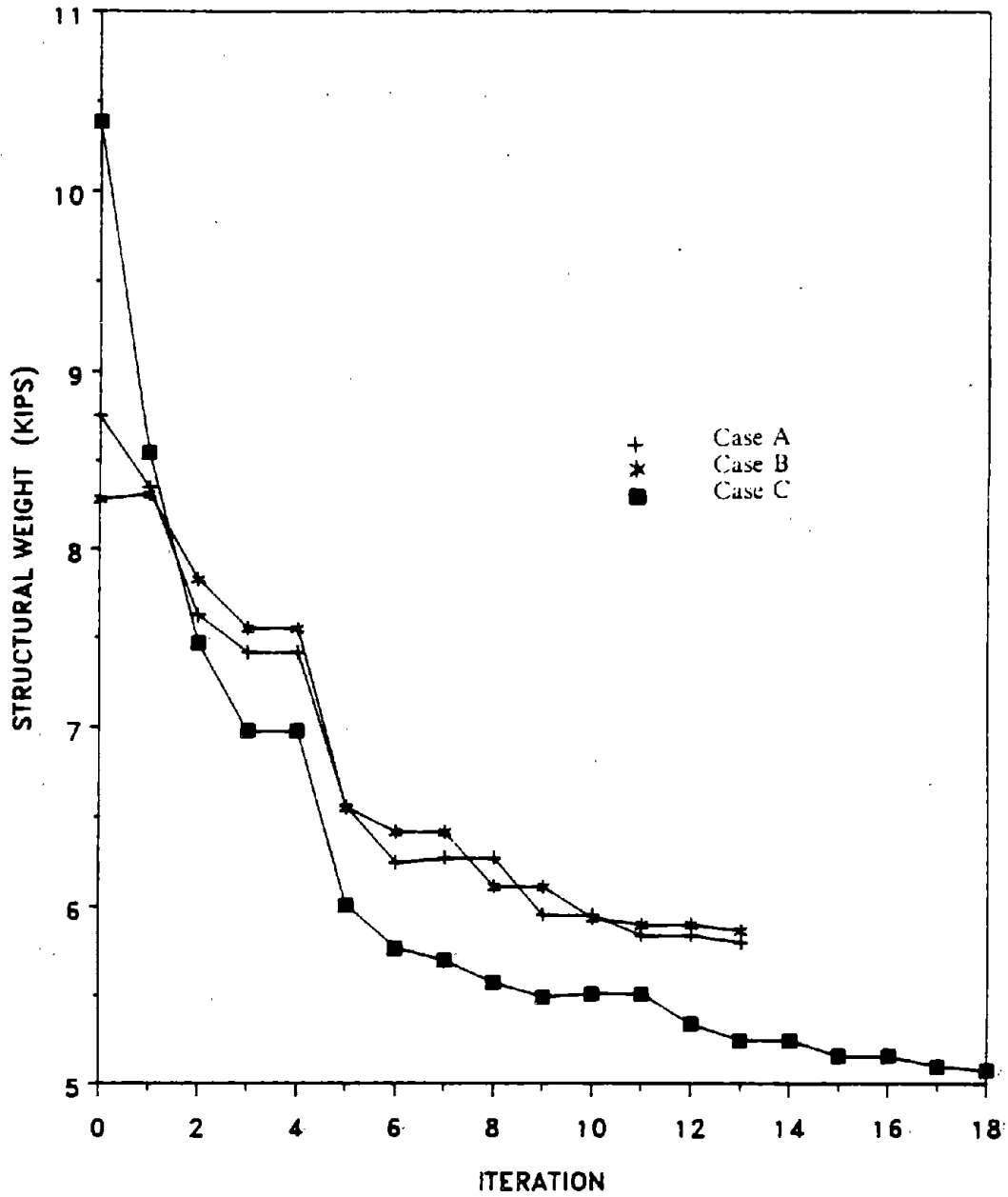
Figure 33.   Structural Weight for Cases A, B, and C
(1 kip = 4.45 kN)

110
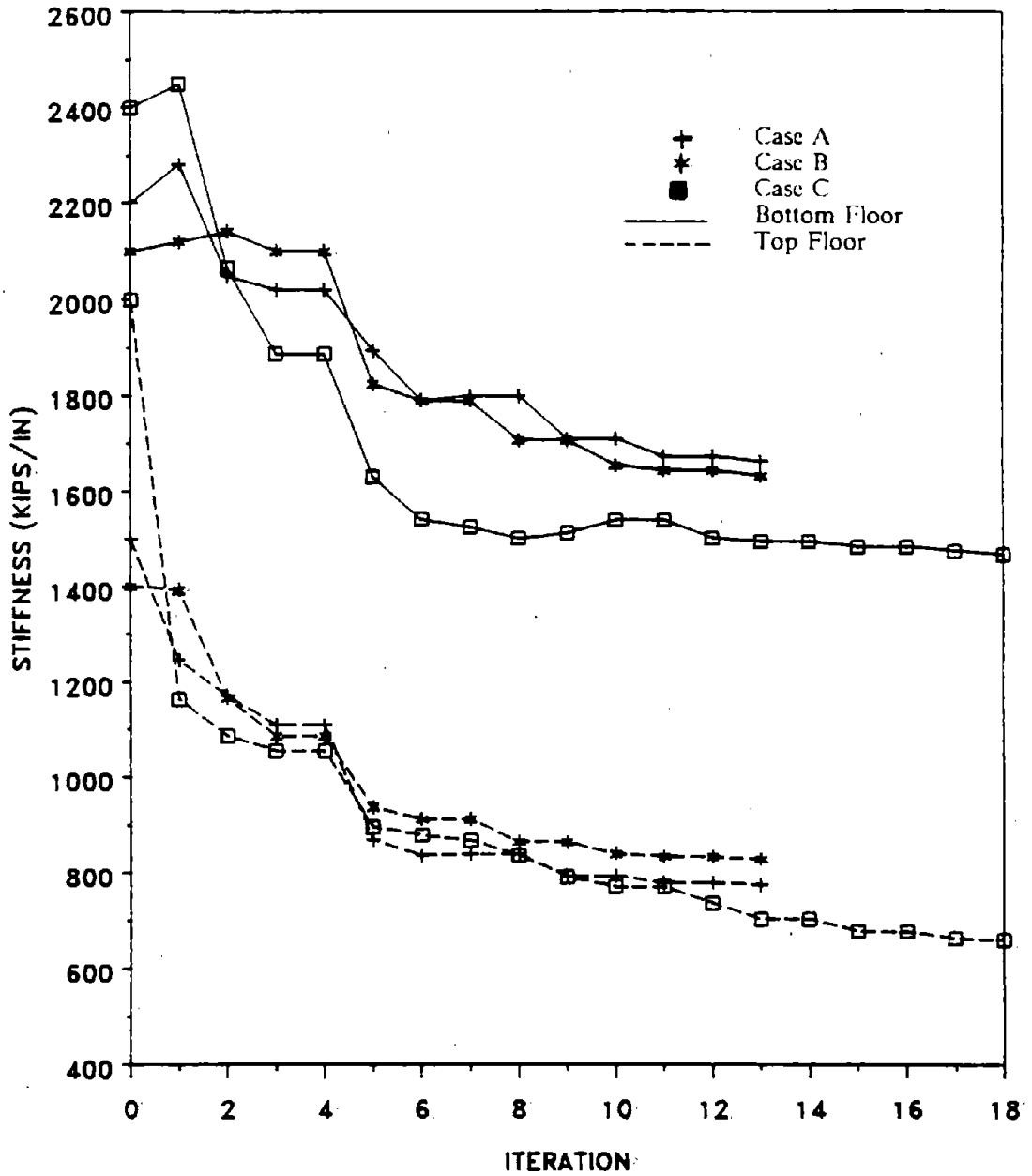
Figure 34. Structural Stiffness for Cases A, B, and C
(1 kip/in = 175.1 kN/m)
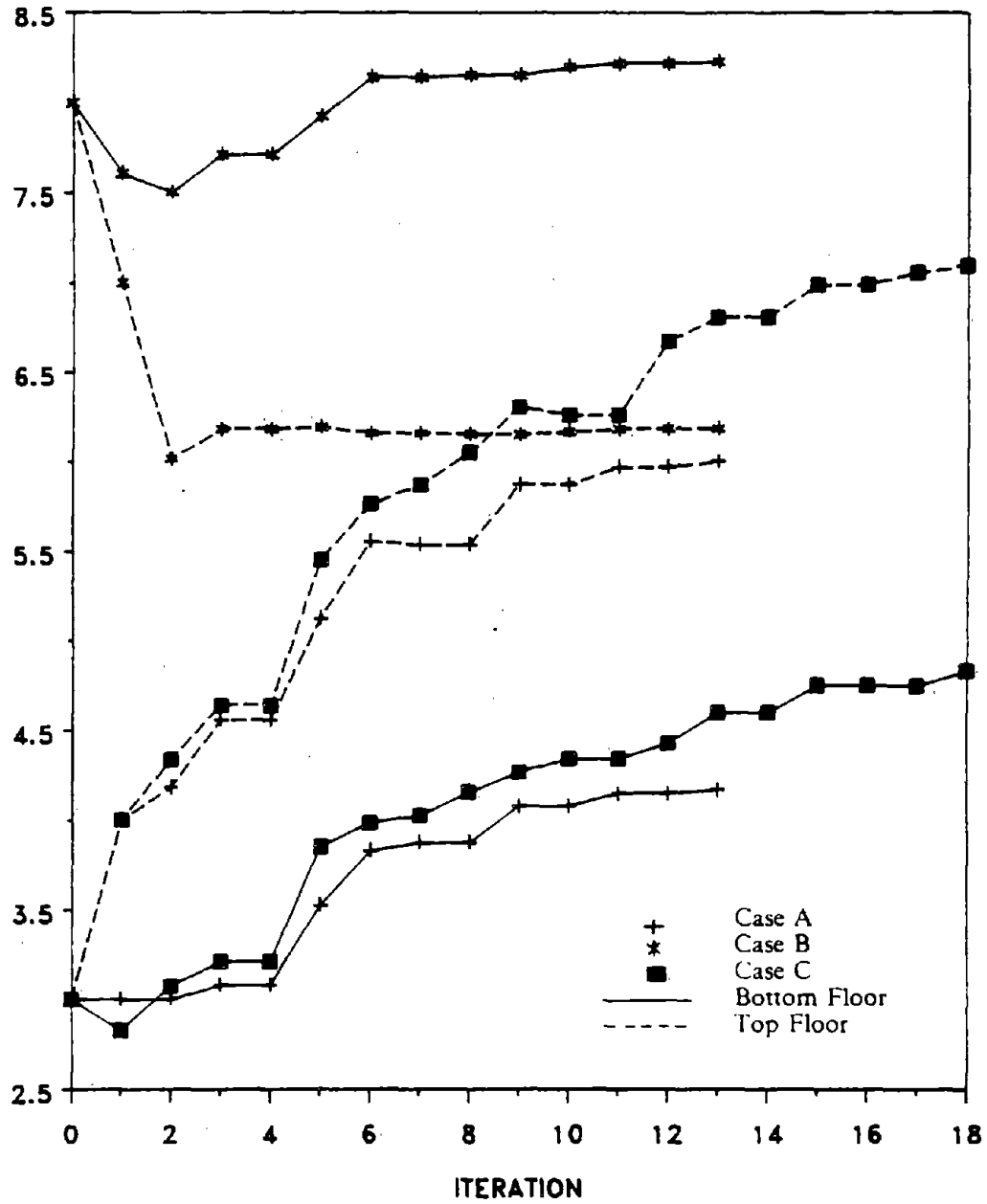
Figure 35. Normalized Feedback Gain of Active Tendons
for Cases A, B, and C
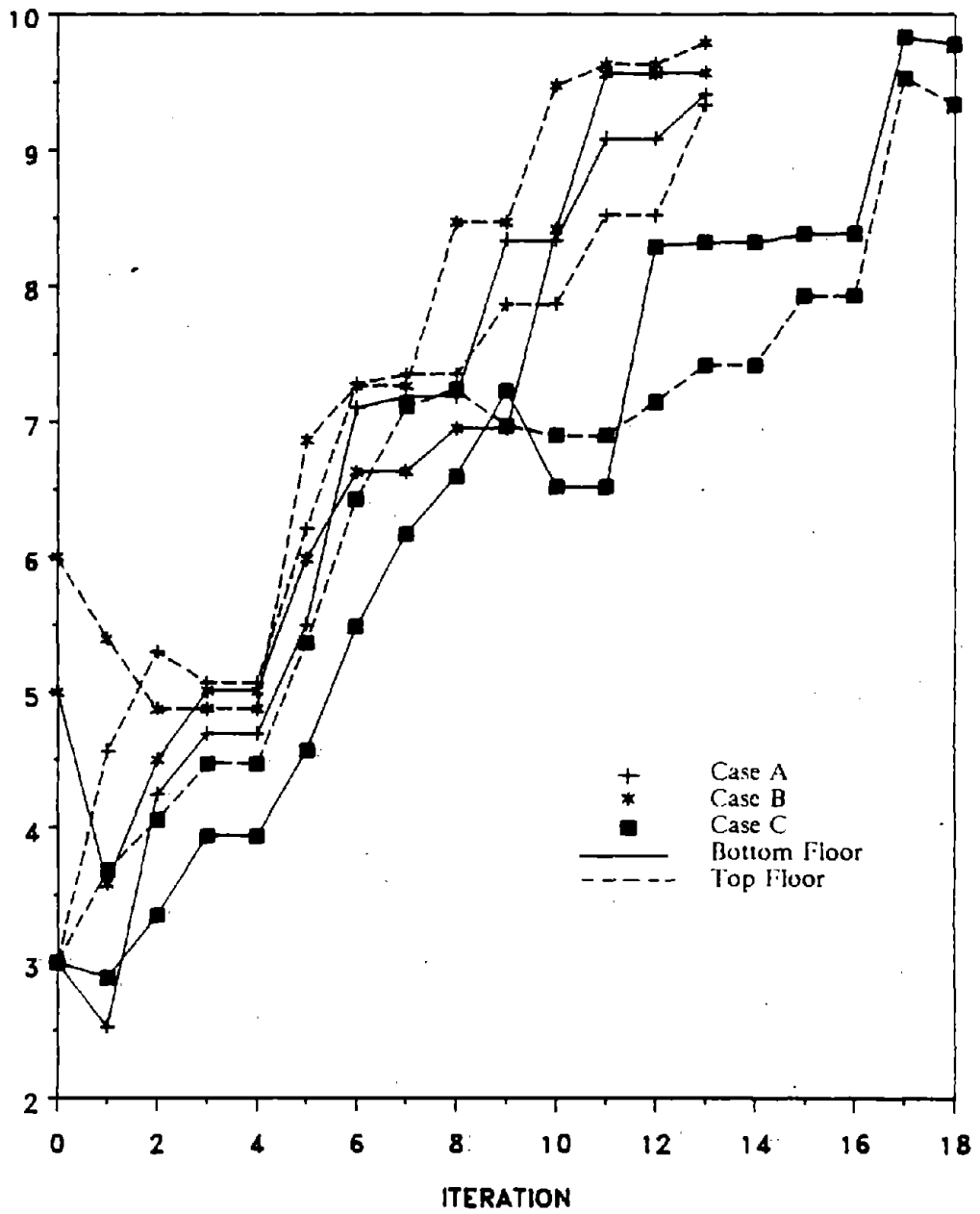
Figure 36.   Normalized Loop Gain of Active Tendons
for Cases A, B, and C
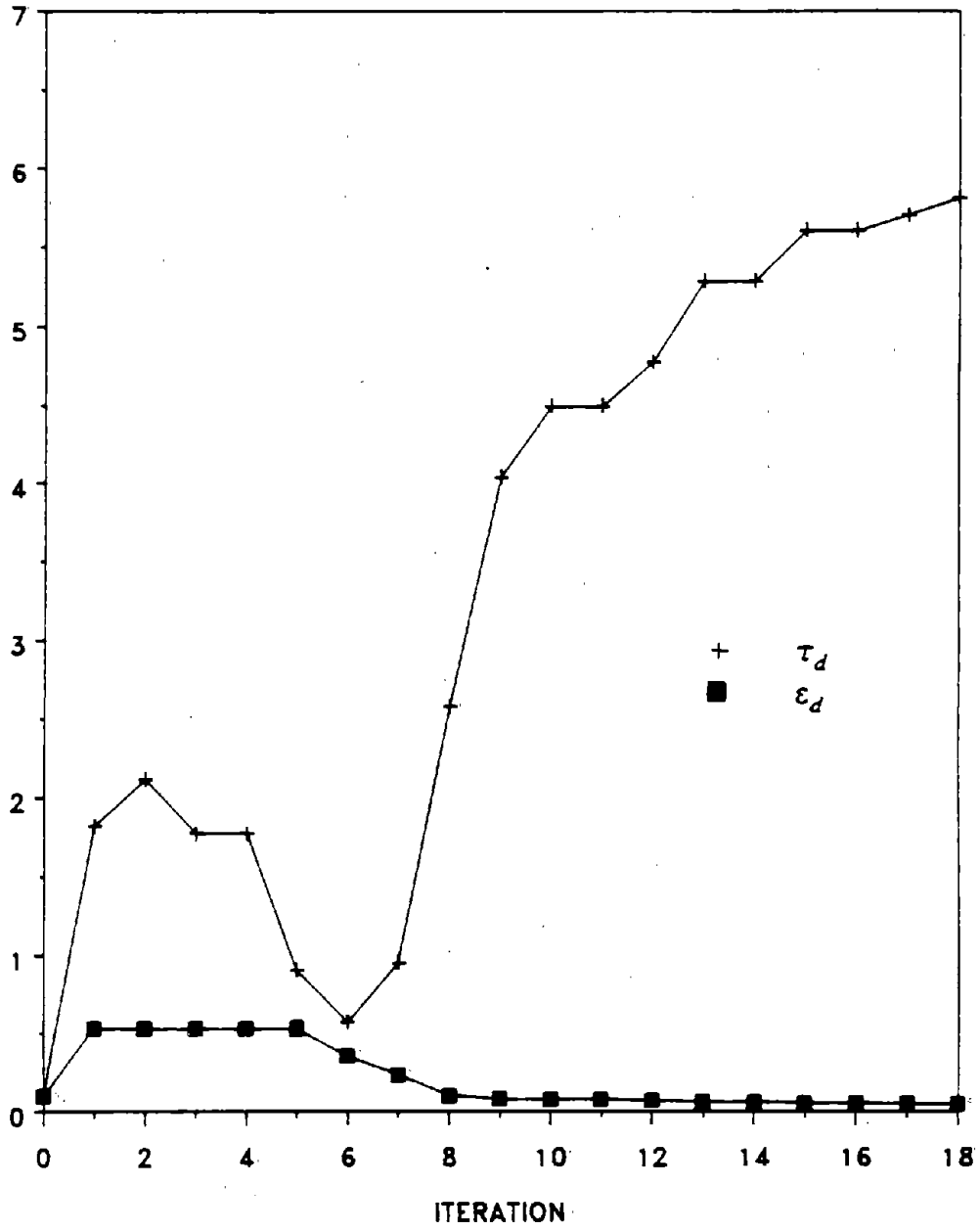
Figure   37.   Normalized Feedback and Loop Gain of Active
              Mass Damper for Case C
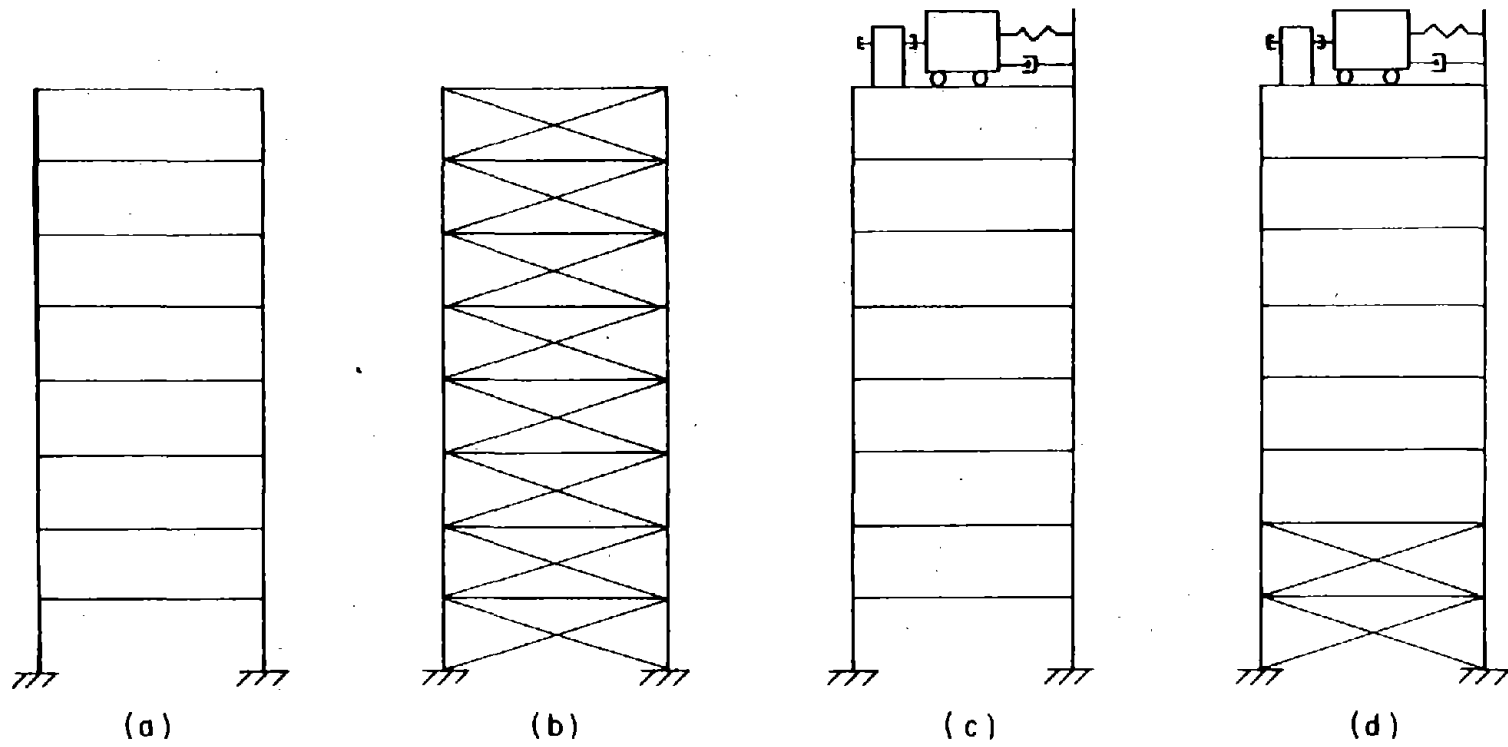
Figure 38. Eight-story Structure: (a) Case 1, (b) Case 2, (c) Case 3, (d) Case 4

by Equation 4.1 with the following parameters: $\omega_g = 18.85 \, rad/\sec$, $\zeta_g = 0.65$, and $S^2 = 4.65 \times 10^{-4} \, m^2/\sec^3 / \text{rad}$. The control parameters are also the same as the ones used in the example of Section E, in Chapter IV. Note that the normalized loop and feedback gains are not fixed but are allowed to vary as design variables in this example. The constraints for all four cases are: σ_{x1} max $= 6 \times 10^{-4} \, m$, σ_{x2} max $= 1.2 \times 10^{-3} \, m$, σ_{x3} max $= 1.8 \times 10^{-3} \, m$, σ_{x4} max $= 2.4 \times 10^{-3} \, m$, σ_{x5} max $= 3.0 \times 10^{-3} \, m$, σ_{x6} max $= 3.6 \times 10^{-3} \, m$, σ_{x7} max $= 4.2 \times 10^{-3} \, m$, σ_{x8} max $= 4.8 \times 10^{-3} \, m$, τ max $= \varepsilon$ max $= 8$, and k min $= 1.5 \times 10^5 \, kN/m$. For Case 2 σ_{ti} max $= 200 \, kN$, $i = 1, \dots, 8$. For Case 4, σ_{ti} max $= 200 \, kN$, $i = 1, \dots, 2$.

The optimization results are shown in Figures 39 through 42. From Figure 39 we observe that the structure without controls requires a very large weight. Comparing the three control configurations, we note from Figures 40 and 41 that the combined system of Case 4, gives the least weight. The optimum stiffness distribution for all four cases is shown in Figure 42. The values of the normalized loop and feedback gains for Case 4 are given in Figure 43. It is observed that τ_{t1} reaches an upper bound, τ_{t2} is close to the upper bound, but τ_d is low. Similar results are obtained for ε_{t1}, ε_{t2}, and ε_d. The power spectral densities of the response for the four optimal cases were calculated; the spectral density of the eighth floor relative displacement and the spectral density of the base shear force are shown in Figures 44 and 45, respectively. From these figures it is obvious that the no-control case is the worst case. Cases 3 and 4 control the response effectively; Case 4, however has the least weight and it reduces the

116
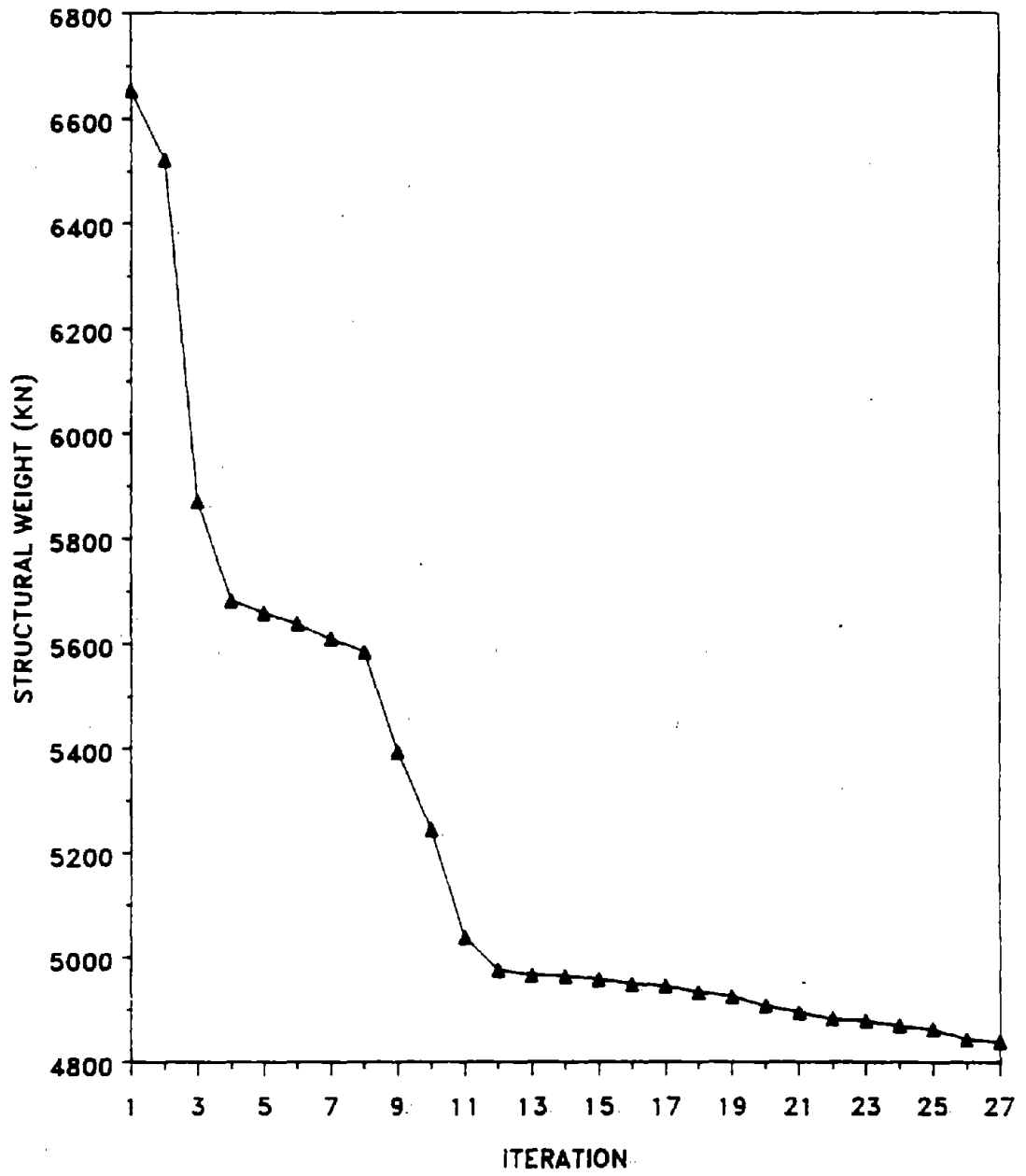
Figure 39. Structural Weight: Case 1 - No Control
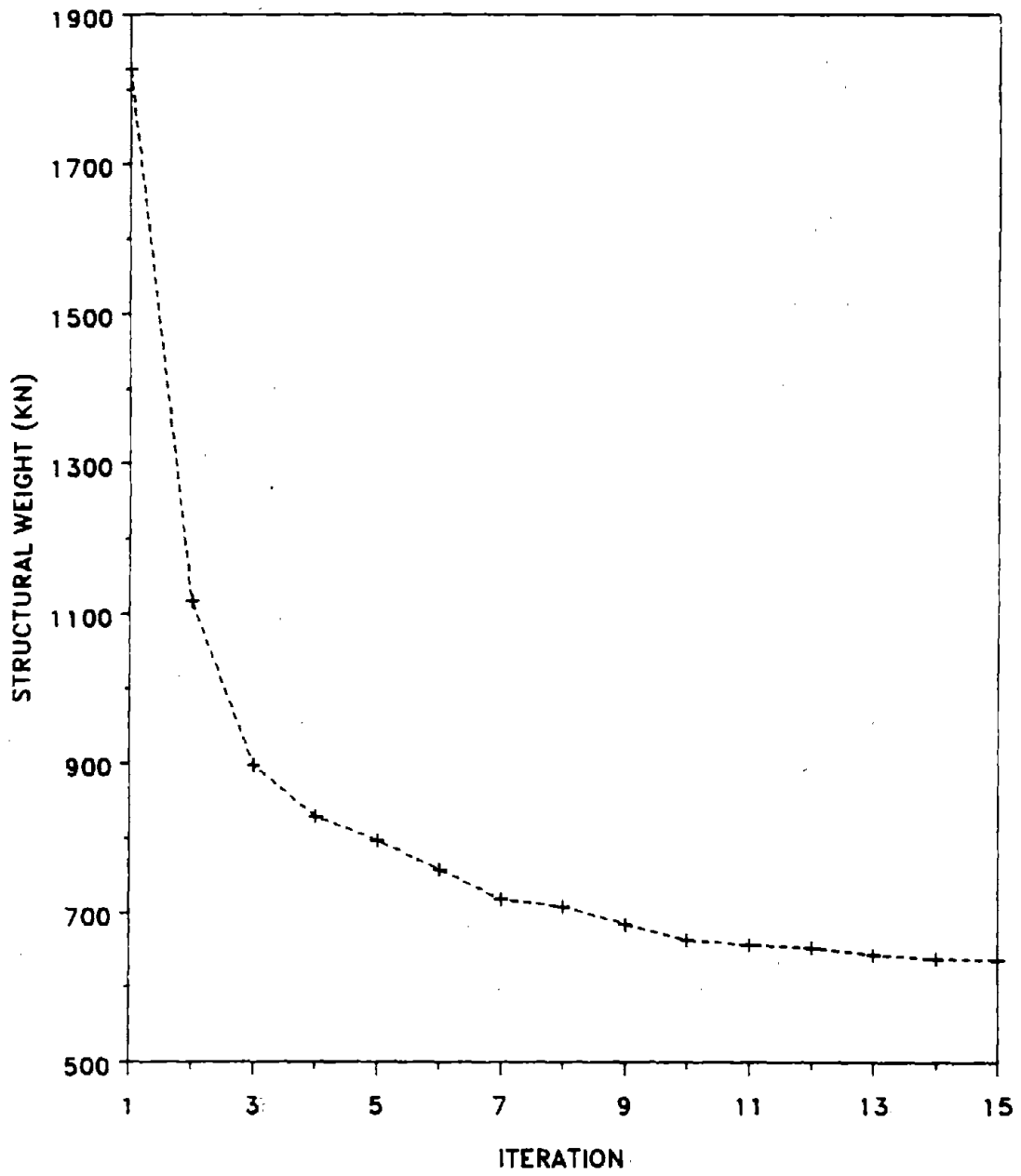
Figure 40. Structural Weight: Case 2 - Eight Active Tendons
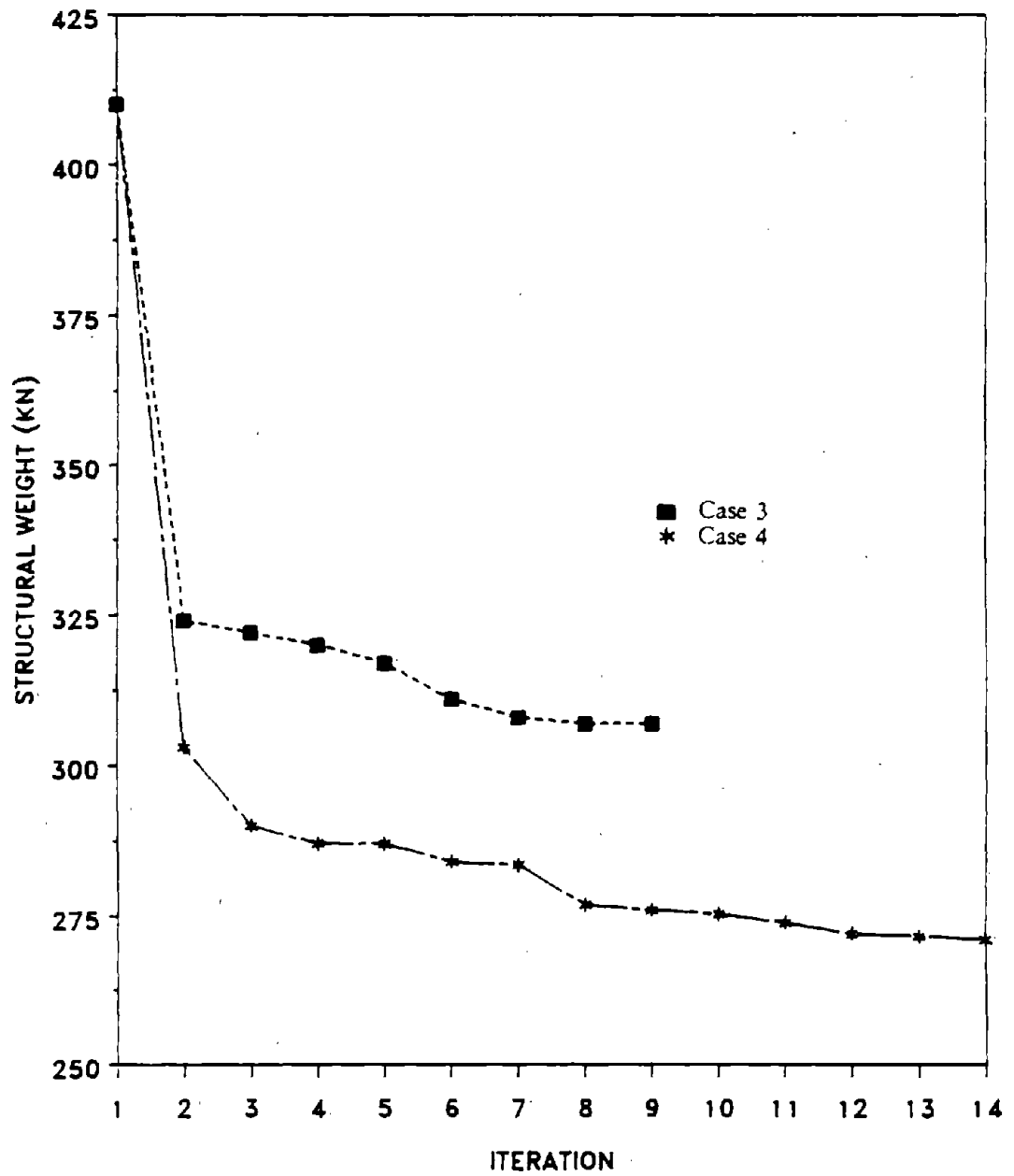
Figure 41. Structural Weight: Case 3 - Active Mass Damper,
Case 4 - Active Mass Damper and Two Active Tendons

119
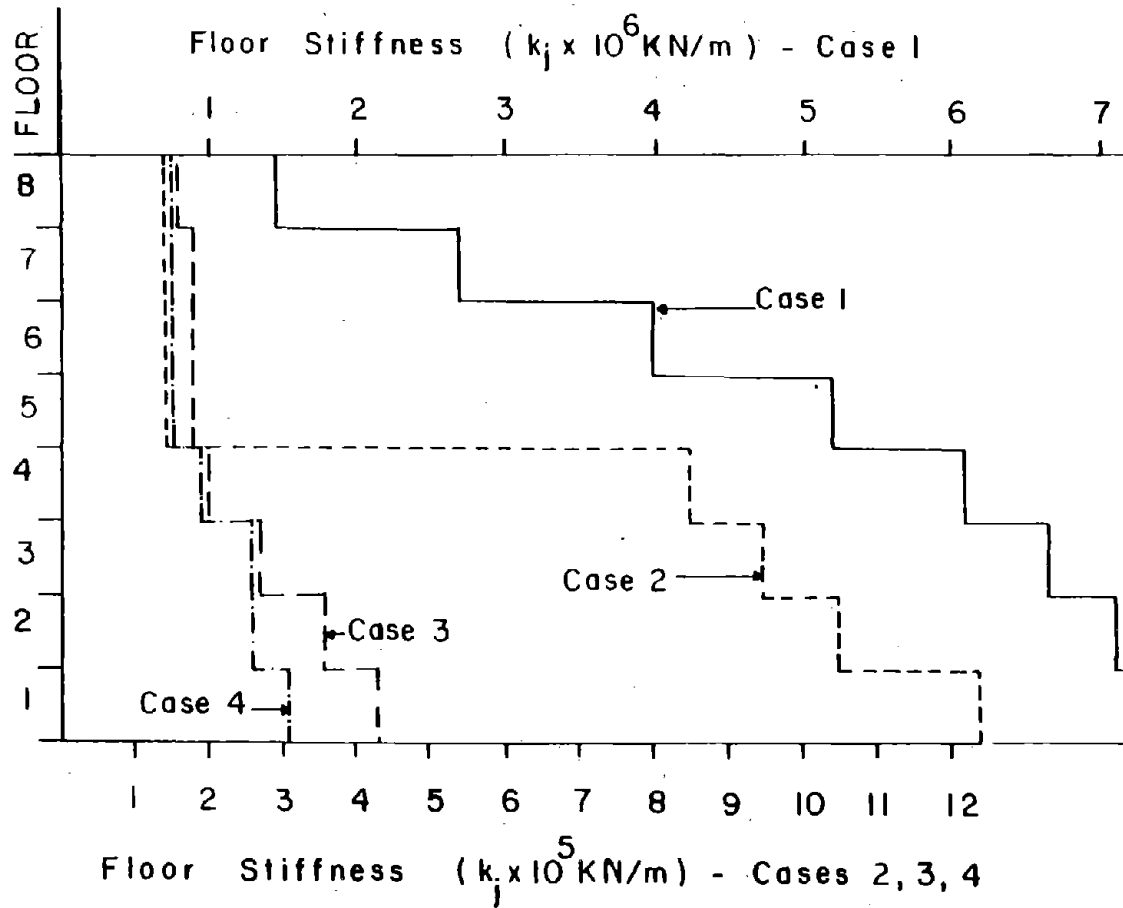
Figure 42. Optimum Stiffness Distribution: Cases 1-4

120
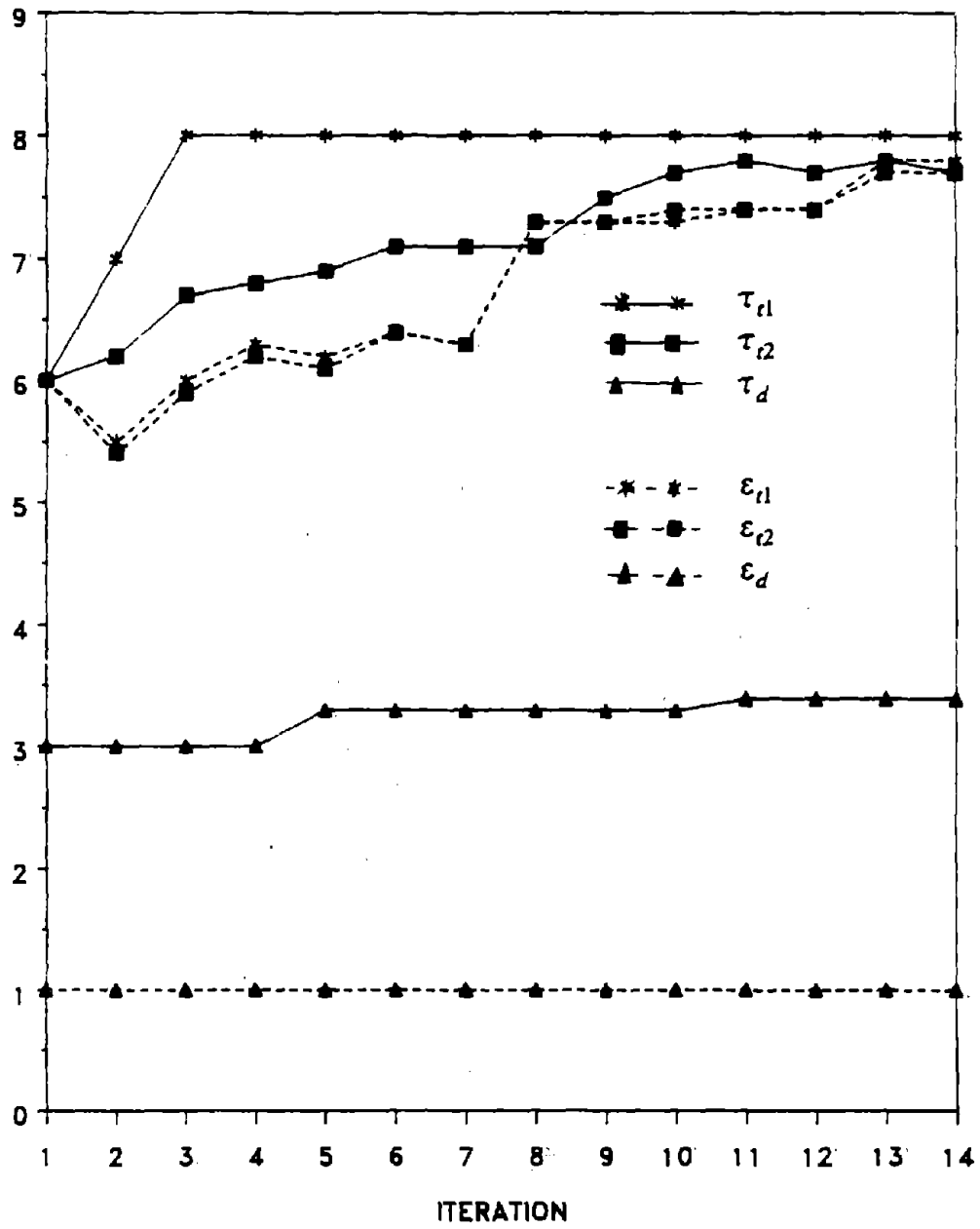
Figure 43. Normalized Feedback and Loop Gains for Case 4
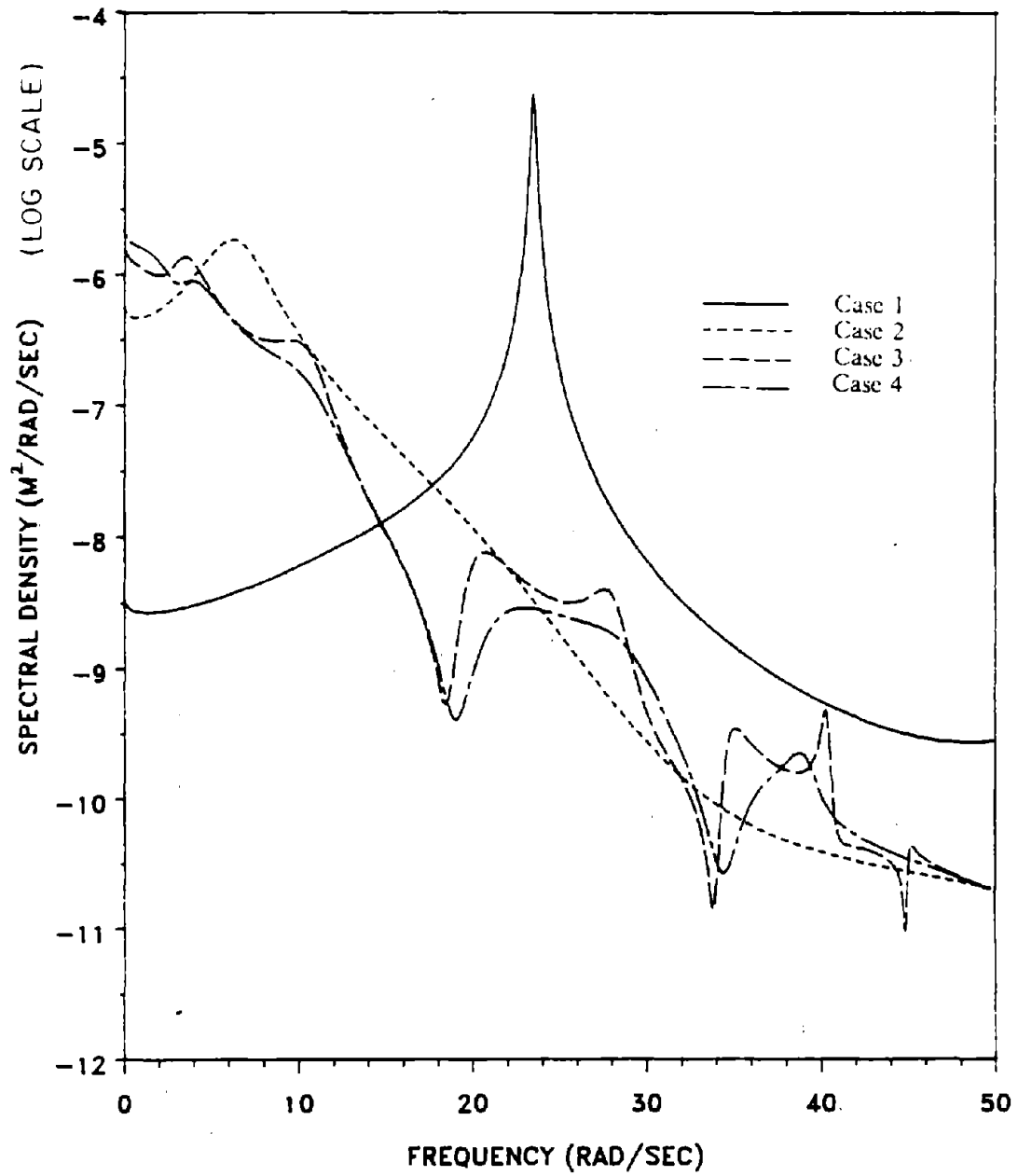
Figure 44. Spectral Density of Eighth Floor Relative Displacement for Cases 1-4
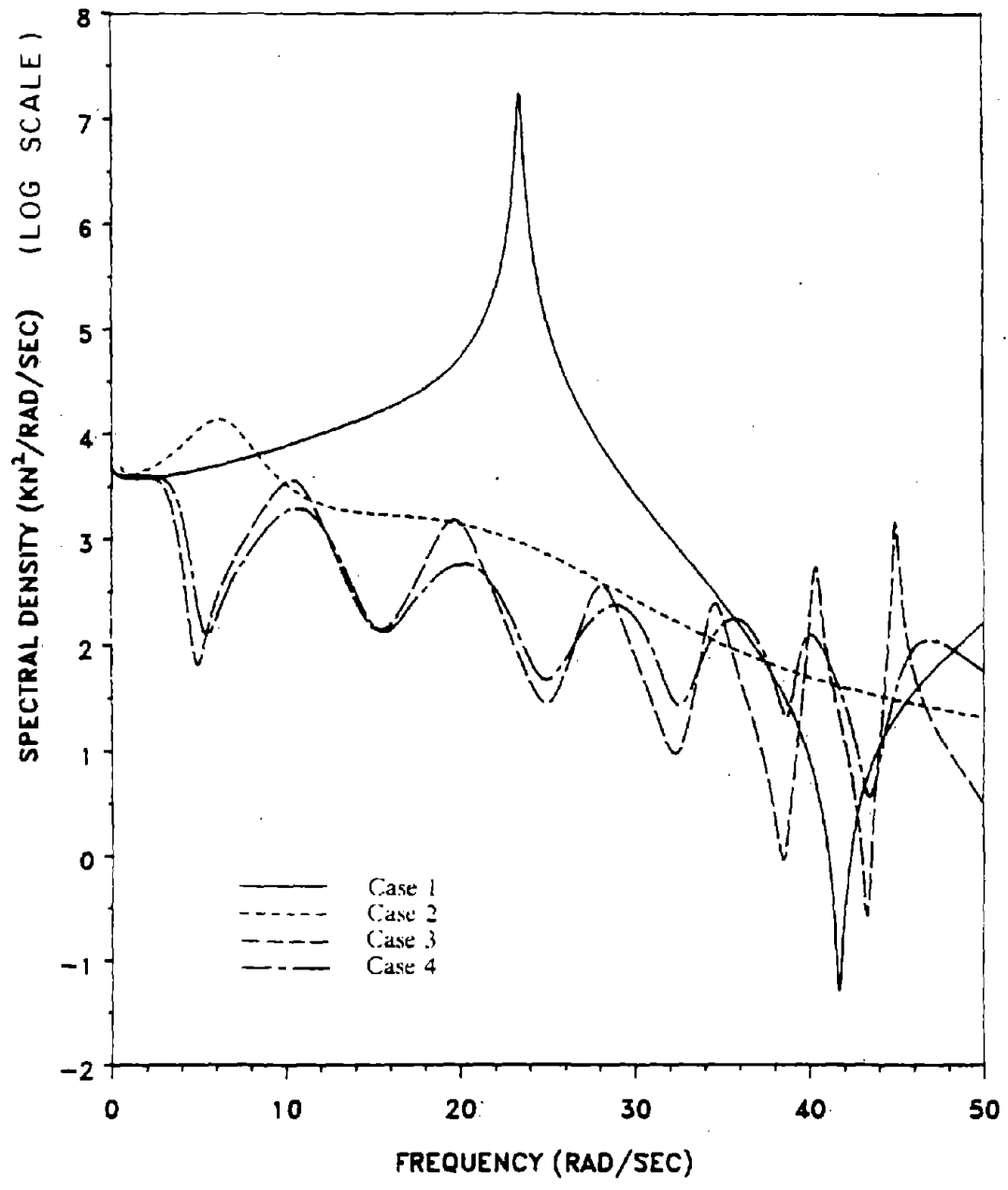
Figure 45. Spectral Density of Base Shear Force for Cases 1-4

higher modes better than Case 3. Case 2 reduces the higher modes best, but of the three control cases has the most weight.

D. OPTIMUM STRUCTURAL DESIGN USING OPTIMAL OPEN-LOOP CONTROL

The instantaneous optimal open-loop control algorithm is used in this example. An eight-story shear building is considered. The structural properties are: $m_j = 105\,Mg$, $c_j = 1138\,Mg/\sec$, $j = 1,...,8$. The earthquake excitation used is the N-S component of the El-Centro earthquake of May 18, 1940, shown in Figure 23. The structure is equipped with eight active tendons, or an active mass damper. The properties of the mass damper are as follows: $m_d = 9\,Mg$, $k_d = 736\,kN/m$, and $c_d = 11\,Mg/\sec$. The weighting matrices, $[Q]$ and $[R]$, are assumed diagonal. From extensive numerical calculations it was found that the ratio of the diagonal elements of the matrices $[Q]$ and $[R]$ is of importance in determining the level of response, and not their absolute values. From a practical point of view, it is desirable to have equal maximum values for the required control forces on all floors. This is achieved by adjusting the ratio of the elements of the weighting matrices. The weighting matrices are then fixed at these values for the structural optimization.

The constraints used for both the eight active tendons case and the active mass damper are: x_1 max $= 0.015\,m$, x_2 max $= 0.025\,m$, x_3 max $= 0.035\,m$, x_4 max $= 0.045\,m$, x_5 max $= 0.050\,m$, x_6 max $= 0.055\,m$, x_7 max $= 0.060\,m$, x_8 max $= 0.065\,m$. The control forces are constrained at: u_i max $= 650\,kN$, $i = 1,...,8$, u_d max $= 650\,kN$, and k min $= 1.5 \times 10^5\,kN/m$. The optimization cycles for the structural weight are shown in Figure 46.
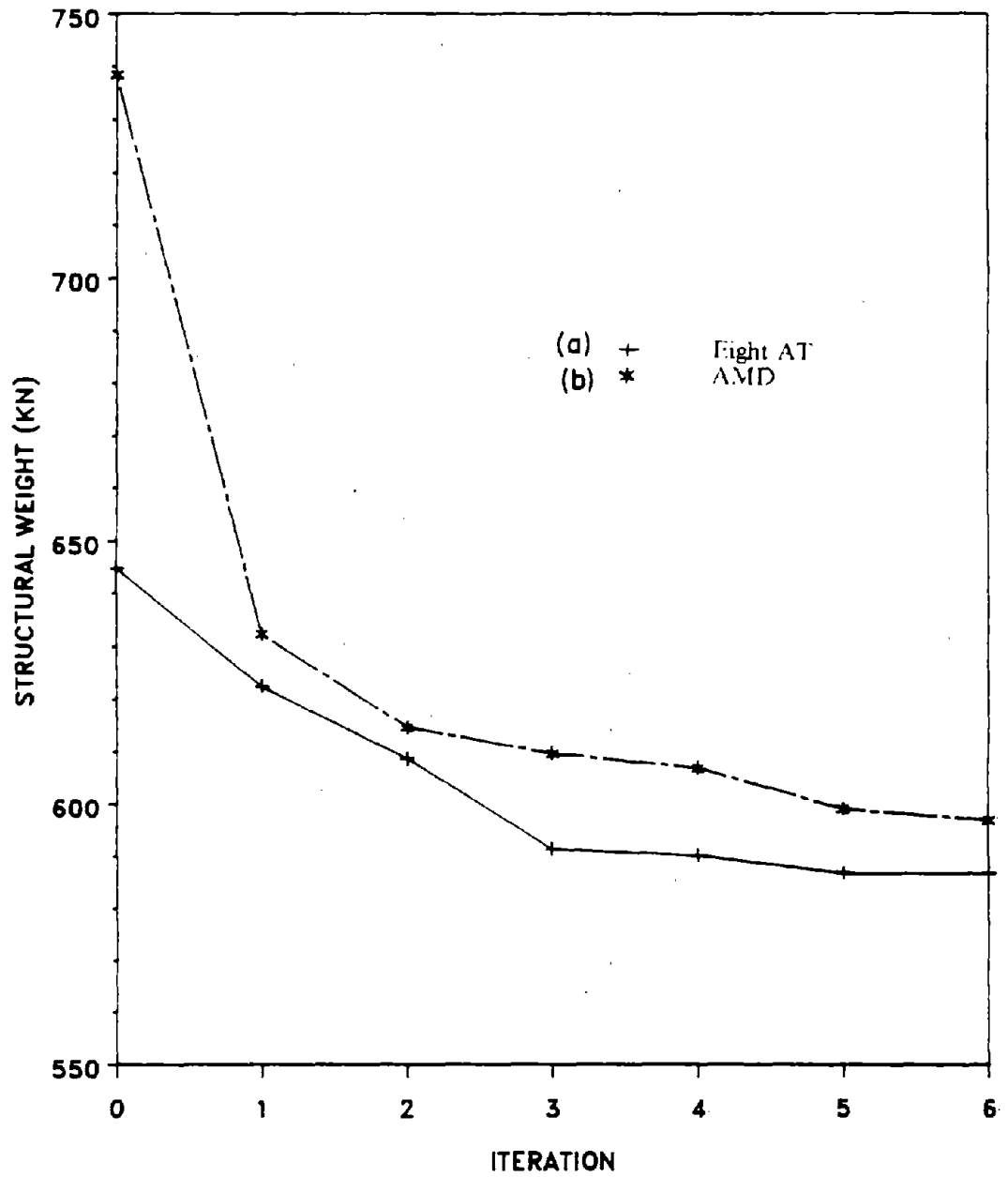
Figure 46. Structural Weight for Building with:
(a) Eight Active Tendons, (b) Active Mass Damper

125

The optimum stiffness distribution at the final iteration is shown in Figure 47. The optimum weight for the AT case is $586.6\,kN$, and for the AMD case $596.8\,kN$. For the AT case, the following constraints are active: x_6, x_7, u_1, u_7, and u_8. For the AMD case, x_8 is active.

The optimal designs found above for the AT and AMD cases were subjected to the same earthquake excitation, but without the active control systems. Figures 48 through 51 describe the response for the optimal structure with and without the active tendons, and Figures 53 through 56 describe the response for the optimal structure with and without the active mass damper. From Figure 48, it is obvious that the eighth floor relative displacement has been reduced by using the active tendon system. Although the maximum displacement of the controlled response has been reduced by only about 60 % as compared to the no-control case, it is evident that for the rest of the time history, the reduction is much greater. The maximum relative velocity and maximum acceleration of the eighth floor have been, respectively, reduced by 55 % and 70 % as compared to the no-control case as shown in Figures 49 and 50. In Figure 51 the maximum first floor drift has been reduced by 60 %. The first floor drift is defined as the algebraic difference in displacements between the first and second floors. The active tendon control force for the first floor tendon is shown in Figure 52. This control force reaches its maximum value for a very short time, while for the rest of the time-record its value is less than half of its maximum.
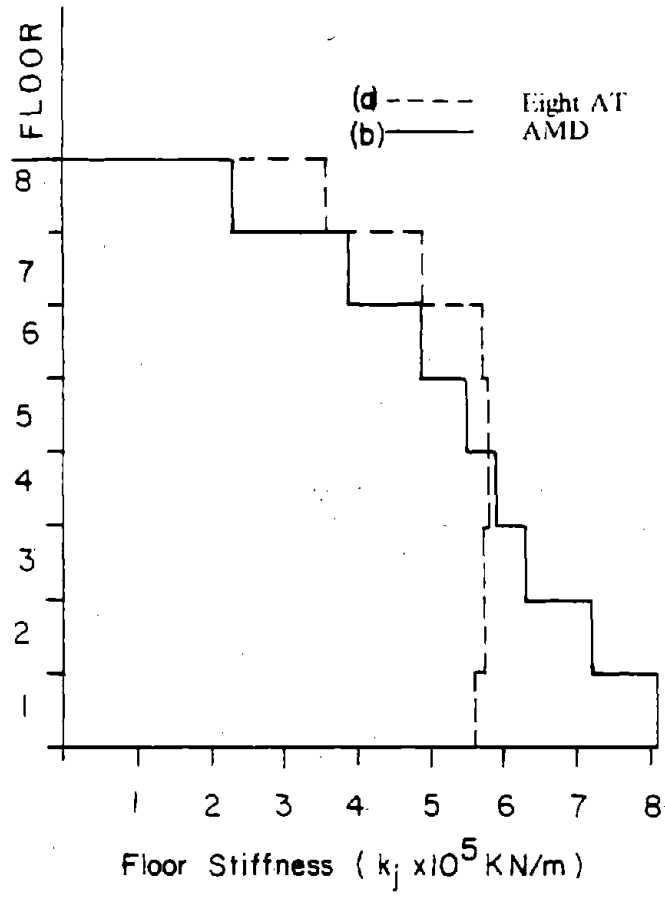
Figure 47. Optimum Stiffness Distribution for Building with:
(a) Eight Active Tendons, (b) Active Mass Damper

127
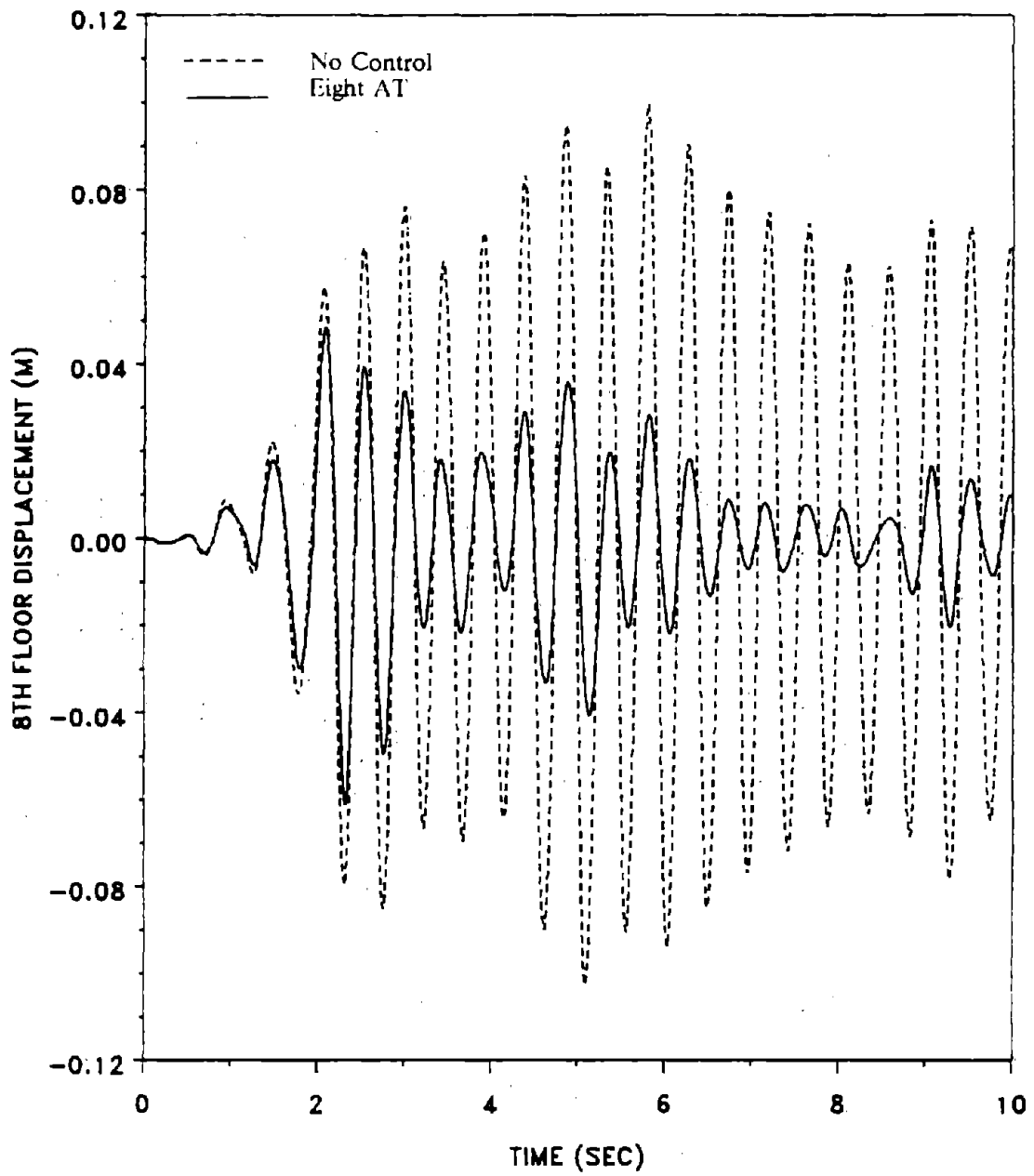
Figure 48. Comparison of Eighth Floor Relative Displacement of
Optimum Structure with and without Active Tendons

128
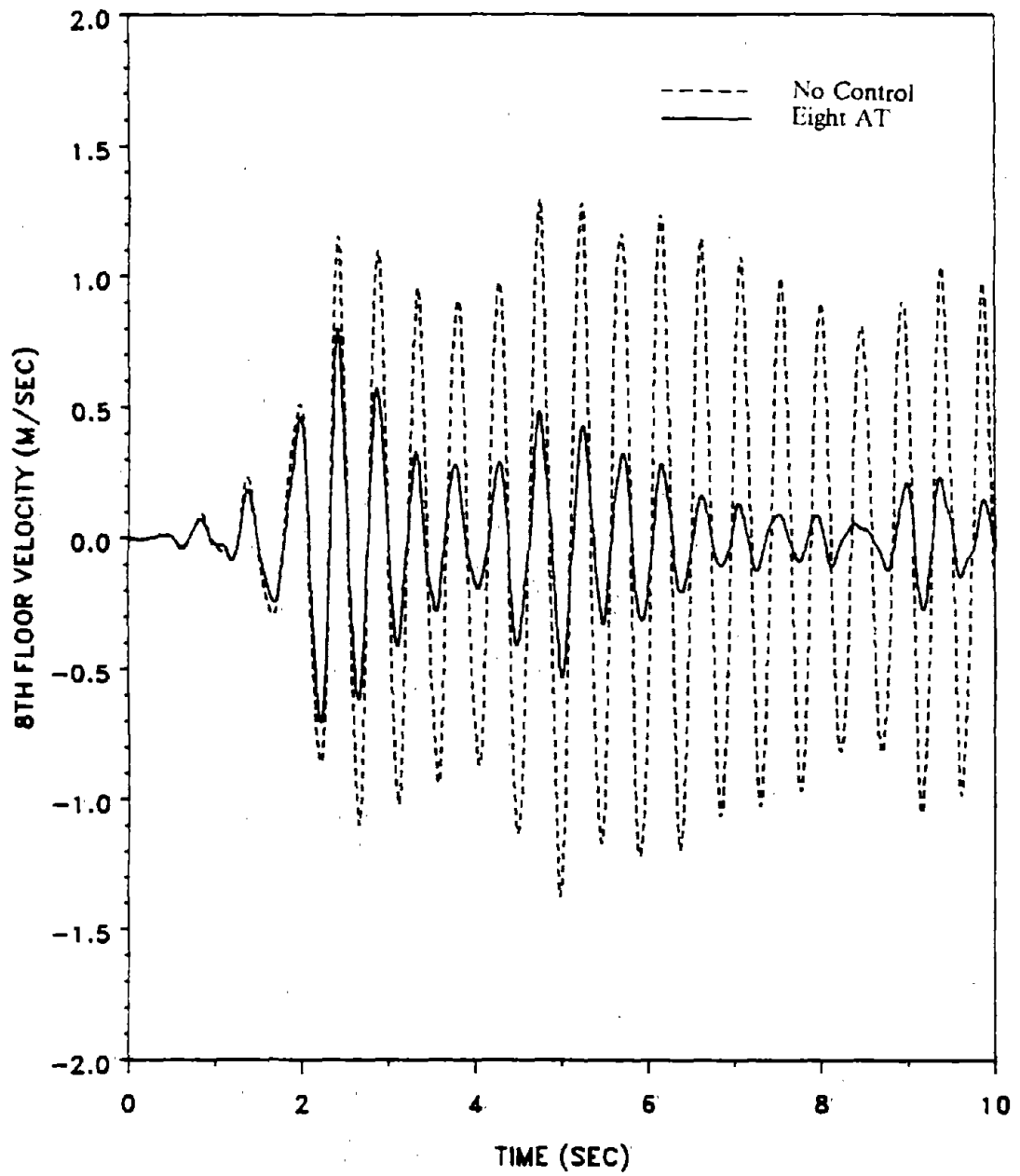
Figure   49.   Comparison of Eighth Floor Relative Velocity of
Optimum Structure with and without Active Tendons

129
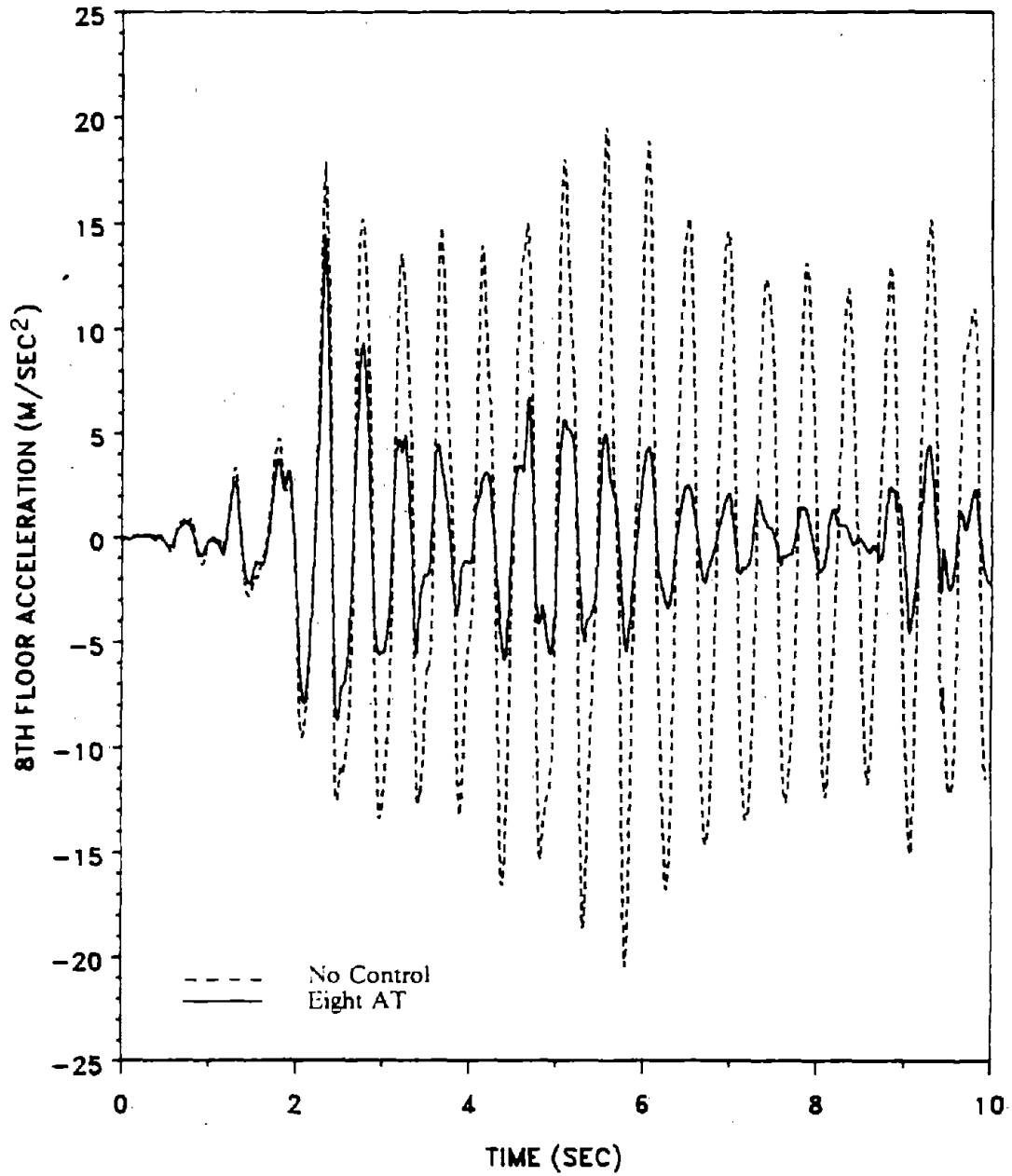
Figure 50. Comparison of Eighth Floor Relative Acceleration of
Optimum Structure with and without Active Tendons
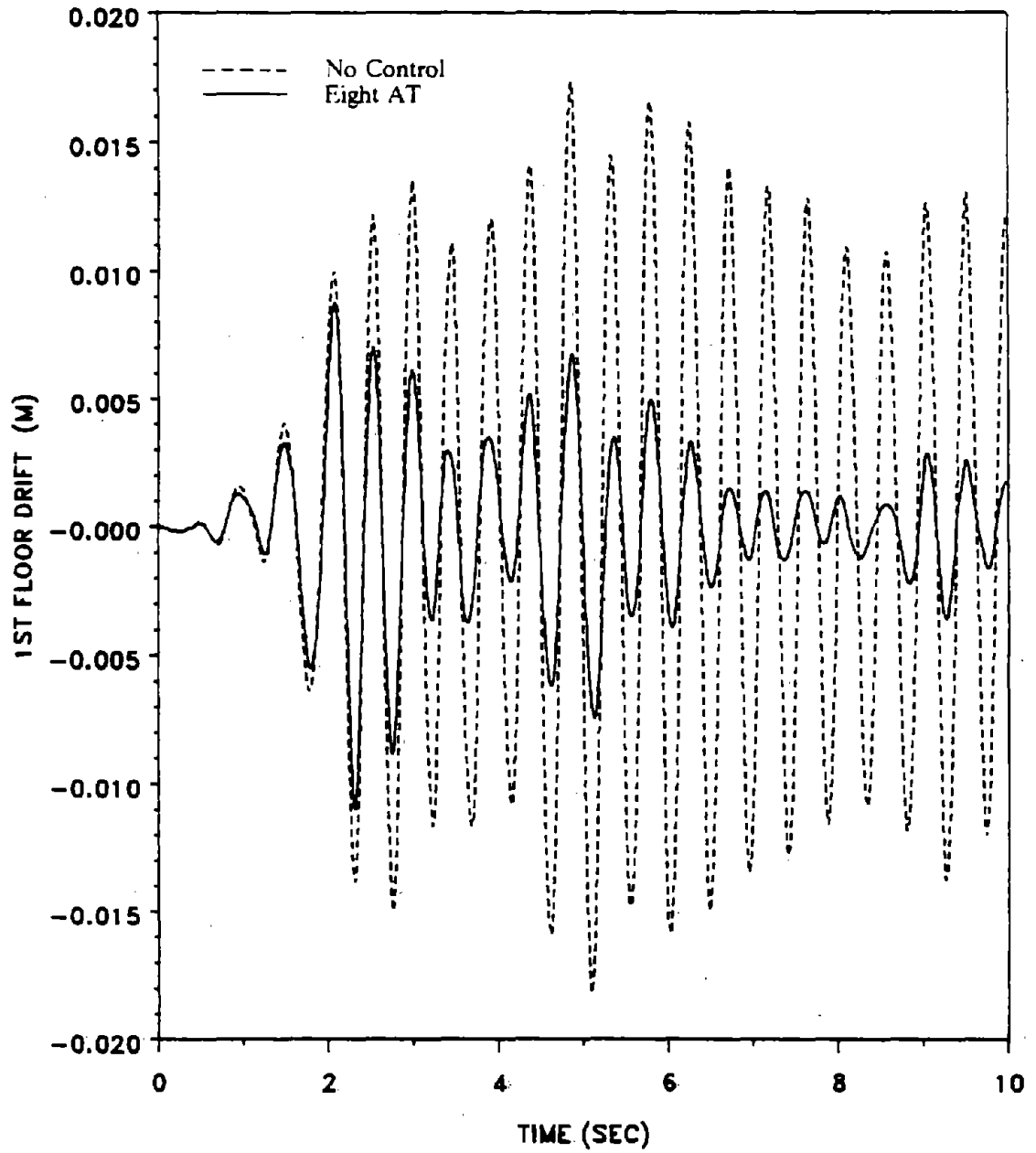
Figure 51. Comparison of First Floor Relative Drift of
Optimum Structure with and without Active Tendons

131
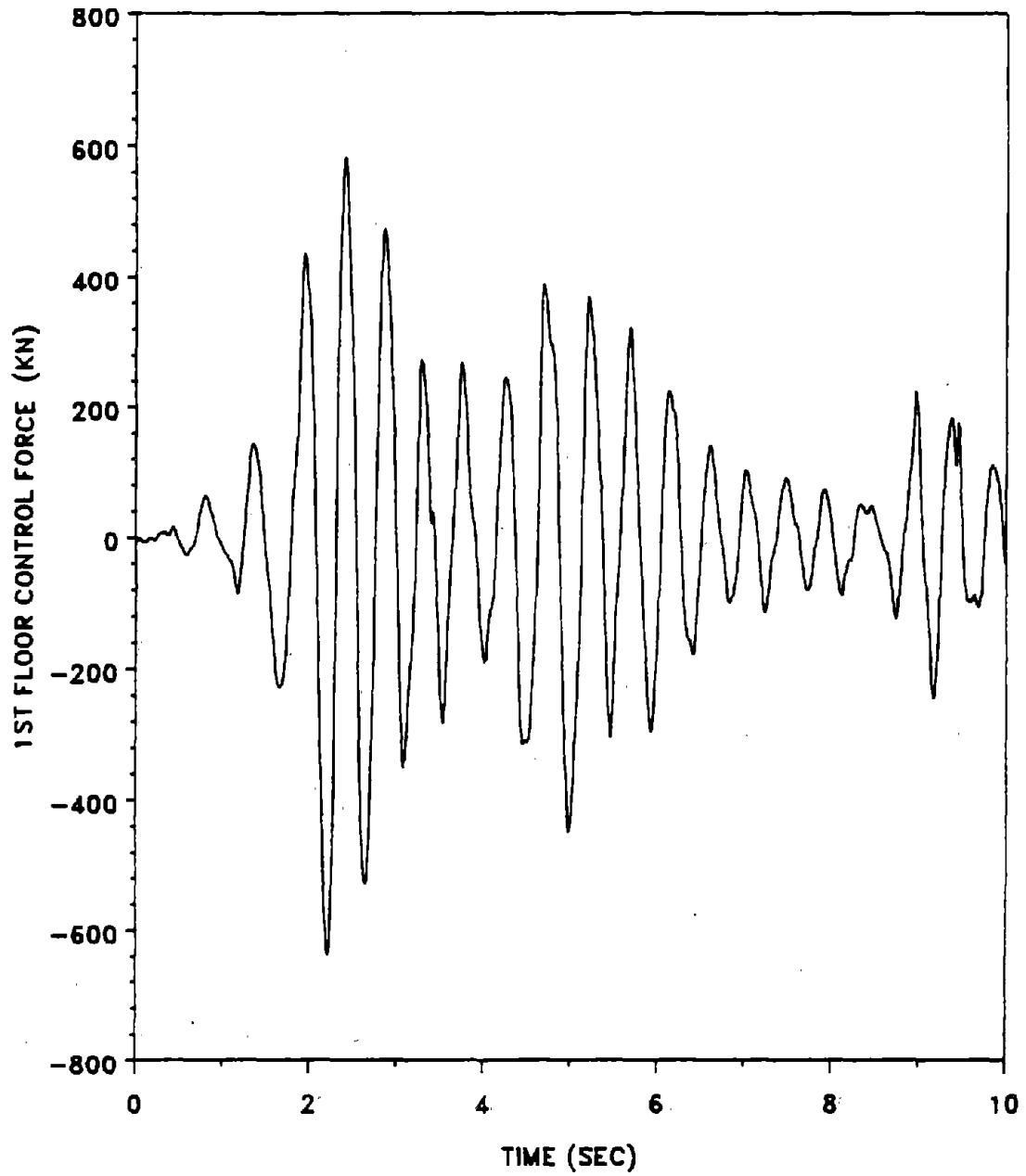
Figure 52. First Floor Active Tendon Control Force
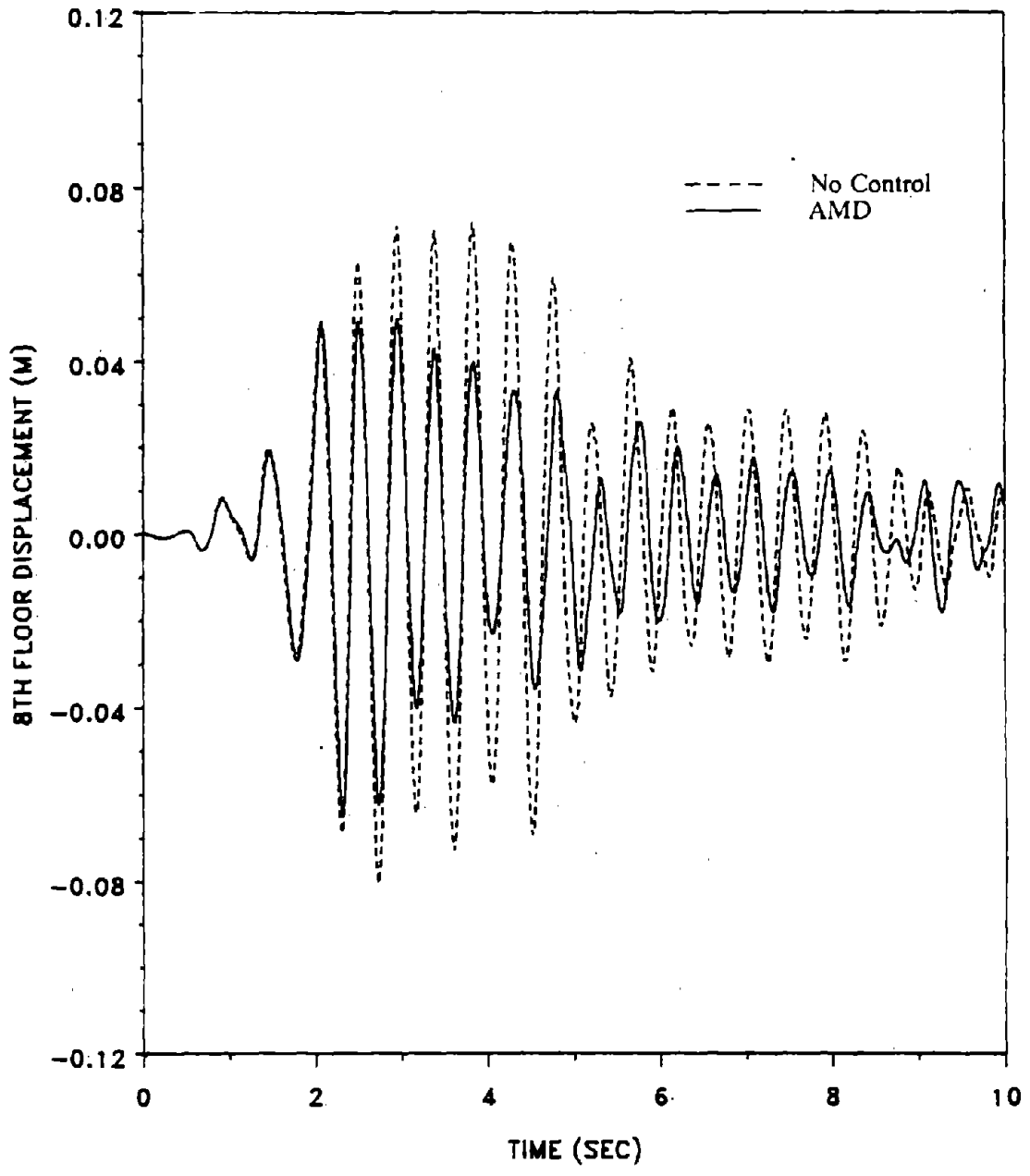
Figure 53. Comparison of Eighth Floor Relative Displacement of
Optimum Structure with and without Active Mass Damper

133
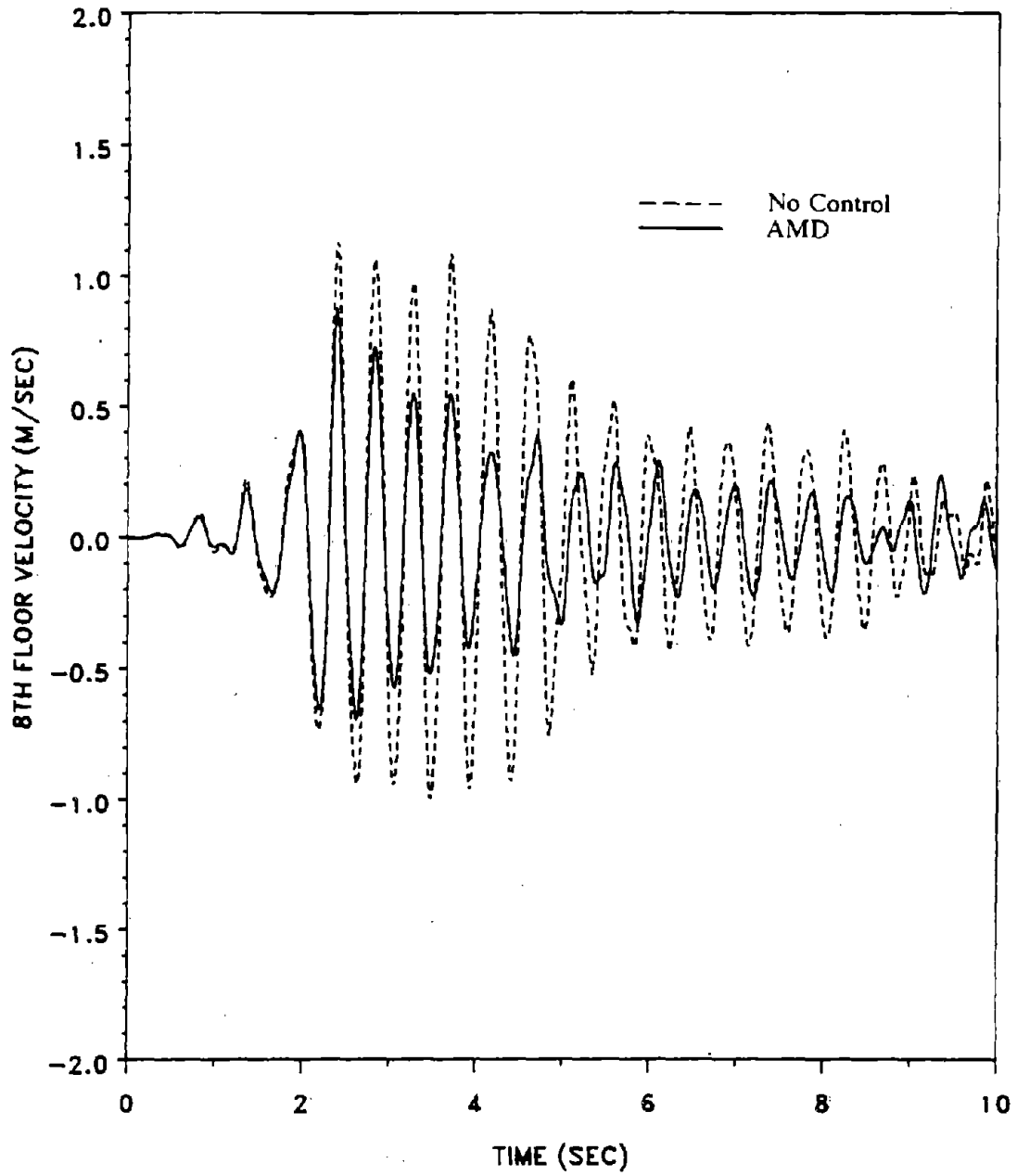
Figure 54.   Comparison of Eighth Floor Relative Velocity of
            Optimum Structure with and without Active Mass Damper

134
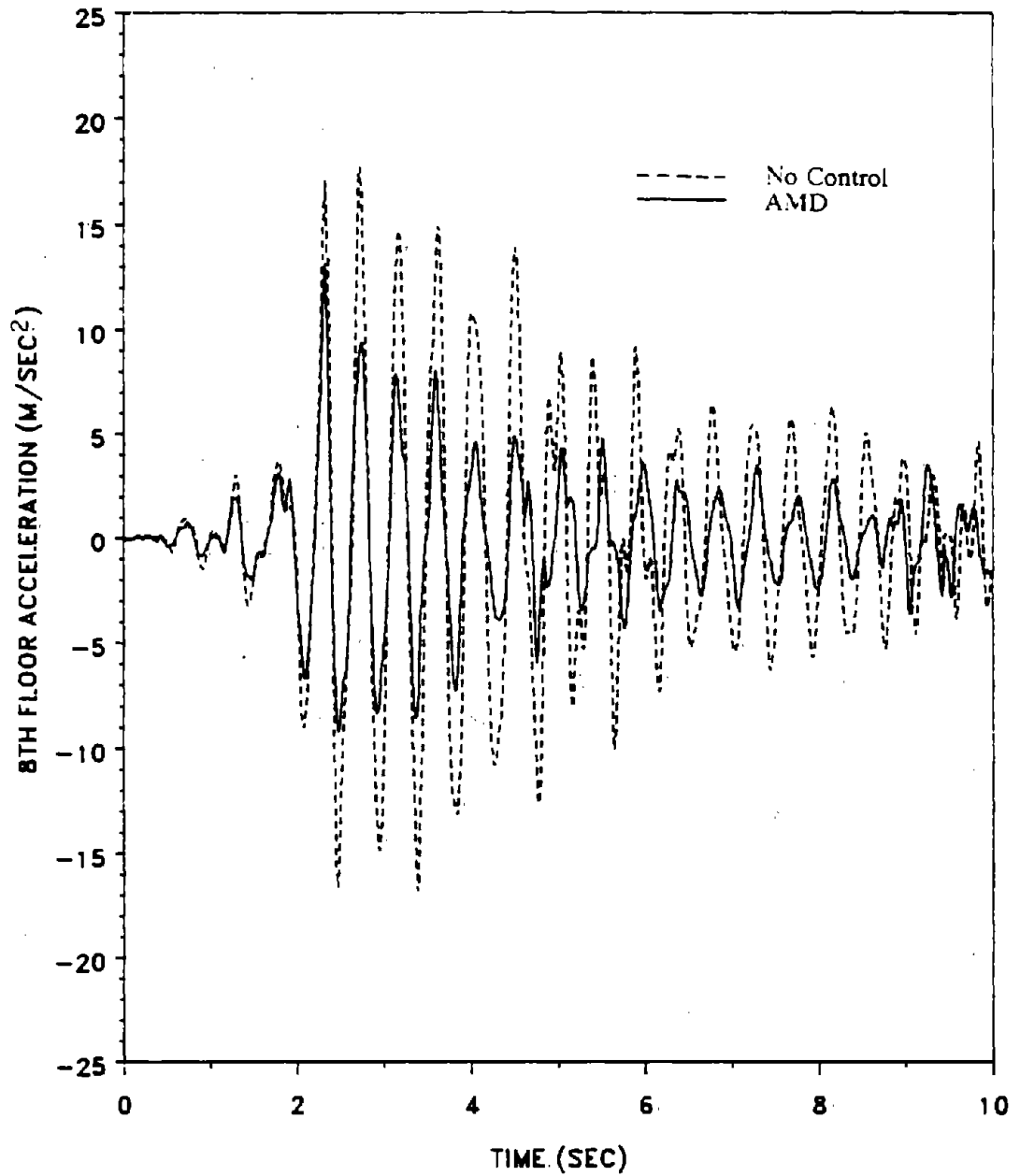
Figure 55. Comparison of Eighth Floor Relative Acceleration of
Optimum Structure with and without Active Mass Damper

135
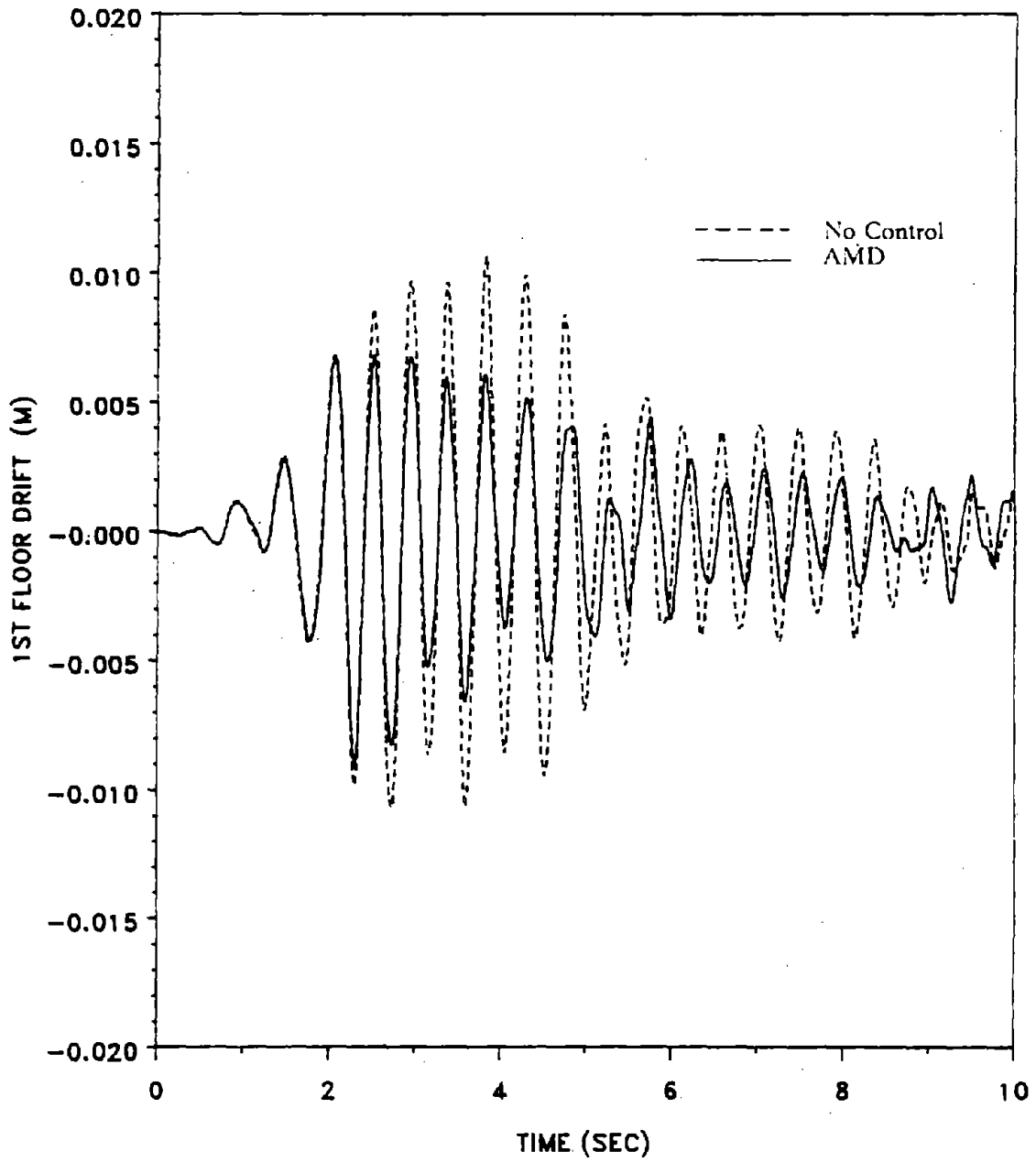
Figure 56. Comparison of First Floor Relative Drift of
Optimum Structure with and without Active Mass Damper

From Figure 53, the eighth floor relative displacement has been reduced by using the active mass damper system. The reduction is about 80 % as compared to the no-control case. The maximum relative velocity and acceleration of the eighth floor have both been reduced by 85 % as compared to the no-control case as shown in Figures 54 and 55, respectively. The maximum first floor drift has been reduced by 80 % as shown in Figure 56. The active mass damper control force is shown in Figure 57. The damper control force is about one third of the allowable at its maximum value. This is the reason why the active mass damper system does not reduce the response as much as the active tendon system. However, the active mass damper performance could be improved by adjusting the elements of the weighting matrices, so as to yield a larger control force.

E.   OPTIMUM STRUCTURE USING OPTIMAL CLOSED-LOOP CONTROL

The instantaneous optimal closed-loop control algorithm is used in this example to illustrate the benefits of combinining structural optimization with active control. An eight-story shear building is considered. The structural properties are: $m_j = 2\,kip - \sec^2/in$ ($350\ Mg$), $j = 1, \ldots, 8$, and 1 % critical damping in all the modes. The earthquake excitation used is the N-S component of the El-Centro earthquake of May 18, 1940, shown in Figure 23. The structure is equipped with eight active tendons, one on each floor. The weighting matrices [Q] and [R] are assumed diagonal with the values $R(i,i) = 0.06$, $i = 1, \ldots, 8$ and $Q(l,l) = 1500$, $l = 1, \ldots, 16$. The choice of these matrices at this stage

137
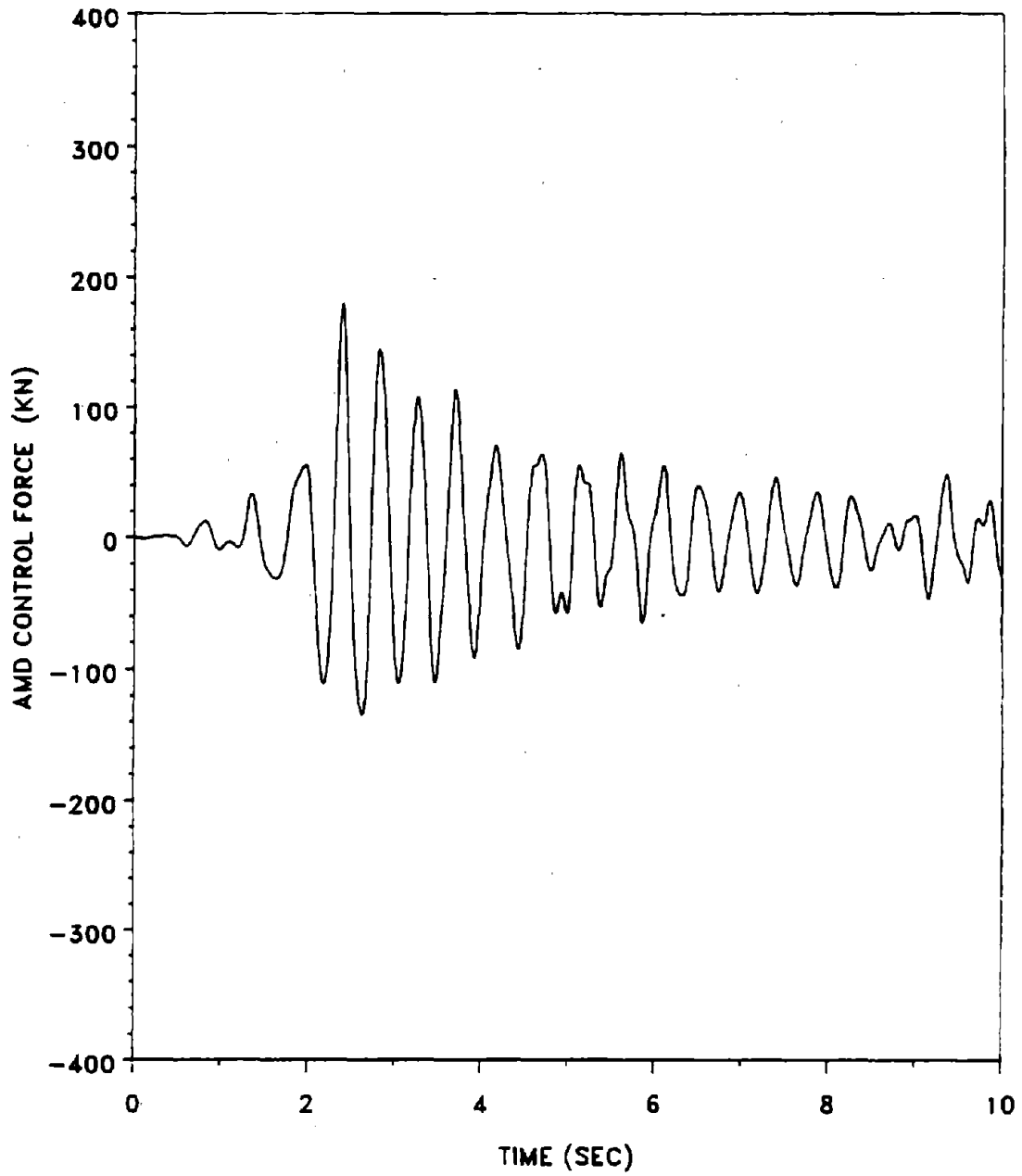
Figure 57. Active Mass Damper Control Force

is arbitrary, and they are fixed at this values during the structural optimization.

The constraints used in this case (Case 1) are: x_1 max = 0.72 in (.018 m), x_2 max = 1.44 in (.037 m), x_3 max = 2.16 in (.055 m), x_4 max = 2.88 in (.073 m), x_5 max = 3.60 in (.091 m), x_6 max = 4.32 in (.110 m), x_7 max = 5.04 in (.128 m), x_8 max = 5.76 in (.146 m), u_i max = 300 kips (133 kN), $i = 1, ..., 8$, and k min = 400 kips/in (70040 kN/m). The optimization cycles for the structural weight are shown in Figure 58. The optimum stiffness distribution at the final iteration is shown in Figure 59. The optimum weight for Case 1 is 42.12 kips (187.35 kN). The following constraints are active: x_2, x_3, and x_4. To illustrate the usefulness and versatility of the optimization process, a second optimization of the same structure-control system was carried out, with the following difference: The displacement constraints of Case 1 were reduced by 70 % for this case (Case 2). The rest of the constraints are kept at the same values. The resulting design for Case 2 is also shown in Figures 58 and 59. As expected the optimum weight for Case 2 is higher, at 116.34 kips (517.48 kN). The following constraints are active: x_1, x_3, x_4, x_5, and x_8. It can be seen that optimization is not intended just to reduce the structural weight, but to achieve optimal structural strength through rational stiffness redistribution based on a given set of constraints. The limitations of the control system were observed by retaining the same constraints on the maxima of the control forces for both Cases 1 and 2, and two different designs were obtained to satisfy the two situations.
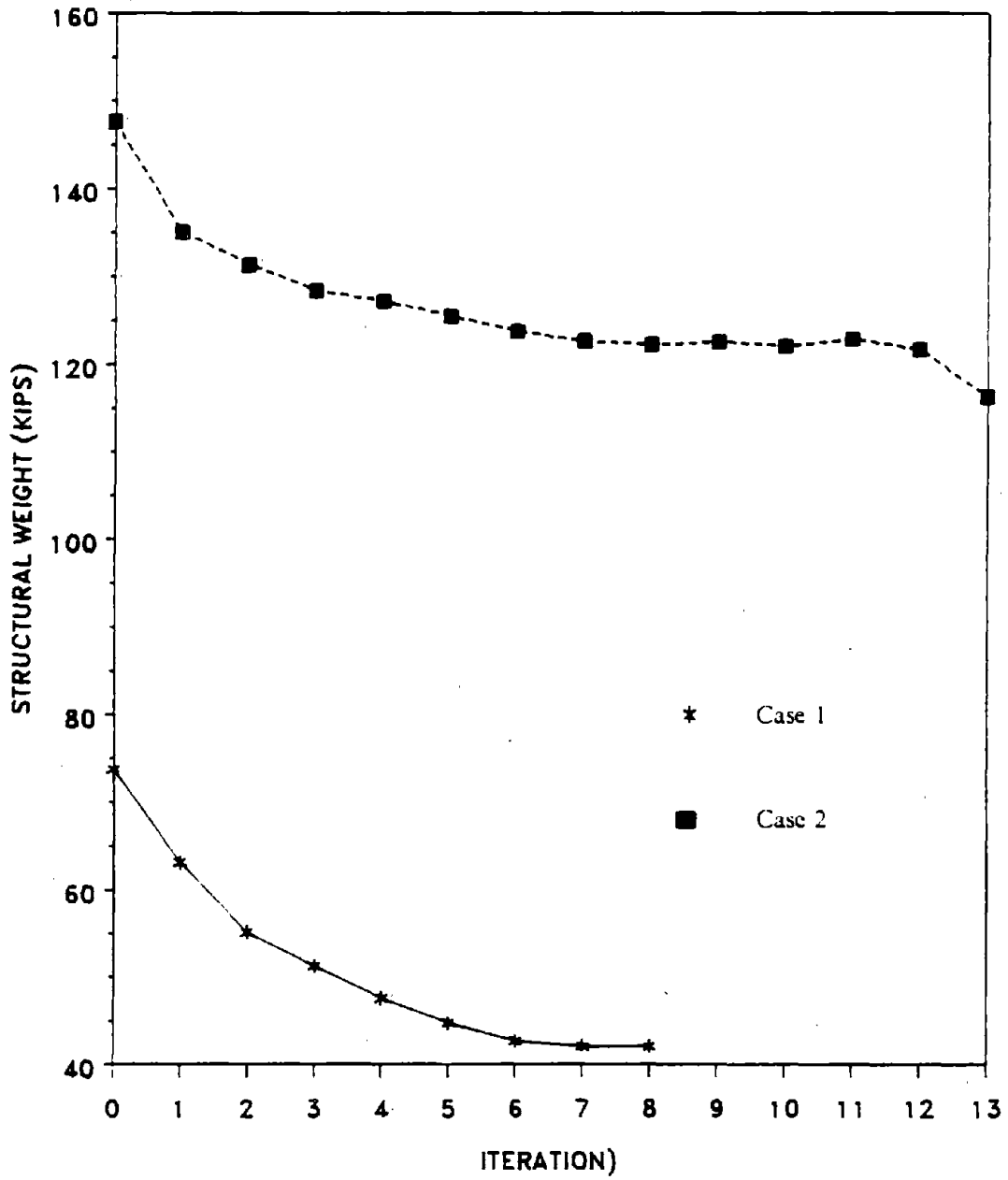
Figure 58. Structural Optimization using Instantaneous
Closed-loop Control
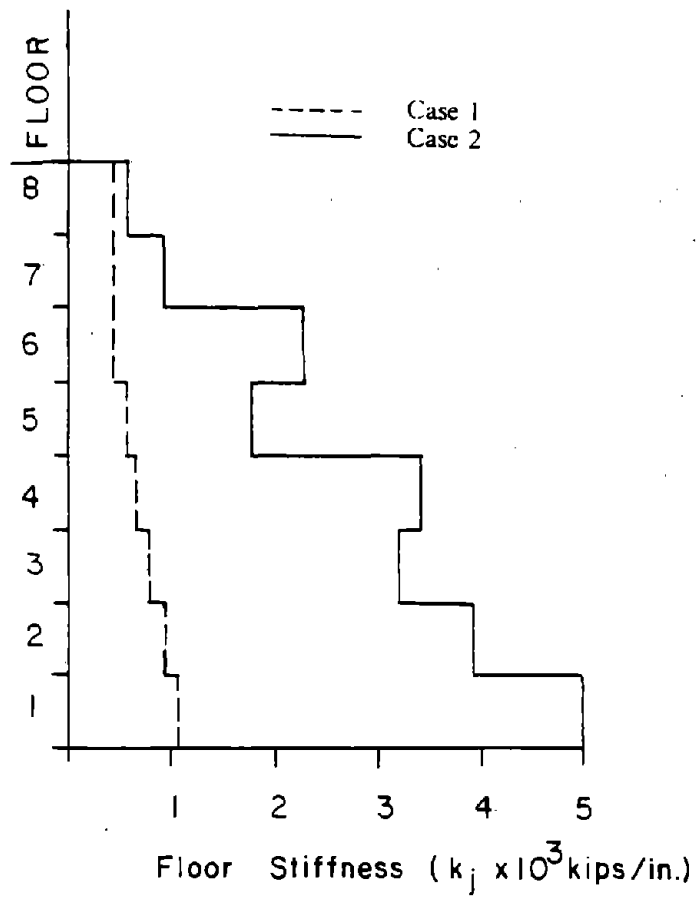
Figure 59. Optimum Stiffness Distribution for Cases 1 and 2

F.   OPTIMUM STRUCTURAL DESIGN WITH FREQUENCY CONSTRAINTS

The instantaneous optimal open-loop control algorithm is used in this example that demonstrates the use of frequency constraints. The frequency constraints are imposed so that the resulting optimum structure with the active system will have its natural period removed from the seismic spectral peak period. An eight-story shear building is considered. The structural properties are: $m_j = 105\,Mg$, $c_j = 1138\,Mg/\,sec$, $j = 1,...,8$. The earthquake excitation used is the N-S component of the El-Centro earthquake of May 18, 1940, and the structure is equipped with eight active tendons.

The displacement constraints used are: x_1 max $= 0.018\,m$, x_2 max $= 0.037\,m$, x_3 max $= 0.055\,m$, x_4 max $= 0.073\,m$, x_5 max $= 0.092\,m$, x_6 max $= 0.110\,m$, x_7 max $= 0.128\,m$, x_8 max $= 0.146\,m$. The control forces are constrained at: u_i max $= 650\,kN$, $i = 1,...,8$. The frequency constraints are imposed as follows: ω_1 min $= 0.90\,Hz$, ω_1 max $= 1.25\,Hz$, and k min $= 1.0 \times 10^4\,kN/m$. The optimization cycles for the structural weight are shown in Figure 60a. The optimum weight is $164.4\,kN$. The frequency constraint is active at $\omega_1 = 0.90\,Hz$. At the optimum, $x_8 = 0.0568\,m$, which is lower than the allowable. The first and second mode frequencies are given in terms of the optimization cycles in Figures 60b and 60c, respectively. The optimum stiffness distribution at the final iteration is shown in Figure 61.
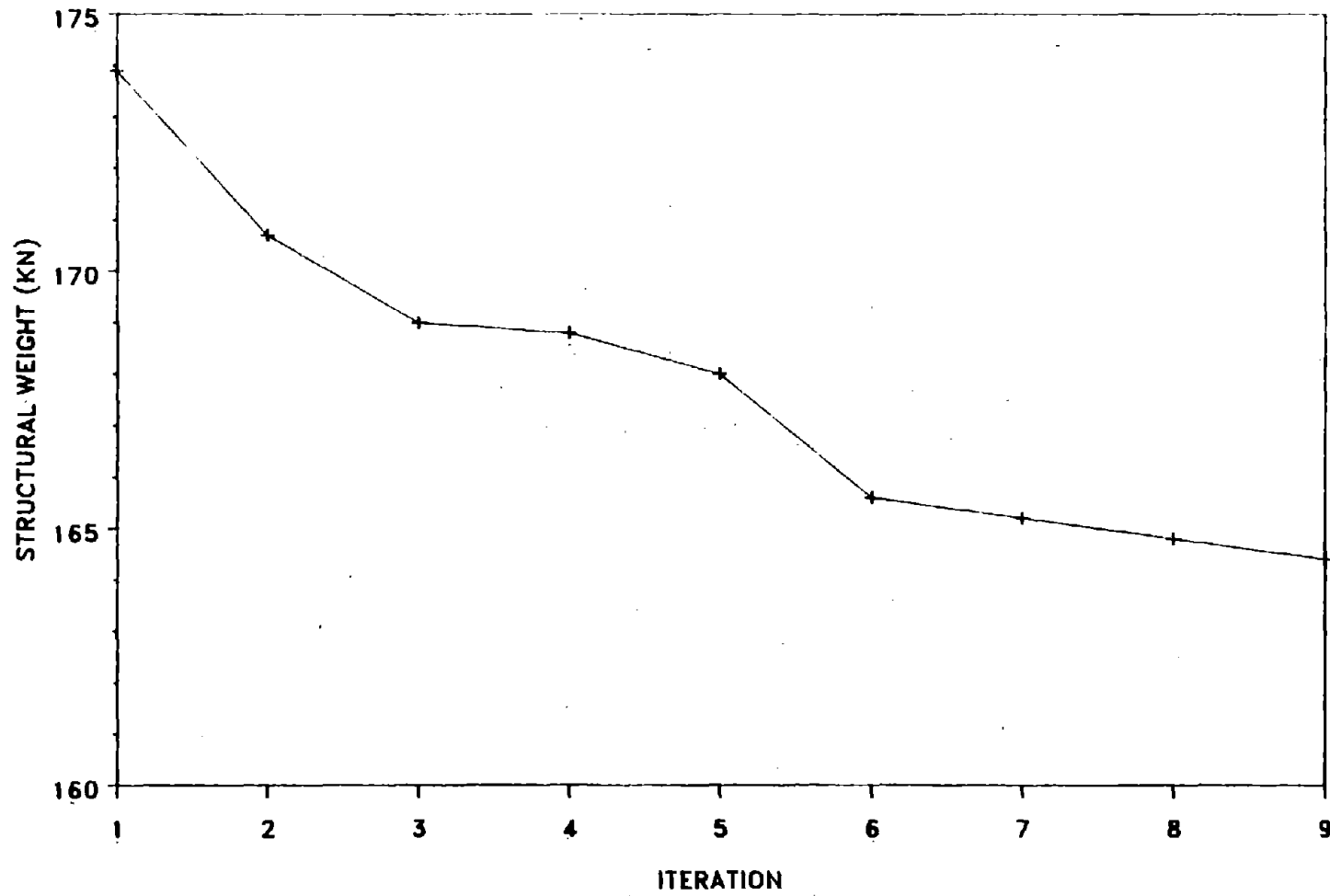
Figure 60. Structural Optimization using Frequency Constraints: (a) Structural Weight
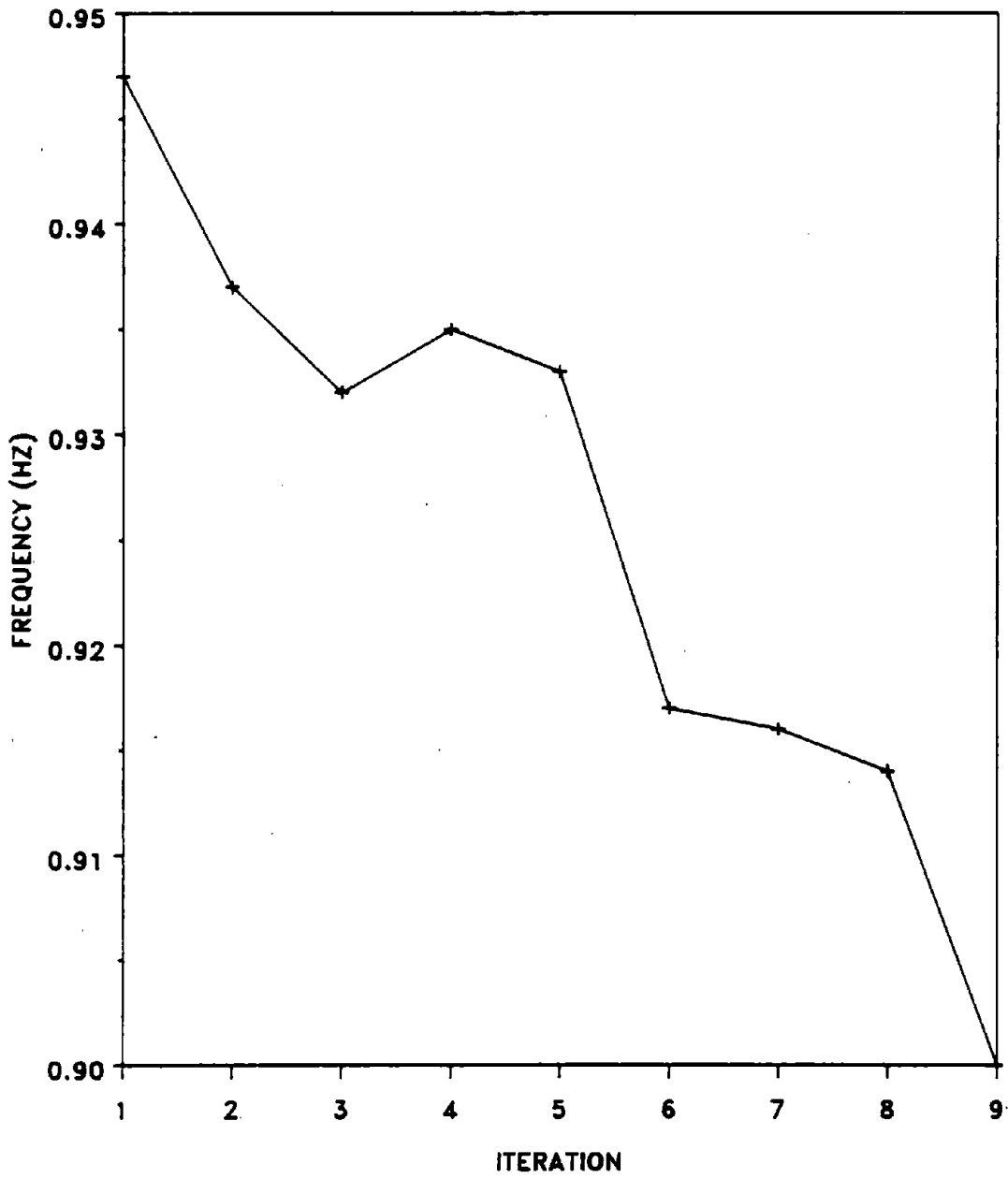
Figure 60. (cont'd)
          (b) First Mode Frequency
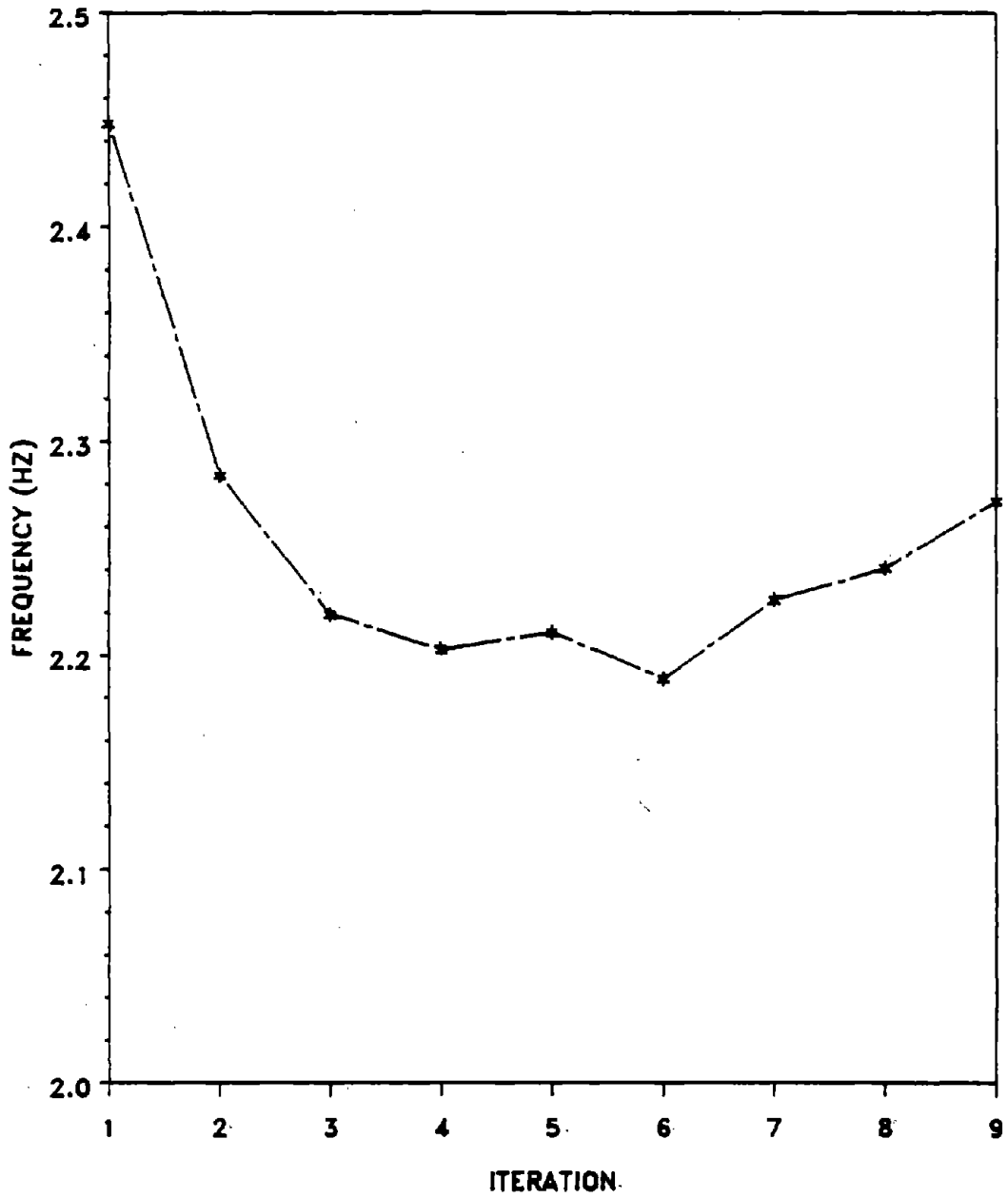
Figure 60. (cont'd)
          (c) Second Mode Frequency
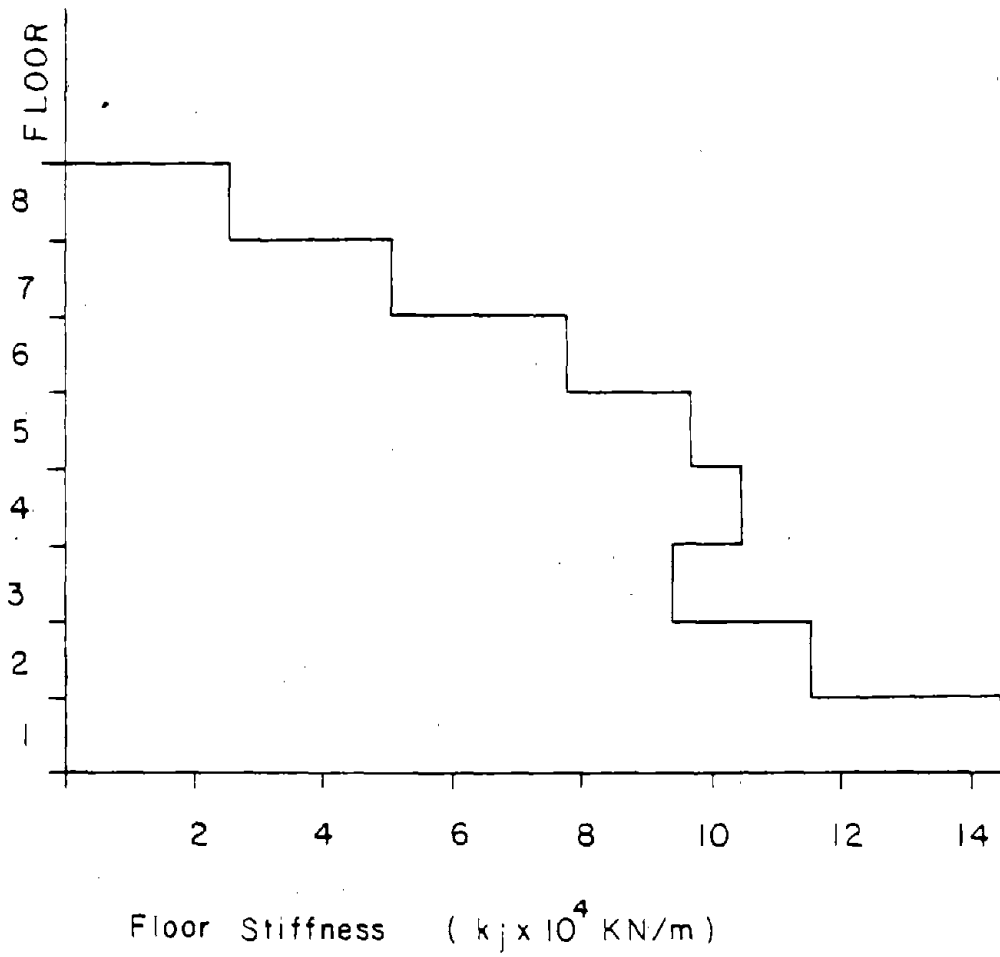
Figure 61. Optimum Stiffness Distribution for Frequency Costraints

VII. CONTROL ENERGY MINIMIZATION

Through the course of this study it has been shown that the weighting matrices are influential in shaping the response. When the elements of the response weighting matrix $[Q]$ are large the response is reduced, but at the expense of large control forces. When the elements of the control weighting matrix $[R]$ are large the control forces are small, however the displacement response is increased. Evidence of these observations was shown in Figure 31 in Chapter V for a wind-excited structure, but similar results are obtained under earthquake excitations.

Physical limitations of the actuator impose an upper bound on the maximum control force magnitude that can be achieved. Considerations of power limit the control energy available. Various objectives and constraints can be met by judicious selection of the elements of the weighting matrices. Physically the weighting matrices affect the gain matrix for the system and they are implemented in terms of the amplifier gains that produce the control forces.

From extensive numerical results carried out during this study it was observed that when the weighting matrices $[Q]$ and $[R]$ are assumed diagonal, it is not the absolute value of the elements of these matrices that influences the response but the ratio of the elements (11). Thus the problem can be simplified by keeping the elements of matrix $[Q]$ constant and varying the elements of $[R]$ only. A trial-and-error approach was used in order to search for the elements of the weighting matrix $[R]$ that will produce approximately equal

maxima for the control forces on all the floors. This is desirable from a practical point of view.

A more rational procedure is developed herein in order to obtain the optimal weighting matrix $[R]$. The control energy is chosen as the objective function to be minimized. The constraints are the same as those used in the structural optimization using optimal control algorithms. The optimization problem is as follows: Find the elements $R(i,i)$ of the weighting matrix $[R]$, assumed diagonal, that will minimize the control energy defined as

$$JE = \frac{1}{2} \int_{t_0}^{t_f} \{u(t)\}^T [R] \{u(t)\} \, dt \tag{7.1}$$

subject to constraints on the maximum allowable floor relative displacements and maximum allowable control forces

$$x_j(t) \leq x_j \max \qquad\qquad j = 1, \dots, N \tag{7.2}$$

$$u_i(t) \leq u_i \max \qquad\qquad i = 1, \dots, M \tag{7.3}$$

where N is the number of floors, and M is the number of controllers. The objective here is to obtain the optimum weighting matrices that will reduce the control forces, while the response still remains within the constraint limitations. In this sense, a combination of structural optimization and optimal active control yields an economical design that both determines the optimal structure stiffnesses and the optimum control parameters as expressed by the optimum weighting matrices.

The optimal weight structure obtained in Case 1 of Section E in Chapter VI is used as the structure for applying the control energy minimization procedure. The structure and the weighting matrix $[Q]$ are fixed. The constraints for allowable displacements and control forces are the same as before for Case 1. The objective is to determine the optimum elements of the diagonal weighting matrix $R(i,i)$, $i = 1,...,8$, that will minimize the control energy as defined by Equation 7.1. From the results shown in Figure 62 and Table III, it can be observed that by finding the optimal weighting matrices, the maxima of the control forces have been reduced. The first floor control force at iteration 1 and iteration 5 are compared in Figure 63. It is clear that the energy minimization has resulted in reduction of the control force. The maxima displacements, of course, are still bound by the constraints used in Case 1.
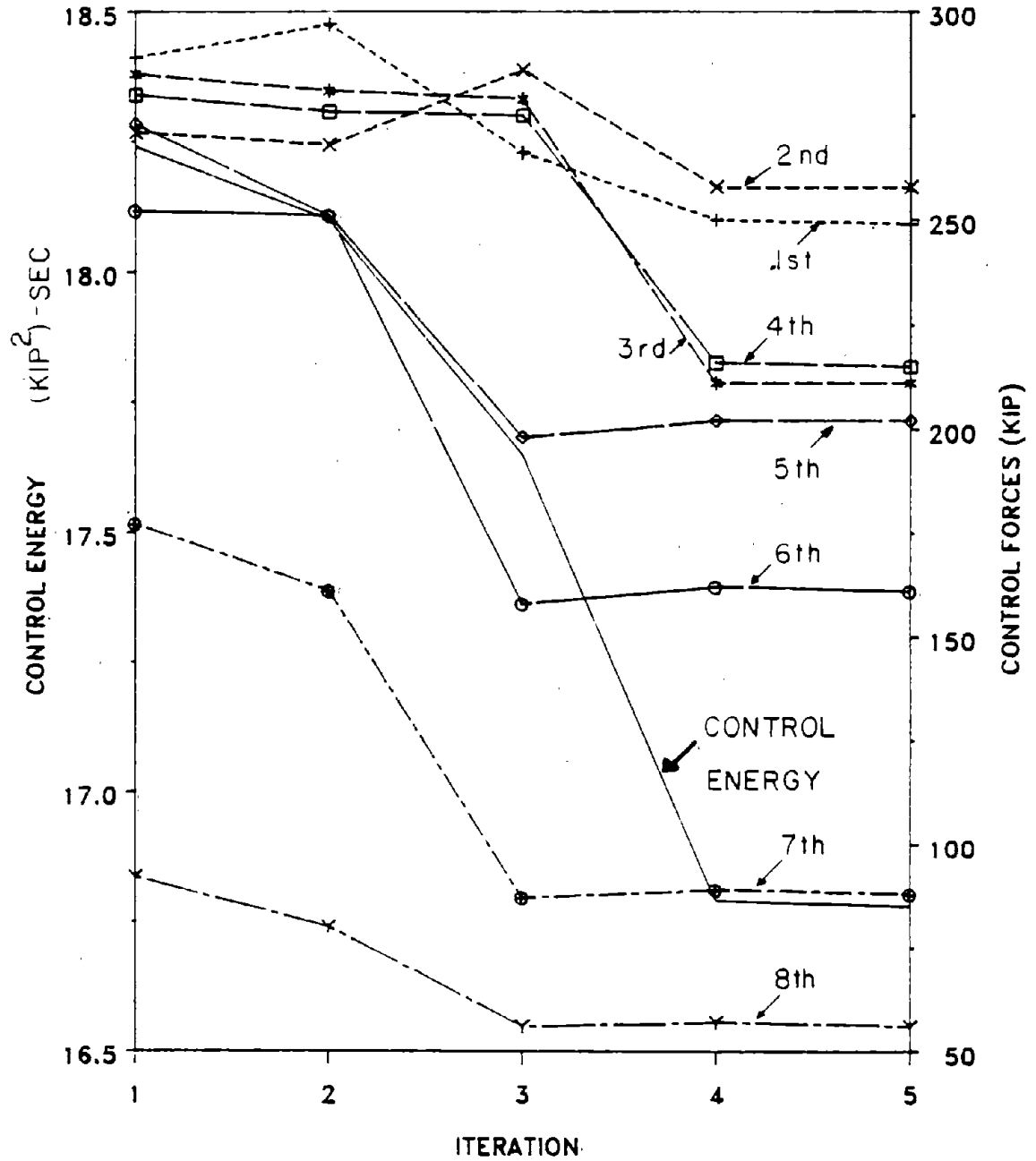
Figure 62. Optimal Weighting Matrices and Control Energy
(1 kip = 4.45 kN), (1 (kip)^2-sec = 19.8 (kN)^2-sec)

TABLE III. CONTROL ENERGY MINIMIZATION RESULTS

Maxima of Control Forces (kip)
(1 kip = 4.45 kN)

Iteration Number	Floor Number							
	1	2	3	4	5	6	7	8
1	289	271	285	280	273	252	177	92
5	250	258	211	216	202	162	89	57

Weighting Variables $R(i,i) \times 10^{-3}$

Iteration Number	Floor Number							
	1	2	3	4	5	6	7	8
1	.070	.070	.070	.070	.070	.070	.070	.070
5	.110	.076	.100	.095	.109	.169	.274	.240

300

FIRST FLOOR CONTROL FORCE (KIP)

200

100

0

-100

-200

-300

0   1   2   3   4   5   6   7   8   9   10

TIME (SEC)

——— Iteration 1
- - - - Iteration 5

152
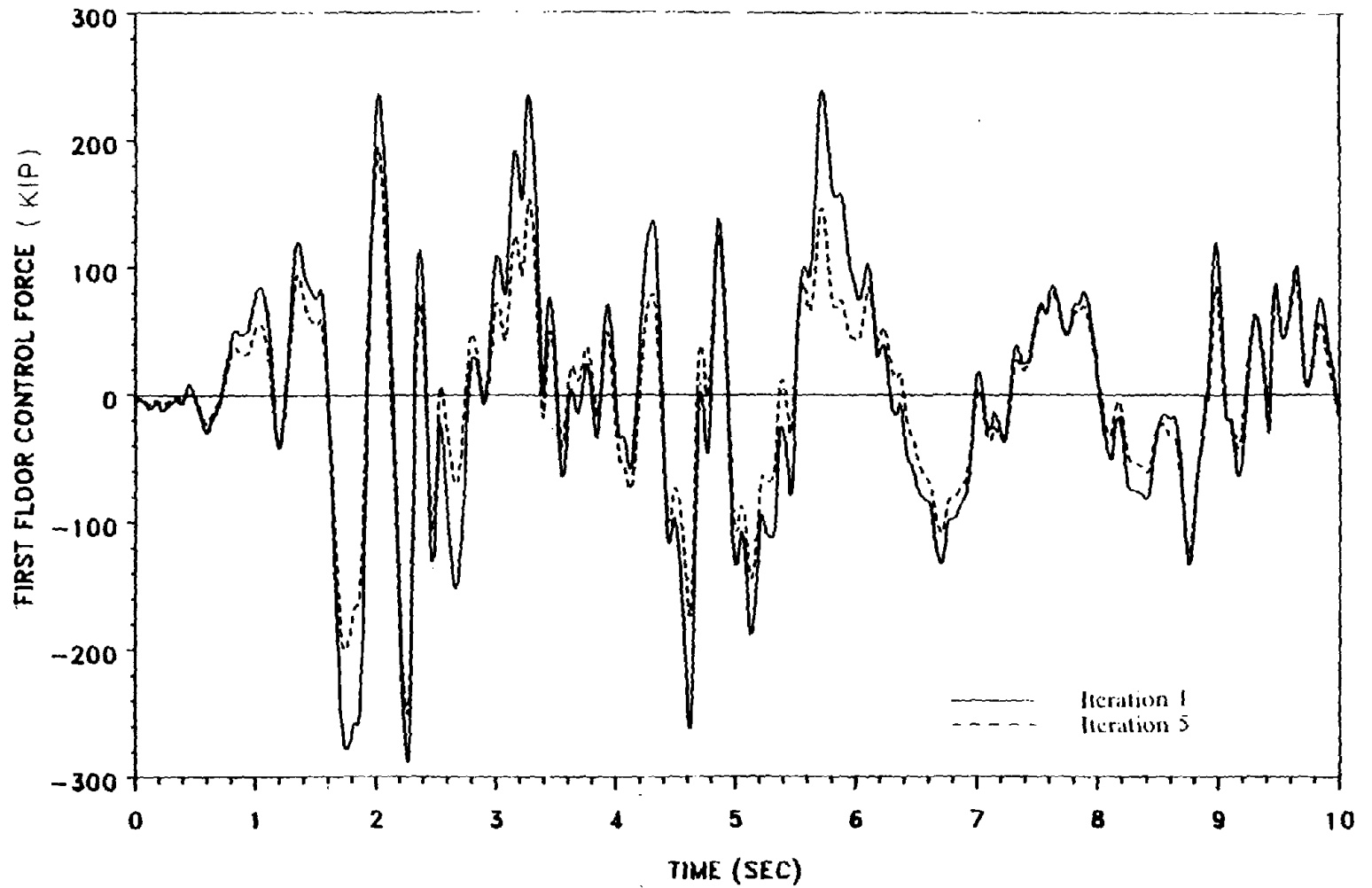
Figure 63.   Comparison of Control Forces at First Floor
(1 kip = 4.45 kN)

VIII. TIME-DELAY IN APPLICATION OF CONTROL

A very important issue in the implementation of active control is that of time-delay. Time-delay can cause unsychronized application of the control force. More importantly, due to time-delay the control forces may be applied at a time at which they are not needed. It is plausible that such delay in the application of the control forces may lead to instability, because the control forces may deteriorate the situation if they are applied at the wrong time.

Although time-delay may be attributed to a variety of factors, the reasons for it can be classified in two categories. First, time-delay is caused due to on-line computation and execution of the control forces. Secondly, it can be caused from delay in measuring on-line the base acceleration. Note that the first category is unavoidable no matter which control algorithm is being used. However the second category will occur only if the open-loop, or open-closed-loop control algorithms are utilized, as shown by Chung, Reinhorn and Soong (15).

A. ON-LINE COMPUTATION AND EXECUTION OF CONTROL FORCES

This category of time-delay arises from the delay caused by the computer in calculating the optimal control forces according to the algorithm currently in use, and the delay caused in the movement of the actuator. This type of delay can be compensated for. Assume that the structure oscillates with a dominant frequency, ω_1. The feedback

force is in general of two types, displacement feedback force (DFF), and velocity feedback force (VFF),

$$u(t) = G1\,x(t) + G2\,\dot{x}(t) \tag{8.1}$$

where the first term on the right side of Eqs. 8.1 is the DFF, and the second term the VFF. If the DFF lags the measurement of the displacement, t_x units of time, and the VFF lags the measurement of the velocity, $t_{\dot{x}}$ units of time, their corresponding phase lags are $\omega_1 t_x$ and $\omega_1 t_{\dot{x}}$, respectively. The ideal and the real system are shown in Figure 64. The ideal or theoretical gains are $G1$ and $G2$ as shown in Figure 64(a), and the real gains are denoted by g_1 and g_2 as shown in Figure 64(b). By resolving the DFF and VFF in the real system one obtains the situation shown in Figure 64(c). Note that the DFF produces a negative component which reduces the control force effect of the real system. Thus time-delay may cause instability. The time-delay is compensated for in the real system as follows: 1) precalculate the feedback gains $G1$ and $G2$, and the fundamental frequency of the structure, ω_1, for the ideal or theoretical system, 2) determine the time-lag in the measurement of the displacement t_x and the velocity $t_{\dot{x}}$ experimentally; this can be done by measuring the phase shift of the transfer function of the real system, when the structure is subjected to a white noise excitation, 3) use the information from 1), and 2) to calculate the real gains g_1 and g_2 with time compensation. From Figure 64, the equivalence of the real and ideal control forces gives

$$(G1)\,x(t) = (g_1 \cos \omega_1 t_x)\,x(t) + (g_2 \sin \omega_1 t_{\dot{x}})\,\omega_1\,x(t) \tag{8.2}$$

154
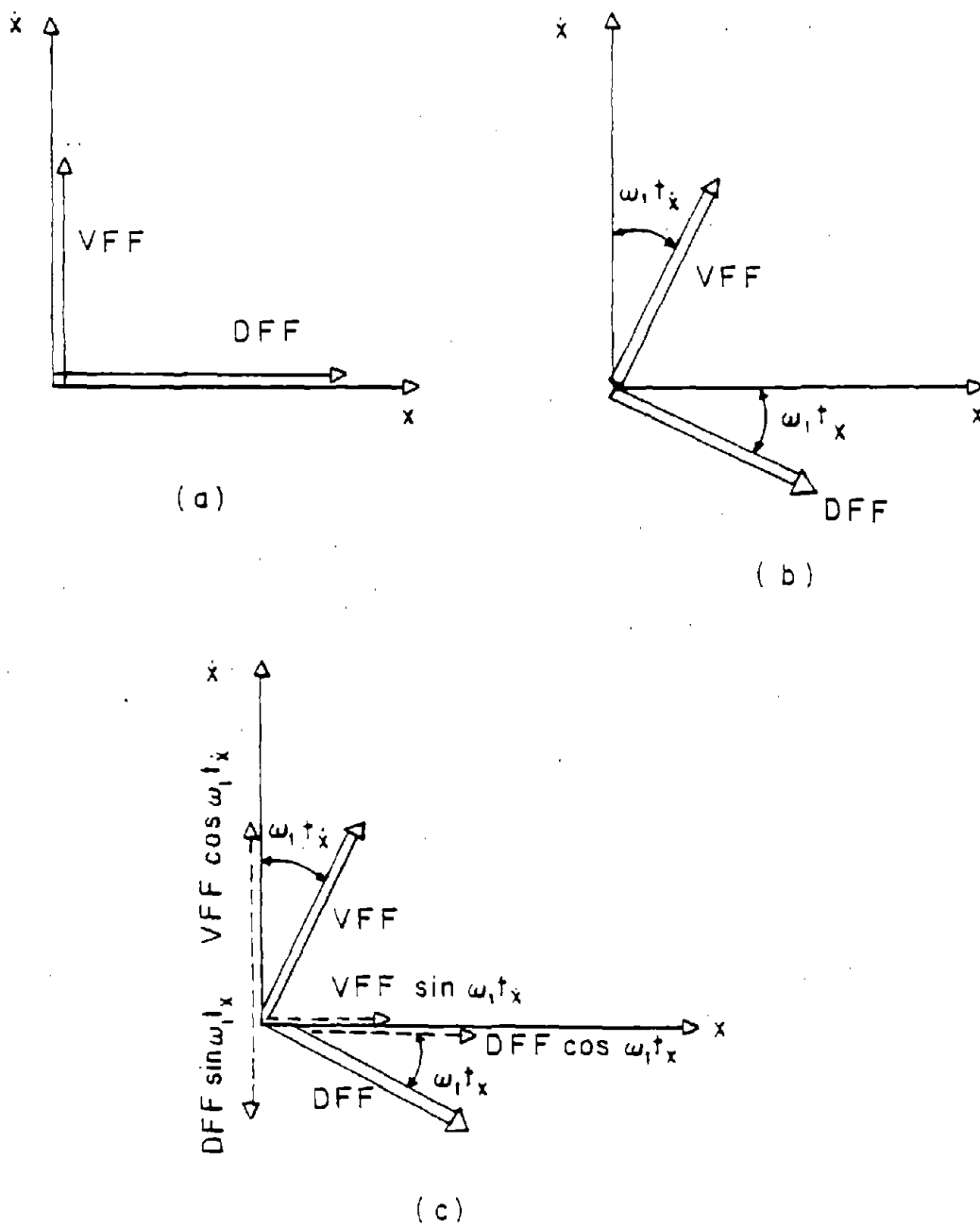
Figure 64. DFF and VFF for Ideal and Real System:
(a) Ideal System, (b) Real System, (c) Resolution

$$(G2) \; \dot{x}(t) \;\; = \;\; (-g_1 \sin \omega_1 \, t_x) \frac{\dot{x}(t)}{\omega_1} + (g_2 \cos \omega_1 \, t_x) \, \dot{x}(t) \qquad\qquad (8.3)$$

Thus in order to have the ideal system produce the control forces required by the real system the following relation must hold

$$\begin{bmatrix} \cos \omega_1 \, t_x & \omega_1 \sin \omega_1 \, t_x \\ -\dfrac{1}{\omega_1} \sin \omega_1 \, t_x & \cos \omega_1 \, t_x \end{bmatrix} \begin{Bmatrix} g_1 \\ g_2 \end{Bmatrix} = \begin{Bmatrix} G1 \\ G2 \end{Bmatrix} \qquad\qquad (8.4)$$

Therefore the real system gains can be obtained from those of the ideal system by

$$\begin{Bmatrix} g_1 \\ g_2 \end{Bmatrix} = \frac{1}{\cos \omega_1 \, (t_x - t_x)} \begin{bmatrix} \cos \omega_1 \, t_x & \dfrac{1}{\omega_1} \sin \omega_1 \, t_x \\ -\omega_1 \sin \omega_1 \, t_x & \cos \omega_1 \, t_x \end{bmatrix} \begin{Bmatrix} G1 \\ G2 \end{Bmatrix} \qquad (8.5)$$

B. COMPENSATION METHOD FOR TIME-DELAY

For multiple degree-of-freedom systems with more than one controller, the same concepts can be applied as for the single degree-of-freedom system. Being a distributed parameter system, the structure will be controlled at discrete locations. The active tendons will be located at various floors of the building. Assuming for the present discussion that an eight-story building will be equipped with eight active tendons, we note the following: 1) the time delays in the VFF and DFF will in general not be the same for every controller, 2) for the purpose of calculating time-delays assume that the structure is vibrating at its controlled fundamental frequency, 3) the controlled fundamental frequency can be obtained from the closed-loop plant matrix. Following the discussion for the single

degree-of-freedom system, Eqs. 8.5 will still be valid for the ith tendon control force

$$\begin{Bmatrix} g_1 \\ g_2 \end{Bmatrix}_i = [TR]_i \begin{Bmatrix} G1 \\ G2 \end{Bmatrix}_i \qquad (8.6)$$

where $[TR]_i$ was given in Eqs. 8.5. Note that for the particular tendon ι_x and $\iota_{\dot{x}}$ may be different, and therefore the elements of $[TR]_i$ will be different. The ideal gain matrix $[IK]$ for the instantaneous optimal closed-loop control was derived in Chapter V, and is given by

$$[IK] = -\left(\frac{\Delta\iota}{2}\right)[R]^{-1}[B_i]^T[Q] \qquad (8.7)$$

If we consider that the weighting matrices $[Q]$ and $[R]$ are diagonal, and that the time-delay for each controller is the same, then it can be shown that the real gain matrix for the present example is an $[8 \times 16]$ matrix. Because of the form of the controller location matrix, the real gain matrix is given by

$$[RK] = [[0] | [RKR]] \qquad (8.8)$$

where $[RKR]$ is an $[8 \times 8]$ submatrix whose non-zero elements are: $(1,1)$, $(2,1)$, $(2,2)$, $(3,2)$, $(3,3)$, $(4,3)$, $(4,4)$, $(5,4)$, $(5,5)$, $(6,5)$, $(6,6)$, $(7,6)$, $(7,7)$, $(8,7)$, and $(8,8)$. The non-zero elements of the real gain matrix are related to those of the ideal gain matrix as follows

$$g_{i,j} = \frac{G(i,j)}{\cos(\omega \iota_{\dot{x}})} \qquad (8.9)$$

It is important to note that as more advanced control software and hardware becomes available, the magnitude of time-delay is expected to

157

decrease. In the experiment carried out by Chung, Reinhorn and Soong for a single degree-of-freedom system, it was found that the values for t_x and $t_{\dot{x}}$ were 30 msec, and 36 msec, respectively (15). It was also stated that since real structures vibrate at a lower fundamental frequency as compared with the test-model, time-delay is expected to produce minor effects. The issue of time-delay is investigated in order to be utilized in the optimal control algorithms used in the structural optimization process.

C. APPLICATION OF TIME-DELAY COMPENSATION

For the purpose of illustrating the time-compensation method, a numerical simulation of the real system was attempted. A SDOF structural system equipped with an active tendon is considered. The structural and control properties are described in Table IV. The elements of the weighting matrices $[Q]$ and R are chosen as

$$[Q] = \left[\begin{array}{c|c} 2k & 0 \\ \hline 0 & 0 \end{array}\right], \qquad R = (2 \times 10^{-3})\, k_t \qquad (8.10)$$

where k is the structure stiffness, k_t is the tendon stiffness and their values are given in Table IV. The time-delay values were assumed as follows: $t_x = 30$ msec and $t_{\dot{x}} = 36$ msec, respectively. The results for a system compensated for time-delay and an identical system for which time-delay was not considered are shown in Figures 65 through 67. From these results it can be seen that time delay has some influence on the response and the applied control force.

TABLE IV. TIME-DELAY SIMULATION DATA
(1 lb-sec^2/in = 175 Kg)
(1 lb/in = 175 N/m)

Parameter	Quantity
mass	16.69 lb-sec^2/in
structure stiffness	7934 lb/in
tendon stiffness	2124 lb/in
tendon angle	36 degrees
natural frequency	3.47 Hz
damping factor	1.24 %
earthquake excitation	30 % of El-Centro 1940
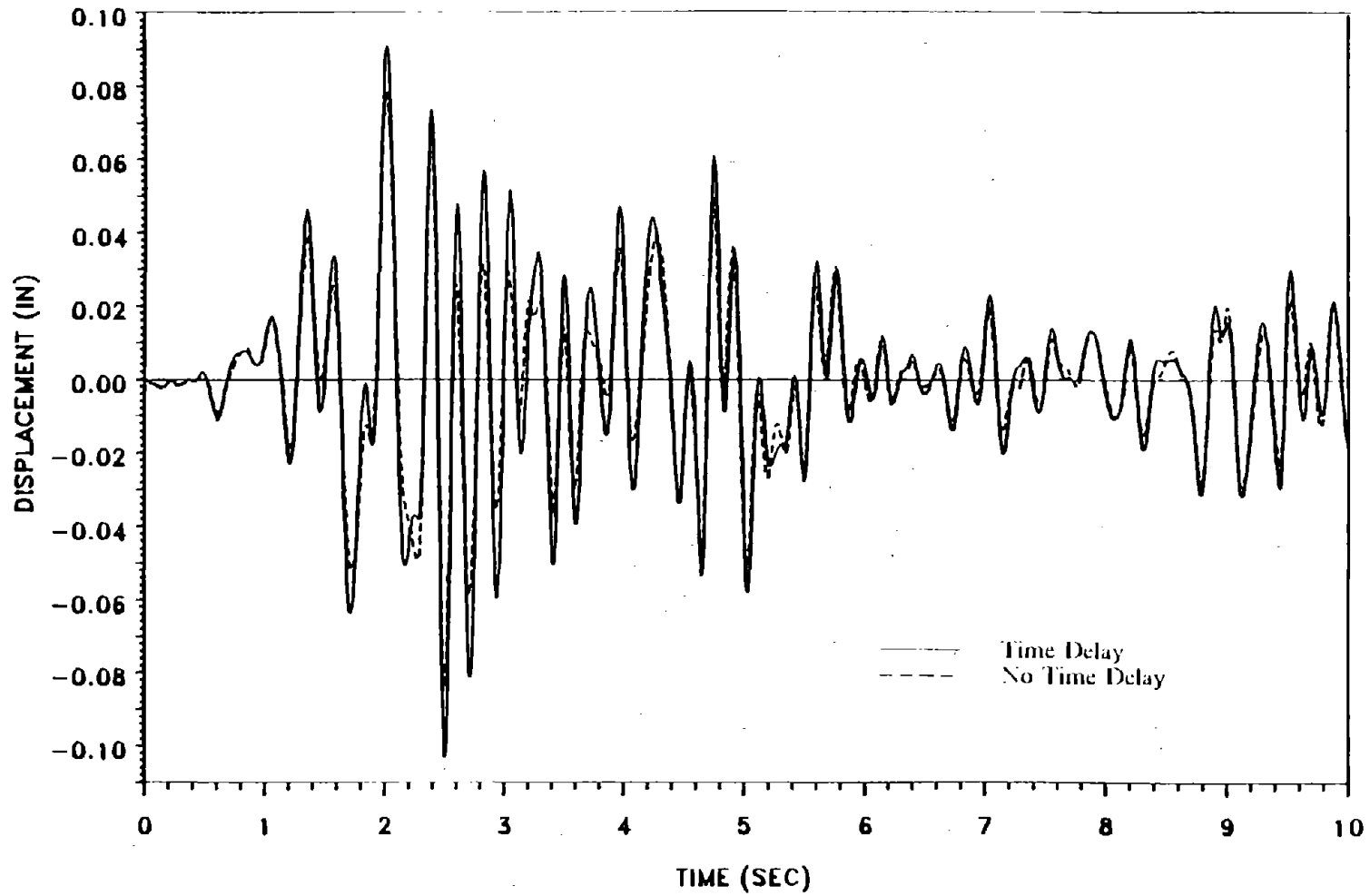
Figure 65. Displacement for SDOF with Time-delay
(1 in = 25.4 mm)
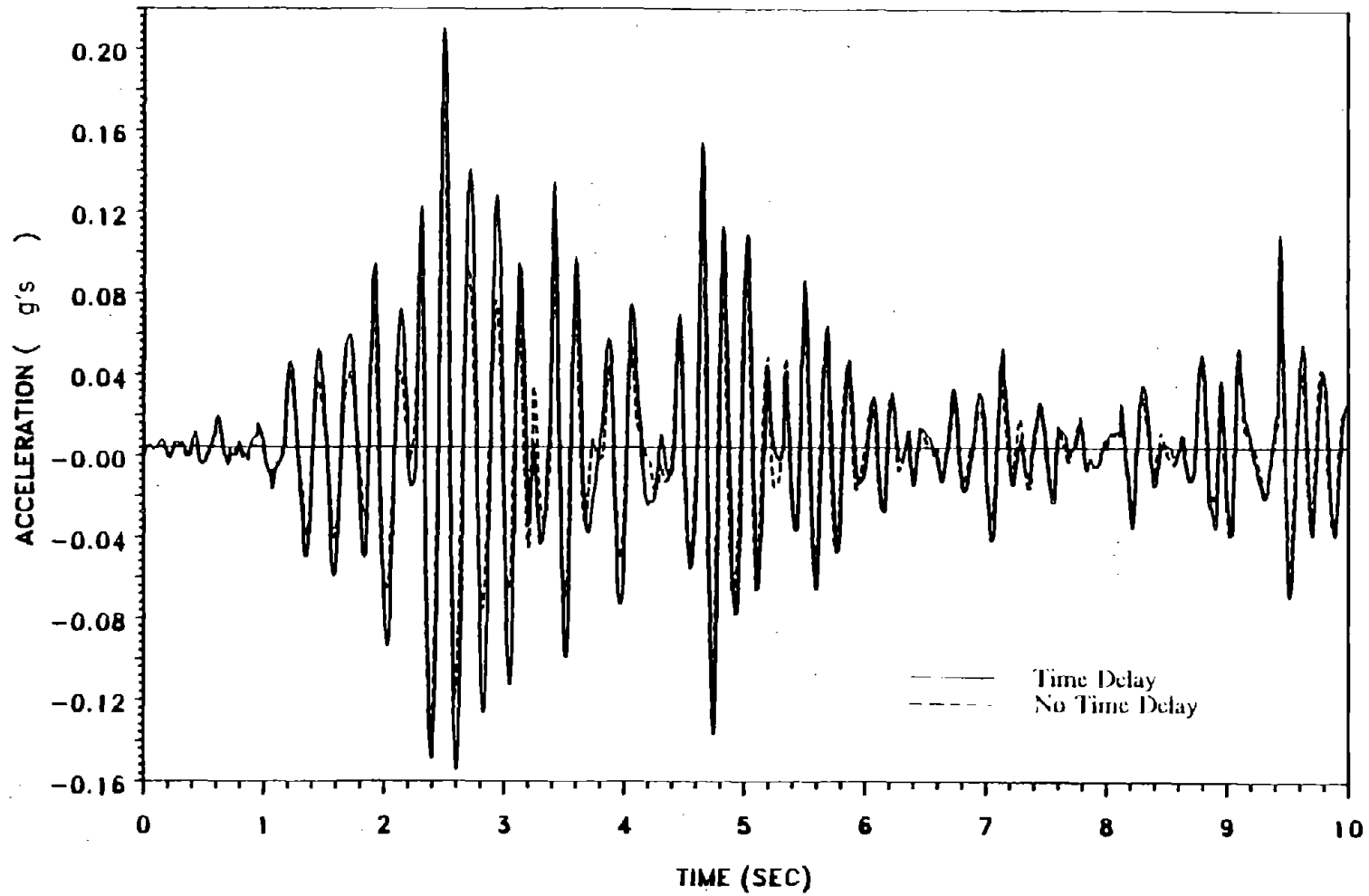
Figure 66. Acceleration for SDOF with Time-delay
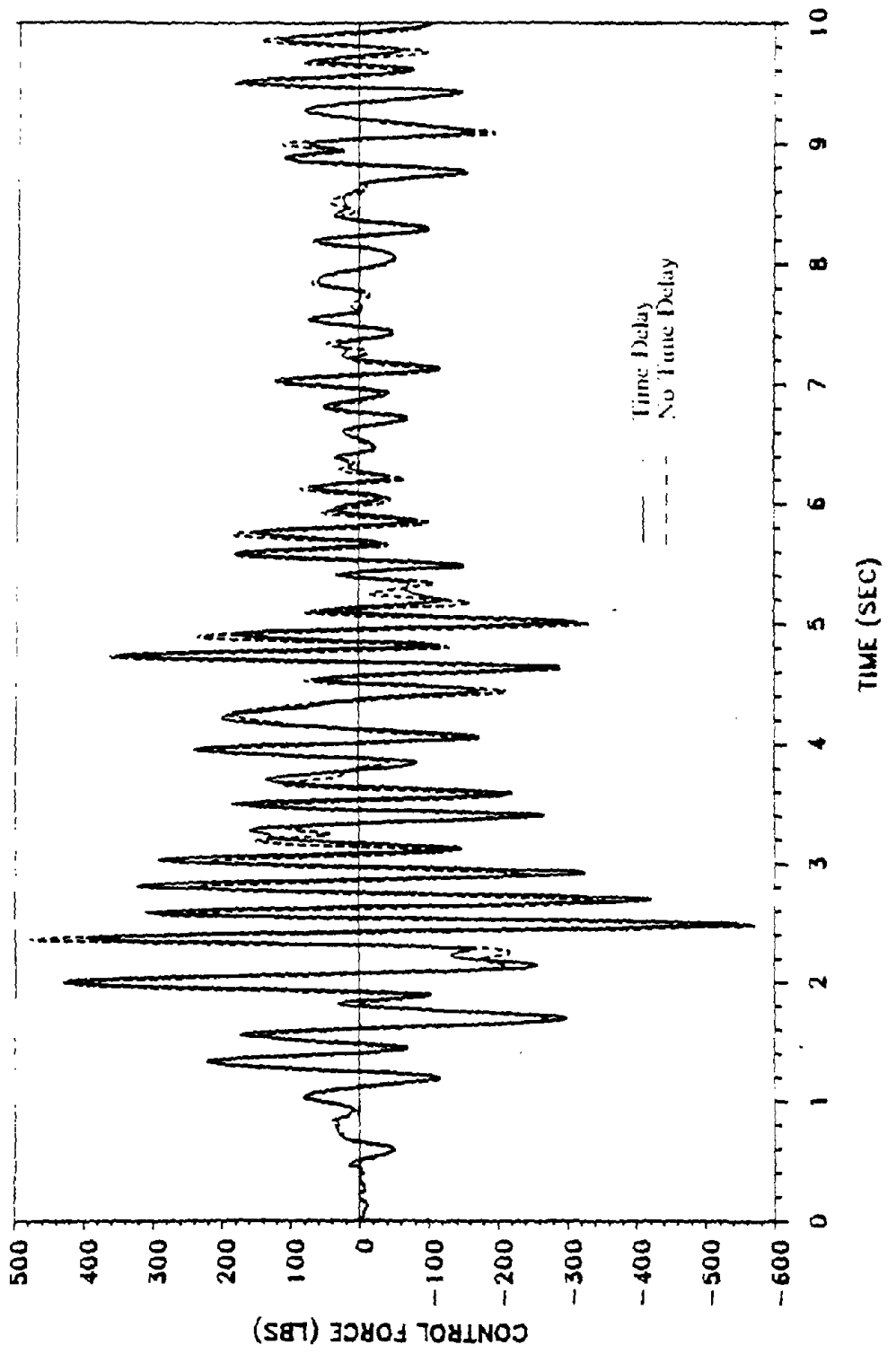
Figure 67. Control Force for SDOF with Time-delay
(1 lb = 4.45 N)

162

IX. CRITICAL-MODE CONTROL ALGORITHM

As it was pointed out in the Introduction, the optimal critical-mode control is likely to be as effective as the optimal global control, since the response of tall buildings under earthquake excitations is usually dominated by a few lowest modes. The critical-mode control is also superior to the global control, as far as the amount of on-line computations is concerned. For global control of a structure with N degrees of freedom, the instantaneous algorithms require the solution of $2N$ differential equations. However, if only $\bar{m}$ critical modes are controlled where $(\bar{m} < N)$, only $2\bar{m}$ differential equations have to be solved. The critical-mode control algorithm is developed in order to reduce the amount of computation, which is important in the structural optimization procedure.

In this Chapter the critical-mode control algorithm is derived based on the instantaneous closed-loop algorithm. The spillover effect is demonstrated theoretically and through the use of numerical examples. The algorithm is then used as a tool for establishing optimal locations of active tendon controllers when only a limited number of controllers are available.

A. CRITICAL-MODE CONTROL USING INSTANTANEOUS CLOSED-LOOP ALGORITHM

The formulation follows the developments of Chapter V. The modal state-equation can be written in an expanded form using Equations 5.5 through 5.7 as follows

$$\{\dot{\psi}_t(t)\} = [\varphi_t]\{\psi_t(t)\} + [T_t]^{-1}[B_t]\{u(t)\} + [T_t]^{-1}\{C_t\}\ddot{X}_g(t) \qquad (9.1)$$

Our interest is in controlling only the lowest modes $\{\psi_t(t)\}_c$. The remaining residual modes are denoted as $\{\psi_t(t)\}_r$. By partitioning $[\varphi_t]$ according to the critical and residual modes, Equation 9.1 can be written in the form

$$\left\{\frac{\{\dot{\psi}_t(t)\}_c}{\{\dot{\psi}_t(t)\}_r}\right\} = \left[\begin{array}{c|c} [\varphi_t]_c & [0] \\ \hline [0] & [\varphi_t]_r \end{array}\right]\left\{\frac{\{\psi_t(t)\}_c}{\{\psi_t(t)\}_r}\right\} + \left[\frac{[TB]_c}{[TB]_r}\right]\{u(t)\}$$
$$+ \left\{\frac{\{TC\}_c}{\{TC\}_r}\right\}\ddot{X}_g(t) \qquad (9.2)$$

where the following definitions have been used

$$[TB] = [T_t]^{-1}[B_t], \qquad \qquad \{TC\} = [T_t]^{-1}\{C_t\} \qquad (9.3)$$

Rewriting Equation 9.2 in two separate equations, one for the critical and one for the residual modes

$$\{\dot{\psi}_t(t)\}_c = [\varphi_t]_c\{\psi_t(t)\}_c + [TB]_c\{u(t)\} + \{TC\}_c\ddot{X}_g(t) \qquad (9.4)$$

$$\{\dot{\psi}_t(t)\}_r = [\varphi_t]_r\{\psi_t(t)\}_r + [TB]_r\{u(t)\} + \{TC\}_r\ddot{X}_g(t) \qquad (9.5)$$

The critical-mode control algorithm is based entirely on the dynamics of Equation 9.4. The residual modes of Equation 9.5 are ignored in the derivation of the optimal control law. The instantaneous performance

164

index has to be expressed in terms of the critical modes only. This can be achieved by substituting Equation 5.2 into Equation 5.1, and retaining the term containing the critical modes $\{\psi_t(t)\}_c$ only. The expression for Equation 5.1 becomes

$$J_p(t) = \{[T_t]\{\psi_t(t)\}\}^T [Q] \{[T_t]\{\psi_t(t)\}\} + \{u(t)\}^T [R]\{u(t)\} \tag{9.6}$$

Substituting the partitioned modal state-vector $\{\psi_t(t)\}$

$$\{\psi_t(t)\} = \left\{ \frac{\{\psi_t(t)\}_c}{\{\psi_t(t)\}_r} \right\} \tag{9.7}$$

in Equation 9.6, performing the algebra, and ignoring terms that involve the residual modes $\{\psi_t(t)\}_r$, the critical-mode performance index is

$$J_c(t) = \{\psi_t(t)\}_c^T [Q]_c \{\psi_t(t)\}_c + \{u(t)\}^T [R]\{u(t)\} \tag{9.8}$$

in which $[Q]_c$ is a $\overline{2m} \times \overline{2m}$ matrix obtained form partitioning the following matrix product

$$[T_t]^T [Q][T_t] = \left[\begin{array}{c|c} [Q]_c & [Q]_{cr} \\ \hline [Q]_{rc} & [Q]_r \end{array} \right] \tag{9.9}$$

More details about Equations 9.8 and 9.9 can be found in Appendix C. The critical-mode optimal control problem is as follows: Find the optimal control $\{u^\bullet(t)\}$ that minimizes the critical-mode performance index $J_c(t)$ and satisfies the state-equation for the critical modes Equation 9.4. Following the derivation for the global control algorithm, the critical-mode closed-loop optimal control is found in Appendix D as

165

$$\{u^{\cdot}(t)\} = -\left(\frac{\Delta t}{2}\right)[R]^{-1}[TB]_c^T[Q]_c\{\psi_t(t)\}_c \qquad (9.10)$$
$$= [K]_c\{\psi_t(t)\}_c$$

Note that the optimal control is given as a function of the modal state-vector. Specifically, only the critical modes $\{\psi_t(t)\}_c$ are of interest. However the displacement and velocity sensors measure the actual state-vector $\{z(t)\}$. The modal states can be estimated using modal filters, as pointed out by Meirovitch and Baruh (38). The modal filters produce estimates of modal states from distributed measurements of the actual states. For simulation purposes we assume that the modal state-vector can be recovered from the actual state-vector $\{z(t)\}$ by using the inverse of Equation 5.2 in the following form,

$$\left\{\frac{\{\psi_t(t)\}_c}{\{\psi_t(t)\}_r}\right\} = [T_t]^{-1}\{z(t)\} \qquad (9.11)$$

The solution of the motion equation Equation 9.1 proceeds in two parts. First the critical modes are obtained by solving Equation 9.4, and the residual modes are obtained by solving Equation 9.5. The solution of Equation 9.4 for the critical modes can be written as

$$\{\psi_t(t)\}_c = \int_0^t \exp[[\varphi_t]_c(t-\tau)]\left\{[TB]_c\{u(t)\} + \{TC\}_c \ddot{X}_g(t)\right\}d\tau \qquad (9.12)$$

Proceeding for the numerical integration in the same manner performed for the global control in Equations 5.12 through 5.16 and 5.33, we obtain

$$\{\psi_t(t)\}_c = [\hat{P}1(t)]\{\hat{P}2(t)\} \qquad (9.13a)$$

$$[\hat{P}1(t)] = \left[[I]_c + \frac{(\Delta t)^2}{4} [TB]_c [R]^{-1} [TB]_c^T [Q]_c \right]^{-1} \tag{9.13b}$$

$$\{\hat{P}2(t)\} = \left\{ \{\Lambda_t(t - \Delta t)\}_c + \{TC\}_c \cdot \ddot{X}_g(t) \left(\frac{\Delta t}{2} \right) \right\} \tag{9.13c}$$

The derivation of Equation 9.13 is given in Appendix D. The solution for the residual modes can be obtained in a similar manner from Equation 9.5. Finally the actual state-vector $\{z(t)\}$ is retrieved from Equation 5.2. The derivative of the state-vector can then be obtained from Equation 3.13. The effectiveness of critical-mode control applied to seismic structures is illustrated in the numerical examples.

B. SPILLOVER EFFECT

It is known that any modal control technique has as an objective to control only some of the modes. The control forces may excite the remaining uncontrolled modes. This is shown here for the instantaneous closed-loop algorithm. Substituting Equation 9.10 in Equation 9.2 we obtain

$$\left\{ \begin{matrix} \{\dot{\psi}_t(t)\}_c \\ \{\dot{\psi}_t(t)\}_r \end{matrix} \right\} = \left[\begin{matrix} [\varphi_t]_c & [0] \\ [0] & [\varphi_t]_r \end{matrix} \right] \left\{ \begin{matrix} \{\psi_t(t)\}_c \\ \{\psi_t(t)\}_r \end{matrix} \right\} + \left[\begin{matrix} [TB]_c [K]_c \\ [TB]_r [K]_c \end{matrix} \right] \{\psi_t(t)\}_c \tag{9.14}$$
$$+ \left\{ \begin{matrix} \{TC\}_c \\ \{TC\}_r \end{matrix} \right\} \ddot{X}_g(t)$$

Collecting terms

$$\left\{ \begin{matrix} \{\dot{\psi}_t(t)\}_c \\ \{\dot{\psi}_t(t)\}_r \end{matrix} \right\} = \left[\begin{matrix} [\varphi_t]_c + [TB]_c [K]_c & [0] \\ [TB]_r [K]_c & [\varphi_t]_r \end{matrix} \right] \left\{ \begin{matrix} \{\psi_t(t)\}_c \\ \{\psi_t(t)\}_r \end{matrix} \right\} \tag{9.15}$$
$$+ \left\{ \begin{matrix} \{TC\}_c \\ \{TC\}_r \end{matrix} \right\} \ddot{X}_g(t)$$

167

Rewriting the equation for the residual modes by partitioning Equation 9.15

$$\{\psi_t(t)\}_r = [\varphi_t]_r \{\psi_t(t)\}_r + \{TC\}_r \dot{X}_g(t) + [TB]_r [K]_c \{\psi_t(t)\}_c \qquad (9.16)$$

By comparison, note that for an uncontrolled system, the last term would be absent. Thus the last term is an excitation of the residual modes by the control forces. This term produces the control spillover effect, the influence of which is examined in the numerical examples. If critical-mode control is to be effective, the spillover effect should be minimized.

C.   OPTIMAL LOCATION OF CONTROLLERS

The objective of this Section is to establish criteria for the optimal location of a limited number of controllers. The critical-mode optimal control algorithm derived in this Chapter is used to control the lowest modes of a seismic structure. It is quite plausible that in the application of active control systems to structures, it may be more economical to place the controllers at a few preselected locations. The term optimal locations reflects on the reduction of the structural response, while using the minimum control effort. The location of the controllers with respect to the structure is reflected in the matrix $[\gamma]$ in Equation 3.7, and the state-form matrix $[B_t]$ in Equation 3.14. By varying the locations of the controllers, the entries in the aforementioned location matrix will be changed, thus the dynamic response will be modified.

168

One method of selecting the optimal controller locations is to consider the modal shapes of the structure. The modal shapes of the few lowest modes that we select to control give useful information about the most beneficial locations. The maxima of these modal shapes in a given mode are obviously advantageous locations for the controllers. However the determination of the optimal locations for a combination of modes is more of an intuitive procedure, but nevertheless very useful. Another method for the optimal locations selection is one proposed by Martin and Soong (34). In this approach a performance index of control energy is minimized in the time period of interest. This performance index is defined by the integral

$$J_E = \int_0^{t_f} \{u(t)\}^T \{u(t)\} \, dt \tag{9.17}$$

where t_f is the final time. The concept here is that if the choice of the controller locations is to be optimal, the control work performed by the control system as reflected in Equation 9.17 is to be a minimum. In the course of the present study it has become obvious that minimization of the performance index of Equation 9.17 alone may not lead to the optimal solution since when the control energy is reduced the response is bound to be increased. Therefore a new performance index is suggested that reflects upon the measure of the reduction of the structural response, given as

$$J_R = \int_0^{t_f} \{z(t)\}^T \{z(t)\} \, dt \tag{9.18}$$

169

This index should also be considered in deciding whether or not a given combination of controllers is truly optimal. Extensive discussion of these criteria is given in the numerical examples.

D. COMPARISON OF GLOBAL AND CRITICAL-MODE CONTROL

A comparison of the global instantaneous closed-loop algorithm derived in Section D of Chapter V, and the critical-mode control algorithm derived in Section A of the present Chapter is carried out. An eight-story shear building is considered whose structural properties are: $k_1 = 1026.3\ kip/in\ (179700\ kN/m)$, $k_2 = 937.4\ kip/in\ (164140\ kN/m)$, $k_3 = 790.6\ kip/in\ (138430\ kN/m)$, $k_4 = 684.1\ kip/in\ (119790\ kN/m)$, $k_5 = 538.5\ kip/in\ (94290\ kN/m)$, $k_6 = 400.0\ kip/in\ (70040\ kN/m)$, $k_7 = 400.0\ kip/in\ (70040\ kN/m)$, $k_8 = 400.0\ kip/in\ (70040\ kN/m)$, $m_j = 2\ kip-sec^2/in\ (350\ Mg)$, $j = 1, ..., 8$, and 3 % critical damping in all the modes. The earthquake excitation used is the N-S component of the El-Centro earthquake of May 18, 1940, shown in Figure 23. The structure is equipped with eight active tendons, one on each floor. The weighting matrices $[Q]$, and $[R]$, are assumed diagonal with the values $R(i,i) = 0.06$, $i = 1, ..., 8$ and $Q(l,l) = 1500$, $l = 1, ..., 16$. The global algorithm considers control of all eight modes as was done in Chapter V, and the critical-mode algorithm considers control of only the first and second mode. The results are shown in Figures 68 and 69. In Figure 68 the eighth floor relative displacement is shown. It can be observed that the two-mode control is almost as effective as the global control for this structure and excitation. Figure 69 shows the first floor

170
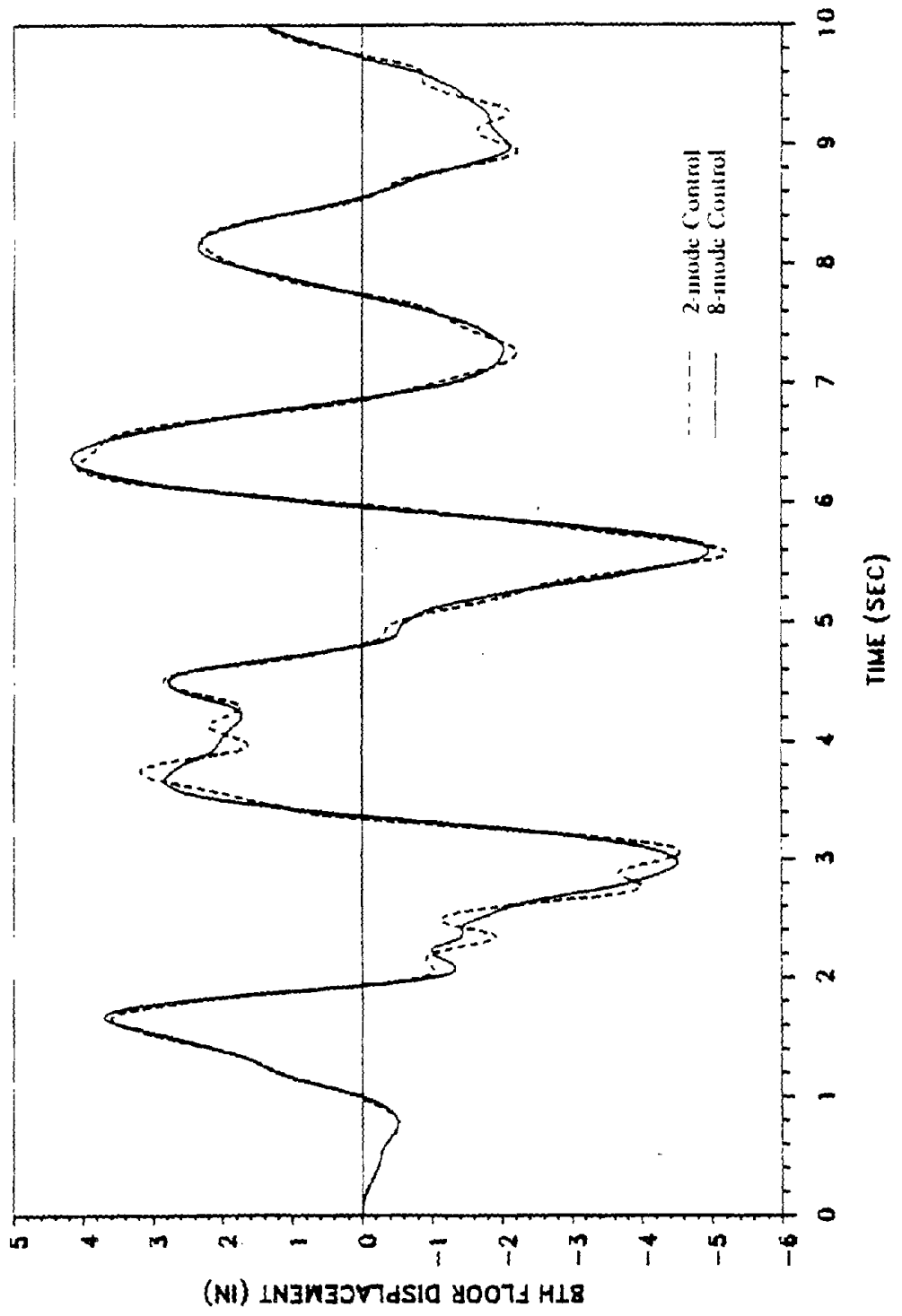
Figure 68. Response for Global and Critical-Mode Control
(1 in = 25.4 mm)
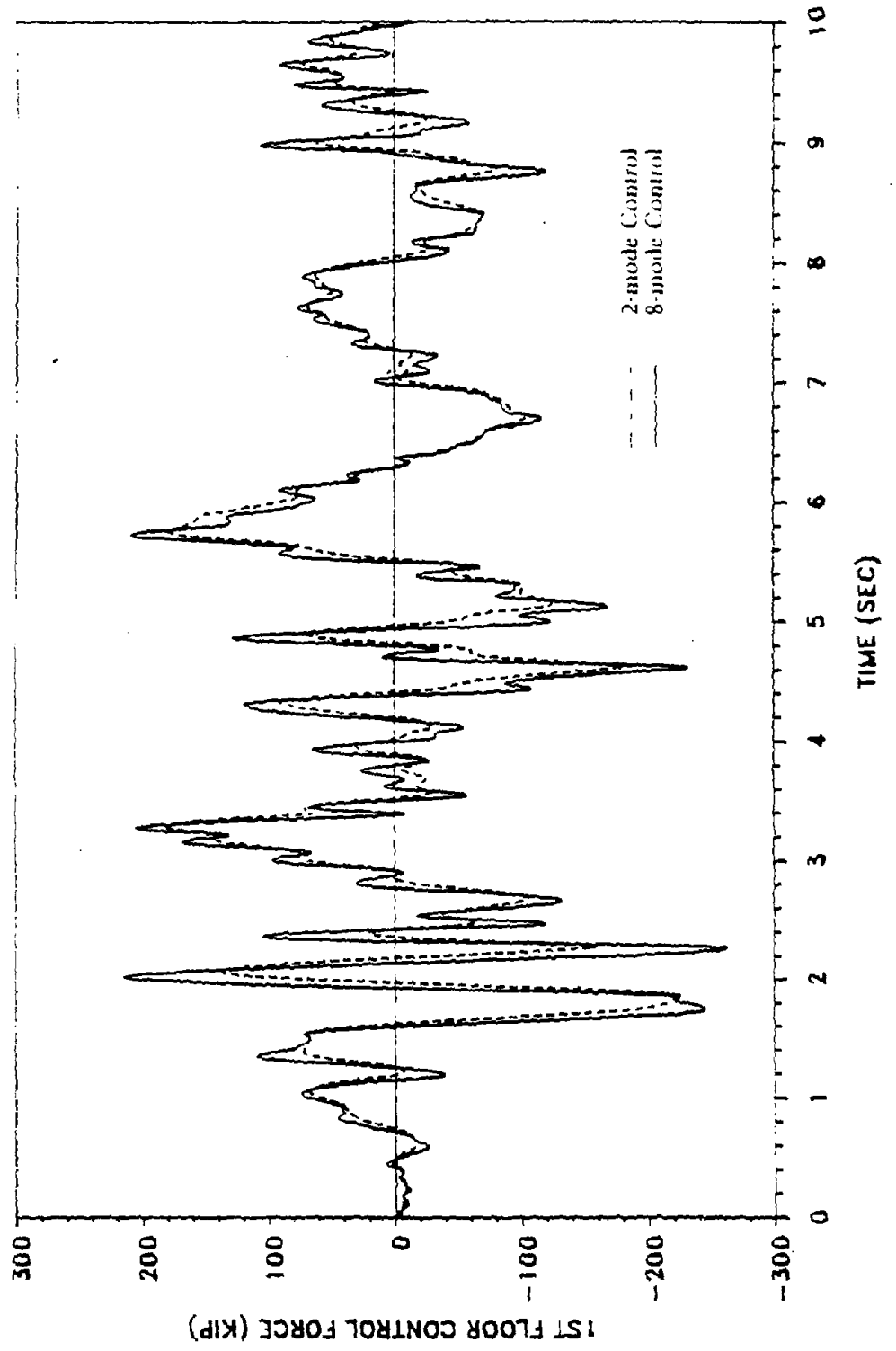
Figure 69. Control Force for Global and Critical-Mode Control
(1 kip = 4.45 kN)

172

control force and we can observe that in general the two algorithms require similar control forces.

E. SPILLOVER USING ARTIFICIAL EXCITATION

The structure of Section D equipped with only two active tendons located at the two bottom floors is subjected to an artificial earthquake ground acceleration. The excitation is a combination of three sinusoids centered around the first, second and third frequencies of the structure of 3.5 rad/sec, 9 rad/sec and 15 rad/sec, respectively. These sinusoids are weighted and scaled to reflect a peak magnitude of ground acceleration of 0.21 g and to excite the first three modes. The purpose here is to evaluate the spillover effect. The artificial excitation, designated as Excitation 1, is given by

$$\ddot{X}_g(t) = .05 g (.2 \sin 3.5t + \sin 9t + 3 \sin 15t) \tag{9.19}$$

and is shown in Figure 70. The critical-mode algorithm was used to control the first and second modes. The comparison of the no-control and the two-mode control response of the eighth-floor relative displacement subject to Excitation 1 is given in Figure 71. The required control forces for the first and second floor tendon controllers are shown in Figures 72 and 73. The eighth floor relative displacement shown in Figure 71 is split into the modal contributions of the first three modes and is compared with the no-control case. Figure 74 shows the first mode response, Figure 75 the second, and Figure 76 the third mode response. While modes one and two are controlled, mode three is not, which shows the spillover effect. This

173
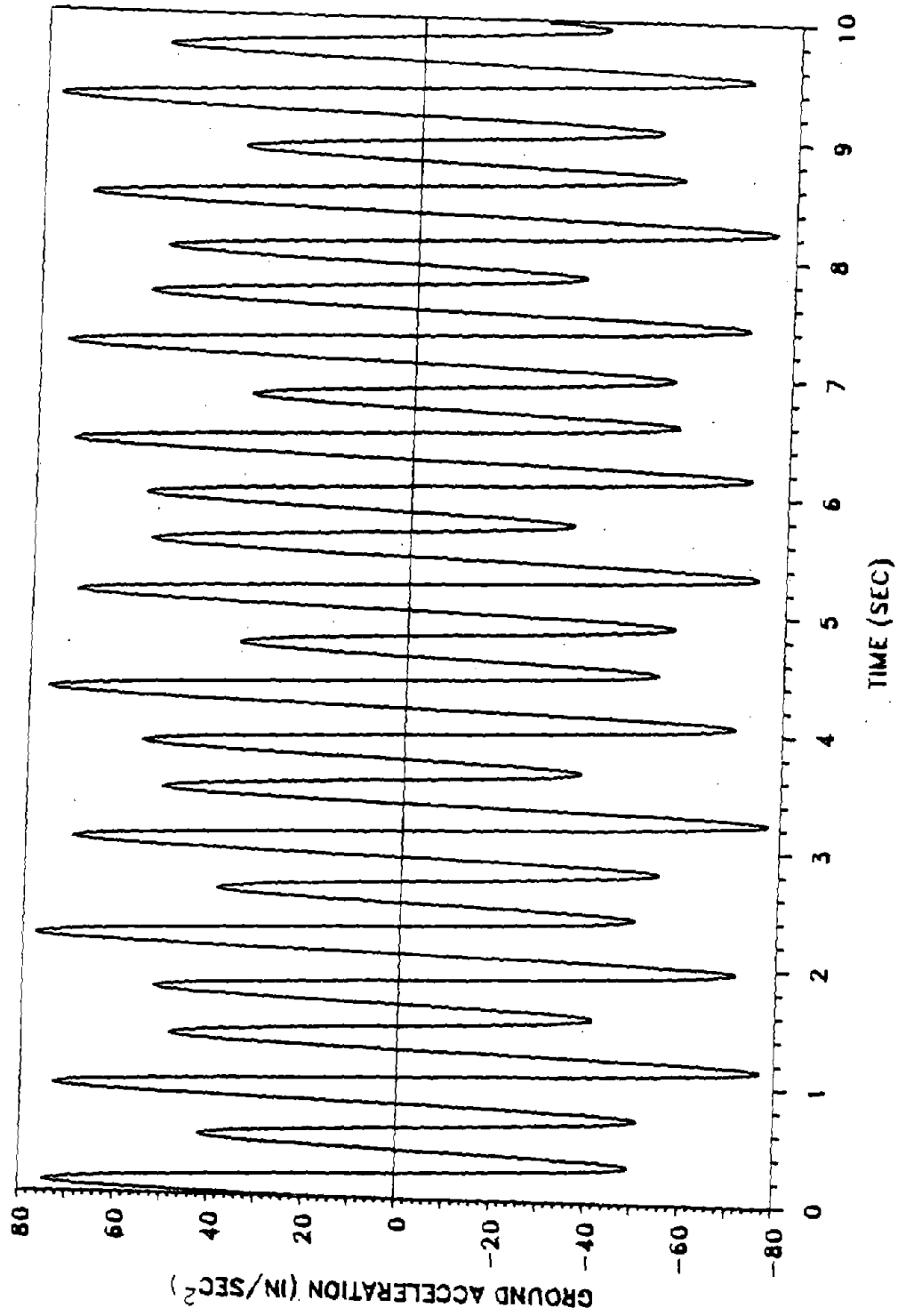
Figure 70. Artificial Ground Excitation 1 (1 in/sec² = 25.4 mm/sec²)

174

TIME (SEC)

8TH FLOOR DISPLACEMENT (IN)

No Control
2-mode Control

175
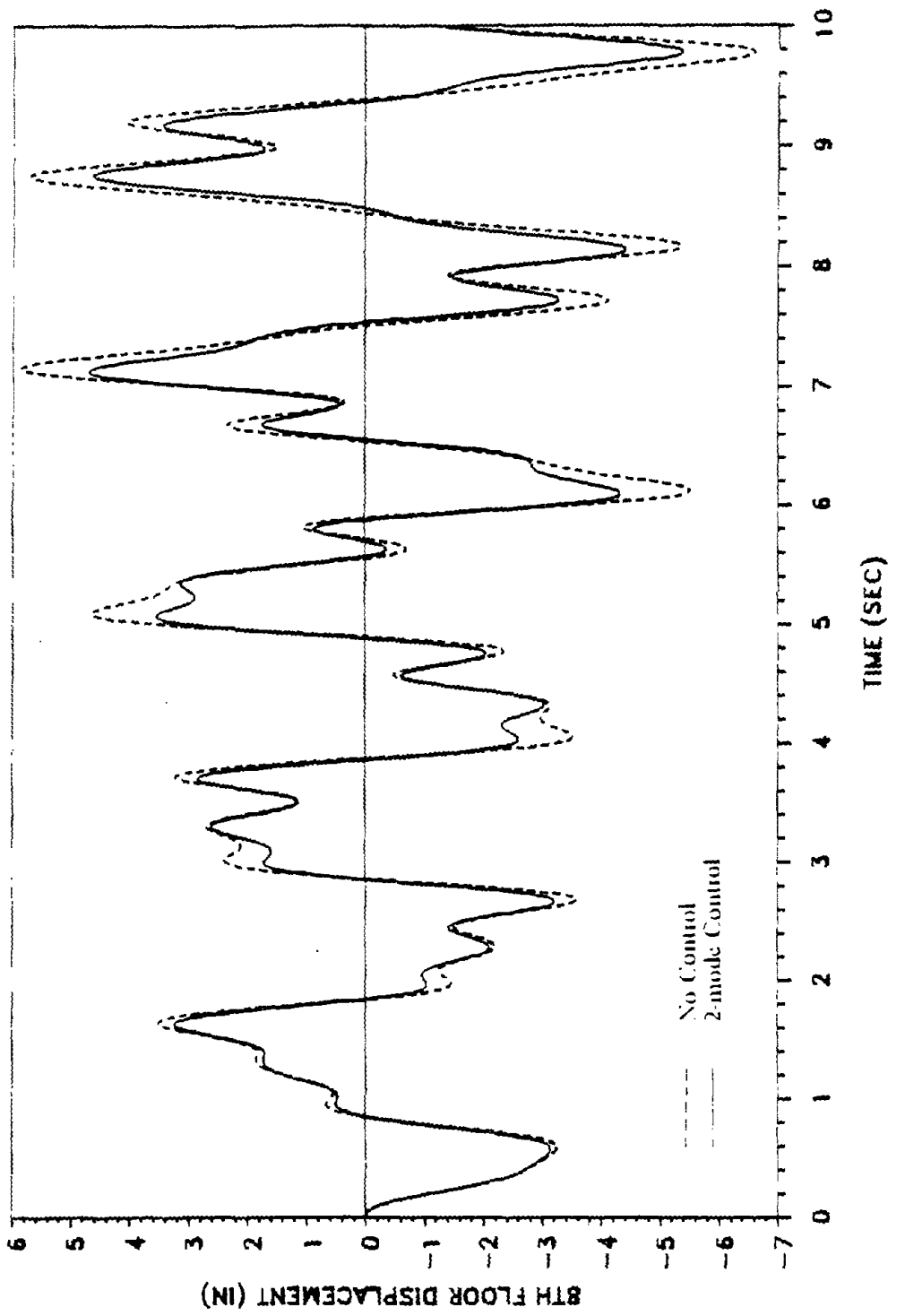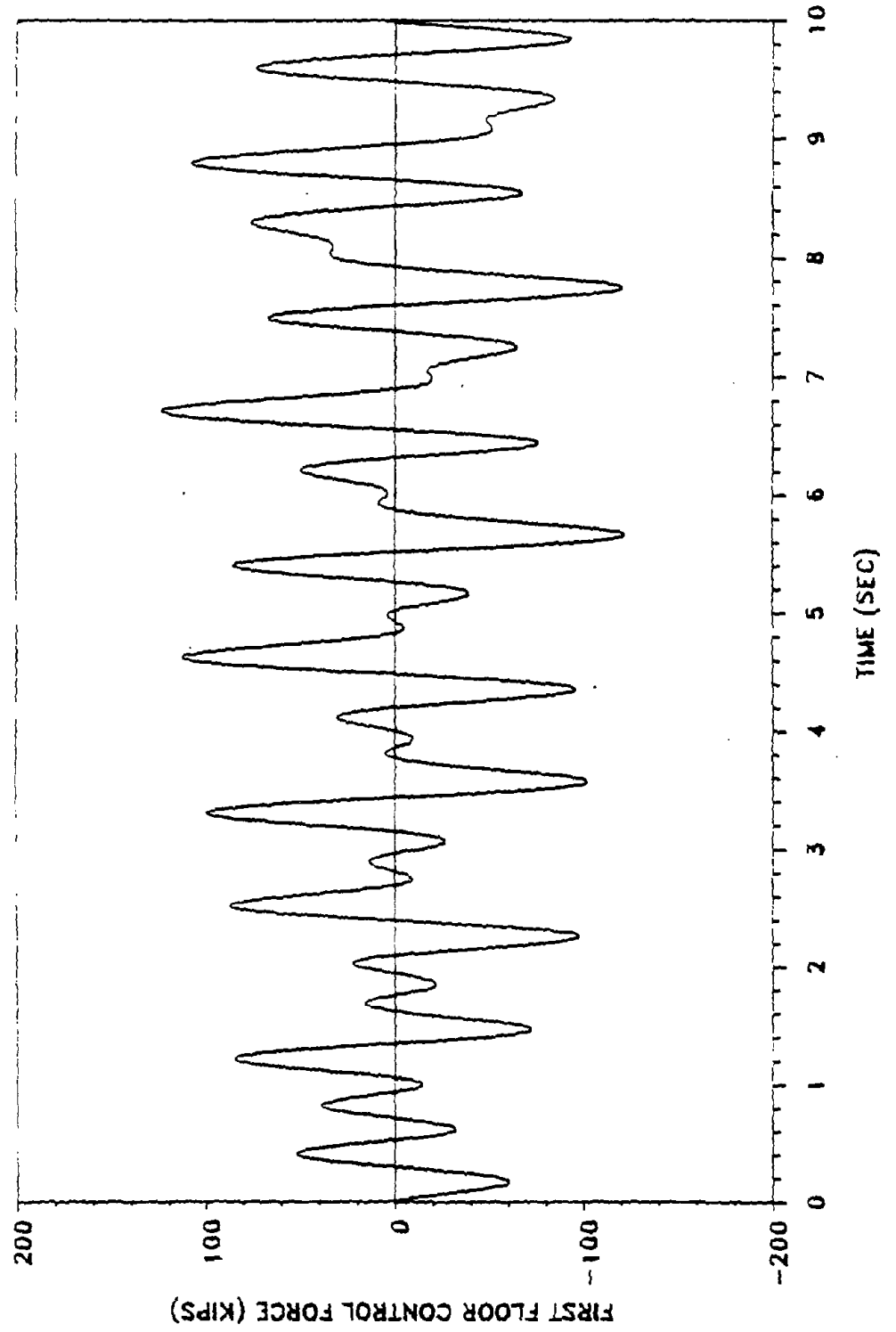
Figure 72. First Floor Control Force for Critical-mode Control
(1 kip = 4.45 kN)

176
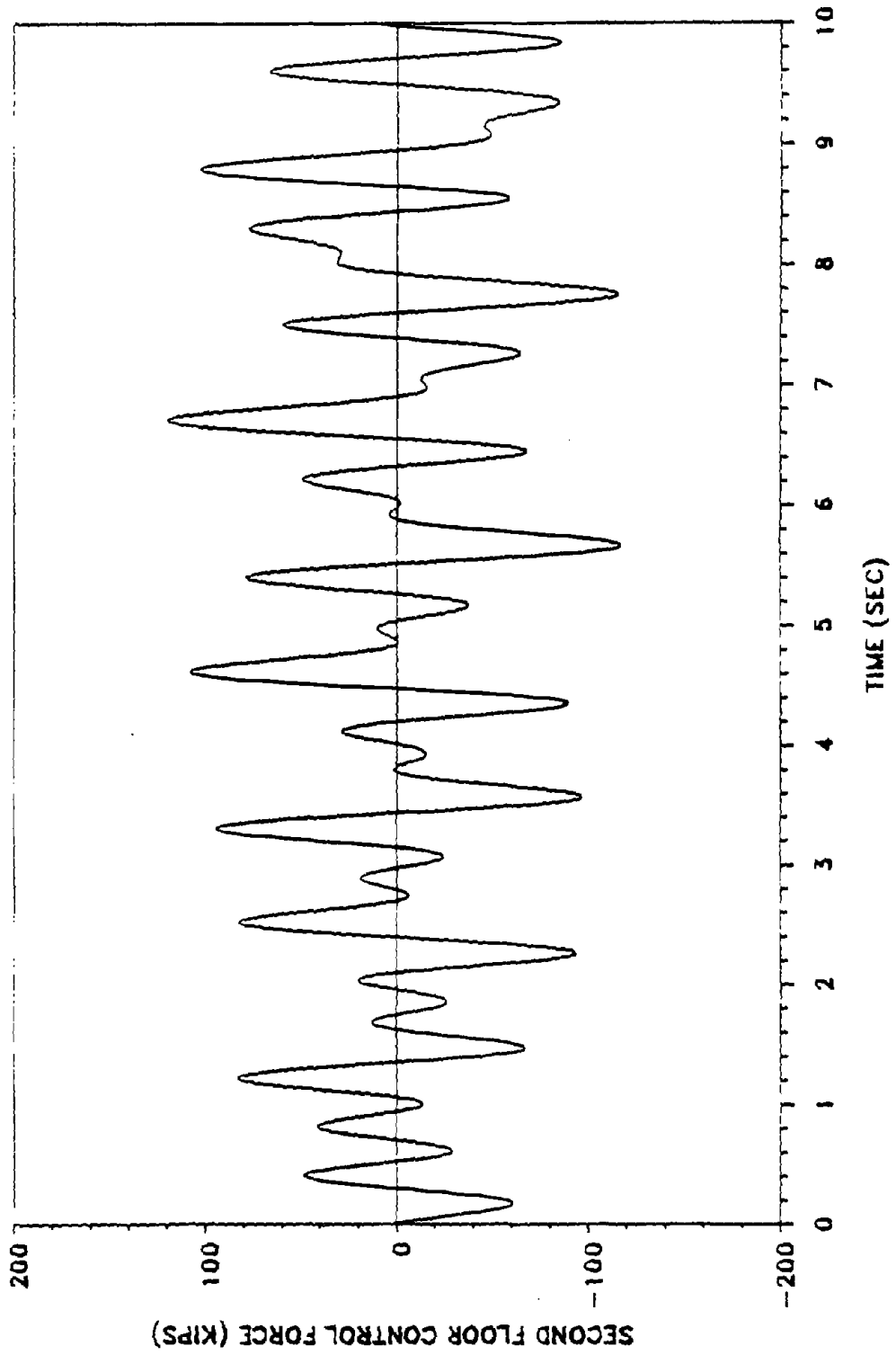
Figure 73. Second Floor Control Force for Critical-mode Control
(1 kip = 4.45 kN)
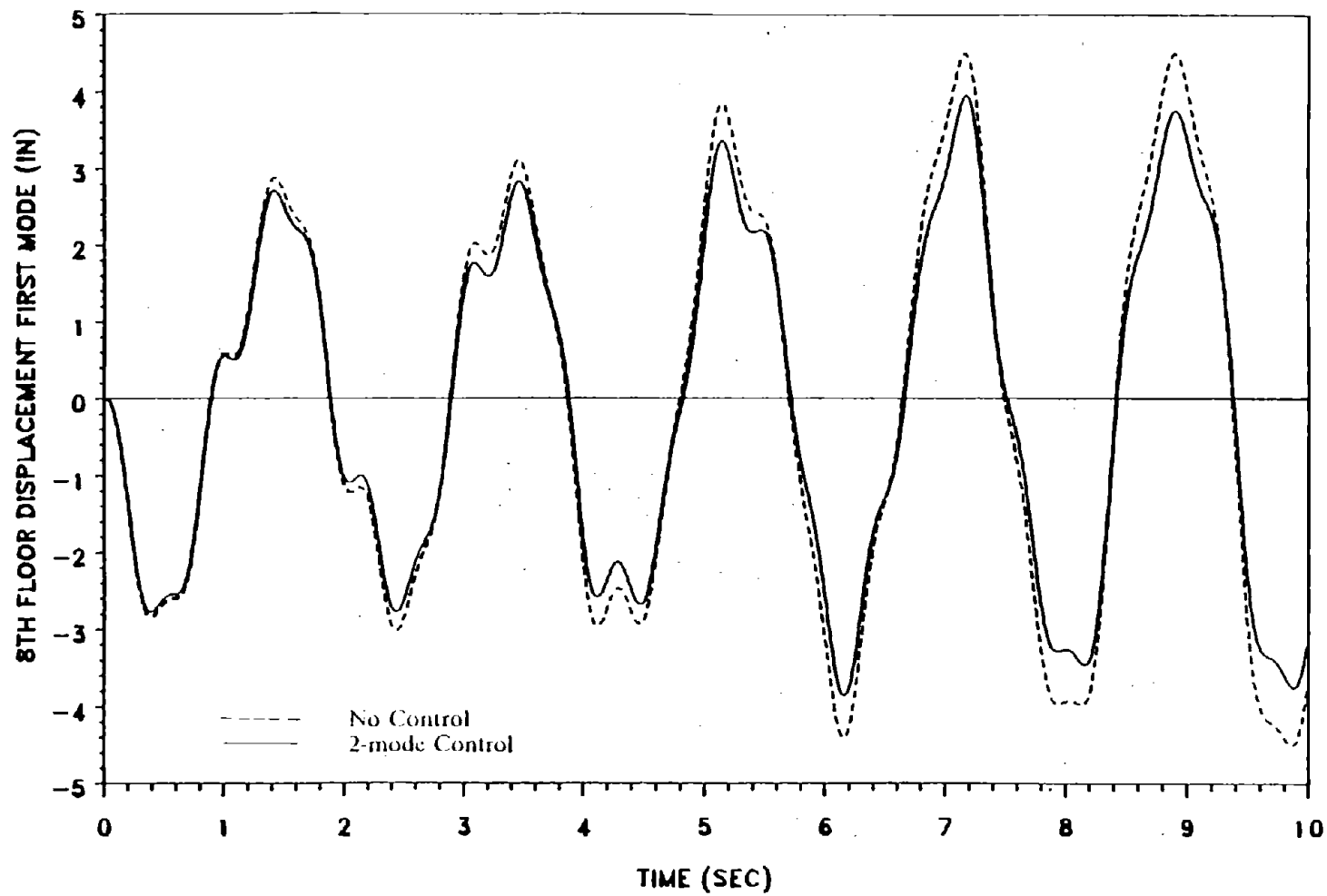
Figure 74. First Mode Response for Critical-mode Control
(1 in = 25.4 mm)

178
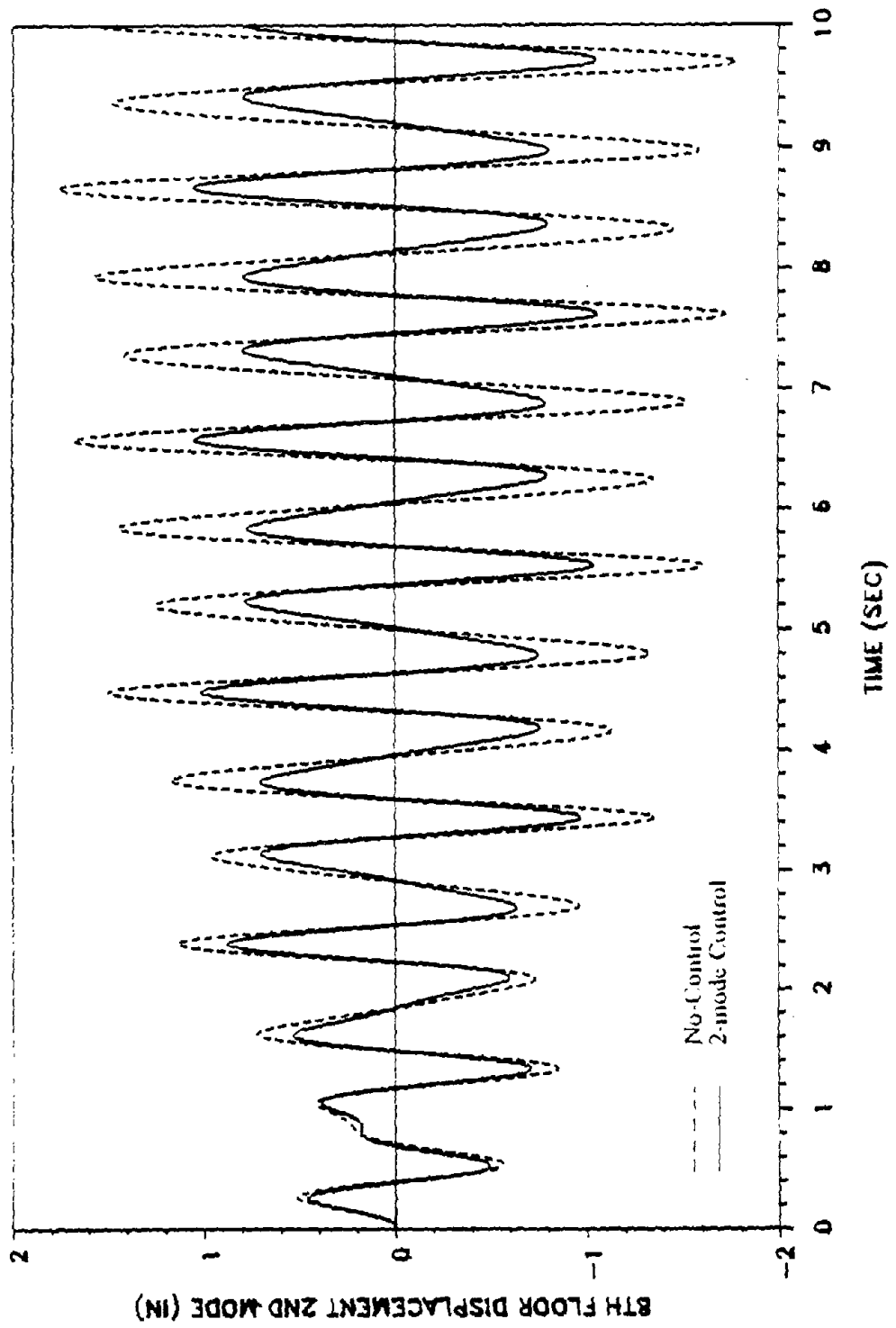
Figure 75. Second Mode Response for Critical-mode Control
(1 in = 25.4 mm)

179
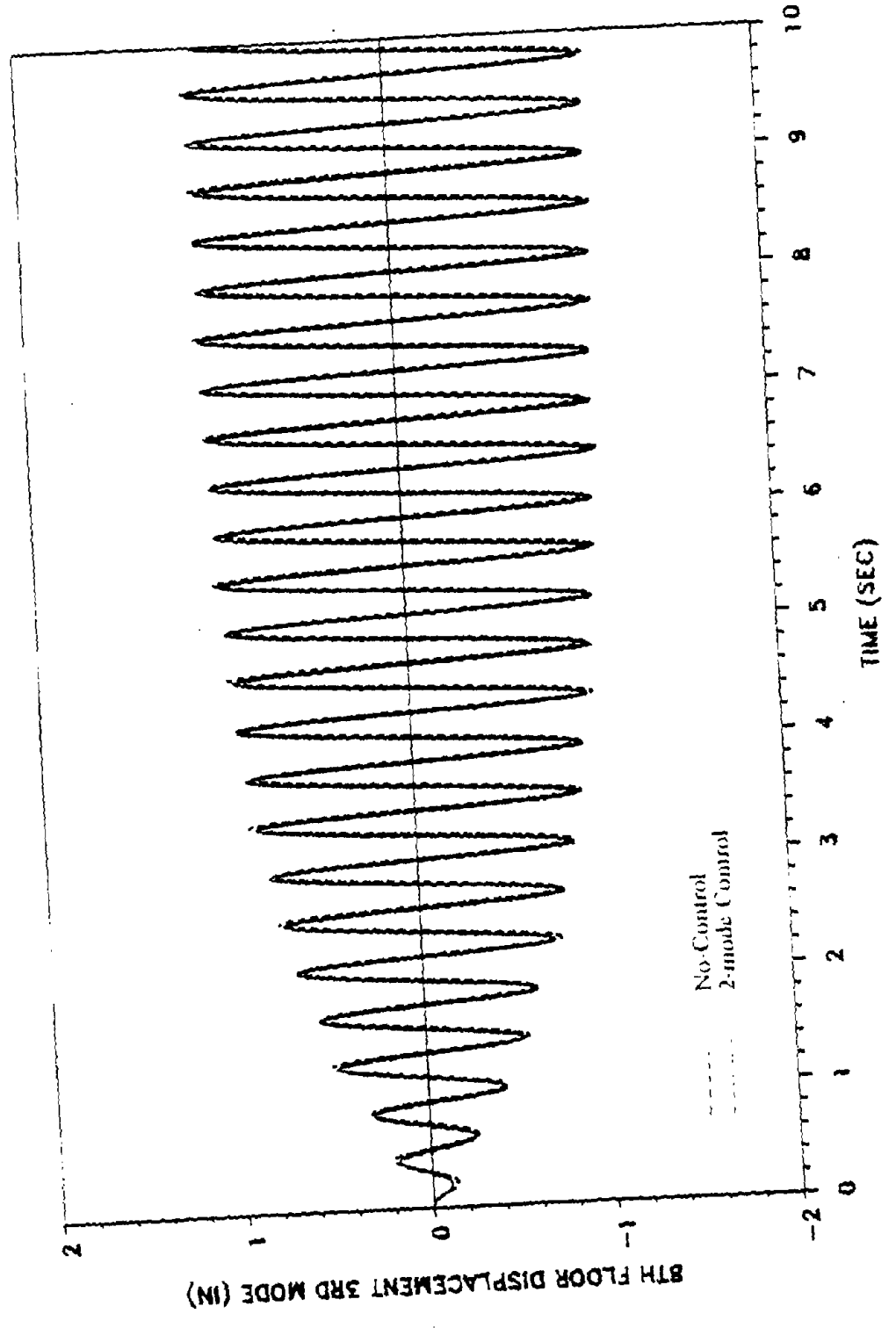
Figure 76. Third Mode Response for Critical-Mode Control
(1 in = 25.4 mm)

is because the critical-mode algorithm we have used attempts to control only the first two modes, which in turn excite the third mode.

F. OPTIMAL LOCATION OF CONTROLLERS: EXCITATION 1

The two approaches outlined in Section C for selecting the optimal locations of controllers are applied to an eight-story shear building with two active tendons. The two tendons can be located on any of the eight possible locations. The critical-mode algorithm is used and the first and second mode are controlled. The earthquake excitation is Excitation 1 shown in Figure 70. The structural properties are the same as those of the example in Section D, except that only 1 % critical damping is considered in the present example. The weighting matrix $[Q]$ is the same as in the example of Section D, but matrix $[R]$ has only two elements at the diagonal fixed at the values $R(1,1) = R(2,2) = 0.15$. The modal choice is made from a plot of the first two modes as shown in Figure 77. It is suggested that for the first mode the 8th floor would be a suitable choice, and for the second mode the 4th floor. For the performance indices choice, using Equations 9.17 and 9.18, several trials were made and the best choice was for the 5th and 6th floors. A comparison of the performance indices for control energy given in Equation 9.17 and for controlled response given in Equation 9.18 is shown in Table V. As can be seen both the control energy and response indices are less for the 5th and 6th floor choice. The maximum relative displacements and accelerations for all the floors are less for the 5th and 6th floor choice. The

181
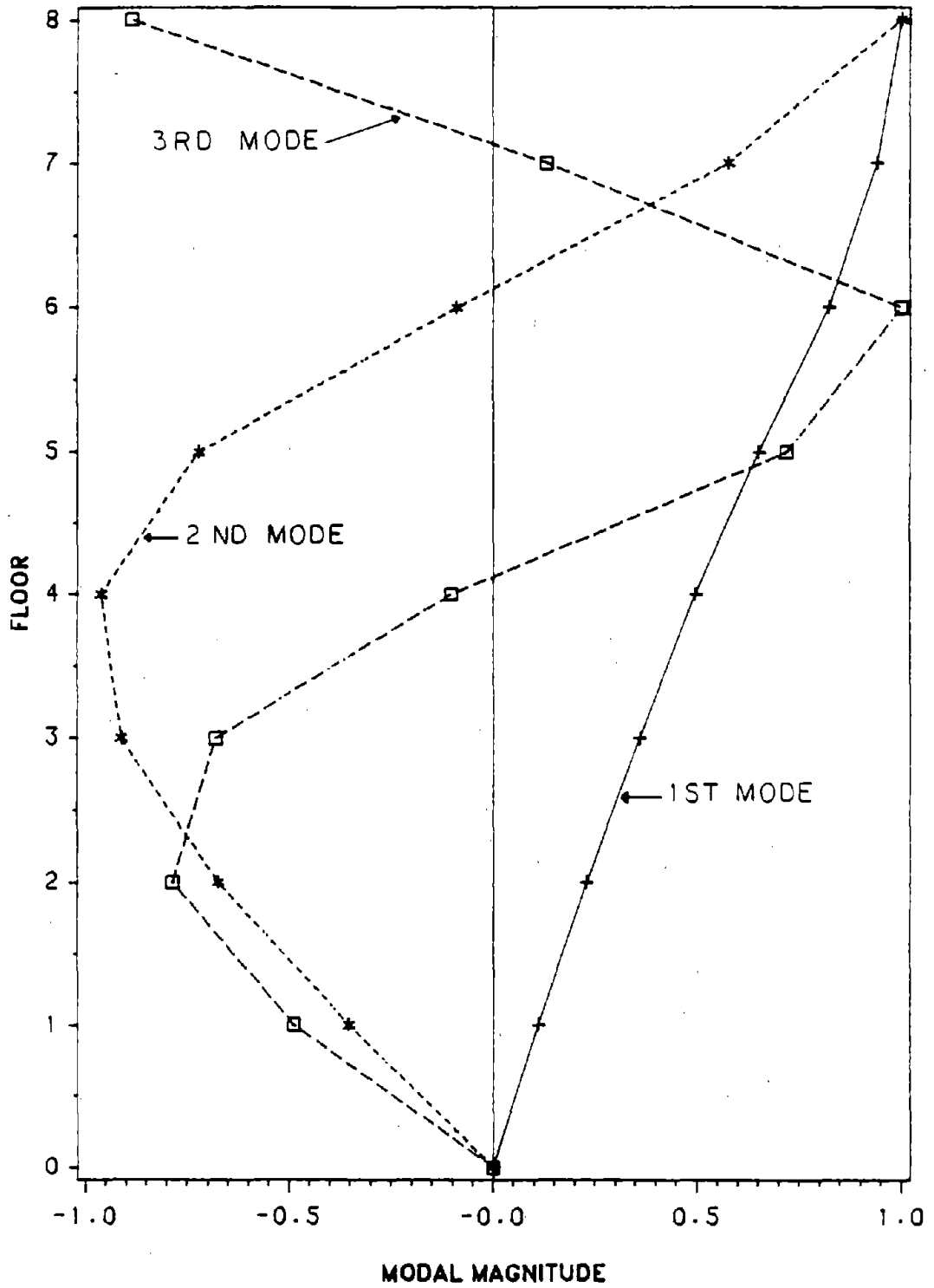
Figure 77. First Three Modes for Eight-story Building

TABLE V. OPTIMAL CONTROLLER LOCATIONS : FIXED R(I,I) - EXCITATION 1
(1 kip = 4.45 kN), (1 in = 25.4 mm)

Locations	4 & 8	5 & 6
Control Energy	74829	74132
Response Index	368	266
Maximum Displacement	(in.)	(in.)
Floor 1	1.94	1.72
Floor 2	3.27	2.95
Floor 3	3.43	3.21
Floor 4	3.40	2.45
Floor 5	5.95	4.74
Floor 6	6.67	5.78
Floor 7	5.61	4.16
Floor 8	8.64	6.89
Maximum Acceleration	(% g)	(% g)
Floor 1	90	80
Floor 2	146	127
Floor 3	134	109
Floor 4	55	40
Floor 5	148	140
Floor 6	189	173
Floor 7	59	47
Floor 8	179	152
	(kip)	(kip)
Maximum	4th 8th	5th 6th
Control Forces	92 164	95 179
R(1,1)	.15	.15
R(2,2)	.15	.15

maxima of the control forces for the 5th and 6th floor choice is slightly greater.

For the same structure, another comparison is made between the two cases of modal shape and performance index choices. This time the elements of the weighting matrix $[R]$ are allowed to be different in the two choices. The elements of matrix $[Q]$ are still fixed. The reason for allowing the elements of matrix $[R]$ to be different in the two choices is to make the maxima of the control forces for both choices equal. In this sense a better comparison can be carried out. The results of this comparison are shown in Table VI and Figures 78 through 84. Both the control energy and response performance indices are less for the 5th and 6th floor choice. Similarly the maxima of the relative displacements and accelerations for all the floors are less for the 5th and 6th floor choice. The maxima of the control forces are equal and the elements of matrix $[R]$ are different as shown in Table VI. Figure 78 shows the response for the 8th floor relative displacement without control, split into the first three modes. It can be seen that Excitation 1 excites the second and third modes considerably. A comparison of the required control forces for the two choices given in Figures 79 and 80 indicates that they are approximately equal. The two choices are compared for the 8th floor relative displacement in Figure 81. It is seen that the 5th and 6th floor choice reduces the response more effectively.

TABLE VI. OPTIMAL CONTROLLER LOCATIONS - EXCITATION 1
(1 kip = 4.45 kN), (1 in = 25.4 mm)

Locations	4 & 8	5 & 6
Control Energy	93283	83716
Response Index	331	249
Maximum Displacement	(in.)	(in.)
Floor 1	1.96	1.71
Floor 2	3.31	2.93
Floor 3	3.44	3.17
Floor 4	3.20	2.38
Floor 5	5.70	4.64
Floor 6	6.29	5.59
Floor 7	5.09	4.03
Floor 8	8.06	6.64
Maximum Acceleration	(% g)	(% g)
Floor 1	92	80
Floor 2	149	127
Floor 3	138	110
Floor 4	55	41
Floor 5	149	138
Floor 6	189	172
Floor 7	57	47
Floor 8	180	152
	(kip)	(kip)
Maximum	4th 8th	5th 6th
Control Forces	150 154	149 151
$R(1,1)$	.085	.095
$R(2,2)$	.160	.180
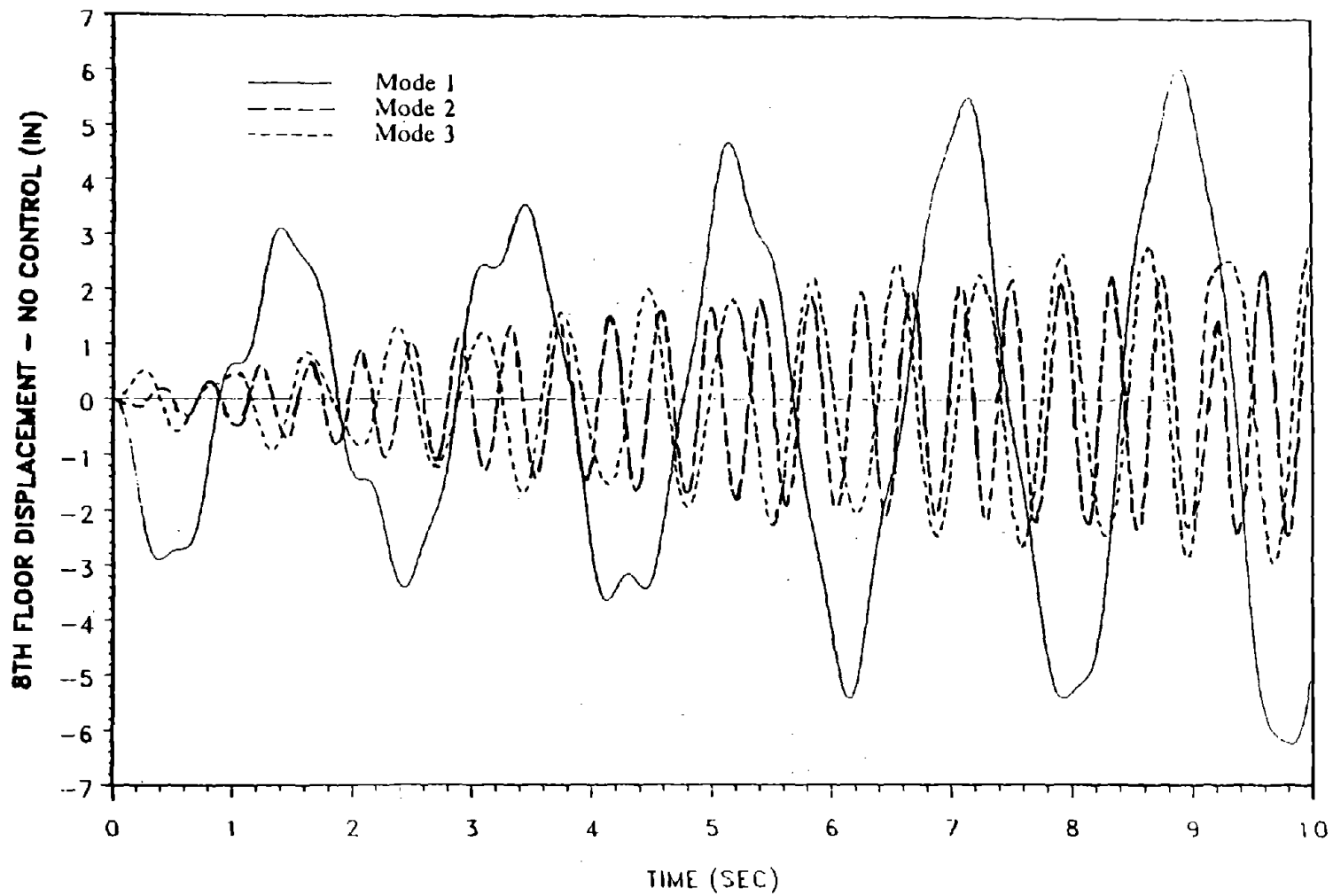
Figure 78. Response for No-control: First Three Modes
(1 in = 25.4 mm)

186
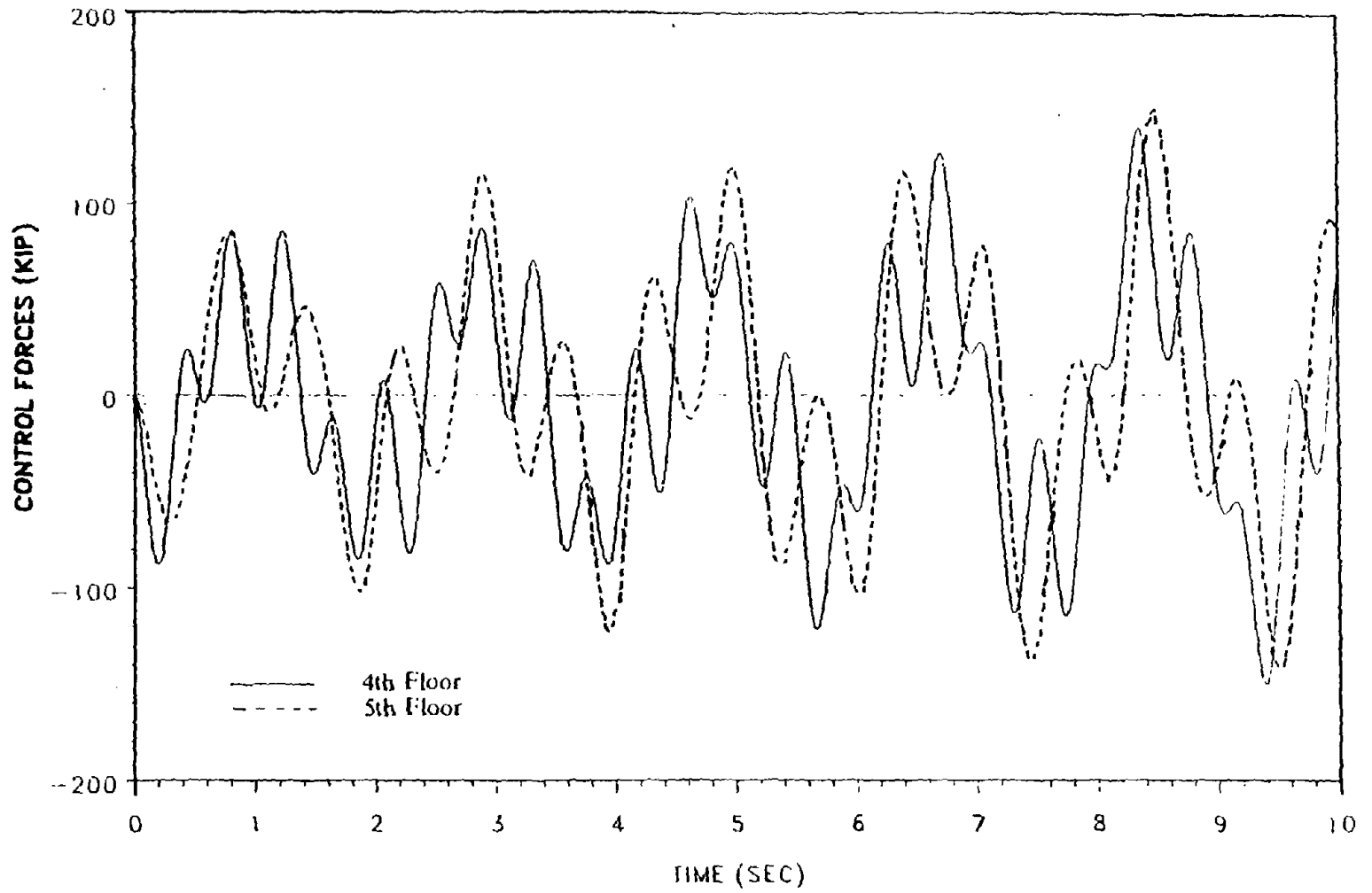
Figure 79. Control Forces for 4th and 5th Floors: Excitation 1
(1 kip = 4.45 kN)

187
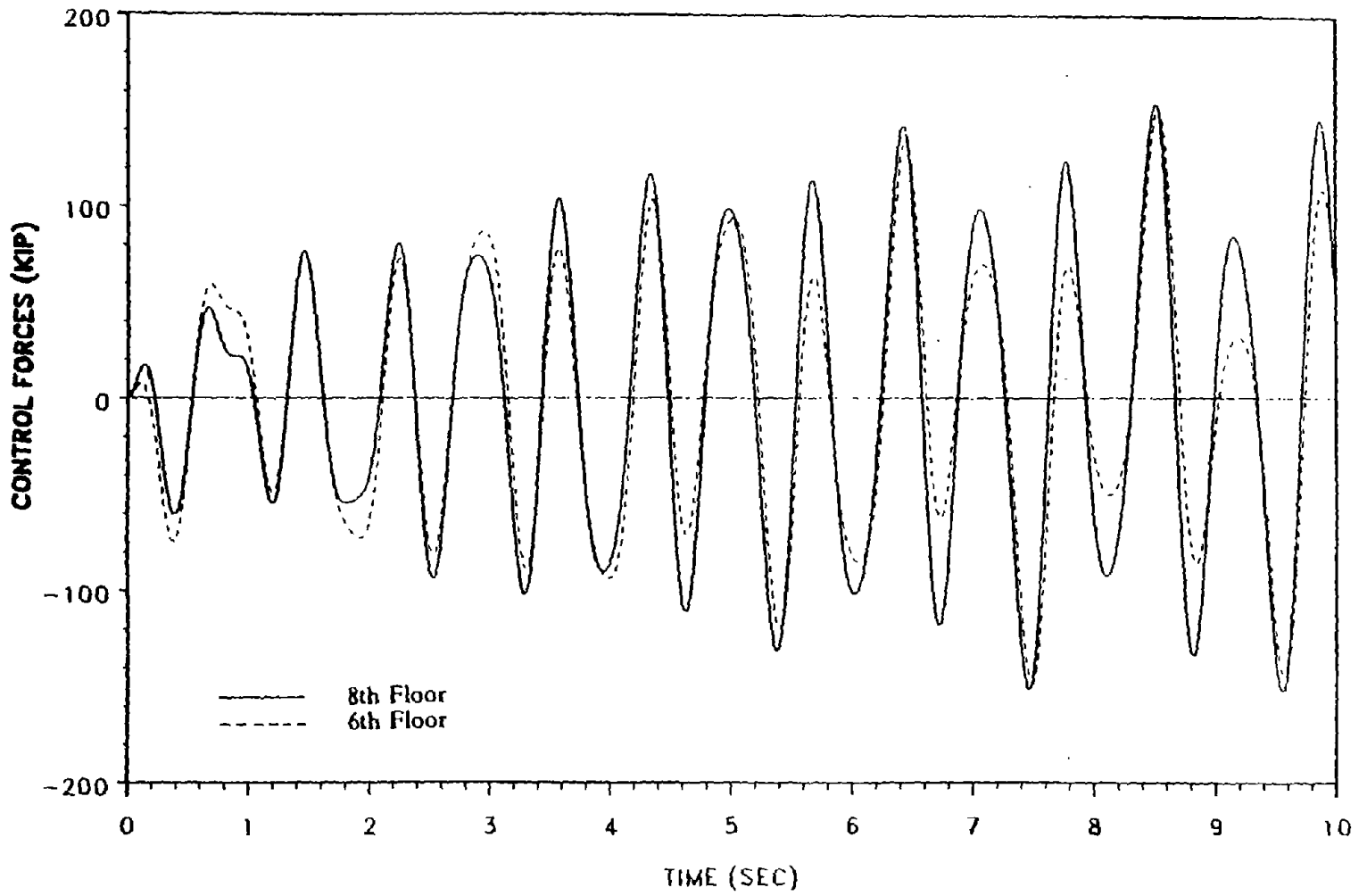
Figure 80. Control Forces for 8th and 6th Floors: Excitation 1
(1 kip = 4.45 kN)

188
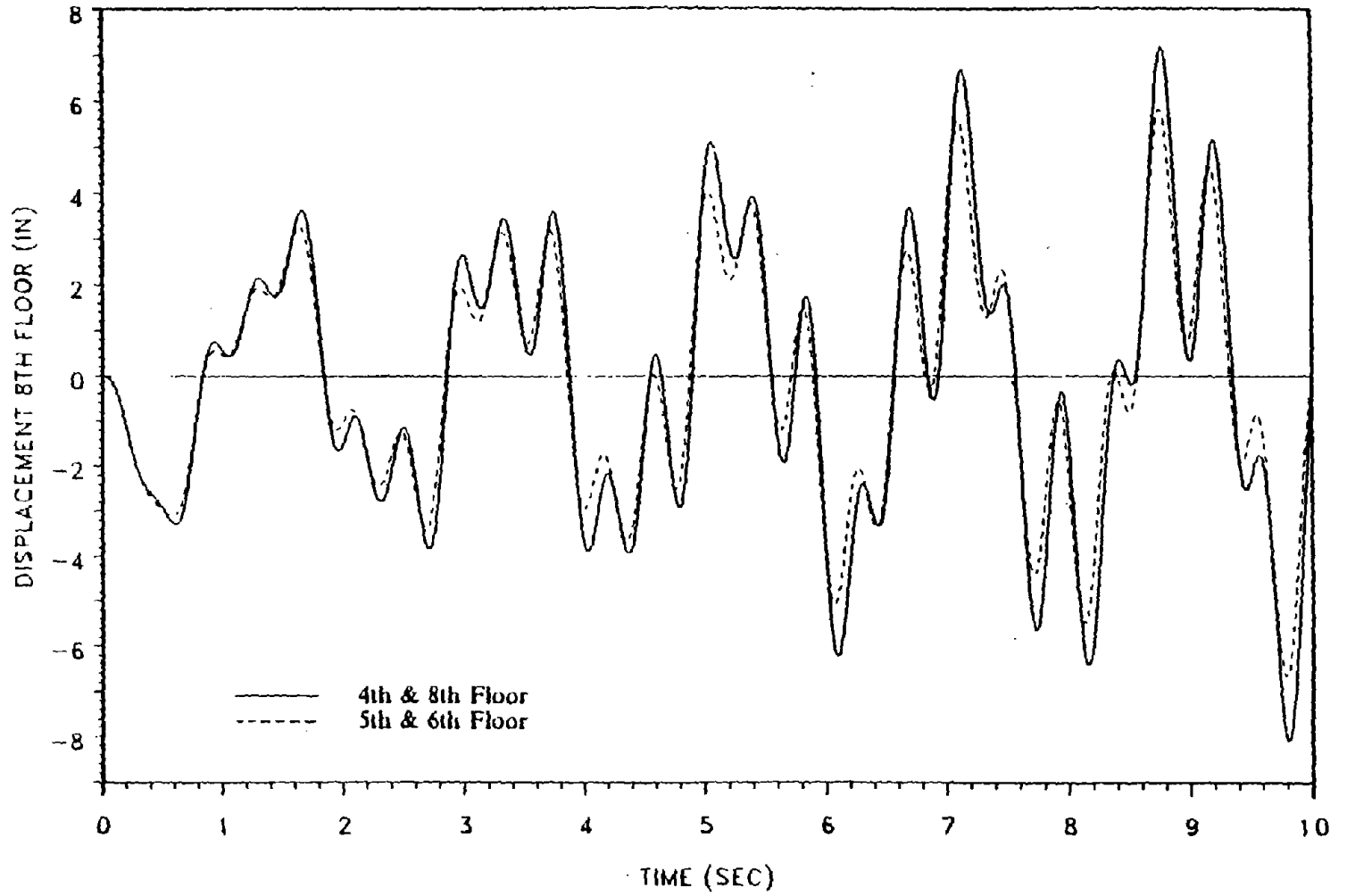
Figure 81. Controller Choices: Total Response – Excitation 1
(1 in = 25.4 mm)

189

The 8th floor controlled response is split into the first three modes in Figures 82 through 84. The 5th and 6th floor choice is more effective for the first and second mode response. From Figure 84 note the presence of the spillover effect on the third mode, which is to be expected since we control only the first and second mode.

G. OPTIMAL LOCATION OF CONTROLLERS: EXCITATION 2

A second excitation, Excitation 2, is applied to the same structure presented in Section F. The purpose of this example is to test whether the optimal locations of the two tendons is still optimal for a different earthquake excitation. Excitation 2 is given by

$$\ddot{X}_g(t) = .02\,g\,(\,.2\,\sin 3.5t + 7.\,\sin 9t + 3.3\,\sin 15t\,) \tag{9.20}$$

and is shown in Figure 85. It excites the second mode more than the other modes. Figure 86 shows the response of the 8th floor for the three modes without control. The elements of the weighting matrix $[R]$ are different in the two choices. The elements of matrix $[Q]$ are fixed. The results are shown in Table VII. The 5th and 6th floor choice is still better than the modal choice of 4th and 8th floor. Note that the response index is less and control energy is higher for the 5th and 6th floor choice. The simulation shows that the response index may be a better measurement than the control energy. A comparison of control forces is given in Figures 87 and 88, and we observe that they are reasonably close. The two choices are compared for the eighth

191
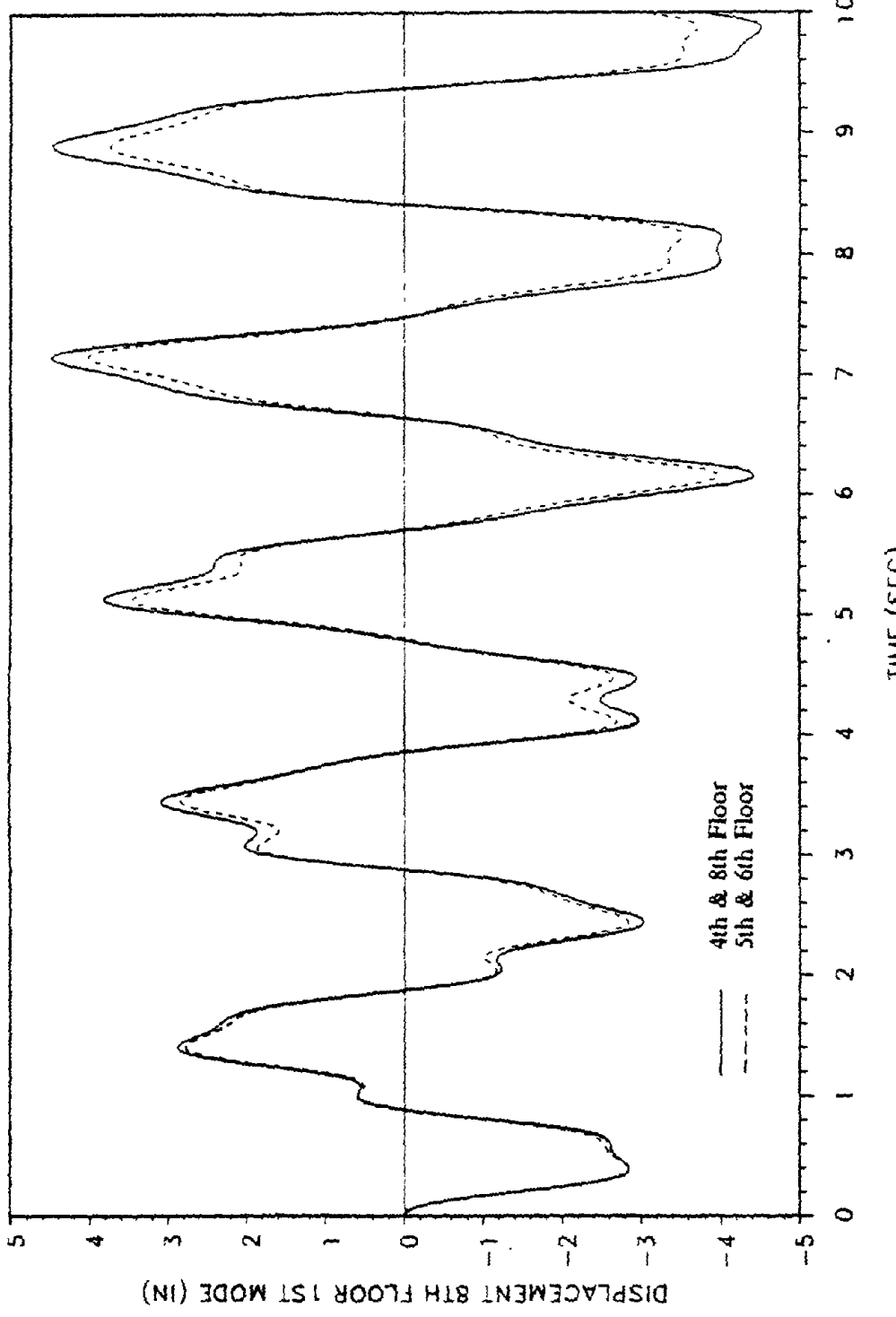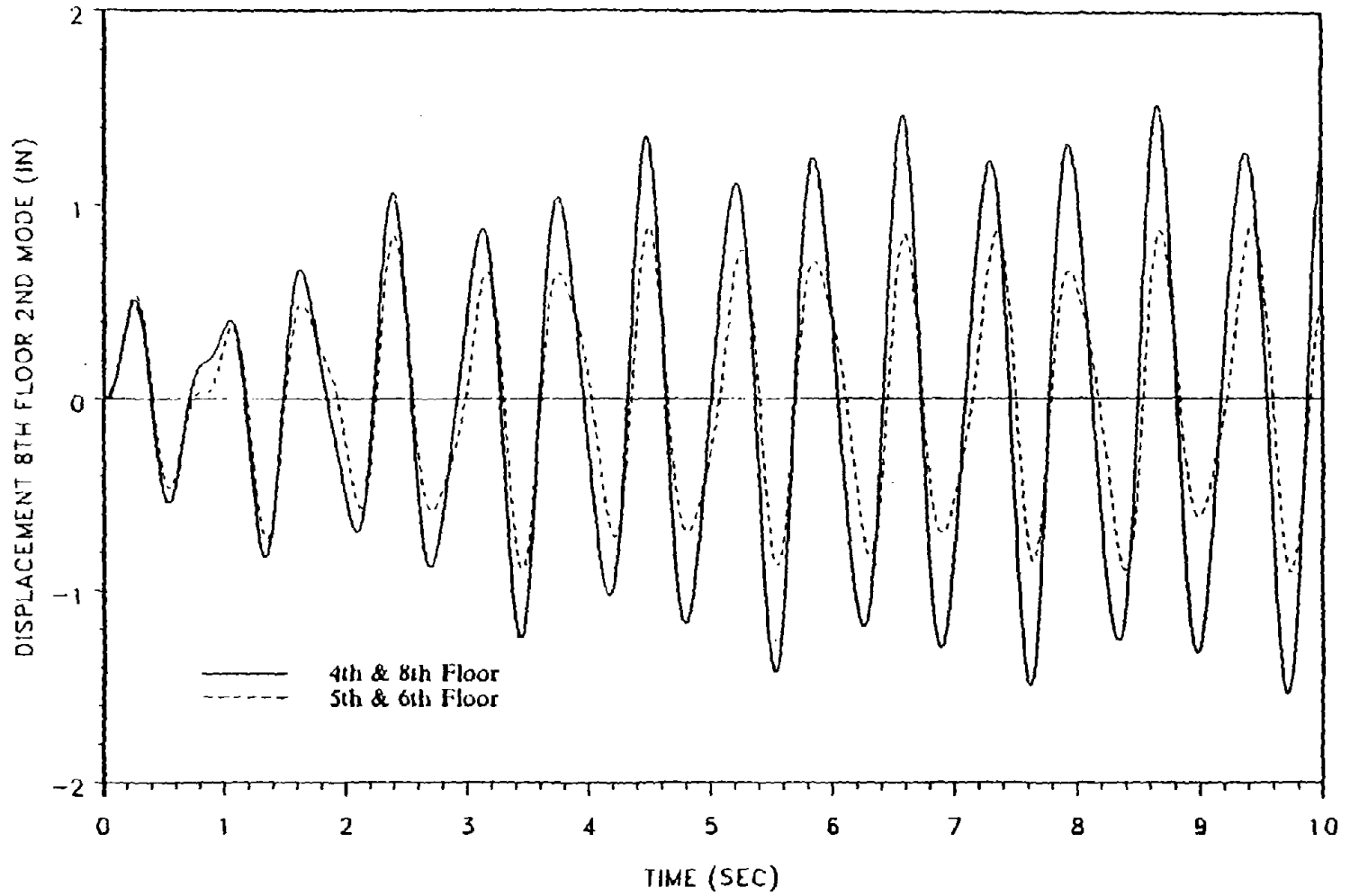
Figure 83. Controller Choices: Second Mode Response - Excitation 1
(1 in ≈ 25.4 mm)

192
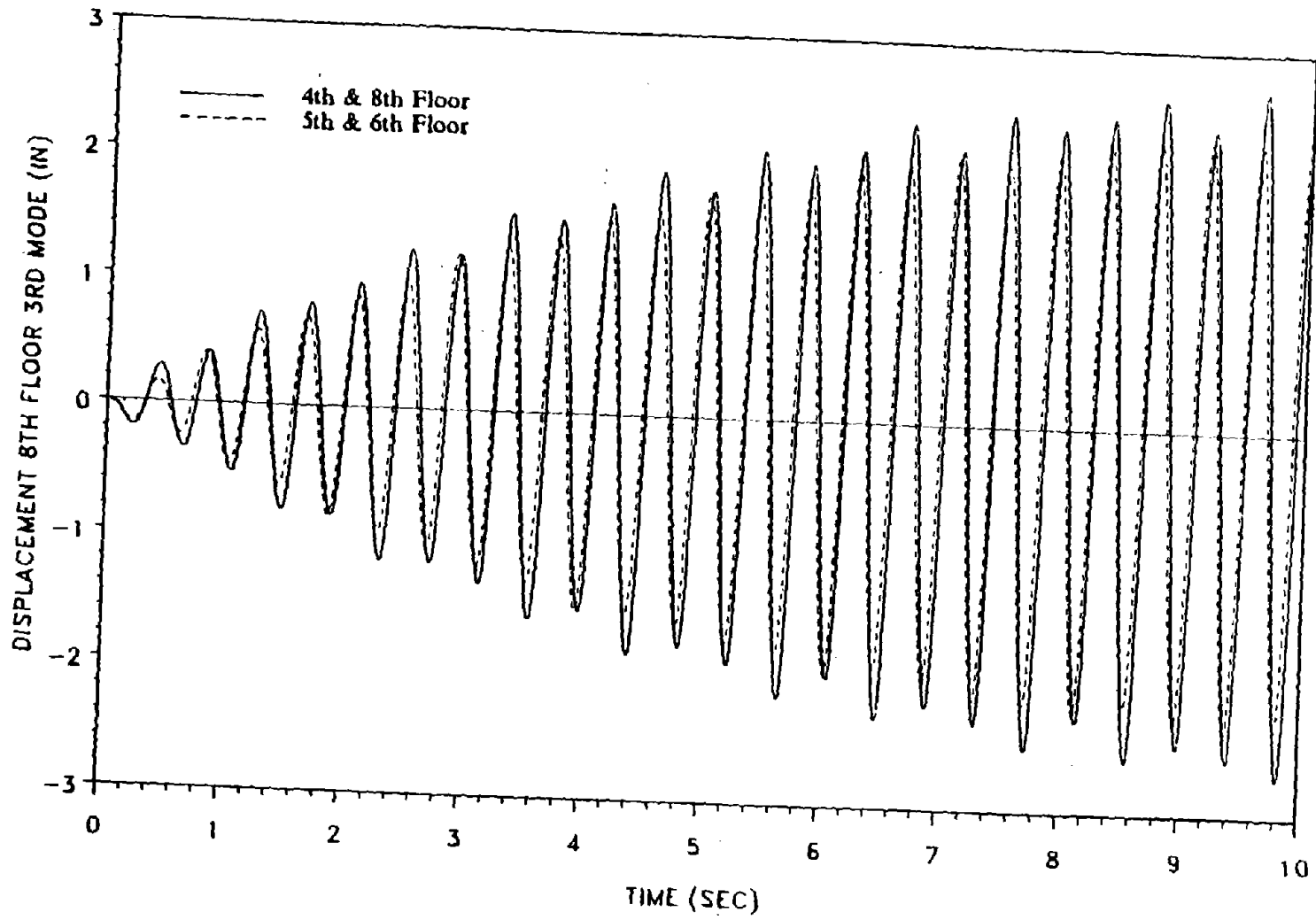
Figure 84. Controller Choices: Third Mode Response - Excitation 1
(1 in = 25.4 mm)
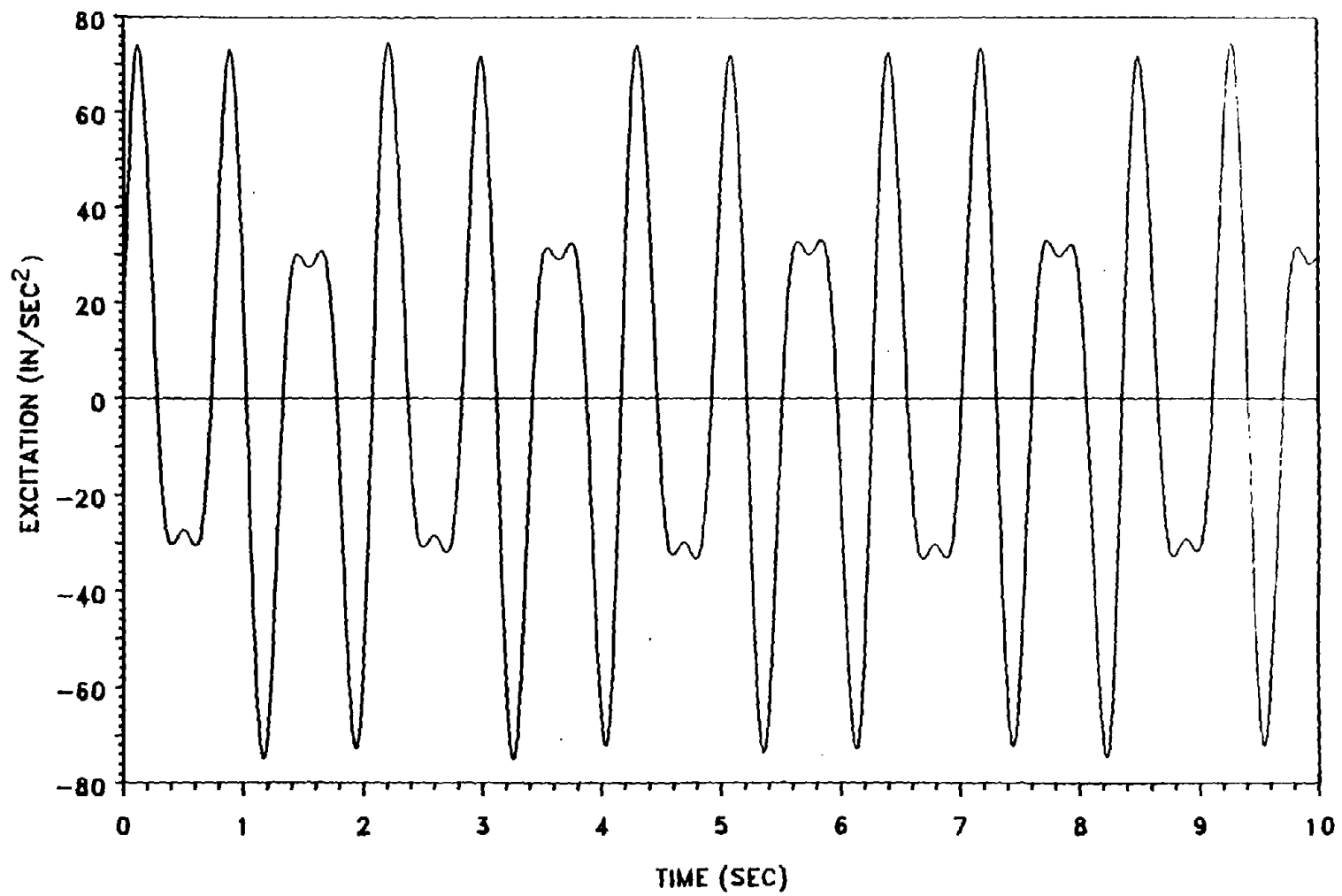
Figure 65. Artificial Ground Excitation 2 (1 in/sec^2 = 25.4 mm/sec^2)
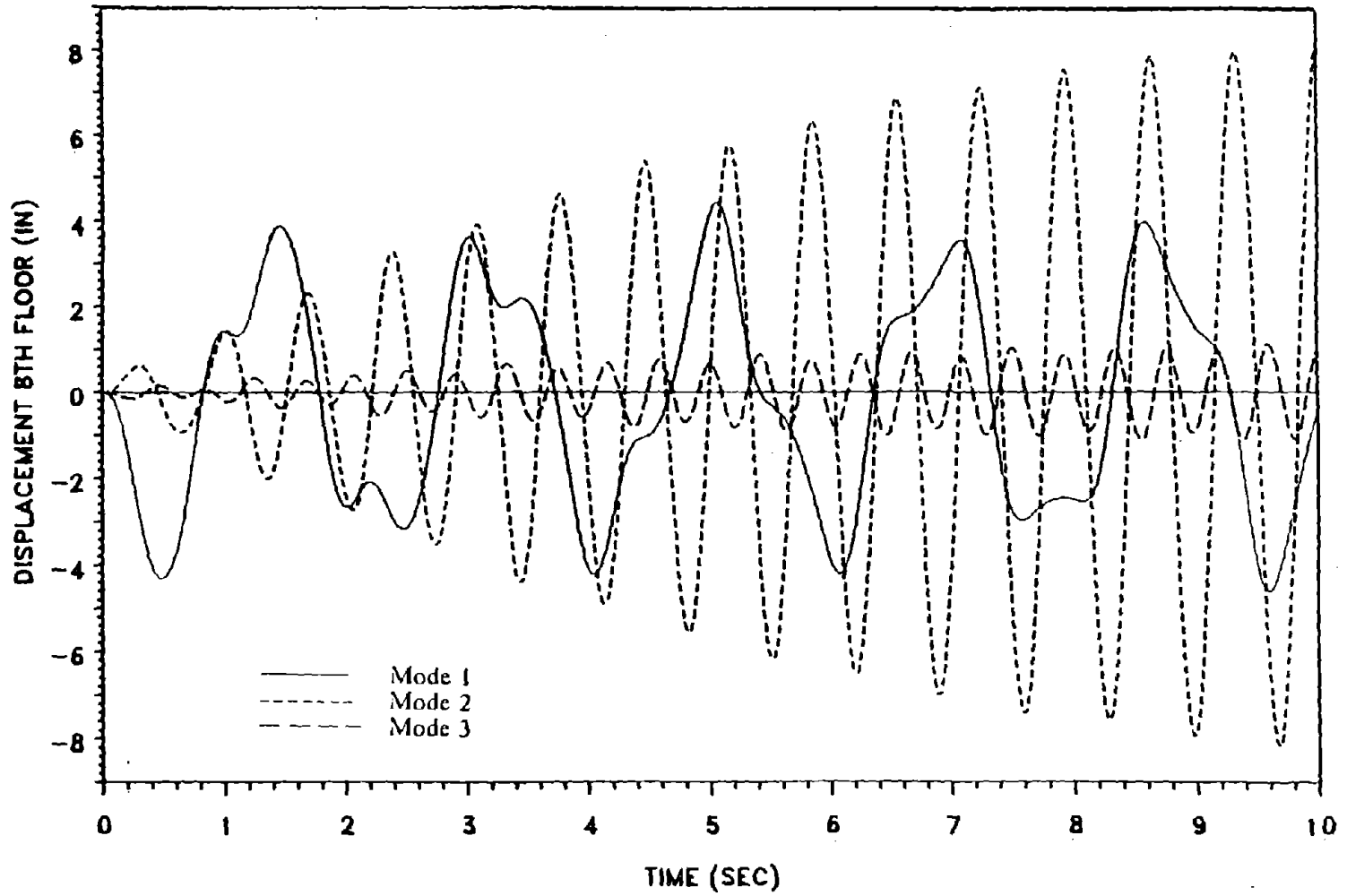
Figure 86.   Response for No-control: First Three Modes
(1 in = 25.4 mm)

TABLE VII. OPTIMAL CONTROLLER LOCATIONS - EXCITATION 2
(1 kip = 4.45 kN), (1 in = 25.4 mm)

Locations	4 & 8	5 & 6
Control Energy	124996	130195
Response Index	604	480
Maximum Displacement	(in.)	(in.)
Floor 1	2.77	2.39
Floor 2	5.07	4.37
Floor 3	6.39	5.46
Floor 4	6.39	5.39
Floor 5	6.05	5.25
Floor 6	3.65	4.05
Floor 7	6.49	6.05
Floor 8	8.75	8.18
Maximum Acceleration	(% g)	(% g)
Floor 1	298	80
Floor 2	149	127
Floor 3	138	110
Floor 4	55	41
Floor 5	149	138
Floor 6	189	172
Floor 7	57	47
Floor 8	180	152
	(kip)	(kip)
Maximum Control Forces	4th 8th	5th 6th
	150 152	153 152
R(1,1)	.075	.30
R(2,2)	.620	.720
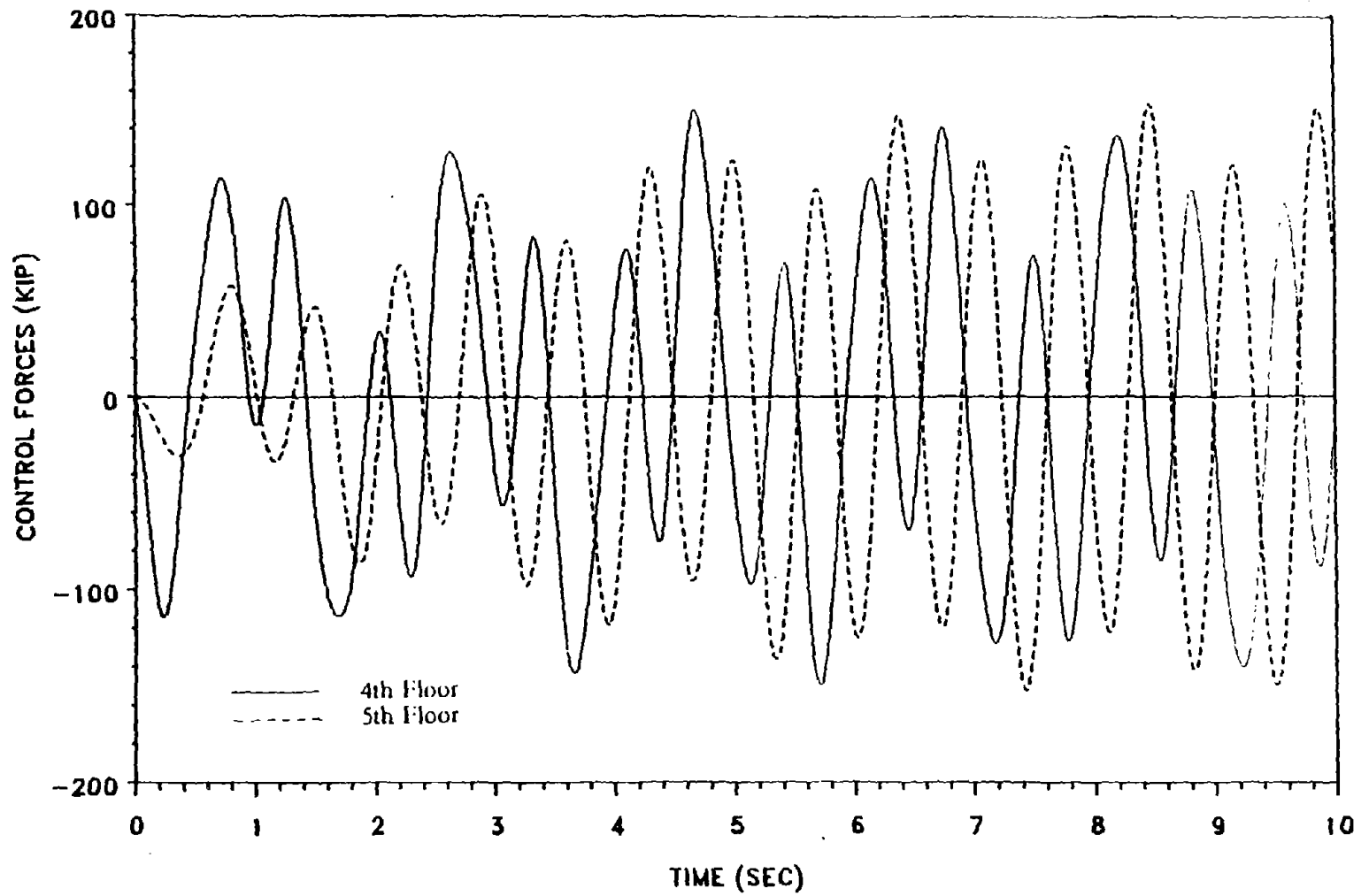
Figure 87. Control Forces for 4th and 5th Floors: Excitation 2
(1 kip = 4.45 kN)
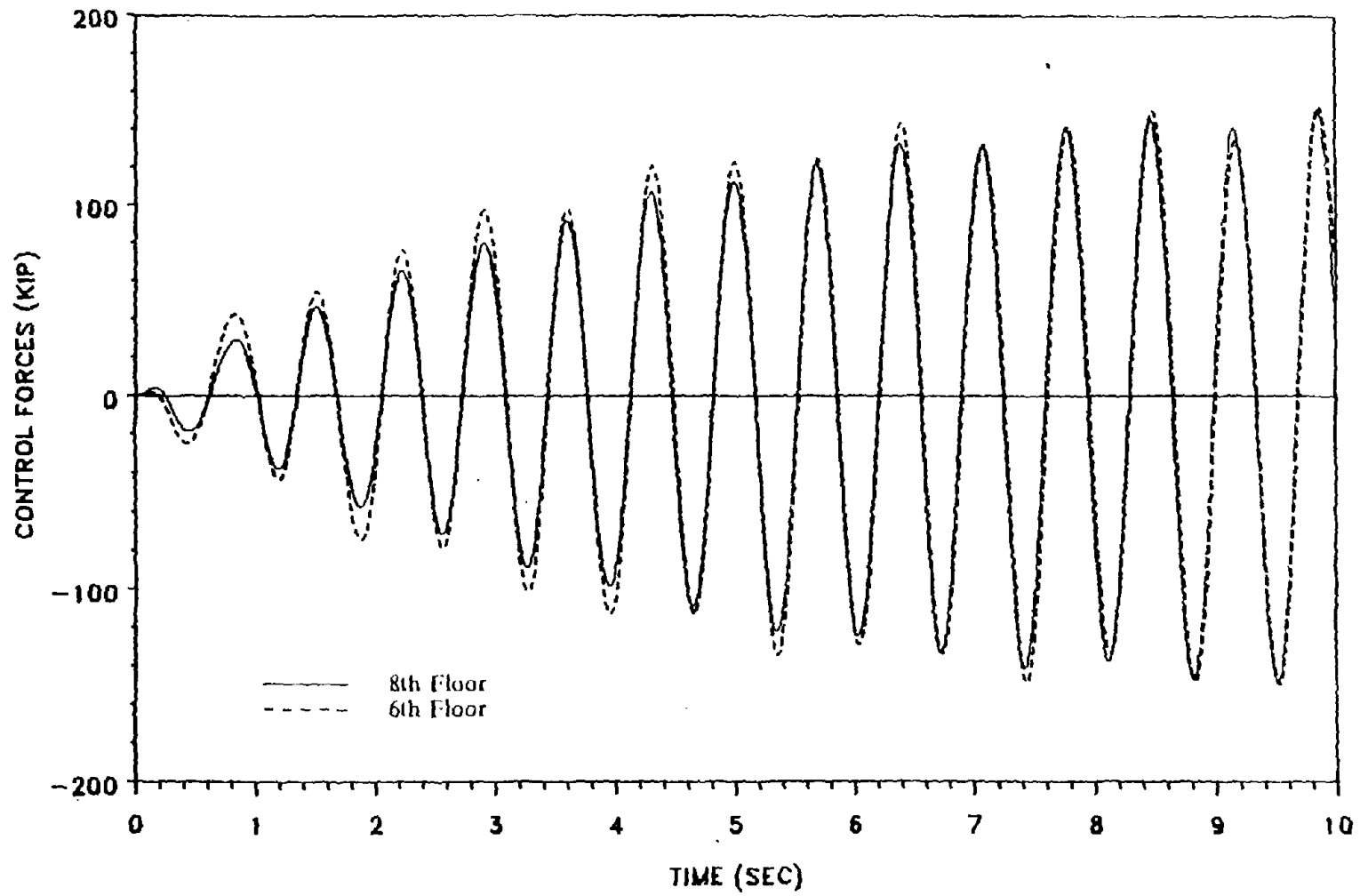
Figure 88.   Control Forces for 8th and 6th Floors: Excitation 2
(1 kip = 4.45 kN)

198

floor relative displacement, and its first three modal contributions
in Figures 89 through 92. It is observed that overall the performance
index choice of 5th and 6th floors is better. It produces a slightly
higher response in the first mode but less response in the second and
third modes.

A note has to be made about the modal choice. It is interesting
to note that after a modal choice has been made, the modal shapes of
the controlled system are no longer the same as those of the original
uncontrolled system. This fact is illustrated by finding the
closed-loop eigenvalues and eigenvectors of the controlled structure.
The procedure used calculates the eigenvalues from the state-equation
as follows. The optimal control of Equation 5.32 is substituted in the
state-equation, Equation 3.13, to give

$$\{\dot{z}(t)\} = \left[[A_t] - \frac{(\Delta t)}{2} [B_t] [R]^{-1} [B_t]^T [Q] \right] \{z(t)\} + \{C\} \ddot{X}_g(t) \tag{9.21}$$

from which the closed-loop-system eigenvalues and eigenvectors are
calculated. The procedure is the same as the one used for the standard
eigenvalue problem,

$$\{\dot{z}(t)\} = [A] \{z(t)\} \tag{9.22}$$

with the matrix $[A]$ defined as the closed-loop-system matrix

$$[A] = \left[[A_t] - \frac{(\Delta t)}{2} [B_t] [R]^{-1} [B_t]^T [Q] \right] \tag{9.23}$$

The no-control and closed-loop-system eigenvalues and eigenvectors of
the structure of the present example are shown in Tables VIII and IX.
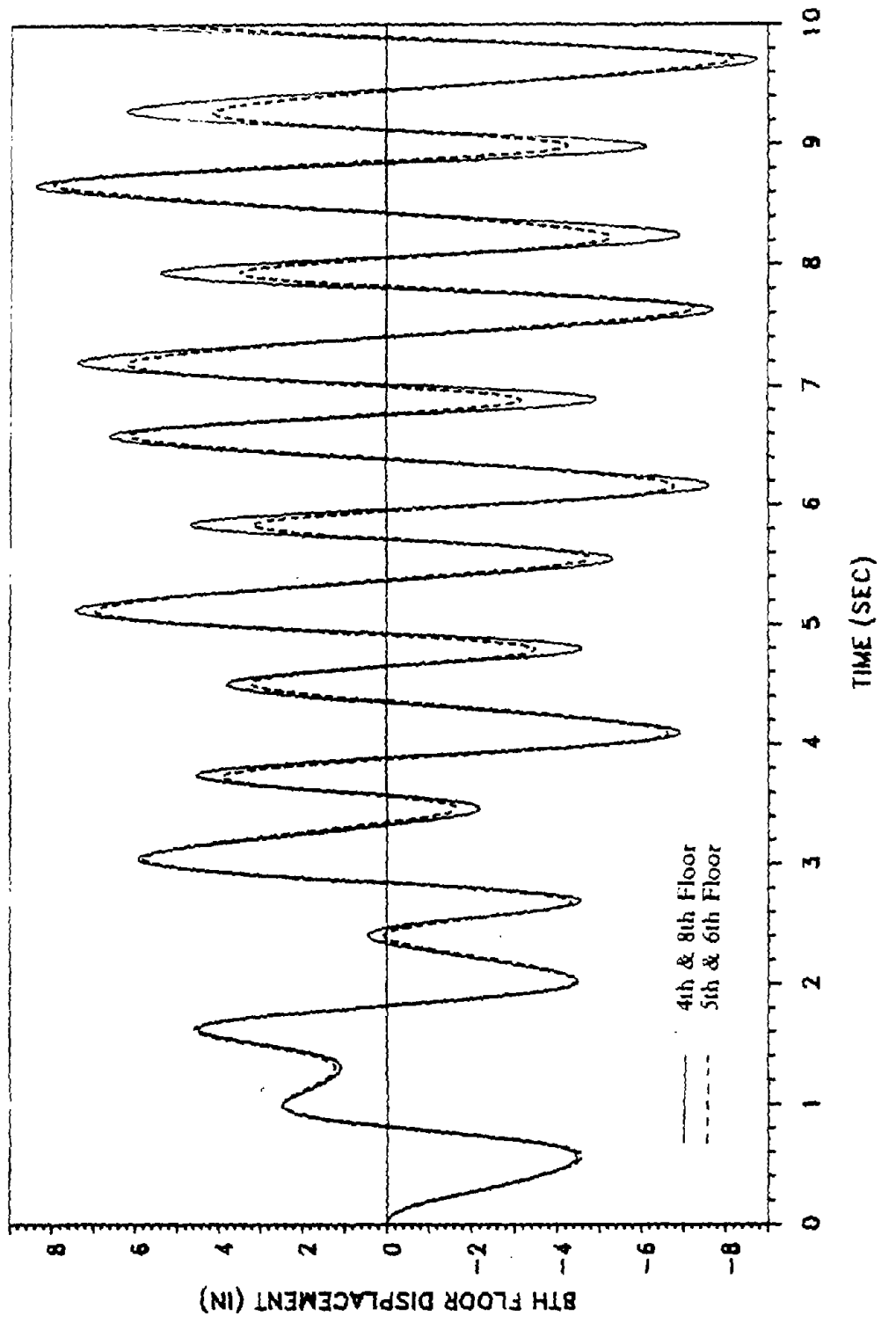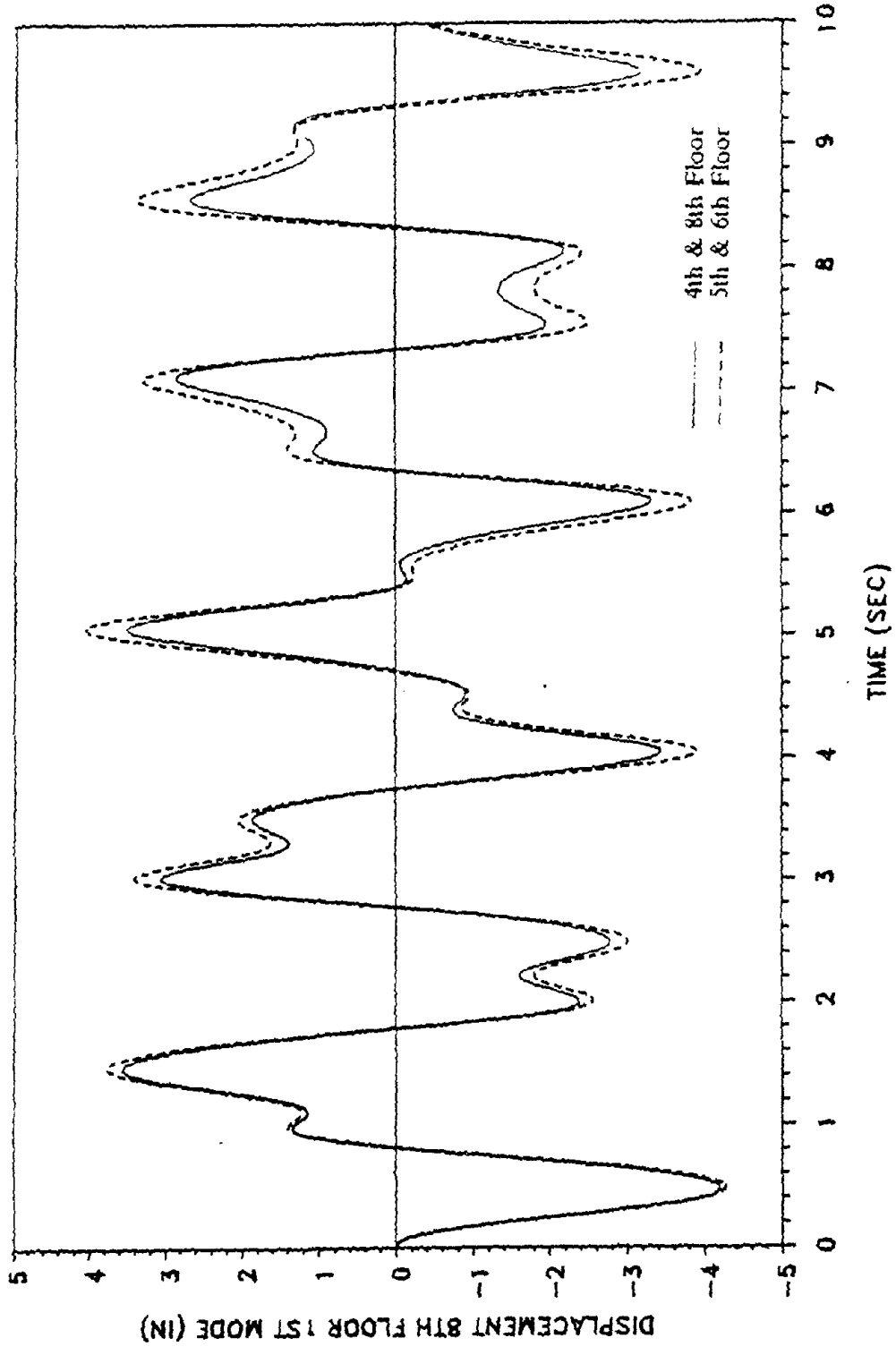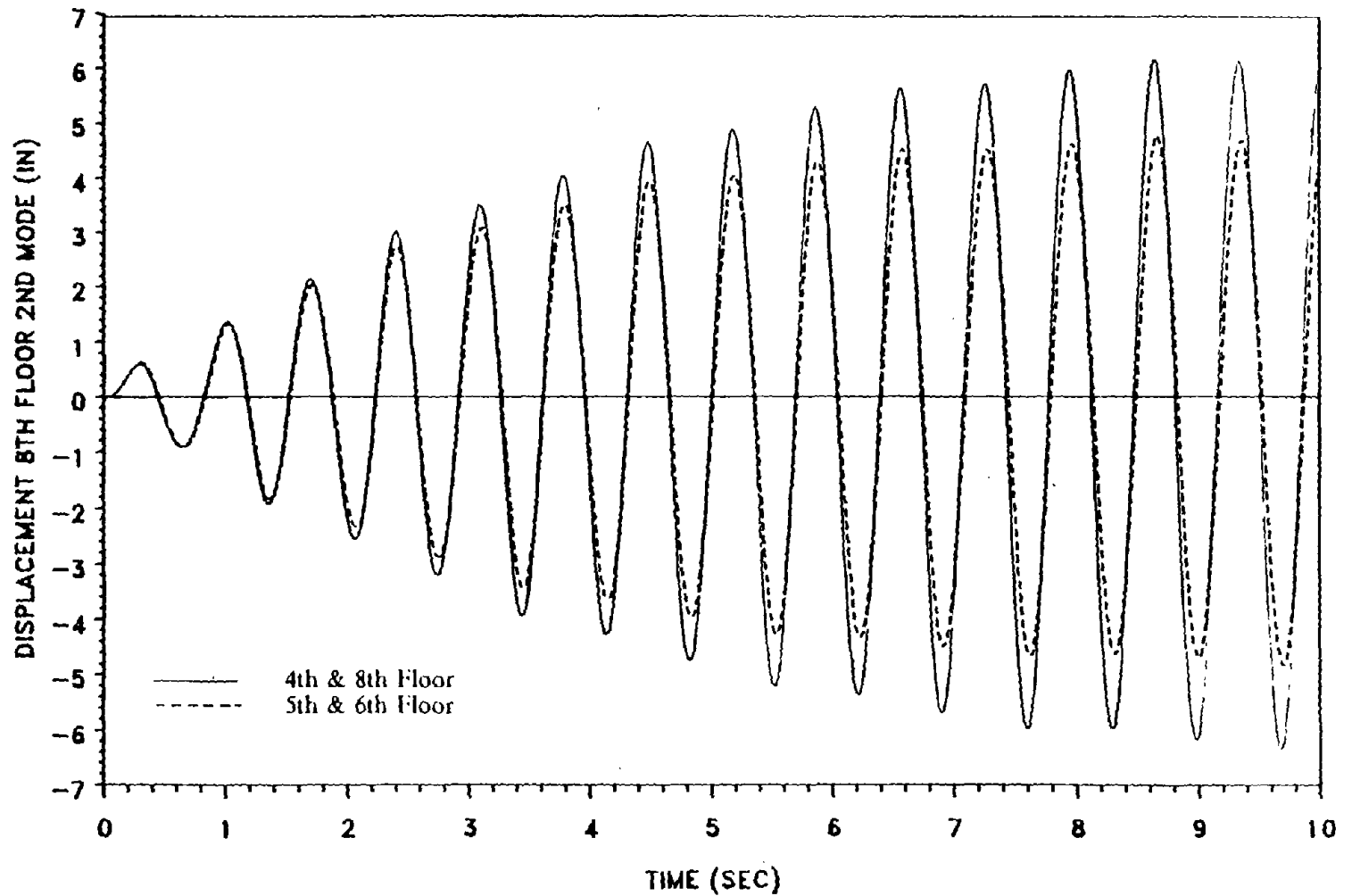
Figure 91. Controller Choices: Second Mode Response - Excitation 2
(1 in = 25.4 mm)

202

203
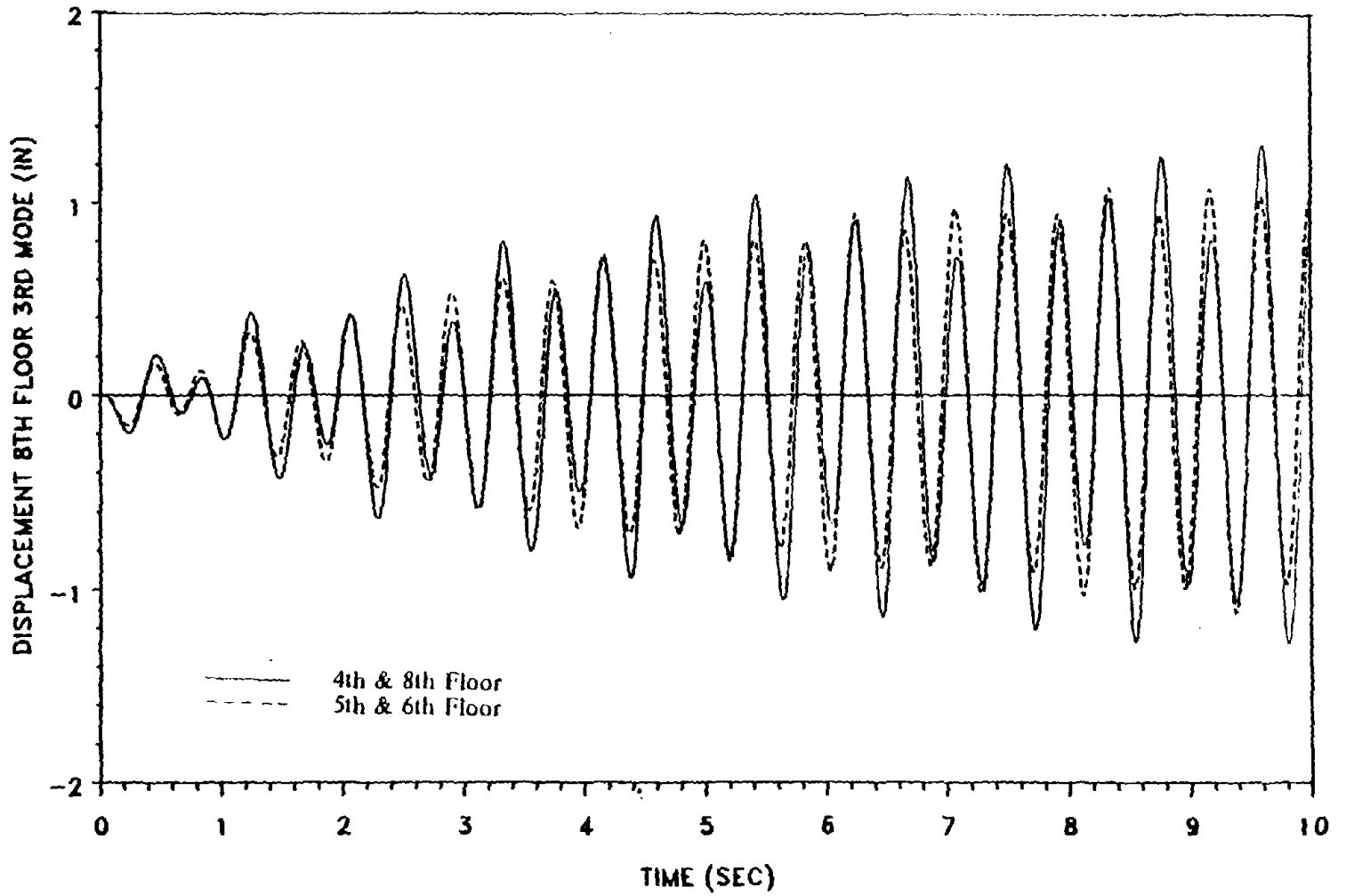
Figure 92. Controller Choices: Third Mode Response - Excitation 2
(1 in = 25.4 mm)

TABLE VIII. NO-CONTROL AND CLOSED-LOOP EIGENVALUES

NO-CONTROL EIGENVALUES

Mode	Eigenvalue	Frequency	% Damping
1st	-.035 + 3.493 i	3.493 rad/sec	1.00
2nd	-.092 + 9.203 i	9.203 rad/sec	1.00

4th & 8th Floors (CLOSED-LOOP EIGENVALUES)

Mode	Eigenvalue	Frequency	% Damping
1st	-.077 + 3.497 i	3.498 rad/sec	2.20
2nd	-.265 + 9.297 i	9.301 rad/sec	2.85

5th & 6th Floors (CLOSED-LOOP EIGENVALUES)

Mode	Eigenvalue	Frequency	% Damping
1st	-.107 + 3.499 i	3.501 rad/sec	3.06
2nd	-.545 + 9.291 i	9.307 rad/sec	5.86

From Table VIII one may note that the magnitude of the frequency in the two modes is slightly increased. Also note that the 5th and 6th floor choice produces higher closed-loop damping ratios for both the first and second mode. From Table IX, the magnitude of the eigenvectors is slightly modified, but more significantly the phase angle varies in the closed-loop cases from that of the no-control case. This is important as shown in Figure 93 for a simple two degree-of-freedom structure. The structure on the left is vibrating in a proportionally damped mode, in which the two degrees of freedom are vibrating either in-phase or at a phase angle of 180 degrees. The structure on the right has a varying phase angle as would be the case for a controlled structure. In Figure 93 the phase angle is 135 degrees. It can be seen that the modal shape is complex in this case and that the fixed mode shape assumed for the uncontrolled structure is no longer present. The performance index choice is definitely better than the modal choice and this can be attributed to the more rational procedure of calculating the indices for all the possibilities and then choosing the best combination.

TABLE IX. NO CONTROL AND CLOSED-LOOP EIGENVECTORS

NO CONTROL EIGENVECTORS

1st mode		2nd mode	
Magnitude	Phase (deg)	Magnitude	Phase (deg)
.109	-90.	-.352	90.
.226	-90.	-.674	90.
.358	-90.	-.913	90.
.498	-90.	-.960	90.
.652	-90.	-.720	90.
.821	-90.	-.091	90.
.939	-90.	.576	90.
1.000	-90.	1.000	90.

4th & 8th Floors (CLOSED-LOOP EIGENVECTORS)

1st mode		2nd mode	
Magnitude	Phase (deg)	Magnitude	Phase (deg)
.110	-90.	.375	-90.
.227	-90.	.717	-90.
.360	-90.	.966	-90.
.498	-92.	1.000	-92.
.653	-91.	.735	-94.
.822	-91.	.091	-141.
.940	-91.	-.648	95.
1.000	-91.	-.987	82.

TABLE IX. (continued)
5th & 6th Floors (CLOSED-LOOP EIGENVECTORS)

1st mode		2nd mode	
Magnitude	Phase (deg)	Magnitude	Phase (deg)
.110	-89.	-.343	79.
.228	-89.	-.655	78.
.360	-89.	-.883	77.
.500	-89.	-.925	75.
.653	-91.	-.685	76.
.820	-92.	-.142	126.
.939	-92.	.571	-98.
1.000	-92.	1.000	-93.
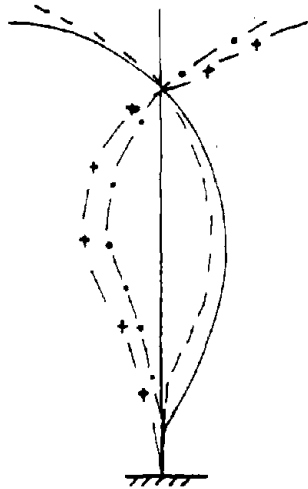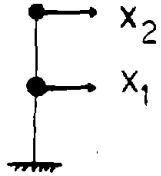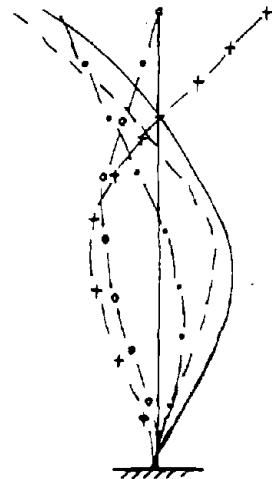
Figure 93. Complex Modal Shapes

X. CONCLUSIONS

This study has shown that active control systems, including the active mass damper and active tendons system, are effective in reducing the response of building structures to earthquake and wind loads. The active tendons system implemented with the Ricatti closed-Loop algorithm showed good agreement when compared to experimental results.

The non-optimal closed-loop, Ricatti optimal closed-loop and instantaneous optimal open-loop, optimal closed-loop and optimal open-closed-loop algorithms were reviewed and discussed. All of these algorithms can be used for the implementation of active control for both earthquake and wind excitations. From the point of view of reliability of measurements the instantaneous optimal closed-loop control algorithm is favored, especially in the case of wind excitations. It is also favored because time-delay in the measurement of the excitation is eliminated. In addition, since the feedback gain matrix for the closed-loop control does not involve the structural properties of mass, stiffness, and damping, the instantaneous optimal closed-loop control algorithm is insensitive to imprecise estimation of the structure's properties.

The structural optimization of building structures equipped with active control systems was carried out, with constraints imposed on the allowable floor displacements, control forces, and natural frequencies. The objective function chosen is structural weight and the design variables are the floor stiffnesses and some control

209

parameters. Structural weight is effective in redistributing the structural stiffness to the different floors for increased structural strength. The structural optimization is followed by minimization of control energy, in order to obtain the optimal weighting matrices that will reduce the level of the optimal control forces. The design variables are the elements of the weighting matrices, which are assumed diagonal matrices.

The optimal design of building structures equipped with active control systems is shown to be economical in both saving structural material and reducing the control energy demand. The structure is strengthened by the optimal redistribution of the stiffnesses and can resist the earthquake and wind excitations effectively using the active control systems. Structural optimization has the capability of varying the constraints imposed on structural response and the magnitude of the control forces; this allows the designer a wide spectrum of options.

A critical-mode optimal closed-loop algorithm was developed, and the spillover effect was shown to be considerable. For seismic structures the prospect of applying the critical-mode control is very promising since the response is governed by the lowest few modes.

Two methods for determining the optimal locations of a limited number of controllers have been investigated. The first method is based on the modal shapes of the uncontrolled structure. However these modal shapes are changed when the control system is enforced and therefore the optimal locations may be difficult to be determined.

This is especially true when a large number of modes is to be controlled. The second method is based on finding the locations of controllers that will minimize the control energy and response indices. The second method is preferable and this can be attributed to the more rational procedure of calculating the performance indices for all the possibilities and then choosing the best combination. It was found that the response index is a better measurement than the control energy and that the optimal locations of the tendons remained optimal for two different artificial earthquake excitations.

The issue of time-delay was explored and ways of compensating for it were suggested. However as the control system technology advances, the effect of time-delay may become negligible.
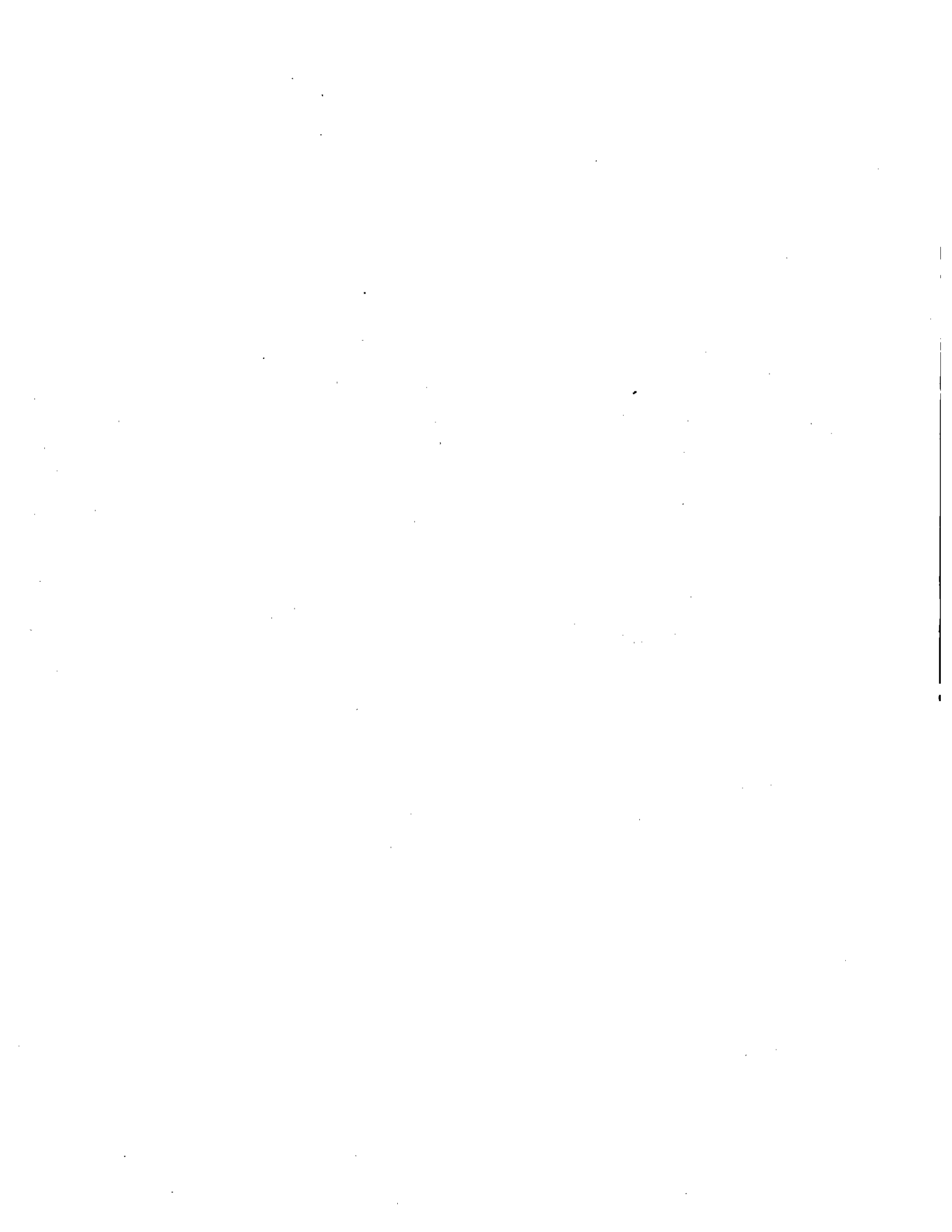
BIBLIOGRAPHY

1. Abdel-Rohman, M., and Leipholz, H. H. E., "A General Approach to Active Structural Control," <u>Proceedings of the IUTAM Symposium on Structural Control</u>, H. H. E. Leipholz, ed., North-Holland Publishing Company and SM Publications, 1980, pp. 1-28.

2. Abdel-Rohman, M., Quintana, V., and Leipholz, H. H. E., "Optimal Control of Civil Engineering Structures," <u>Journal of the Engineering Mechanics Division</u>, ASCE, Vol. 106, No. EM1, 1980, pp. 55-73.

3. Balas, M., "Modal Control of Certain Flexible Systems," <u>SIAM Journal of Control and Optimization</u>, Vol. 16, No. 3, May 1978, pp. 450-462.

4. Basharkhah, M. A., and Yao, J. T. P., "Application of Modern Control Theory for Building Structures," <u>Proceedings of the Third Specialty Conference on Dynamic Response of Structures</u>, ASCE/EMD, Los Angeles, April 1986, pp. 772-779.

5. Chang, F. K., "Human Response to Motions in Tall Buildings," <u>Journal of the Structural Division</u>, ASCE, Paper No. 9811, 1973, pp. 1259-1272.

6. Chang, J. C. H., and Soong, T. T., "Structural Control Using Active Tuned Mass Dampers," <u>Journal of the Engineering Mechanics Division</u>, ASCE, Vol. 106, No. EM6, 1980, pp. 1091-1098.

7. Cheng, F. Y., and Botkin, M. E., "Nonlinear Optimum Design of Dynamic Damped Frames," <u>Journal of the Structural Division</u>, ASCE, 102, ST3, March 1976, pp. 609-628.

8. Cheng, F. Y., and Juang, D. S., "Optimum Design of Braced and Unbraced Frames Subjected to Static, Seismic, and Wind Forces with UBC, ATC-3 and TJ-11," National Science Foundation Report, 1985 (376 pages), NTIS PB87-162988/AS.

9. Cheng, F. Y., and Pantelides, C. P., "Optimal Control of Seismic Structures," Proceedings of the Third Specialty Conference on Dynamic Response of Structures, ASCE/EMD, Los Angeles, April 1986, pp. 764-771.

10. Cheng, F. Y., and Pantelides, C. P., "Optimization of Structures and Controls Under Seismic Loading," International Conference on Computational Mechanics, ICCM-86, Tokyo, May 1986, Vol.II, pp. X-135 - X-140.

11. Cheng, F. Y., and Pantelides, C. P., "Optimum Seismic Structural Design with Tendon and Mass Damper Controls and Random Process," Proceedings of Structures Congress, Recent Developments in Structural Optimization, ASCE, F. Y. Cheng, ed., New Orleans, Sept. 1986, pp. 40-53.

12. Cheng, F. Y., and Pantelides, C. P., "Developments in Combining Structural Optimization and Control for Earthquake and Wind Forces," Proceedings of U.S.-Korea Seminar on Critical Engineering Systems, Seoul, May 1987, Vol. I, pp. 80-95.

13. Cheng, F. Y., and Pantelides, C. P., "Optimum Structural Design of Seismic Structures with Active Controls," Proceedings of the Sixth Specialty Conference, ASCE/EMD, Buffalo, May 1987, pp. 197.

14. Cheng, F. Y., and Truman, K. Z., "Optimum Design of 3-D Reinforced Concrete and Steel Buildings Subjected to Static and Seismic Loads Including Code Provisions," National Science Foundation Report, 1985 (414 pages), NTIS PB86-168564/AS.

15. Chung, L. L., Reinhorn, A. M., and Soong, T. T., "An Experimental Study of Active Control," Proceedings of the Third Specialty Conference on Dynamic Response of Structures, ASCE/EMD, Los Angeles, April 1986, pp. 795-802.

16. Davenport, A. G., "The Dependence of Wind Load upon Meteorological Parameters," Proceedings of International Research Seminar on Wind Effects on Buildings and Structures, University of Toronto Press, Toronto, 1968, pp. 19-82.

17. Davenport, W. B., Probability and Random Process, McGraw-Hill Book Company, New York, 1970, pp. 345-348.

18. Davison, E. J., and Maki, M. C., "The Numerical Solution of the Matrix Ricatti Equation," IEEE Transactions on Automatic Control, Vol. AC-18, No. 1, Feb. 1973, pp. 71-73.

19. Den Hartog, J. P., Mechanical Vibrations, McGraw-Hill, New York, 1947.

20. Elbert, T. F., Estimation and Control of Systems, Van Nostrand Reinhold Company Inc., New York, 1984.

21. Hallauer, W. L. Jr., Skidmore, G. R., and Gehling, R. N., "Modal-Space Active Damping of a Plane Grid: Experiment and Theory," Journal of Guidance, Control, and Dynamics, Vol. 8, No. 3, May-June 1985, pp. 366-373.

22. Iliff, K. W., "Identification and Stochastic Control of an Aircraft Flying in Turbulence," <u>Journal of Guidance and Control</u>, Vol. 1, No. 2, March-Apr. 1978, pp. 101-108.

23. Juang, D. S., "Optimum Design of Braced and Unbraced Frameworks Subjected to Static, Seismic, and Wind Forces with Building Code Provisions," Ph. D. Dissertation, Civil Engineering Department, University of Missouri-Rolla, 1986.

24. Kanai, K., "Semi-Empirical Formula for Seismic Characterization of the Ground," <u>Bulletin of Earthquake Research Institute</u>, University of Tokyo, Tokyo, Japan, Vol. 28, 1964, pp. 1967.

25. Khot, N. S., Eastep, F. E., and Venkayya, V. B., "Optimal Structural Modifications to Enhance the Optimal Active Vibration Control of Large Flexible Structures," <u>Proceedings of the 26th Structures and Dynamic Materials Conference</u>, <u>AIAA Paper No. 85-0627</u>, Orlando, April 1985.

26. Kleinman, D. L., "On An Iteration Technique for Ricatti Equation Computations," <u>IEEE Transactions on Automatic Control</u>, Vol. AC-13, No. 1, Feb. 1968, pp. 114-115.

27. Kobori, T., Kanayama, H., and Kamagata, S., "New Philosophy of Aseismic Design - Approach on Dynamic Intelligent Buildings," <u>Proceedings of the Sixth Specialty Conference</u>, ASCE/EMD, Buffalo, May 1987, pp. 196.

28. Lam, R. P., and Lam, L. C. H., "Assessment of Wind Loading on the Claddings of High-rise Buildings," <u>Proceedings of the Institute of Civil Engineers</u>, <u>Part 2</u>, 73, Sept. 1982, pp. 653-666.

29. Laub, A. J., "A Schur Method for Solving Algebraic Ricatti Equations," <u>IEEE Transactions on Automatic Control</u>, Vol. AC-24, No. 6, Dec. 1979, pp. 913-921.

30. Lewis, F. M., "Extended Theory of the Viscous Vibration Damper," <u>Journal of Applied Mechanics</u>, Transactions of ASME, Vol. 22, 1955, pp. 377-382.

31. Likins, P., "Spacecraft Attitude Dynamics and Control-A Personal Perspective on Early Developments," <u>Journal of Guidance</u>, <u>Control</u>, <u>and Dynamics</u>, Vol. 9, No. 2, March-Apr. 1986, pp. 129-134.

32. Lin, R. C., Chung, L. L., Soong, T. T., and Reinhorn, A. M., "Experimental Evaluation of Optimal Control Algorithms for Seismic Applications," <u>Proceedings of the Sixth Specialty Conference</u>, ASCE/EMD, Buffalo, May 1987, pp. 194.

33. Lin, R. C., Soong, T. T., and Reinhorn, A. M., "Experimental Evaluation of Instantaneous Optimal Algorithms for Structural Control," <u>Report No. 86-14</u>, Department of Civil Engineering, State University of New York at Buffalo, Buffalo, New York 14260

34. Martin, C. R., and Soong, T. T., "Modal Control of Multistory Structures," <u>Journal of the Engineering Mechanics Division</u>, ASCE, Vol. 102, No. EM4, 1976, pp. 613-623.

35. Masri, S. F., Bekey, G. A., and Caughey, T. K., "Optimum Pulse Control of Flexible Structures," <u>Journal of Applied Mechanics</u>, ASME Transactions, Vol. 48, Sep. 1981, pp. 619-626.

36. Mayne, J. R., "A Wind-Pressure Transducer," <u>Physics E: Scientific Instruments</u>, Vol. 3, May 1970, pp. 248-250.

37. Meirovitch, L., and Baruh, H., "Control of Self-Adjoint Distributed-Parameter Systems," Journal of Guidance and Control, AIAA, Vol. 5, No. 1, Jan.-Feb. 1982, pp. 60-66.

38. Meirovitch, L., and Baruh, H., "The Implementation of Modal Filters for Control of Structures," Journal of Guidance, Control, and Dynamics, Vol. 8, No. 6, Nov.-Dec. 1985, pp. 707-716.

39. Meirovitch, L., Baruh, H., Montgomery, R. C., and Williams, J. P., "Nonlinear Natural Control of an Experimental Beam," Journal of Guidance, Control, and Dynamics, Vol. 7, No. 4, Jul.-Aug. 1984, pp. 437-442.

40. Meirovitch, L., and Öz, H., "Modal-Space Control of Large Flexible Spacecraft Possessing Ignorable Coordinates," Journal of Guidance and Control, Vol. 3, No. 6, Nov.-Dec. 1980, pp. 569-577.

41. Meirovitch, L., and Öz, H., "Active Control of Structures by Modal Synthesis," Proceedings of the IUTAM Symposium on Structural Control, H. H. E. Leipholz, ed., North-Holland Publishing Company and SM Publications, 1980, pp. 505-521.

42. Meirovitch, L., and Silverberg, L. M., "Control of Structures Subjected to Seismic Excitation," Journal of the Engineering Mechanics Division, ASCE, Vol. 109, No. 2, April 1983, pp. 604-618.

43. Ormonroyd, J. and Den Hartog, J. P., "Theory of the Dynamic Vibration Absorber," Transactions of ASME, Vol. 50, PAPM-241, 1928, pp. 9-22.

44. Öz, H., and Meirovitch, L., "Optimal Modal-Space Control of Flexible Gyroscopic Systems," *Journal of Guidance and Control*, Vol. 3, No. 3, May-June 1980, pp. 218-226.

45. Öz, H., and Meirovitch, L., "Stochastic Independent Modal-Space Control of Distributed-Parameter Systems," *Journal of Optimization Theory and Applications*, Vol. 40, No. 1, May 1983, pp. 121-154.

46. Petersen, N. R., "Design of Large Scale Tuned Mass Dampers," *ASCE Convention and Exposition*, Preprint 3578, Boston, April 1979.

47. Powell, M. J. D., "An Efficient Method for Finding the Minimum of a Function of Several Variables without Calculating Derivatives," *Computer Journal*, Vol. 7, No. 2, 1964, pp. 155-162.

48. Saridis, G. N., and Lobbia, R. N., "Parameter Identification and Control of Linear Discrete-Time Systems," *IEEE Transactions on Automatic Control*, Vol. AC-17, No. 1, Feb. 1972, pp. 52-60.

49. Schaechter, D. B., "Hardware Demonstration of Flexible Beam Control," *Journal of Guidance, Control, and Dynamics*, Vol. 5, No. 1, Jan.-Feb. 1982, pp. 48-53.

50. Shinozuka, M., and Jan, C. M., "Digital Simulation of Random Processes and its Applications," *Journal of Sound and Vibration*, Vol. 25, No. 1, 1972, pp. 111-128.

51. Simiu, E., and Scanlan, R. H., *Wind Effects on Structures*, Second Edition, John Wiley and Sons Inc., New York, 1986.

52. Soong, T. T., and Chang, M. I. J., "On Optimal Control Configuration in Theory of Modal Control," *Structural Control*, H. H. E. Leipholz, ed., North Holland, Amsterdam, 1980, pp. 723-738.

53. Soong, T. T., Reinhorn, A. M., and Yang, J. N., "A Standard Model for Structural Control Experiments and Experimental Results," 2nd International Symposium on Structural Control, Waterloo, Ontario, July 1985.

54. Soong, T. T., and Skinner, G., "Experimental Study of Active Structural Control," Journal of the Engineering Mechanics Division, ASCE, Vol. 107, No. EM6, 1981, pp. 1057-1067.

55. Truman, K. Z., "Optimal Design of 3-D Reinforced Concrete and Steel Buildings Subjected to Static and Seismic Loads," Ph. D. Dissertation, Civil Engineering Department, University of Missouri-Rolla, 1985.

56. Truman, K. Z., and Cheng, F. Y., "Optimum Design of Steel and Reinforced Concrete 3-D Seismic Building Systems," Proceedings of the 8th World Conference on Earthquake Engineering, San Francisco, Vol. V, July 1984, pp. 475-482.

57. Vaughan, D. R., "A Negative Exponential Solution for the Matrix Ricatti Equation," IEEE Transactions on Automatic Control, Vol. AC-14, No. 1, Feb. 1969, pp. 72-75.

58. Vickery, B. J., "On the Reliability of Gust Loading Factors," Proceedings of Technical Meeting Concerning Wind Loads on Buildings and Structures, National Bureau of Standards, Building Science Series 30, Washington, D. C., 1970, pp. 93-104.

59. Warwaruk, J., "Deflection Requirements-History and Background Related to Vibrations," Vibrations of Concrete Structures, SP 60-2, American Concrete Institute, Detroit, 1979, pp. 13-41.

60. Wiesner, K. B., "Tuned Mass Dampers to Reduce Building Wind Motion," *ASCE Convention and Exposition*, Preprint 3510, Boston, April 1979.

61. Yang, J. N., "Control of Tall Buildings under Earthquake Excitation," *Journal of the Engineering Mechanics Division*, ASCE, Vol. 108, No. EM5, October 1982, pp. 833-849.

62. Yang, J. N., Akbarpour, A., and Gaemmaghami, P., "Instantaneous Optimal Control Laws for Tall Buildings Under Seismic Excitations," *Technical Report NCEER-87-0007*, June 10, 1987.

63. Yang, J. N., and Lin, M. J., "Optimal Critical Mode Control of Building under Seismic Load," *Journal of the Engineering Mechanics Division*, ASCE, Vol. 108, No. EM6, 1982, pp. 1167-1185.

64. Yang, J. N., and Lin, M. J., "Building Critical-Mode Control: Nonstationary Earthquake," *Journal of the Engineering Mechanics Division*, ASCE, Vol. 109, No. EM6, 1983, pp. 1375-1389.

65. Yang, J. N., and Samali B., "Control of Tall Buildings in Along-Wind Motion," *Journal of Structural Engineering*, ASCE, Vol. 109, No. 1, January 1983, pp. 50-68.

APPENDICES

EARTHQUAKE EXCITATION - KANAI-TAJIMI SPECTRAL DENSITY

The earthquake excitation derived herein is known as the Kanai-Tajimi power spectral density (24). This earthquake excitation is used as a ground acceleration input for the non-optimal closed-loop control algorithm of Chapter IV. Consider a white noise process having a power spectral density function of amplitude S^2 to be the input to the ground, which is modelled as a linear filter shown in Figure 94. The ground properties depending on the particular geological location are specified as $\omega_g =$ ground frequency, and $\zeta_g =$ ground damping. The power spectral density of the output $\Phi \ddot{X}_g(\omega)$ from the linear filter of the ground model is to be derived. Let z_g be the ground displacement, x_g be the input displacement, and the quantities k_g, c_g, and m_g, be the "stiffness", "damping", and "mass" of the ground, respectively; the equation of motion can be written

$$m_g \ddot{z}_g + c_g(\dot{z}_g - \dot{x}_g) + k_g(z_g - x_g) = 0 \qquad (A.1)$$

where in Equation $A.1$ a dot denotes differentiation with respect to time. Using the relations for frequency and damping

$$\frac{k_g}{m_g} = \omega_g^2, \qquad\qquad \frac{c_g}{m_g} = 2\,\omega_g\,\zeta_g \qquad (A.2)$$

Equation $A.1$ can be written as

$$\ddot{z}_g + 2\,\omega_g\,\zeta_g\,\dot{z}_g + \omega_g^2\,z_g = 2\,\omega_g\,\zeta_g\,\dot{x}_g + \omega_g^2\,x_g \qquad (A.3)$$
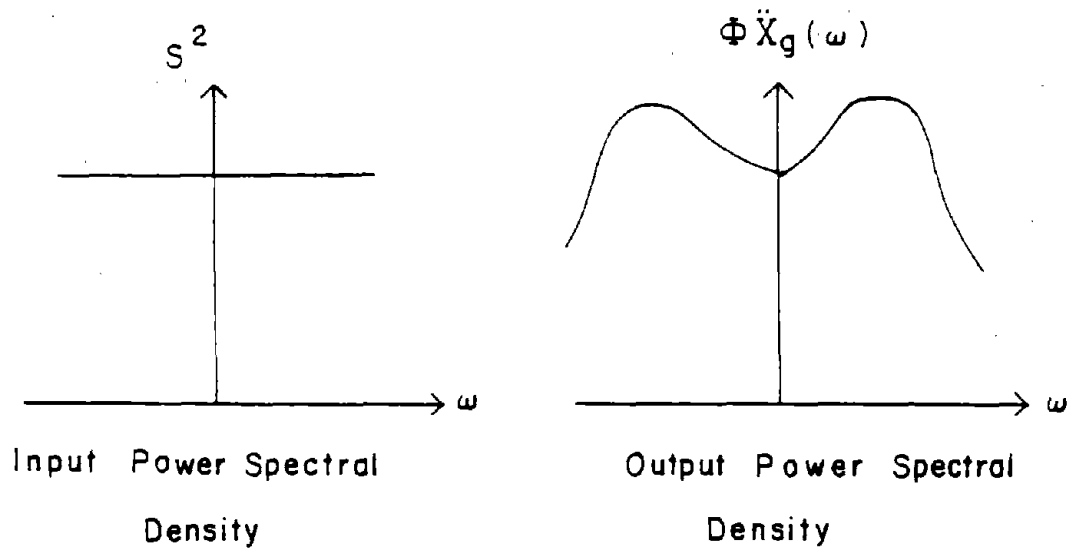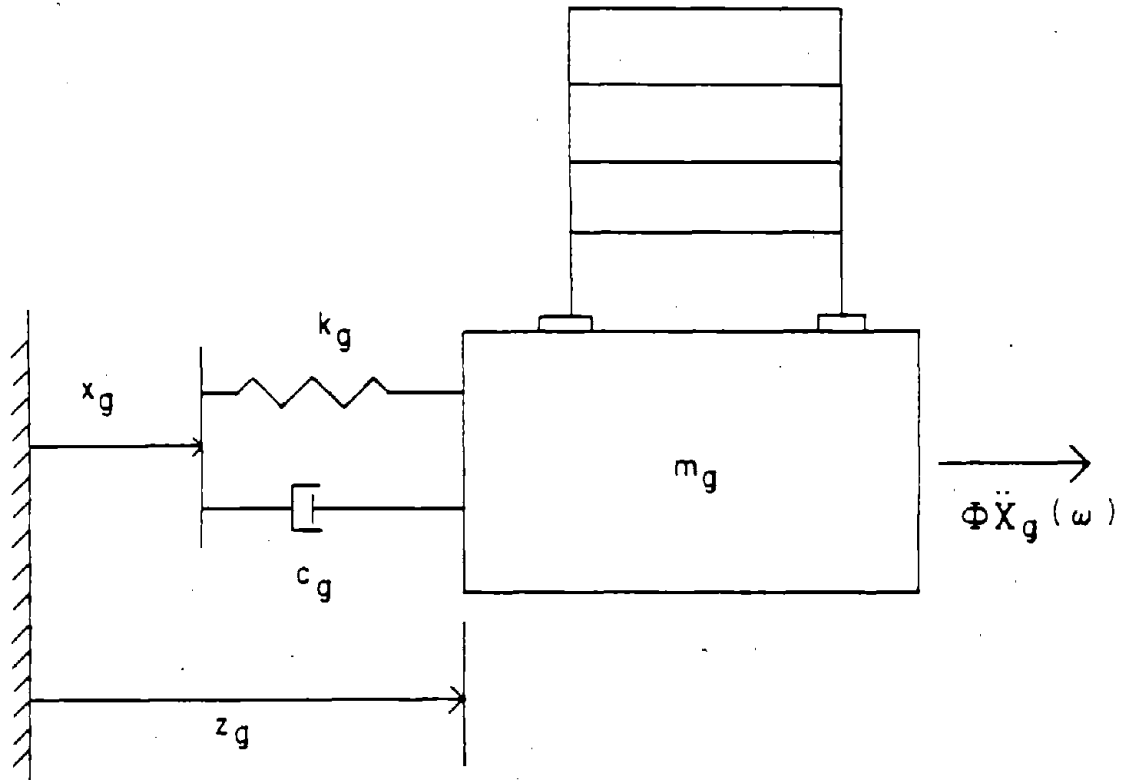
Figure 94. SDOF Model for Earthquake Excitation

Taking the Laplace transform of Equation $A.3$

$$(s^2 \bar{z}_g - z_g(0) s - \dot{z}_g(0)) + 2 \omega_g \zeta_g (s \bar{z}_g - z_g(0)) + \omega_g^2 \bar{z}_g$$
$$= 2 \omega_g \zeta_g (s \bar{x}_g - x_g(0)) + \omega_g^2 \bar{x}_g$$

$$(A.4)$$

where the overbar denotes the Laplace transform of a quantity, and s is the Laplace operator. Assuming zero initial conditions

$$x_g(0) = z_g(0) = 0, \qquad\qquad \dot{z}_g(0) = 0 \qquad\qquad (A.5)$$

and collecting terms, Equation $A.4$ becomes

$$\bar{z}_g(s^2 + 2 \omega_g \zeta_g s + \omega_g^2) = \bar{x}_g (2 \omega_g \zeta_g s + \omega_g^2) \qquad\qquad (A.6)$$

Therefore the transfer function of the filter is

$$H_g(s) = \frac{\bar{z}_g}{\bar{x}_g} = \frac{\omega_g^2 + 2 \omega_g \zeta_g s}{\omega_g^2 + 2 \omega_g \zeta_g s + s^2} \qquad\qquad (A.7)$$

The frequency response function $H_g(i\omega)$ can be obtained from the transfer function $H_g(s)$, by replacing s with $(i\omega)$, where $i = \sqrt{-1}$. The frequency response function becomes

$$H_g(i\omega) = \frac{1 + 2\zeta_g \dfrac{i\omega}{\omega_g}}{(1 - \dfrac{\omega^2}{\omega_g^2}) + 2\zeta_g \dfrac{i\omega}{\omega_g}} \qquad\qquad (A.8)$$

The power spectral density of the response is given by the well known expression

$$\Phi \ddot{X}_g(\omega) = \|H_g(i\omega)\|^2 \ S^2 \qquad\qquad (A.9)$$

in which S^2 is the amplitude of the power spectral density function of the input acceleration, and

$$\|H_g(i\omega)\|^2 = \|H_g(i\omega) \, H_g^*(i\omega)\| \qquad\qquad (A.10)$$

where $\|.\|$ denotes magnitude, and $H_g^*(i\omega)$ is the complex conjugate of $H_g(i\omega)$. Performing the algebra one can show using Equations $A.8$ and $A.10$ that

$$\|H_g(i\omega)\|^2 = \frac{1 + 4\zeta_g^2 \dfrac{\omega^2}{\omega_g^2}}{\left(1 - \dfrac{\omega^2}{\omega_g^2}\right)^2 + 4\zeta_g^2 \dfrac{\omega^2}{\omega_g^2}} \qquad\qquad (A.11)$$

Substituting the expression for $\|H_g(i\omega)\|^2$ in Equation $A.9$, the power spectral density of filtered white noise is obtained

$$\Phi\ddot{X}_g(\omega) = \frac{\left[1 + 4\zeta_g^2 \dfrac{\omega^2}{\omega_g^2}\right] S^2}{\left(1 - \dfrac{\omega^2}{\omega_g^2}\right)^2 + 4\zeta_g^2 \dfrac{\omega^2}{\omega_g^2}} \qquad\qquad (A.12)$$

APPENDIX B

WIND EXCITATION

In order to test the Ricatti closed-loop and instantaneous algorithms, a set of artificial wind excitations was generated based on design spectra for wind. The artificially generated wind velocities are used to create correlated wind pressures that are then applied on the individual floors of the structure. These artificial wind excitations can be applied for all three cases of open-loop, closed-loop, and open-closed-loop control.

The wind flow is assumed stationary in time and non-homogenous in space. Physically the wind is composed of two velocity components, steady and turbulent flow. The wind velocity vector at discrete points can be expressed as

$$\{F(h,t)\} = \{\overline{F}(h)\} + \{f(h,t)\} \qquad (B.1)$$

where $\{\overline{F}(h)\}$ is the mean wind velocity vector at different heights, h_j, and $\{f(h,t)\}$ is the dynamic component of the velocity. The procedure for determining the mean wind velocity at any height h_j is as follows : The reference wind velocity at $h = 10$ meters is adjusted for different averaging times and different terrain conditions, and the logarithmic law (51) is used to obtain the mean wind velocity

$$\{\overline{F}(h)\} = \frac{1}{\kappa} \tilde{f} \ln \frac{h}{h_0} \qquad (B.2)$$

in which κ = Von Karman's constant, $\tilde{f}$ = shear velocity constant, and h_0 = roughness length which depends on the terrain roughness.

The dynamic component of the wind velocity is considered to be a stationary random process. The power spectrum of the longitudinal fluctuations accepted for design, given by Simiu and Scanlan (51), is

$$\frac{n\ S(h,n)}{\tilde{f}^2} = \frac{200\ E}{(1 + 50\ E)^{5/3}} \qquad\qquad (B.3)$$

$$E = \frac{n\ h}{\bar{F}(h)} \qquad\qquad (B.4)$$

where n is the frequency of the velocity components of the fluctuating part of the wind velocity. Using Equations $B.3$ and $B.4$ one can determine the dynamic component of the velocity, $\{f(h,t)\}$. The vector $\{f(h,t)\}$ is descretized into N components $f_j(t)$, $j = 1,\dots,N$ corresponding to the N floors of the structure. From Equations $B.3$ and $B.4$ one may note that the wind spectrum varies with height, hence each floor has a unique spectrum. A random process is created that has a specific correlation, based on an experimentally derived coherence function developed by Davenport (16), for the entire structure. Consider the spectra of the first and Nth floor, as shown in Figure 95. Using the common part ACD between the two spectra (shown shaded in Figure 95), with the corresponding spectral density S_{ACD}, N uncorrelated velocities $\beta_j(t)$ are generated. The algorithm proposed by Shinozuka and Jan (50) is used

$$\beta_j(t) = \sqrt{2}\ \sum_{i=1}^{L} \sqrt{S_{ACD}(n_i)\ \Delta n_i}\ \ \cos(2\pi\ n_i\ t + \phi_{ji}), \qquad j = 1,\dots,N \qquad (B.5)$$

227
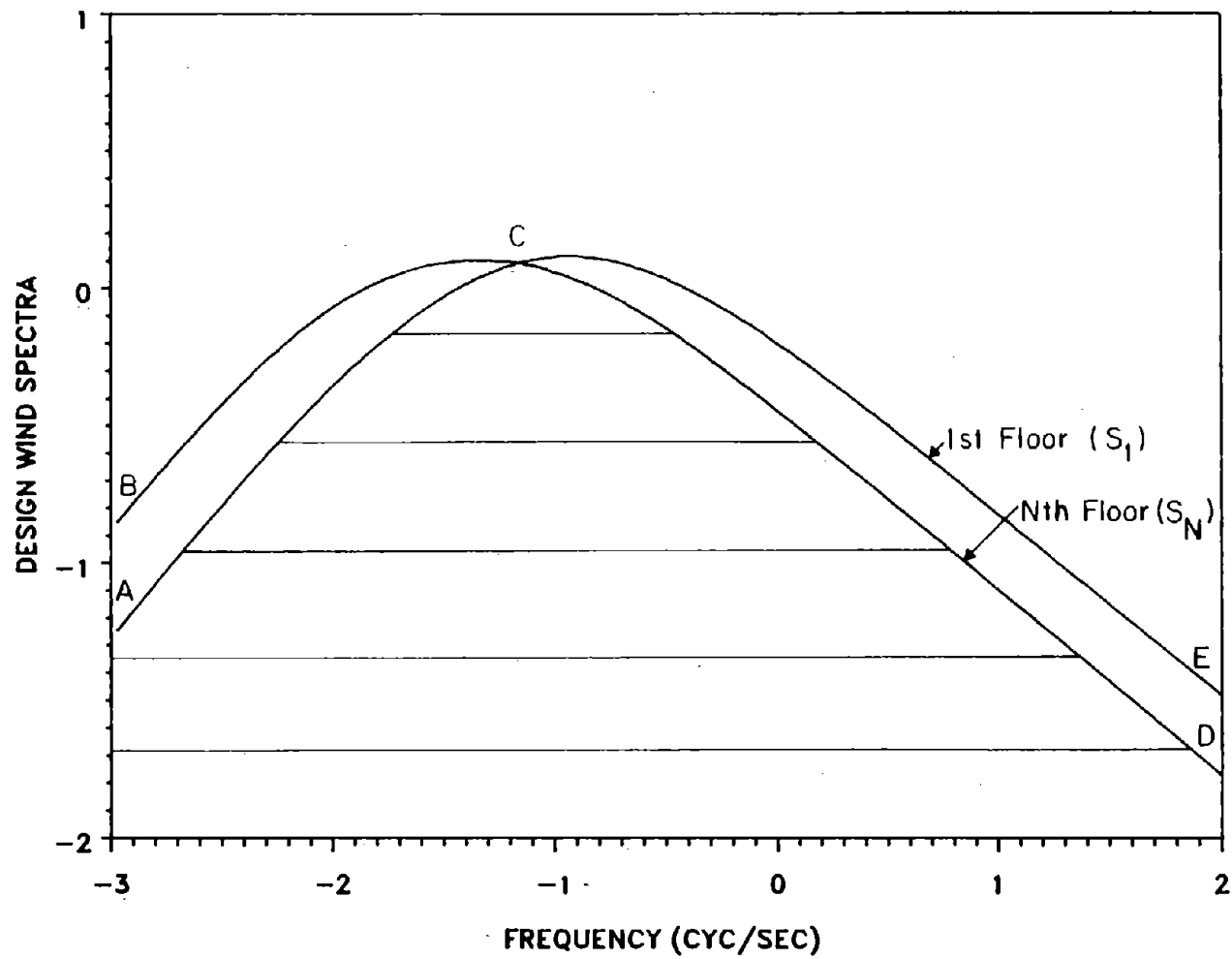
Figure 95. Wind Design Spectra

in which the range of frequencies containing the natural frequencies of the structure has been divided into L parts. Note that $\Delta n_i = n_{(i+1)} - n_i$. The angle ϕ_{ji} is a phase angle which varies randomly between zero and 2π, with a uniform probability distribution. The elements of $\{\beta(t)\}$ are then spatially correlated by using the transformation

$$\{\eta(t)\} = [D]\,\{\beta(t)\} \tag{B.6}$$

where $[D]$ is a lower-triangular matrix derived on the basis of the cross-correlation matrix $[\tilde{H}]$ of the process $\{\eta(t)\}$. The elements of $[\tilde{H}]$ are derived by using numerical integration of the co-spectrum between points j and $j+1$. The co-spectrum given by Vickery (58) is used

$$S^C(r,n) = \sqrt{S_j(n)\,S_{j+1}(n)}\ \ coh(r,n) \tag{B.7}$$

where r is the relative distance between points j and $j+1$, and $coh(r,n)$ is the coherence function proposed by Davenport (16), given by

$$coh(r,n) = e^{-\nu} \tag{B.8}$$

$$\nu = \frac{2\,n\left[C_h^2\,(h_j - h_{j+1})^2 + C_\chi^2\,(\chi_j - \chi_{j+1})^2\right]^{1/2}}{\bar{F}(h_j) + \bar{F}(h_{j+1})} \tag{B.9}$$

where C_h and C_χ are experimentally determined exponential decay coefficients. Note that the symbol χ denotes the horizontal dimension.

According to Simiu and Scanlan (51) the mean square value of the area under curve ACE or BCD in Figure 95 is equal to $6\tilde{f}^2$. Hence the common area ACD is equal to $\alpha(6\tilde{f}^2)$, where $\alpha < 1$. It is known that if $[\tilde{B}]$ is the cross-correlation matrix of process $\{\beta(t)\}$, then the

cross-correlation matrix of the process $\{\eta\}$ is $[\tilde{H}]$ given by Davenport (17)

$$[\tilde{H}] = [D][\tilde{B}][D]^T \tag{B.10}$$

Since $\beta_j(t)$ are stochastically independent and all have the variance $\alpha(6\tilde{f}^2)$, matrix $[\tilde{B}]$ is a diagonal matrix

$$[\tilde{B}] = \alpha(6\tilde{f}^2)[I] \tag{B.11}$$

In Equation $B.10$ the elements of matrix $[\tilde{H}]$ are given by the integration of the co-spectrum

$$\tilde{H}(j,k) = \int_0^\infty S^C(r,n)\, dn \tag{B.12}$$

and hence the elements of $[D]$ matrix can be obtained from Equation $B.10$ by using Cholesky Decomposition.

Finally to account for areas ABC and CDE in Figure 95, N uncorrelated velocities $\{\xi(t)\}$ are generated by using the difference between the first and and Nth floor spectra with the common spectrum (ACD). Define

$$S_{ABC} = S_N - S_{ACD}, \qquad\qquad S_{CDE} = S_1 - S_{ACD} \tag{B.13}$$

and use Equation $B.5$ with S_{ABC} and S_{CDE} to obtain $\{\xi(t)\}$.

The dynamic component of the velocity is given by

$$\{f(h,t)\} = [D]\{\beta(t)\} + \{\xi(t)\} \tag{B.14}$$

The mean pressures on the windward side of the structure are given by Simiu and Scanlan (51) as follows: For the steady-state

$$\overline{P}_r(h_j) = \frac{\rho}{2} \overline{F}^2(h_j) C_p \qquad (B.15)$$

where ρ is the air-density, and C_p is a pressure coefficient. For the fluctuating component

$$P_r(h_j, t) = \rho \, \overline{F}(h_j) f(h_j, t) C_w \qquad (B.16)$$

where C_w is an average pressure coefficient. Similar relations can be written for the leeward side. Finally the windward pressures given by Equations B.15 and B.16 are added to those of the leeward side and are then multiplied by the tributary area of each floor to provide the wind force for each floor. These wind forces at each floor constitute the wind force vector $\{W(t)\}$ to be used in the analysis.

APPENDIX C

PERFORMANCE INDICES

1. Ricatti Closed-loop.

In order to derive an optimal control force vector a suitable
performance index should be minimized. In the case of the Ricatti
closed-loop algorithm of Chapter 3, the performance index is chosen so
as to minimize the structural response and the control energy over the
time period from t_0 to t_f. Thus the expression of Equation 3.16

$$ J = \frac{1}{2} \int_{t_0}^{t_f} \left(\{z(t)\}^T [Q] \{z(t)\} + \{u(t)\}^T [R] \{u(t)\} \right) \, dt \qquad (C.1) $$

implies that it is important that at every time instant between t_0 and
t_f, both the structural response and control energy should be at a
minimum. If it is more important that the response be small, we should
choose the elements of $[Q]$ to be large. If it is more important,
however, that the control energy be small, then we should select the
elements of $[R]$ to have large values. One may note that while the
system dynamics are fixed as given by Equations 3.15 or 3.32, the
performance index is chosen in order to achieve a specific control
objective. Equation C.1 is for the AT case. For the AMD case, since
there is only one control force, matrix $[R]$ is reduced to just one
element and the performance index is given by Equation 3.47.

2. Instantaneous Optimal Control Algorithms.

The performance index of Equation C.1 leads to an optimal control law which requires the solution of Equation 3.34. This equation has to be solved backwards in time but since the earthquake excitation is not known apriori, its solution is not feasible. Based on the studies of Saridis and Lobbia (48) for stochastic control, the overall performance index of Equation C.1 can also be written in discrete form as

$$ J = \frac{1}{2} \sum_{i=1}^{n-1} (\{z(t)\}^T [Q] \{z(t)\} + \{u(t)\}^T [R] \{u(t)\}) \qquad (C.2) $$

defined over the time interval of interest (1,n). The objective is to find the control sequence $\{u_1(t)\}$, $\{u_2(t)\}$, ... , $\{u_{n-1}(t)\}$ that minimizes J. In their formulation Saridis and Lobbia, instead of minimizing a stochastic performance index similar to Equation C.2, suggest a step-by-step process. Equivalently in terms of the overall performance index of Equation C.2 we can define an instantaneous performance index as

$$ J_p(t) = \{z(t)\}^T [Q] \{z(t)\} + \{u(t)\}^T [R] \{u(t)\} \qquad (C.3) $$

This performance index was suggested by Yang, Akbarpour and Gaemmaghami for the instantaneous active control of earthquake-excited structures (62). One may note that the instantaneous performance index of Equation C.3 is time-dependent. This expression implies that the structural response and the control energy are minimized at every time instant in the time interval of interest. The performance index of

233

Equation C.3 is used in Chapter V for finding the optimal control for the open, closed and open-closed-loop strategies. The resulting expressions for the optimal control laws are simpler than those resulting from the classical performance index of Equation C.1. Using Equation C.3 instead of Equation C.1 can be justified in terms of the interpretation of Equation C.1 as an area integral between times t_0 to t_f. Thus minimization of Equation C.1 is equivalent to minimization of the area integral, and minimization of Equation C.3 is equivalent to minimization of the individual ordinates.

3. Critical-mode Algorithm.

The performance index derived for the instantaneous algorithms is modified in order to be expressed in terms of the $\overline{m}$ critical modes only. Substituting Equation 5.2 in Equation 5.1

$$J_p(t) = \{[T_t]\{\psi_t(t)\}\}^T [Q] \{[T_t]\{\psi_t(t)\}\} + \{u(t)\}^T [R] \{u(t)\} \qquad (C.4)$$

Performing the algebra

$$J_p(t) = \{\psi_t(t)\}^T [T_t]^T [Q][T_t]\{\psi_t(t)\} + \{u(t)\}^T [R]\{u(t)\} \qquad (C.5)$$

Substituting the partitioned modal state-vector of Equation 9.7 in Equation C.5

$$J_p(t) = \left\{ \frac{\{\psi_t(t)\}_c}{\{\psi_t(t)\}_r} \right\}^T [T_t]^T [Q][T_t] \left\{ \frac{\{\psi_t(t)\}_c}{\{\psi_t(t)\}_r} \right\} \\ + \{u(t)\}^T [R]\{u(t)\} \qquad (C.6)$$

$$J_p(t) = \left[\{\psi_t(t)\}_c^T \quad \{\psi_t(t)\}_r^T \right] [T_t]^T [Q][T_t] \left\{ \frac{\{\psi_t(t)\}_c}{\{\psi_t(t)\}_r} \right\} \\ + \{u(t)\}^T [R]\{u(t)\} \qquad (C.7)$$

The product of the three matrices in the first term is partitioned as follows

$$[T_i]^T [Q] [T_i] = \left[\begin{array}{c|c} [Q]_c & [Q]_{cr} \\ \hline [Q]_{rc} & [Q]_r \end{array} \right] \qquad\qquad (C.8)$$

where $[Q]_c$ is a $\overline{2m} \times \overline{2m}$ matrix and $[Q]_r$ is a $2(N - \overline{m}) \times 2(N - \overline{m})$ matrix. Substituting Equation C.8 in Equation C.7

$$J_p(t) = \left[\left\{ \{\psi_i(t)\}_c^T [Q]_c + \{\psi_i(t)\}_r^T [Q]_{rc} \right\} \quad \left\{ \{\psi_i(t)\}_c^T [Q]_{cr} + \{\psi_i(t)\}_r^T [Q]_r \right\} \right]$$
$$* \left\{ \frac{\{\psi_i(t)\}_c}{\{\psi_i(t)\}_r} \right\} + \{u(t)\}^T [R] \{u(t)\} \qquad\qquad (C.9)$$

$$J_p(t) = \{\psi_i(t)\}_c^T [Q]_c \{\psi_i(t)\}_c + \{\psi_i(t)\}_r^T [Q]_{rc} \{\psi_i(t)\}_c$$
$$+ \{\psi_i(t)\}_c^T [Q]_{cr} \{\psi_i(t)\}_r + \{\psi_i(t)\}_r^T [Q]_r \{\psi_i(t)\}_r + \{u(t)\}^T [R] \{u(t)\} \qquad (C.10)$$

For controlling the critical modes only, terms that contain products involving the residual modes are ignored. Hence the performance index to be minimized for controlling the critical modes becomes

$$J_c(t) = \{\psi_i(t)\}_c^T [Q]_c \{\psi_i(t)\}_c + \{u(t)\}^T [R] \{u(t)\} \qquad\qquad (C.11)$$

APPENDIX D

OPTIMAL CONTROL DERIVATIONS

Herein the derivations of the optimal control forces for the Ricatti closed-loop and instantaneous optimal control algorithms are presented.

1. <u>Ricatti Closed-loop</u>.

The derivation of the optimal control forces for the Ricatti closed-loop follows the classical control derivation for the linear regulator problem. A regulator is a feedback control law which maintains the state of the system close to a desired reference state during the interval (t_0, t_f), using reasonable values of the control force vector. Here the state is the displacement and velocity response, and the desired reference state is the equilibrium state. The optimal control force vector $\{u^*(t)\}$ is to be derived by minimizing a standard quadratic performance index given by

$$J = \frac{1}{2} \int_{t_0}^{t_f} \left(\{z(t)\}^T [Q] \{z(t)\} + \{u(t)\}^T [R] \{u(t)\} \right) dt \qquad (D.1)$$

and satisfying the state-equation

$$\{\dot{z}(t)\} = [A_t] \{z(t)\} + [B_t] \{u(t)\} \qquad (D.2)$$

Define the Hamiltonian as

$$\mathcal{H} = \frac{1}{2}\{z(t)\}^T [Q] \{z(t)\} + \frac{1}{2}\{u(t)\}^T [R] \{u(t)\}$$
$$+ \{\lambda(t)\}^T \left([A_t] \{z(t)\} + [B_t] \{u(t)\} - \{\dot{z}(t)\} \right) \tag{D.3}$$

where $\{\lambda(t)\}$ is the vector of Lagrange multipliers of dimension $[2N \times 1]$. The necessary conditions for optimality are

$$\frac{\partial \mathcal{H}}{\partial \{z(t)\}} = -\{\dot{\lambda}(t)\} \quad \rightarrow \quad -\{\dot{\lambda}(t)\} = [Q]\{z(t)\} + [A_t]^T\{\lambda(t)\} \tag{D.4}$$

$$\frac{\partial \mathcal{H}}{\partial \{u(t)\}} = \{0\} \quad \rightarrow \quad [R]\{u(t)\} + [B_t]^T\{\lambda(t)\} = \{0\} \tag{D.5}$$

$$\frac{\partial \mathcal{H}}{\partial \{\lambda(t)\}} = \{0\} \quad \rightarrow \quad [A_t]\{z(t)\} + [B_t]\{u(t)\} - \{\dot{z}(t)\} = \{0\} \tag{D.6}$$

with the transversality condition

$$\{\lambda(t_f)\} = \{0\} \tag{D.7}$$

From Equation D.5 the optimal control is derived as

$$\{u^*(t)\} = -[R]^{-1} [B_t]^T \{\lambda(t)\} \tag{D.8}$$

In order to find $\{\lambda(t)\}$, Equations D.4, D.6 and D.7 are utilized. Assume a solution of the form

$$\{\lambda(t)\} = [P(t)] \{z(t)\} \tag{D.9}$$

Substitute Equation D.9 in Equation D.4

$$-\left([\dot{P}(t)] \{z(t)\} + [P(t)] \{\dot{z}(t)\}\right) = [Q] \{z(t)\} + [A_t]^T [P(t)] \{z(t)\} \tag{D.10}$$

Substitute Equation D.6 in Equation D.10

$$[\dot{P}(t)]\,\{z(t)\} + [P(t)]\,([A_t]\,\{z(t)\} + [B_t]\,\{u(t)\}) + [Q]\,\{z(t)\}$$
$$+ [A_t]^T\,[P(t)]\,\{z(t)\} = \{0\} \tag{D.11}$$

Substitute Equations D.8 and D.9 in Equation D.11

$$\left([\dot{P}(t)] + [P(t)]\,[A_t] + [A_t]^T\,[P(t)] - [P(t)]\,[B_t]\,[R]^{-1}\,[B_t]^T\,[P(t)] + [Q]\right)\{z(t)\}$$
$$= \{0\} \tag{D.12}$$

From Equations D.7 and D.9 we get

$$[P(t_f)]\,\{z(t_f)\} = \{0\} \tag{D.13}$$

For a non-zero state $\{z(t)\}$ the non-trivial solution is from Equations D.12 and D.13

$$-[\dot{P}(t)] = [P(t)]\,[A_t] + [A_t]^T\,[P(t)] - [P(t)]\,[B_t]\,[R]^{-1}\,[B_t]^T\,[P(t)] + [Q] \tag{D.14}$$

$$[P(t_f)] = [0] \tag{D.15}$$

which are given in Chapter III as Equations 3.27 and 3.28. Similar derivations lead to Equation 3.34 for the case of the Ricatti closed-loop algorithm for external disturbances.

2. <u>Instantaneous Open-loop</u>.

The derivation of the optimal control forces for the instantaneous open-loop case of Chapter V follows. Find the optimal control forces $\{u^*(t)\}$ that minimize the instantaneous performance index of Equation 5.1 given by

$$J_p(t) = \{z(t)\}^T\,[Q]\,\{z(t)\} + \{u(t)\}^T\,[R]\,\{u(t)\} \tag{D.16}$$

and satisfy the state-equation, Equation 3.13, which can be used in the alternative form given by Equation 5.16 as

$$\{z(t)\} = [T_t]\left\{\{\Lambda_t(t - \Delta t)\} + \{\Gamma(t)\}\left(\frac{\Delta t}{2}\right)\right\} \tag{D.17}$$

Substituting Equation D.17 in Equation D.16

$$J_p(t) = \left\{[T_t]\left\{\{\Lambda_t(t - \Delta t)\} + \{\Gamma(t)\}\left(\frac{\Delta t}{2}\right)\right\}\right\}^T [Q]$$
$$\cdot \left\{[T_t]\left\{\{\Lambda_t(t - \Delta t)\} + \{\Gamma(t)\}\left(\frac{\Delta t}{2}\right)\right\}\right\} + \{u(t)\}^T [R]\{u(t)\} \tag{D.18}$$

Simplifying the first term

$$J_p(t) = \left\{\{\Lambda_t(t - \Delta t)\}^T + \{\Gamma(t)\}^T\left(\frac{\Delta t}{2}\right)\right\}[T_t]^T [Q]$$
$$\cdot [T_t]\left\{\{\Lambda_t(t - \Delta t)\} + \{\Gamma(t)\}\left(\frac{\Delta t}{2}\right)\right\} + \{u(t)\}^T [R]\{u(t)\} \tag{D.19}$$

The conditions for minimizing $J_p(t)$ are

$$\delta^{(1)}J_p(t) \equiv 0, \qquad \delta^{(2)}J_p(t) > 0 \tag{D.20}$$

$$\delta J_p(t) = \delta\{\Gamma(t)\}^T[T_t]^T [Q][T_t]\left(\frac{\Delta t}{2}\right)\left\{\{\Lambda_t(t - \Delta t)\} + \{\Gamma(t)\}\left(\frac{\Delta t}{2}\right)\right\}$$
$$+ \left\{\{\Lambda_t(t - \Delta t)\}^T + \{\Gamma(t)\}^T\left(\frac{\Delta t}{2}\right)\right\}[T_t]^T [Q][T_t]\delta\{\Gamma(t)\}\left(\frac{\Delta t}{2}\right) \tag{D.21}$$
$$+ \delta\{u(t)\}^T [R]\{u(t)\} + \{u(t)\}^T [R]\delta\{u(t)\}$$

The variation of $\{\Gamma(t)\}$ can be expressed in terms of the variation of $\{u(t)\}$ using Equation 5.7

$$\{\Gamma(t)\} = [T_t]^{-1}[B_t]\{u(t)\} + [T_t]^{-1}\{C_t\}\ddot{X}_g(t) \tag{D.22}$$

Hence

239

$$\delta\{\Gamma(t)\} = [T_t]^{-1}[B_t]\,\delta\{u(t)\} \qquad (D.23)$$

Substituting Equation D.23 in Equation D.21 we obtain

$$
\begin{aligned}
\delta J_p(t) = {} & \delta\{u(t)\}^T [B_t]^T ([T_t]^{-1})^T [T_t]^T [Q][T_t]\left(\frac{\Delta t}{2}\right)\left\{ \{\Lambda_t(t-\Delta t)\} + \{\Gamma(t)\}\left(\frac{\Delta t}{2}\right)\right\} \\
& + \left\{ \{\Lambda_t(t-\Delta t)\}^T + \{\Gamma(t)\}^T\left(\frac{\Delta t}{2}\right)\right\}[T_t]^T [Q][T_t][T_t]^{-1}[B_t]\,\delta\{u(t)\}\left(\frac{\Delta t}{2}\right) \qquad (D.24) \\
& + \delta\{u(t)\}^T [R]\{u(t)\} + \{u(t)\}^T [R]\,\delta\{u(t)\}
\end{aligned}
$$

Simplifying

$$
\begin{aligned}
\delta J_p(t) = {} & \left[\delta\{u(t)\}^T [B_t]^T [Q][T_t]\left(\frac{\Delta t}{2}\right)\left\{ \{\Lambda_t(t-\Delta t)\} + \{\Gamma(t)\}\left(\frac{\Delta t}{2}\right)\right\}\right. \\
& \left. + \delta\{u(t)\}^T [R]\{u(t)\}\right] + \left[\{u(t)\}^T [R]\,\delta\{u(t)\}\right. \qquad (D.25) \\
& \left. + \left\{ \{\Lambda_t(t-\Delta t)\}^T + \{\Gamma(t)\}^T\left(\frac{\Delta t}{2}\right)\right\}[T_t]^T [Q][B_t]\,\delta\{u(t)\}\left(\frac{\Delta t}{2}\right)\right]
\end{aligned}
$$

The terms in the brackets are the transpose of each other provided that $[Q]$ and $[R]$ are symmetric matrices. In order to satisfy Equation D.20 it suffices to set one of them equal to zero. Therefore the necessary condition becomes

$$
\begin{aligned}
& \delta\{u(t)\}^T [B_t]^T [Q][T_t]\left(\frac{\Delta t}{2}\right)\left\{ \{\Lambda_t(t-\Delta t)\} + \{\Gamma(t)\}\left(\frac{\Delta t}{2}\right)\right\} \\
& + \delta\{u(t)\}^T [R]\{u(t)\} = 0
\end{aligned} \qquad (D.26)
$$

Substitute $\{\Gamma(t)\}$ from Equation D.22 in Equation D.26

$$
\begin{aligned}
& \delta\{u(t)\}^T [B_t]^T\left(\frac{\Delta t}{2}\right)[Q][T_t]\left[\{\Lambda_t(t-\Delta t)\} + [T_t]^{-1}[B_t]\{u(t)\}\left(\frac{\Delta t}{2}\right)\right. \\
& \left. + [T_t]^{-1}\{C_t\}\,\ddot{X}_g(t)\left(\frac{\Delta t}{2}\right)\right] + \delta\{u(t)\}^T [R]\{u(t)\} = 0
\end{aligned} \qquad (D.27)
$$

Simplifying

240

$$\delta\{u(t)\}^T\left[\ [B_l]^T[Q][T_l]\{\Lambda_t(t-\Delta t)\}\left(\frac{\Delta t}{2}\right)+[B_l]^T[Q][B_l]\{u(t)\}\left(\frac{\Delta t}{2}\right)^2\right.$$
$$\left.+[B_l]^T[Q]\{C_l\}\ddot{X}_g(t)\left(\frac{\Delta t}{2}\right)^2+[R]\{u(t)\}\ \right]\ =\ 0 \qquad (D.28)$$

For a non-trivial solution the terms inside the brackets should be set equal to zero

$$[B_l]^T[Q][T_l]\{\Lambda_t(t-\Delta t)\}\left(\frac{\Delta t}{2}\right)+[B_l]^T[Q]\{C_l\}\ddot{X}_g(t)\left(\frac{\Delta t}{2}\right)^2$$
$$+\left[\ [B_l]^T[Q][B_l]\left(\frac{\Delta t}{2}\right)^2+[R]\ \right]\{u(t)\}\ =\ 0 \qquad (D.29)$$

Solving in terms of $\{u(t)\}$

$$\{u^{\bullet}(t)\}\ =\ [G_l]\{\Theta_t(t)\} \qquad (D.30a)$$

where

$$[G_l]\ =\ \left[[B_l]^T[Q][B_l]\left(\frac{\Delta t}{2}\right)^2+[R]\ \right]^{-1} \qquad (D.30b)$$

$$\{\Theta_t(t)\}\ =\ -[B_l]^T[Q][T_l]\{\Lambda_t(t-\Delta t)\}\left(\frac{\Delta t}{2}\right)-[B_l]^T[Q]\{C_l\}\ddot{X}_g(t)\left(\frac{\Delta t}{2}\right)^2 \qquad (D.30c)$$

which is exactly the solution given in Equations 5.18 through 5.20. The second condition in Equation D.20 can be satisfied by arguing on physical grounds.

3. Instantaneous Closed-loop.

The derivation of the optimal control forces for the instantaneous closed-loop case of Chapter V follows. Find the optimal control forces $\{u^{\bullet}(t)\}$ that minimize the instantaneous performance index of Equation D.16 and satisfy the state-equation Equation 3.13 or

241

equivalently Equation D.17. In addition we want the control force vector to be regulated only by the feedback response vector $\{z(t)\}$ as follows

$$\{u(t)\} = [T1]\{z(t)\} \qquad (D.31)$$

where $[T1]$ is a time-independent gain matrix. The Lagrangian function is given by

$$
\begin{aligned}
LF = {} & \{z(t)\}^T [Q]\{z(t)\} + \{u(t)\}^T [R]\{u(t)\} \\
& + \{\lambda(t)\}^T \left\{ \{z(t)\} - [T_t]\{\Lambda_t(t-\Delta t)\} - [T_t]\{\Gamma(t)\}\left(\frac{\Delta t}{2}\right) \right\}
\end{aligned} \qquad (D.32)
$$

Substituting $\{\Gamma(t)\}$ from Equation D.22

$$
\begin{aligned}
LF = {} & \{z(t)\}^T [Q]\{z(t)\} + \{u(t)\}^T [R]\{u(t)\} \\
& + \{\lambda(t)\}^T \left\{ \{z(t)\} - [T_t]\{\Lambda_t(t-\Delta t)\} - \left\{[B_t]\{u(t)\} + \{C_t\}\ddot{X}_g(t)\right\}\left(\frac{\Delta t}{2}\right) \right\}
\end{aligned} \qquad (D.33)
$$

The necessary conditions for optimality are

$$\frac{\partial LF}{\partial\{z(t)\}} = \{0\} \quad \rightarrow \quad 2[Q]\{z(t)\} + \{\lambda(t)\} = \{0\} \qquad (D.34)$$

$$\frac{\partial LF}{\partial\{u(t)\}} = \{0\} \quad \rightarrow \quad 2[R]\{u(t)\} - [B_t]^T\{\lambda(t)\}\left(\frac{\Delta t}{2}\right) = \{0\} \qquad (D.35)$$

$$\frac{\partial LF}{\partial\{\lambda(t)\}} = \{0\} \rightarrow \{z(t)\} - [T_t]\{\Lambda_t(t-\Delta t)\} - \left\{[B_t]\{u(t)\} + \{C_t\}\ddot{X}_g(t)\right\}\left(\frac{\Delta t}{2}\right) = \{0\} \quad (D.36)$$

From Equation D.35

$$\{u(t)\} = \frac{1}{2}\left(\frac{\Delta t}{2}\right)[R]^{-1}[B_t]^T\{\lambda(t)\} \qquad (D.37)$$

From Equation D.34

242

$$\{\lambda(t)\} \,. = \; -2\,[Q]\,\{z(t)\} \tag{D.38}$$

Substituting Equation D.38 in Equation D.37 we get the optimal control force

$$\{u^{\bullet}(t)\} \;=\; -\left(\frac{\Delta t}{2}\right)[R]^{-1}\,[B_t]^T\,[Q]\,\{z(t)\} \tag{D.39}$$

To obtain the state-vector in closed form, first substitute Equation D.39 in Equation D.22

$$\{\Gamma(t)\} \;=\; [T_t]^{-1}\,\{C_t\}\,\ddot{X}_g(t) - [T_t]^{-1}\,[B_t]\,[R]^{-1}\,[B_t]^T\,[Q]\,\{z(t)\}\left(\frac{\Delta t}{2}\right) \tag{D.40}$$

Substitute Equation D.40 in the state-equation Equation D.17

$$\{z(t)\} \;=\; [T_t]\left\{ \{\Lambda_t(t - \Delta t)\} + [T_t]^{-1}\,\{C_t\}\,\ddot{X}_g(t)\left(\frac{\Delta t}{2}\right) \right. $$
$$\left. - [T_t]^{-1}\,[B_t]\,[R]^{-1}\,[B_t]^T\,[Q]\,\{z(t)\}\left(\frac{\Delta t}{2}\right)^2 \right\} \tag{D.41}$$

$$\{z(t)\} \;=\; [T_t]\{\Lambda_t(t - \Delta t)\} + \{C_t\}\,\ddot{X}_g(t)\frac{(\Delta t)}{2} $$
$$- [B_t]\,[R]^{-1}\,[B_t]^T\,[Q]\,\{z(t)\}\left(\frac{\Delta t}{2}\right)^2 \tag{D.42}$$

Collecting terms

$$\{z(t)\}\left[\; [I]\, + [B_t]\,[R]^{-1}\,[B_t]^T\,[Q]\left(\frac{\Delta t}{2}\right)^2 \;\right]$$
$$= \; [T_t]\{\Lambda_t(t - \Delta t)\} + \{C_t\}\,\ddot{X}_g(t)\left(\frac{\Delta t}{2}\right) \tag{D.43}$$

Finally we obtain by inversion

$$\{z(t)\} \;=\; [\hat{\bar{\Xi}}(t)]\,\{\hat{\xi}(t)\} \tag{D.44a}$$

243

$$[\hat{\Xi}(t)] = \left[[I] + \frac{(\Delta t)^2}{4} [B_t][R]^{-1} [B_t]^T [Q] \right]^{-1}$$ (D.44b)

$$\{\hat{\xi}(t)\} = \left\{ [T_t]\{\Lambda_t(t-\Delta t)\} + \{C_t\}\ddot{X}_g(t)\left(\frac{\Delta t}{2}\right) \right\}$$ (D.44c)

which is the desired solution given in Equation 5.33.

4. Instantaneous Open-closed-loop.

The derivation of the optimal control forces for this algorithm follows that of the instantaneous closed-loop control. The difference is that the optimal control force is to be regulated by both the ground excitation and the structural response, and is to be of the form

$$\{u(t)\} = [S1]\{z(t)\} + \{S2(t)\}$$ (D.45)

where $[S1]$ is a time-independent gain matrix expressing the closed-loop feedback, and vector $\{S2(t)\}$ is a time-dependent vector as required by the earthquake excitation measurement for open-loop control. The Lagrangian function is identical to Equation D.32, and the optimality conditions are exactly the same as Equations D.34 through D.36. Substitute Equation D.35 into Equation D.36

$$\{z(t)\} = [T_t]\{\Lambda_t(t-\Delta t)\} + [B_t][R]^{-1}[B_t]^T\{\lambda(t)\}\frac{(\Delta t)^2}{8}$$
$$+ \{C_t\}\ddot{X}_g(t)\left(\frac{\Delta t}{2}\right)$$ (D.46)

From Equation D.34

$$\{\lambda(t)\} = -2[Q]\{z(t)\} = -[Q](\{z(t)\} + \{z(t)\})$$ (D.47)

244

Substitute one term for $\{z(t)\}$ from Equation D.46 in Equation D.47

$$\{\lambda(t)\} = -[Q]\Bigg[\{z(t)\} + [T_t]\{\Lambda_t(t-\Delta t)\}$$
$$+ [B_t][R]^{-1}[B_t]^T \{\lambda(t)\} \frac{(\Delta t)^2}{8} + \{C_t\}\ddot{X}_g(t)\left(\frac{\Delta t}{2}\right) \Bigg] \qquad (D.48)$$

Solving for $\{\lambda(t)\}$ from Equation D.48

$$\Bigg[[I] + [Q][B_t][R]^{-1}[B_t]^T \frac{(\Delta t)^2}{8} \Bigg]\{\lambda(t)\}$$
$$= -[Q]\Bigg[\{z(t)\} + [T_t]\{\Lambda_t(t-\Delta t)\} + \{C_t\}\ddot{X}_g(t)\left(\frac{\Delta t}{2}\right) \Bigg] \qquad (D.49)$$

$$\{\lambda(t)\} = -\Bigg[[I] + [Q][B_t][R]^{-1}[B_t]^T \frac{(\Delta t)^2}{8} \Bigg]^{-1}$$
$$\cdot [Q]\Bigg[\{z(t)\} + [T_t]\{\Lambda_t(t-\Delta t)\} + \{C_t\}\ddot{X}_g(t)\left(\frac{\Delta t}{2}\right) \Bigg] \qquad (D.50)$$

Substitute $\{\lambda(t)\}$ from Equation D.50 in Equation D.35

$$2[R]\{u(t)\} = -[B_t]^T \frac{(\Delta t)}{2}\Bigg[[I] + [Q][B_t][R]^{-1}[B_t]^T \frac{(\Delta t)^2}{8} \Bigg]^{-1}$$
$$\cdot [Q]\Bigg[\{z(t)\} + [T_t]\{\Lambda_t(t-\Delta t)\} + \{C_t\}\ddot{X}_g(t)\left(\frac{\Delta t}{2}\right) \Bigg] \qquad (D.51)$$

Substituting $\{u(t)\}$ on the left hand side by Equation D.45

$$2[R]\Big[[S1]\{z(t)\} + \{S2(t)\} \Big]$$
$$= -[B_t]^T\left(\frac{\Delta t}{2}\right)\Bigg[[I] + [Q][B_t][R]^{-1}[B_t]^T \frac{(\Delta t)^2}{8} \Bigg]^{-1}[Q]\{z(t)\}$$
$$- [B_t]^T\left(\frac{\Delta t}{2}\right)\Bigg[[I] + [Q][B_t][R]^{-1}[B_t]^T \frac{(\Delta t)^2}{8} \Bigg]^{-1}$$
$$\cdot [Q]\Bigg[[T_t]\{\Lambda_t(t-\Delta t)\} + \{C_t\}\ddot{X}_g(t)\left(\frac{\Delta t}{2}\right) \Bigg] \qquad (D.52)$$

Equating coefficients in Equation D.52

$$[S1] = -[R]^{-1} [B_t]^T \frac{(\Delta t)}{4} \left[[I] + [Q][B_t][R]^{-1} [B_t]^T \frac{(\Delta t)^2}{8} \right]^{-1} [Q] \quad (D.53)$$

$$\{S2(t)\} = [S1]\left\{ [T_t]\{\Lambda_t(t-\Delta t)\} + \{C_t\}\ddot{X}_g(t)\left(\frac{\Delta t}{2}\right) \right\} \quad (D.54)$$

which are given in Chapter V as Equations 5.36 and 5.37.

The response state-vector can be derived as follows. From Equations D.17 and D.22

$$\{z(t)\} = [T_t]\{\Lambda_t(t-\Delta t)\} + [B_t]\{u^{\bullet}(t)\}\left(\frac{\Delta t}{2}\right) + \{C_t\}\ddot{X}_g(t)\left(\frac{\Delta t}{2}\right) \quad (D.55)$$

Substituting $\{u^{\bullet}(t)\}$ from Equation D.45

$$\{z(t)\} = [T_t]\{\Lambda_t(t-\Delta t)\} + [B_t]\{ [S1]\{z(t)\} + \{S2(t)\} \}\frac{(\Delta t)}{2}$$
$$+ \{C_t\}\ddot{X}_g(t)\left(\frac{\Delta t}{2}\right) \quad (D.56)$$

Collecting terms

$$\left[[I] - [B_t][S1]\left(\frac{\Delta t}{2}\right) \right]\{z(t)\}$$
$$= [T_t]\{\Lambda_t(t-\Delta t)\} + [B_t]\{S2(t)\}\left(\frac{\Delta t}{2}\right) + \{C_t\}\ddot{X}_g(t)\left(\frac{\Delta t}{2}\right) \quad (D.57)$$

Substituting for $\{S2(t)\}$ in terms of $[S1]$ from Equation D.54

$$\left[[I] - [B_t][S1]\left(\frac{\Delta t}{2}\right) \right]\{z(t)\}$$
$$= [T_t]\{\Lambda_t(t-\Delta t)\} + [B_t][S1][T_t]\{\Lambda_t(t-\Delta t)\}\frac{(\Delta t)}{2} \quad (D.58)$$
$$+ [B_t][S1]\{C_t\}\ddot{X}_g(t)\left(\frac{\Delta t}{2}\right)^2 + \{C_t\}\ddot{X}_g(t)\left(\frac{\Delta t}{2}\right)$$

Collecting terms

246

$$\left[\; [I] - [B_t][S1]\left(\frac{\Delta t}{2}\right) \; \right]\{z(t)\}$$

$$= \left[\; [I] + [B_t][S1]\left(\frac{\Delta t}{2}\right) \; \right][T_t]\{\Lambda_t(t - \Delta t)\} \qquad (D.59)$$

$$+ \left[\; [I] + [B_t][S1]\left(\frac{\Delta t}{2}\right) \; \right]\{C_t\}\ddot{X}_g(t)\left(\frac{\Delta t}{2}\right)$$

Simplifying and solving for $\{z(t)\}$

$$\{z(t)\} = [\hat{\Psi}(t)]\{\hat{\xi}(t)\} \qquad (D.60a)$$

$$[\hat{\Psi}(t)] = \left[\; [I] - [B_t][S1]\left(\frac{\Delta t}{2}\right) \; \right]^{-1}\left[\; [I] + [B_t][S1]\left(\frac{\Delta t}{2}\right) \; \right] \qquad (D.60b)$$

$$\{\hat{\xi}(t)\} = \left\{ [T_t]\{\Lambda_t(t - \Delta t)\} + \{C_t\}\ddot{X}_g(t)\left(\frac{\Delta t}{2}\right) \right\} \qquad (D.60c)$$

which is the answer given in Equation 5.38.

5. Critical-mode Closed-loop.

The derivation for the critical-mode closed-loop algorithm follows the same pattern as the derivation for the instantaneous closed-loop algorithm. The problem is to find the optimal control forces $\{u^*(t)\}$ that minimize the performance index of Equation 9.8 and satisfy the state-equation of Equation 9.4. The control force is to be regulated by the modal state-vector as follows

$$\{u(t)\} = [K]_c\{\psi_t(t)\}_c \qquad (D.61)$$

Following the same procedure as for the instantaneous closed-loop algorithm, the optimality conditions are

$$2[Q]_c\{\psi_t(t)\}_c + \{\lambda(t)\} = \{0\} \qquad (D.62)$$

247

$$2 [R] \{u(t)\} - [TB]_c^T \{\lambda(t)\} \left(\frac{\Delta t}{2} \right) = \{0\} \tag{D.63}$$

$$\{\psi_t(t)\}_c - \{\Lambda_t(t - \Delta t)\}_c - \left\{ [TB]_c \{u(t)\} + \{TC\}_c \ddot{X}_g(t) \right\} \left(\frac{\Delta t}{2} \right) = \{0\} \tag{D.64}$$

From Equation D.62

$$\{\lambda(t)\} = -2 [Q]_c \{\psi_t(t)\}_c \tag{D.65}$$

Substituting Equation D.65 in Equation D.63

$$\{u^\cdot(t)\} = - \left(\frac{\Delta t}{2} \right) [R]^{-1} [TB]_c^T [Q]_c \{\psi_t(t)\}_c \tag{D.66}$$

which is the optimal control force given in Equation 9.10. To obtain the critical-mode state-vector, substitute Equation D.66 in the state-equation for the critical modes, Equation D.64

$$\{\psi_t(t)\}_c = \{\Lambda_t(t - \Delta t)\}_c - \frac{(\Delta t)^2}{4} [TB]_c [R]^{-1} [TB]_c^T [Q]_c \{\psi_t(t)\}_c + \{TC\}_c \ddot{X}_g(t) \left(\frac{\Delta t}{2} \right) \tag{D.67}$$

Collecting terms

$$\left[[I]_c + \left(\frac{\Delta t}{2} \right)^2 [TB]_c [R]^{-1} [TB]_c^T [Q]_c \right] \{\psi_t(t)\}_c$$
$$= \{\Lambda_t(t - \Delta t)\}_c + \{TC\}_c \ddot{X}_g(t) \left(\frac{\Delta t}{2} \right) \tag{D.68}$$

which gives the solution

$$\{\psi_t(t)\}_c = [\hat{P}1(t)] \{\hat{P}2(t)\} \tag{D.69a}$$

$$[\hat{P}1(t)] = \left[[I]_c + \frac{(\Delta t)^2}{4} [TB]_c [R]^{-1} [TB]_c^T [Q]_c \right]^{-1} \tag{D.69b}$$

248

$$\{\hat{P}2(t)\} = \left\{ \{\Lambda_t(t - \Delta t)\}_c + \{TC\}_c \, \ddot{X}_g(t) \left(\frac{\Delta t}{2} \right) \right\}$$

(D.69c)

which are given as Equation 9.13.

APPENDIX E

NON-OPTIMAL CLOSED-LOOP DERIVATIONS

This Appendix presents the derivation of the motion equations and statistics of response of the combined AT and AMD systems for the non-optimal closed-loop scheme described in Chapter IV.

Assuming zero initial conditions and taking the Fourier transforms of Equations 4.2 and 4.3 yields

$$\overline{Y}_j = \overline{Y}_{j-1} + m_j\,(i\omega)^2\,\overline{X}_j + c_j\,(i\omega)\,\overline{X}_j\,, \qquad 1 \le j \le (N-1) \tag{E.1}$$

$$\overline{Y}_{j-1} = k_j\,(\overline{X}_j - \overline{X}_{j-1}) + \overline{u}_j\,, \qquad 1 \le j \le (N-1) \tag{E.2}$$

Let the Fourier transform of the AT control force be expressed by Equation 4.36. Substituting Equation 4.36 in Equation E.2

$$\overline{Y}_{j-1} = (k_j + g_i(\omega))\,(\overline{X}_j - \overline{X}_{j-1}) \tag{E.3}$$

Using the definition of Equation 4.16, Equation E.3 can be rewritten as

$$\overline{Y}_{j-1} = Kc_j\,(\overline{X}_j - \overline{X}_{j-1}) \tag{E.4}$$

Solving Equation E.4 for $\overline{X}_j$ and then substituting in Equation E.1 gives

$$\overline{X}_j = \overline{X}_{j-1} + \frac{\overline{Y}_{j-1}}{Kc_j} \tag{E.5}$$

$$\overline{Y}_j = \overline{Y}_{j-1} + (-\omega^2\,m_j + i\omega\,c_j)\left[\overline{X}_{j-1} + \frac{\overline{Y}_{j-1}}{Kc_j}\right] \tag{E.6}$$

250

Rewritting Equation E.6 and collecting terms

$$\overline{Y}_j = \overline{X}_{j-1}(-\omega^2 m_j + i\omega c_j) + \left[1 + \frac{(-\omega^2 m_j + i\omega c_j)}{Kc_j} \right] \overline{Y}_{j-1} \qquad (E.7)$$

Combining Equations E.5 and E.7 in matrix form yields the transfer matrix $[A]_j$ of the jth floor given in Equation 4.14

$$\left\{ \begin{array}{c} \overline{X}_j \\ \overline{Y}_j \end{array} \right\} = \left[\begin{array}{c|c} 1 & \dfrac{1}{Kc_j} \\ \hline (-\omega^2 m_j + i\omega c_j) & 1 + \dfrac{(-\omega^2 m_j + i\omega c_j)}{Kc_j} \end{array} \right] \left\{ \begin{array}{c} \overline{X}_{j-1} \\ \overline{Y}_{j-1} \end{array} \right\} \qquad (E.8)$$

The transfer matrix of Equation E.8 can be written in compact form by using the state-vector of Equation 4.11 as

$$\{Z\}_j = [A]_j \{Z\}_{j-1} \qquad (E.9)$$

Matrix $[A]_j$ represents the transfer mechanism of a story unit. The state-vector $\{Z\}_{j-1}$ at floor level $(j-1)$ is transferred to the state-vector $\{Z\}_j$ at floor level j through the transfer matrix $[A]_j$. If the jth floor unit is not equipped with an active tendon, set $g_t(\omega) = 0$ in Equation 4.16. Applying Equation E.9 to the first floor

$$\{Z\}_1 = [A]_1 \{Z\}_0 \qquad (E.10)$$

where $\{Z\}_0$ is the state-vector at the basement floor. For the second floor

$$\{Z\}_2 = [A]_2 \{Z\}_1 \qquad (E.11)$$

Combining Equations E.10 and E.11

$$\{Z\}_2 = [A]_2 [A]_1 \{Z\}_0 \qquad (E.12)$$

251

Applying Equation E.9 repeatedly gives

$$\{Z\}_L = [A]_L \ \cdots \ [A]_2 \ [A]_1 \ \{Z\}_0 \qquad\qquad (E.13)$$

$$\{Z\}_L = [A(L)] \ \{Z\}_0 , \qquad 1 \le L \le (N-1) \qquad\qquad (E.14)$$

which is given as Equation 4.8. The multiplication of the transfer matrices is manipulated in the computer program. The transfer relation in Equation E.14 is valid only for the floors $1 \le L \le (N-1)$ since we have an AMD on the top floor. For $L = N$, this relation must be modified to include the AMD control force.

Let the Fourier transform of the AMD control force be defined as in Equation 4.39. Taking the Fourier transform of Equations 4.4 and 4.5 and assuming zero initial conditions

$$\overline{Y}_N = k_d (\overline{X}_{N+1} - \overline{X}_N) + c_d (i\omega)(\overline{X}_{N+1} - \overline{X}_N) \qquad\qquad (E.15)$$

$$\overline{u}_d = m_d (i\omega)^2 \ \overline{X}_{N+1} + \overline{Y}_N \qquad\qquad (E.16)$$

Rewriting Equation E.15 and substituting $\overline{X}_{N+1}$ from Equation E.15 into Equation E.16, give

$$\overline{X}_{N+1} = \overline{X}_N + \frac{\overline{Y}_N}{k_d + i\omega \ c_d} \qquad\qquad (E.17)$$

$$\overline{u}_d = -m_d \omega^2 \ \overline{X}_N + \left[1 - \frac{m_d \omega^2}{k_d + i\omega \ c_d} \right] \overline{Y}_N \qquad\qquad (E.18)$$

Substituting $\overline{u}_d$ from Equation 4.39 into Equation E.18, gives

$$-m_d \omega^2 \ \overline{X}_N + \left[1 - \frac{m_d \omega^2}{k_d + i\omega \ c_d} \right] \overline{Y}_N - g_m(\omega)\overline{X}_N = 0 \qquad\qquad (E.19)$$

252

Combining Equations E.17 and E.19 in matrix form yields Equation 4.10, and the transfer matrix of the AMD, given in Equation 4.18

$$\left\{ \begin{array}{c} \overline{X}_{N+1} \\ 0 \end{array} \right\} = \left[\begin{array}{c|c} 1 & \dfrac{1}{k_d + i\omega\, c_d} \\ \hline -m_d \omega^2 & 1 - \dfrac{m_d \omega^2}{k_d + i\omega\, c_d} \end{array} \right] \left\{ \begin{array}{c} \overline{X}_N \\ \overline{Y}_N \end{array} \right\} - \left\{ \begin{array}{c} 0 \\ g_m(\omega)\overline{X}_N \end{array} \right\} \qquad (E.20)$$

$$\{Z\}_{N+1} = [T]\,\{Z\}_N - \left\{ \begin{array}{c} 0 \\ g_m(\omega)\overline{X}_N \end{array} \right\} \qquad (E.21)$$

$$[T] = \left[\begin{array}{c|c} 1 & \dfrac{1}{k_d + i\omega\, c_d} \\ \hline -m_d \omega^2 & 1 - \dfrac{m_d \omega^2}{k_d + i\omega\, c_d} \end{array} \right] \qquad (E.22)$$

For the Nth floor the effect of the AMD is reflected by Equations 4.6 and 4.7. Assuming zero initial conditions the Fourier transforms of Equations 4.6 and 4.7 are

$$\overline{Y}_N = \overline{Y}_{N-1} + m_N\,(i\omega)^2\,\overline{X}_N + c_N\,(i\omega)\,\overline{X}_N + g_m(\omega)\,\overline{X}_N \qquad (E.23)$$

$$\overline{Y}_{N-1} = k_N\,(\overline{X}_N - \overline{X}_{N-1}) + g_t(\omega)\,(\overline{X}_N - \overline{X}_{N-1}) \qquad (E.24)$$

In Equations E.23 and E.24 the expressions for the Fourier transform of the AT and AMD control forces from Equations 4.36 and 4.39 have been utilized. Collecting terms

$$\overline{Y}_N = \overline{Y}_{N-1} + (\,-m_N \omega^2 + c_N\,(i\omega)\,)\,\overline{X}_N + g_m(\omega)\,\overline{X}_N \qquad (E.25)$$

$$\overline{Y}_{N-1} = [\,k_N + g_t(\omega)\,]\,(\overline{X}_N - \overline{X}_{N-1}) \qquad (E.26)$$

Using Equation 4.16 in Equation E.26

$$\overline{Y}_{N-1} = Kc_N\,(\overline{X}_N - \overline{X}_{N-1}) \qquad (E.27)$$

253

Rewriting Equation E.27 and substituting $\overline{X}_N$ from Equation E.27 into Equation E.25, give

$$\overline{X}_N = \overline{X}_{N-1} + \frac{\overline{Y}_{N-1}}{Kc_N} \qquad (E.28)$$

$$\overline{Y}_N = (-m_N \omega^2 + c_N i\omega) \overline{X}_{N-1} + \left[1 + \frac{(-m_N \omega^2 + c_N i\omega)}{Kc_N} \right] \overline{Y}_{N-1}$$
$$+ g_m(\omega) \overline{X}_N \qquad (E.29)$$

Combining Equations E.28 and E.29 in matrix form yields Equation 4.9 as follows

$$\left\{ \begin{matrix} \overline{X}_N \\ \overline{Y}_N \end{matrix} \right\} = \left[\begin{array}{c|c} 1 & \frac{1}{Kc_N} \\ \hline -m_N \omega^2 + i\omega c_N & 1 + \frac{(-m_N \omega^2 + i\omega c_N)}{Kc_N} \end{array} \right] \left\{ \begin{matrix} \overline{X}_{N-1} \\ \overline{Y}_{N-1} \end{matrix} \right\} \qquad (E.30)$$
$$+ \left\{ \begin{matrix} 0 \\ g_m(\omega)\overline{X}_N \end{matrix} \right\}$$

$$\{Z\}_N = [A]_N \{Z\}_{N-1} + \left\{ \begin{matrix} 0 \\ g_m(\omega)\overline{X}_N \end{matrix} \right\} \qquad (E.31)$$

The boundary conditions for the combined AT and AMD case are given by

$$\{Z\}_{N+1} = \left\{ \begin{matrix} \overline{X}_{N+1} \\ 0 \end{matrix} \right\}, \qquad \{Z\}_0 = \left\{ \begin{matrix} 1 \\ \overline{Y}_0 \end{matrix} \right\} \qquad (E.32)$$

The earthquake ground displacement is assumed to be a Dirac delta function $X_0 = \delta(t)$. In Equation E.32 $\overline{X}_0 = 1$ is the Fourier transform of the Dirac delta function. The response is the impulse response function and the Fourier transform of the response $(\overline{X}_j, \overline{Y}_j)$ is the frequency response function to the ground displacement. The boundary conditions of Equation E.32 can be used to solve for the unknown

254

quantities $\overline{Y}_0$, $\overline{Y}_N$, $\overline{X}_N$ and $\overline{X}_{N+1}$, from Equations E.14, E.21 and E.31. Note that from Equation E.14 once $\overline{Y}_0$ is determined the state-vector for other floors can easily be found. Using Equation E.14 repeatedly to express $\{Z\}_{N-1}$ we get

$$\{Z\}_{N-1} = [A]_{N-1}\ [A]_{N-2}\ \cdots\ [A]_2\ [A]_1\ \{Z\}_0 \tag{E.33}$$

Substituting Equation E.33 in Equation E.31 gives

$$\{Z\}_N = [A]_N\ [A]_{N-1}\ \cdots\ [A]_2\ [A]_1\ \{Z\}_0 + \left\{ \frac{0}{g_m(\omega)\overline{X}_N} \right\} \tag{E.34}$$

and using the notation for the matrix product

$$[A(N)] = [A]_N\ [A]_{N-1}\ \cdots\ [A]_2\ [A]_1 \tag{E.35}$$

in Equation E.34, we obtain

$$\{Z\}_N = [A(N)]\ \{Z\}_0 + \left\{ \frac{0}{g_m(\omega)\overline{X}_N} \right\} \tag{E.36}$$

Simultaneous solution of Equations E.21 and E.36 with the boundary conditions of Equation E.32 yields $\overline{Y}_0$, $\overline{Y}_N$, $\overline{X}_N$. In order to simplify the calculations the following notation is used

$$[A(N)] = \left[\begin{array}{c|c} A11(N) & A12(N) \\ \hline A21(N) & A22(N) \end{array} \right] \tag{E.37}$$

where the elements of the partitioned matrices are known and are manipulated in the computer program. Let $[T]$ be expressed in the symbolic form

$$[T] = \left[\begin{array}{c|c} T11 & T12 \\ \hline T21 & T22 \end{array} \right] \tag{E.38}$$

where, from Equation E.22

$$T11 = 1, \qquad T12 = \frac{1}{k_d + i\omega\, c_d} \qquad (E.39)$$

$$T21 = -m_d\,\omega^2, \qquad T22 = 1 - \frac{m_d\,\omega^2}{k_d + i\omega\, c_d} \qquad (E.40)$$

Rewriting Equations E.21 and E.36 for clarity

$$\left\{ \frac{\overline{X}_{N+1}}{0} \right\} = \left[\begin{array}{c|c} T11 & T12 \\ \hline T21 & T22 \end{array} \right] \left\{ \frac{\overline{X}_N}{\overline{Y}_N} \right\} - \left\{ \frac{0}{g_m(\omega)\overline{X}_N} \right\} \qquad (E.41)$$

$$\left\{ \frac{\overline{X}_N}{\overline{Y}_N} \right\} = \left[\begin{array}{c|c} A11(N) & A12(N) \\ \hline A21(N) & A22(N) \end{array} \right] \left\{ \frac{1}{\overline{Y}_0} \right\} + \left\{ \frac{0}{g_m(\omega)\overline{X}_N} \right\} \qquad (E.42)$$

Substitute Equation E.42 in Equation E.41

$$\begin{aligned}
\left\{ \frac{\overline{X}_{N+1}}{0} \right\} &= \left[\begin{array}{c|c} T11 & T12 \\ \hline T21 & T22 \end{array} \right] \left[\begin{array}{c|c} A11(N) & A12(N) \\ \hline A21(N) & A22(N) \end{array} \right] \left\{ \frac{1}{\overline{Y}_0} \right\} \\
&\quad + \left[\begin{array}{c|c} T11 & T12 \\ \hline T21 & T22 \end{array} \right] \left\{ \frac{0}{g_m(\omega)\overline{X}_N} \right\} - \left\{ \frac{0}{g_m(\omega)\overline{X}_N} \right\}
\end{aligned} \qquad (E.43)$$

Define the matrix product in Equation E.43 as $[E]$

$$[E] = [T][A(N)] = \left[\begin{array}{c|c} E11 & E12 \\ \hline E21 & E22 \end{array} \right] \qquad (E.44)$$

Then Equation E.43 becomes

$$\left\{ \frac{\overline{X}_{N+1}}{0} \right\} = \left[\begin{array}{c|c} E11 & E12 \\ \hline E21 & E22 \end{array} \right] \left\{ \frac{1}{\overline{Y}_0} \right\} + \left\{ \frac{T12}{(T21-1)} \right\} g_m(\omega)\,\overline{X}_N \qquad (E.45)$$

From the second row of Equation E.45

$$0 = E21 + E22\,\overline{Y}_0 + (T22 - 1)\,g_m(\omega)\,\overline{X}_N \qquad (E.46)$$

From the first row of Equation E.42

$$\bar{X}_N = A11(N) + A12(N)\bar{Y}_0 \qquad (E.47)$$

Solving Equations E.46 and E.47 simultaneously and using Equations E.39 and E.40 yields

$$\bar{Y}_0 = -\frac{E21 + T21^*T12^*A11(N)^*g_m(\omega)}{E22 + T21^*T12^*A22(N)^*g_m(\omega)} \qquad (E.48)$$

which when calculated can be substituted in Equation E.47 to yield $\bar{X}_N$. From the second row of Equation E.42 we can obtain $\bar{Y}_N$ as

$$\bar{Y}_N = -A21(N) + A22(N)\bar{Y}_0 + g_m(\omega)\bar{X}_N \qquad (E.49)$$

Finally from the first row of Equation E.41

$$\bar{X}_{N+1} = T11\,\bar{X}_N + T12\,\bar{Y}_N \qquad (E.50)$$

and since from Equation E.39, $T11 = 1$, Equation E.50 can be simplified to

$$\bar{X}_{N+1} = \bar{X}_N + T12\,\bar{Y}_N \qquad (E.51)$$

Thus Equations E.47, E.48, E.49 and E.51 describe all the unknown quantities. The response at any floor level is given by Equation E.14.